AD NUMBER

AD473768

NEW LIMITATION CHANGE

TO

Approved for public release, distribution unlimited

FROM

Distribution authorized to U.S. Gov't. agencies and their contractors; Administrative/Operational Use; AUG 1965. Other requests shall be referred to Air Force Materials Lab., Wright-Patterson AFB, OH 45433.

AUTHORITY

Air Force Materials Lab. ltr dtd 29 Jun 1972

SECURITY MARKING

The classified or limited status of this report applies to each page, unless otherwise marked.
Separate page printouts MUST be marked accordingly.

THIS DOCUMENT CONTAINS INFORMATION AFFECTING THE NATIONAL DEFENSE OF THE UNITED STATES WITHIN THE MEANING OF THE ESPIONAGE LAWS, TITLE 18, U.S.C., SECTIONS 793 AND 794. THE TRANSMISSION OR THE REVELATION OF ITS CONTENTS IN ANY MANNER TO AN UNAUTHORIZED PERSON IS PROHIBITED BY LAW.

NOTICE: When government or other drawings, specifications or other data are used for any purpose other than in connection with a definitely related government procurement operation, the U. S. Government thereby incurs no responsibility, nor any obligation whatsoever; and the fact that the Government may have formulated, furnished, or in any way supplied the said drawings, specifications, or other data is not to be regarded by implication or otherwise as in any manner licensing the holder or any other person or corporation, or conveying any rights or permission to manufacture, use or sell any patented invention that may in any way be related thereto.

AFML-TR-65-284

THE EFFECT OF CERTAIN DAMPING TREATMENTS ON THE RESPONSE OF IDEALIZED AEROPLANE STRUCTURES EXCITED BY NOISE

D. J. MEAD

UNIVERSITY OF SOUTHAMPTON

TECHNICAL REPORT No. AFML-TR-65-284

AUGUST 1965

AIR FORCE MATERIALS LABORATORY
RESEARCH AND TECHNOLOGY DIVISION
AIR FORCE SYSTEMS COMMAND
WRIGHT-PATTERSON AIR FORCE BASE, OHIO

NOTICES

When Government drawings, specifications, or other data are used for any purpose other than in connection with a definitely related Government procurement operation, the United States Government thereby incurs no responsibility nor any obligation whatsoever; and the fact that the Government may have formulated, furnished, or in any way supplied the said drawings, specifications, or other data, is not to be regarded by implication or otherwise as in any manner licensing the holder or any other person or corporation, or conveying any rights or permission to manufacture, use, or sell any patented invention that may in any way be related thereto.

Qualified requesters may obtain copies of this report from the Defense Documentation Center.

The distribution of this report is limited because the report contains technology identifiable with items on the strategic embargo lists excluded from export or re-export under U. S. Export Control Act of 1949 (63 STAT. 7), as amended (50 U.S.C. App. 2020.2031), as implemented by AFR 400-10.

Copies of this report should not be returned to the Research and Technology Division unless return is required by security considerations, contractual obligations, or notice on a specific document.

500 - October 1965 - 773-10-221

THE EFFECT OF CERTAIN DAMPING TREATMENTS ON THE RESPONSE OF IDEALIZED AEROPLANE STRUCTURES EXCITED BY NOISE

D. J. MEAD

UNIVERSITY OF SOUTHAMPTON

FOREWORD

This report was prepared by Dr. D. J. Mead of the University of Southampton, Department of Aeronautics and Astronautics, Southampton, England, under USAF Contract No. AF 61(052)-627. The contract was initiated under Project No. 7351, "Metallic Materials", Task No. 735106, "Behavior of Metals" and it was administered by the European Office, Office of Aerospace Research. The work was monitored by the Metals and Ceramics Division, Air Force Materials Laboratory, Research and Technology Division, under the direction of Mr. W. J. Trapp.

This report covers work performed during the period of January 1963 to January 1964.

The manuscript of this report was released by the author February 1964 for publication as an AFML Technical Report.

The author wishes to acknowledge with gratitude the encouragement and support of this work by Professor B. J. Richards of the Department of Aeronautics and Astronautics at the University of Southampton; also the financial assistance of the U. S. Air Force in Europe who sponsored the work.

This technical report has been reviewed and is approved.

W. J. TRAPP
Chief, Strength and Dynamics Branch
Metals and Ceramics Division
Air Force Materials Laboratory

A B S T R A C T

This report relates to the vibration of aeroplane structures excited by jet-noise or other random pressures. A review is made of those aspects of vibration and transmitted noise which may be alleviated by increasing the structural damping. The damping of conventional untreated structures is then considered, measured values of the damping of model and full-scale structures being discussed in the light of previous studies (by the author) of acoustic and rivet damping.

The common practice of judging a damping treatment by the loss factor increment it produces is then shown to be inadequate for contemporary treatments and thin-plate structures. Alternative "criteria" are therefore derived which describe more adequately the effectiveness of the treatment in attenuating certain random and harmonic vibration phenomena. These have been used to compare two commercial unconstrained treatments and to estimate the reduction of random stresses in an aeroplane structure when the treatments are added.

The response of a two-dimensional flat sandwich plate with a damped core has next been analysed. The dependence of the modal loss factor, stiffness and criteria values on the wavelength and core properties has been studied. Optimum core thicknesses and core properties have been found which minimise the response. Random stresses in a structure with thick-cored sandwich plating have been estimated to be not less than 10% of those in a solid-plate structure of equal weight.

Harmonic experiments on small sandwich specimens have confirmed the theory for the loss factor and stiffness. The special apparatus and techniques of measurement developed for the experiment have been used to assess three commercial sandwich specimens.

A new approach has been initiated to estimate the random response of a very heavily damped system. Its validity has been confirmed for simple random excitation conditions by experiments on the sandwich specimens.

C O N T E N T S

LIST OF TABLES

LIST OF ILLUSTRATIONS

NOTATION

A_m, A_d	cross-sectional areas of metal and treatment
A_{mn}	time dependent coefficient of the pressure series
a, b	plate dimensions
c	speed of sound in medium surrounding plate
C	initial viscous damping coefficient
D	flexural rigidity of a solid plate
E, E_m	Young's Modulus of metal plate
E_d	Young's Modulus of treatment (real part)
e	ratio of Young's Moduli
$F_d(\eta)$, $F_v(\eta)$, $F_a(\eta)$, $F_r(\eta)$	functions of the modal loss factor,
$f_n(y)$	non-dimensional displacement function
$\mathcal{F}_p(i\omega)$	Fourier transform of quantity p(t)
$G_c = G(1 + i\beta)$	complex shear modulus
h_1	face-plate thickness
h_3	core thickness
h	thickness of solid plate equal in weight to the sandwich plate
h_r	a standard thickness of plate
i	$\sqrt{-1}$
I	second moment of area about neutral surface
K	generalised stiffness of untreated plate
K_n, K_r	generalised stiffness in n^{th}, r^{th} mode
k_{mn}	term proportional to the generalised stiffness of a solid plate to thickness $2h_1$
$\mathcal{L}(y)$	non-dimensional loading distribution
M, M_n	generalised mass(of n^{th} mode)

M_x, M_y, M_{xy}	moment resultants in face-plates
m	number of flexural half-waves in plate length
n	number of flexural half-waves in plate width
$P(t)$	time-dependent generalised force
P, P_n	amplitude of harmonic generalised force (in nth mode)
p_i	amplitude of harmonic incident pressure
$\langle p^2 \rangle$	mean square random incident pressure
$\langle p_r^2 \rangle$	mean square random radiation pressure
p_t	amplitude of harmonic transmitted pressure
$p_1(x,y,t)$, $p_2(x,y.t)$	external time dependent pressures on top and bottom face-plates
$p(x,y,t)$	resultant external pressure on plate
q_1, q_2	resultant loadings on top and bottom face-plates
$q, \dot{q}, \ddot{q}$	generalised co-ordinate, velocity and acceleration
$\bar{q}$	amplitude of harmonic displacement
q_{rms}	root mean square value of random displacement
$\langle q^2 \rangle$	mean square value of random displacement
r	lateral semi-wavelength ÷ longitudinal semi-wavelength, $\frac{b/a}{m\ n}$
s, s_r	arc length on vector diagram
t	time
u,v,w	displacement components
U_{mn}, V_{mn}, W_{mn}	coefficients of the displacement series
W_n	generalised displacement in the n^{th} mode
$\bar{W}_n$	amplitude of the harmonic generalised displacement
x,y,z	space-cordinates
Ψ	function of mode and loading distribution (equation 7.41)
$Z_n(\omega)$	complex generalised impedance
$\bar{z}_m$, $\bar{z}_d$	distance from neutral surface to centroid of metal or treatment section.

α, α_{mn}	stress ratio
β	core loss factor (in shear)
ε_x, ε_y	direct strains
η_d	loss factor of unconstrained damping treatment
η, η_{mn}, η_n, η_r	loss factor of the (mn^{th}, n^{th}, r^{th}) flexural mode
η_i	modal loss factor before treatment
θ	mass ratio
λ	wavelength of incident sound waves
λ_t	trace wavelength of incident sound waves on plate
λ_a, λ_b	modal wavelengths
κ, κ_{mn}	stiffness ratio of the (mn^{th}) flexural mode
μ	mass per unit area of sandwich plate
ν	Poisson's ratio
ρ	density of medium surrounding plate
ρ_c, ρ_p	density of core, face-plates
σ_{bx}, σ_{by}	bending stresses in face-plates
σ_{x1}, σ_{y1}	direct stress at mid-plane of top face-plate
σ_{z1}, σ_{z2}	direct stresses in core normal to top and bottom face-plates
τ	thickness of damping material + thickness of face-plate
τ_{xy}, τ_{xz}, τ_{yz}	shear stresses
$\Phi(\omega)$	power spectral density
$\phi(\tau)$	correlation function
ϕ	inclination of plane wave fronts to plate surface
χ	function of loading spectrum (equation 7.40)
Ψ_{mn}	complex shear parameter (equation 5.19)
ψ_{mn},	shear parameter (equation 5.29)
ω	angular frequency

ω_{mn}, ω_n, ω_r	resonant frequency of the mn^{th}, n^{th}, r^{th} mode
ω_{ts}	resonant frequency of the pure thickness-shear mode
ω_c	frequency at which coincidence transmission occurs
Ω	$\omega + \omega_r$

Some other suffices have been used with some of the symbols. The use of these is generally restricted to the section in which they are defined.

Chapter 1
Introduction

1.1 The Context of the Problem

The modern high speed aeroplane is generally known as a prolific source of disturbing noise. On the ground, its jet engines produce noise levels which have been quoted as high as 170 db*. At high speeds, the flow of air over the vehicle is in a turbulent state, generating sound and exerting on the aeroplane surface hydrodynamic pressures of up to 145 db at M = 1.5. Whether stationary on the ground or flying fast through the air, the structure is therefore subjected to intense randomly fluctuating pressure. Since the structure is relatively light and flexible, it responds readily to these pressures. In consequence, noise is transmitted through the walls, inducing passenger discomfort and fatigue, and randomly varying stresses are generated within the structure, leading to metal fatigue.

A reduction of the transmitted noise or of the fluctuating stresses can be achieved by varying the three basic structural parameters, mass, stiffness and damping. Increasing the mass is the well-known method of decreasing transmitted noise, but for obvious reasons is no acceptable solution. Increasing the stiffness, although reducing the stresses in some parts of the structure, has been found in practice sometimes to increase them elsewhere. Furthermore, the extent to which the stiffness can be increased is limited by the amount of extra weight that may be permitted. Increasing the damping can be shown to be beneficial to the stresses in all cases, and under some conditions also to the transmitted sound.

Until recent years, the damping was not considered to be a variable, but with developments in damping treatments, large increases of damping have become possible with relatively little or no increase in weight. Contemporary treatments involve adding a layer of visco-elastic material (usually a high-polymer) to the plates and beams of the structure. As the structure vibrates, the material undergoes fluctuating strains, dissipates energy and damps the motion. Recent developments have led to the manufacture of materials having greater damping capacities than hitherto, which are retained over broad ranges of temperature and frequency. Further increases of damping efficiency have resulted from developments in the techniques of using the materials, notably in the method of constraining the layer to distort in shear, instead of distorting only in flexure, as previously.

The purpose of this report is to conduct investigation into the benefits which might accrue by using certain damping treatments in aeroplane structures subjected to noise excitation. It must first be proved that increasing the damping is, in fact, beneficial. This is so, of course, provided the random response of the structure is predominantly resonant. To establish this, and also to give insight into the problems of the investigation, we shall firstly discuss the nature of the structures and their modes of free vibration, the nature of the excitation fields and also of the corresponding structural response.

*Noise levels quoted are in db's, referred to .0002 dynes cm^{-2}
i.e. db's = $20 \log_{10} p_{r.m.s.} / .0002$

1.2 The Nature of the Structure and its Modes of Natural Vibration

A typical fuselage structure consists of a thin cylindrical shell reinforced longitudinally by stringers and circumferentially by frames. Typical spacings may be 4 - 10 in. between the stringers and 6 - 18 in. between the frames. The stringers may have an open or closed section and are riveted or bonded to the skin. Frames are usually of open section and are riveted to the skin. The stringers are continuous through the frames, being joined to the frames at the intersections by cleats which add torsional stability to the stringers. The modes of vibration which are significant in noise transmission and acoustic fatigue may, for convenience, be classified as long wavelength (or 'overall') modes, and short wavelength (or 'local') modes. (The classification is based essentially on the methods and restrictions used to calculate the modal frequencies, rather than on essential differences in the nature of the modes).

The overall modes involve distortion of the whole cross-section and length. The distortion is periodic around the circumference and along the length. The frames, stringers and skin all take part in the distortion, a typical mode of which is shown in Figure 1. Longitudinal half-wavelengths may occupy several frame spacings. The frequencies of modes of this type have been analysed by P.R. Miller (1), and some typical values are shown in Figure 2.

The local modes have longitudinal half-wavelengths equal to the frame spacing, nodal lines existing at each frame station. The radial displacements around the circumference of the four simplest modes of this type are shown in Figure 3, where a cylinder of infinite radius is shown for simplicity. Lin (2) has discussed and analysed these local modes. It will be noticed that the stringer displacement in any mode is either flexural or torsional, Lin's work having shown (rather dubiously) that for this class of mode flexural and torsional displacements of any one stringer do not occur simultaneously. For the Caravelle fuselage, the natural frequencies of modes A and C of Figure 3 are approximately 700 cps and 1000 cps respectively.

An intermediate class of mode exists with nodal lines at the frames and with circumferential half-wavelengths greater than the stringer spacing. Flexural and torsional displacements now occur simultaneously on one stringer. Ford (3) has shown that the frequencies of these modes lie between the frequencies of modes A and C of Figure 3.

It is clear that these free modes of vibration and their natural frequencies depend on a large number of structural variables, viz. the skin thickness, the frame and stringer spacings, the stringer flexural and torsional stiffnesses and shear centre location, the frame flexural stiffness, the cylinder radius and effective length. The higher order modes will be influenced considerably by "secondary" variables such as rivet stiffness, cleat stiffness and cross-sectional stiffness of the stringers and frames.

The structure of a tail-plane or elevator consists of a thin skin covering reinforced in the spanwise direction by stringers, and in the chordwise direction by thin plate ribs which join the top and bottom surfaces. The modes of vibration which are significant in acoustic fatigue (4) are of the

form shown in Figure 4, where the section is spanwise along the structure. In the chordwise direction the modes of displacements will be similar to those of Figure 3. The stiffness of the rib relative to the stiffness of the surface skins is obviously one of the most important parameters governing these modes of vibration, typical frequencies of which are shown on the figure.

An elevator structure is basically similar to that of the tailplane, but there will be only one or two spanwise stringers. On the Caravelle tailplane (with one stringer) the 18 S.W.G. skin panels were approximately rectangular, having sides of 5 to 9 in. Their measured natural frequencies were in the region of 230 to 340 cps.

1.3 The Nature of the Excitation

1.3.1 Jet Noise

The pressure fluctuations generated by a jet are essentially random in character, deriving from a random array of moving random sources. These sources originate in the turbulence in the jet as it enters and mixes with the surrounding air. Associated with the turbulence are both hydrodynamic and acoustic pressure fluctuations, the former being predominant in the region of the jet itself and near the jet boundary, and the latter predominating in regions far from the jet (say, seven diameters and more away from it). In the intermediate region the effects of each are comparable.

The randomness of the pressure is such that its continuous frequency spectrum may have appreciable components at frequencies as far apart as 50 and 5000 cps, although the really damaging intensities only occur between 100 and 1000 cps. Typical spectra measured at two points near an Avon jet engine (5) are shown in Figure 5. These show the general feature that the peak in the spectrum is quite broad and moves to lower frequencies as the distance from thejet increases.

The sources of the high frequency components are strongest near the jet orifice, whereas those of the low frequencies are strongest further downstream in the 'mixing region' of the jet. The nature of the acoustic sources is such that the radiated sound is quite strongly directional. The maximum <u>total</u> noise is radiated out from the jet along lines at approximately 35° to the jet axis. The maximum high frequency radiation is along lines inclined at larger angles than this. On account of this directionality only limited regions of the whole aeroplane structure are prone to acoustic fatigue.

The response of the structure to these pressure fluctuations depends not only upon the pressure spectra, but also upon the spatial correlation of the pressure over the surface of the structure. One mode of vibration can be excited to a much greater extent than another simply due to the nature of the variation of the correlation coefficient in space compared with the modal displacement pattern. The actual forms of the correlation spatial distribution will not be discussed here, but the reader is referred to the work of Callaghan, Howes and Coles (6) for jet engine correlation measurements. Clarkson (4) also gives a summary account of correlation measurements.

1.3.2 Boundary Layer Pressure Fluctuations

The normal pressure fluctuations on a surface adjacent to the boundary layer of a high speed flow originate in the hydrodynamic pressure associated with the turbulent velocity fluctuations. The turbulence may be regarded as eddies being convected downstream at a mean speed of about 0.8 times the free stream velocity. As in the jet boundary, these eddies build up to a maximum and then decay as others are formed, and are larger in the thicker boundary layers.

The root mean square value of the normal pressure fluctuations exerted on an aeroplane surface has been found to be approximately 0.6% of the free stream dynamic pressure up to a Mach No. of about 1.2, and is virtually independent of the boundary layer thickness (7). The mean square pressures at the front and rear of an aeroplane fuselage are therefore approximately equal. In db's, the empirical pressure level is

$$40 \log_{10} \frac{U_{EAS}}{100} + 105 \text{ db.}$$

i.e. 143 db at 600 mph and at sea level.

This is not so damaging to the structure as jet noise of the same overall intensity, as the spectrum tends to be flat from low frequencies up to a certain "cut-off frequency", given by

$$f(\text{cps}) = \frac{0.2 \times \text{Free stream velocity}}{\text{Boundary layer displacement thickness}}$$

Beyond this frequency, the spectral level falls off quite steeply. At the rear end of a large aeroplane flying at 600 mph the boundary layer thickness may be 6 in. (the displacement thickness is about 1/10 of this), giving a cut-off frequency of about 7000 cps, rising to 42,000 cps upstream where the thickness is only 1 in. Under these two conditions pressure spectra such as those of Figure 6 are obtained.

Space correlation measurements in full-scale boundary layer pressure fields have not yet been made. Laboratory measurements suggest that a curve of a non-dimensional narrow band space correlation coefficient may be constructed, from which may be obtained the correlation coefficient in any frequency band, and at any speed and separation in the streamwise direction. Some measurements have been summarised and discussed by Bull(7).

1.4 The Nature of the Response of the Structure

A system subjected to randomly varying pressure will respond in a random manner. Although the random pressure may have a flat power spectrum, the response spectrum may be 'peaky', having been modified by the receptance of the system. The peaks in the spectrum occur at the natural frequencies of the system, and the height of each is proportional to the square of the damping of the corresponding natural mode. Now the total mean square response is proportional to the area under the whole response power spectrum. If the

peaks are large, the area under them will form the major part of the total mean square response, which may then be described as 'predominantly resonant'. It is then critically dependent on the damping of the modes.

It will now be shown that some of the responses of the structures of para 1.2 are indeed predominantly resonant, and may therefore be attenuated by increasing the damping. By "responses" are implied such quantities as the fluctuating stress in the structure, the sound levels transmitted through the structure and accelerations at points on the structure, etc., etc.

That structural stresses have the resonant character has been shown conclusively by Clarkson and Ford (8) in their experimental analyses of jet-excited fuselage and tailplane vibrations. Figure 7 and 8 show typical spectra of stresses measured at the centres of a fuselage and tailplane panel respectively. The primary peak of Figure 7 has been shown to be due to the excitation of the stringer torsion mode of Figure 3 in the neighbourhood of its natural frequency. The area under the spectral curve in the vicinity of the peak forms a large proportion of the total area under the curve, and the stress is therefore predominantly resonant. The peak in the tailplane stress spectrum (Figure 9) shows an even stronger resonant effect, the mode of vibration having been identified as that of Figure 4. Similar strongly resonant spectra have been obtained from measurements on elevator panels, tailplane ribs and stringers, and fuselage frames. All emphasise the predominance of the resonant portions in the total spectra.

Another significant feature of Figures 7 and 8 is that the response derives primarily from the excitation of a very few modes. Although this is not always the case, it does have an important bearing on the problem of designing the most effective type of damping treatment, for some treatments give their maximum benefit in certain frequency and wavelength ranges.

Convincing experimental evidence is not yet forthcoming that transmitted boundary layer noise is predominantly resonant. However, the results of several independent theoretical investigations (9, 10, 11) have shown that under all conditions the transmitted noise has pronounced peaks in its spectrum at the resonant frequencies of the plate structures considered. This, in itself, does not indicate that the total mean square noise is predominantly resonant (see Chapter III para. 3.4.2), but under the so-called "coincidence" transmission conditions which can occur at high speeds, the peaks are further magnified relative to the non-resonant portions of the spectrum, and the peaks then dominate the spectrum.

"Coincidence" conditions obtain whenever the convection velocity of the boundary layer pressure fluctuations coincides with the phase velocity of a free flexural wave in the skin plating. A large peak then exists in the spectrum of the generalised force corresponding to that mode, at the modal natural frequency. The vibration amplitude and the sound radiated by the plate in that mode are correspondingly magnified. If the plate is (simply) supported on frames which are 7 in. apart and has a fundamental natural frequency of 600 cps, the lowest necessary convection velocity is only 700 ft. per sec. Coincidence transmission is therefore quite likely to occur in quite slow aeroplanes, although the transmitted noise levels will then

be quite low.

It can be shown that the magnitrde of the peak in the generalised force spectrum depends on the period during which an element of turbulence maintains its identity. i.e. on its "lifetime". The thicker the boundary layer, the longer the lifetime and the smaller is the rate of decay of the correlation. This, in turn, can be shown to imply a greater peak in the force spectrum. The resonant portion of the response therefore increases relative to the non-resonant portion, and the damping of the plate plays an increasing part in limiting the response. In particular, Dyer (9) shows that under coincidence conditions, the mean square noise pressure transmitted by a single mode is inversely proportional to the square of the damping for long lifetimes and high natural frequencies, but only to the first power of the damping for short lifetimes. This serves to show that the effectiveness of the damping may be governed by the correlation characteristics and lifetime of the exciting field, as well as by the other obvious field characteristics and structural properties.

Whereas only a few modes may contribute appreciably to the jet-excited stress spectrum, many modes may contribute to the transmitted noise spectrum. This has been shown by Kraichnan's analysis (11). However, if coincidence transmission is occurring, the most important modes will be those "closest" to the coincidence conditions, and the noise spectrum can be expected to have its maximum value in the corresponding frequency range. The wavelengths and frequencies of these modes will be the significant parameters in the design of an optimum damped structure to attenuate the noise.

In an investigation into the effect of damping treatments on structural fatigue life, it is necessary to know specifically the response quantities on which the fatigue life depends. Acoustic fatigue failures in the skin plating of a structure generally occur as cracks along the line of rivets attaching the skin to the stringers or ribs. The stresses causing these failures are the surface bending stresses in the skin generated by the plate flexural motion, and considerably magnified by local stress concentrations at the rivets. Failure of the rivets themselves also occurs, the heads breaking off under the combined action of the normal plate inertia forces and the normal exciting pressure. Fatigue cracking in stringers and ribs occurs along the intersections of their attachment flanges and webs. The stress causing this is proportional to the local bending moment across the cross-section, which, in turn, is proportional to the bending moment in the skin surface.

Now the fatigue life of a component undergoing random stress fluctuations depends on the statistical properties of the temporal stress variation, including its root-mean-square value. When the stress fluctuations are of the predominantly resonant form involving only one mode of vibration, the waveform may be described as "sinusoidal with a randomly varying amplitude", the magnitudes of the peak values forming a Rayleigh Distribution. The statistical properties of the stress are then completely characterised by the natural frequency and the root-mean-square value. Accordingly, it is sufficient (under the above conditions) to assess the fatigue life knowing only the natural frequency and the r.m.s. value of the stress.

1.5 The Proposed Damping Treatments

Having established that under some conditions the responses of the structure are resonant, and that increasing the damping must therefore be beneficial, we now discuss the particular treatments which can be considered. As stated already, these involve adding to the structural surface a layer of material having a high damping capacity. Structural vibration imposes fluctuating strains upon the layer which dissipates energy and damps the vibration. Treatments may be classified as "unconstrained layers" or as "constrained layers".

An unconstrained layer is initially sprayed or trowelled on to the vibrating member in a wet state and is left with one free, or "unconstrained" surface. On drying out, it becomes quite stiff and when the member bends, the layer undergoes direct bending strain (see Figure 9a) and so dissipates energy. As stiff materials are required for maximum damping, developments for this purpose have led to the use of soft resins (PVC, PVA etc) which have been stiffened by vermiculite or china-clay fillers. The complex Young's Modulus of one such material (Aquaplas) is about $10^6(1 + i\ 0.35)$ lb.in.$^{-2}$ at about 200 cps. When applied to an aluminium plate to a thickness equal to that of the plate, a flexural damping ratio of about 0.12 is obtained (= actual damping of a flexural mode ÷ critical damping).

A constrained layer consists of a damping material sandwiched between two plates. As the plates bend, the layer is constrained to undergo shear strain, by virtue of which energy is dissipated. The "double-skin" configuration consists of outer skins of equal thickness, the interfacial damping layer being anything from 'very thin' to three times the plate thickness. This configuration must be pre-fabricated and built into the structure, ab initio. "Sound damping tape", on the other hand, may be applied to an existing plate structure simply by pressing it on. It consists of a thin, pressure-sensitive, high damping adhesive layer backed by a thin metal foil. It is used extensively in certain airliners for sound insulation.

The essential shearing mechanism of the constrained layer is illustrated in Figures 9b and 9c. For most practical applications a soft material is required for a constrained layer, but there is an optimum layer stiffness for maximum damping.

The advantage possessed by unconstrained layer treatments is that they may readily be used as an emergency measure on existing structures. They may be applied not only to plates but also to stringers and frames to damp their flexural motion. Their disadvantage is that they are usually hygroscopic and the moisture absorbed may promote corrosion fatigue on the light alloy surfaces. The layers are not readily removable for fatigue inspection, and once removed cannot be used again. Constrained layers shown promise of providing much higher damping than unconstrained layers, (flexural damping ratios of 0.50 have been measured) and do not suffer from moisture absorption as the constraining foil or plate is impermeable. Damping tape is readily removable for inspection purposes, and afterwards may be replaced, but it may only be used for damping plate flexural motion. The double-skin configuration is similarly restricted and should require no internal inspection. Its prime requirement is for an extremely strong bond between plates and interface. This is met admirably by the "Hycadamp" sandwich plate which has recently been marketed. The main problem associated with its use is in the attachments

to the reinforcing and stiffening structure. Riveting restricts the essential shearing displacements between the two plates, and so reduces the damping effectiveness. Creep of the damping layer under the compressive stress induced by the rivet may cause the rivet to loosen in time. However, it is claimed that Hycadamp may be bonded to reinforcing members, and with suitable production techniques the above two objections should be over-ruled.

It is important to recognise that the addition of a damping layer to a plate may change the plate flexural stiffness very considerably. A layer of Aquaplas on an aluminium plate doubles the stiffness when the Aquaplas weight is one half of the plate weight. On the other hand, the stiffness of a sandwich plate with a thin soft layer may be only one quarter of that of a solid plate of equal weight. If the layer is thick andstiff, the stiffness of the plate may be several times greater than that of the solid plate.

Reference has been made to the complex Young's Modulus of Aquaplas. It is usual to represent the dynamic (harmonic) moduli of linear damping materials in this form with the notation

$$\text{Young's Modulus} = E^* = E'(1 + i\eta_d) = E' + iE'' ,$$

and

$$\text{Modulus of Rigidity} = G^* = G'(1 + i\beta) = G' + iG'' .$$

E' and G' are known as the "storage moduli", E" and G" as the "loss moduli", and η_d and β as the "loss factors".

Each of the terms E' , G' , η_d and β are frequency dependent, varying in the forms of which figures 10 and 11 are typical. The use of the complex stiffness does not therefore imply that the energy dissipated per given strain cycle (which is proportional to E" or G") is the same for all frequencies.

It will be noticed in figures 10 and 11 that the maximum loss factors occur at frequencies at which the storage modulus is varying most rapidly with respect to frequency. This is an inevitable characteristic which stems from the molecular relaxation mechanisms at the root of the visco-elastic behaviour. The frequency at which the maximum loss factors occur can be adjusted by suitably mixing and compounding different materials. Most materials developed for damping treatments have this peak between 100 cps and 3000 cps, which is in the same region as the peaks in jet-noise spectra. The breadth of the peaks can be adjusted in the same way. In general, however, broadening the peak reduces the maximum loss factor but also reduces the rate of change with frequency of the storage modulus.

The general effect of increasing the temperature of the material is to move its curves of storage moduli and loss factors to higher frequencies, without changing the maximum and minimum values. Decreasing the temperature moves the curves to lower frequencies. As may therefore be expected, the materials with the flattest curves of loss factor vs. frequency, also show the least variation of loss factor and storage modulus with temperature changes. Materials designed to have a broad "temperature bandwidth" therefore have lower damping properties than "narrow bandwidth" materials. Since aeroplane structures have to operate between large extremes of temperature,

the desirability of broad temperature-band materials is obvious.

If the temperature changes are too great, the physical nature of the polymer may change. e.g. dropping the temperature will eventually change it from an amorphous to a crystalline material. The simple lateral translation of the curves is then no longer applicable.

1.6 The Problems of the Present Investigation

The stated purpose of this report is to investigate the benefits accompanying the use of certain damping treatments. Particular attention will be given to the use of Aquaplas and the double-skin damping configuration, with particular reference to their effects on structural stresses. Only limited reference will be made to the effects on sound transmissions. It is further required to determine whether certain "optimum configurations" exist which will minimize the response, "optimum configuration" implying either an optimum thickness or stiffness of the damping material.

The fundamental problem involved is firstly to determine the response of a multi-freedom stiffened structure to the random excitation, and then to determine the dependence of this response on the stiffness, mass and damping of the damped elements of the structure (i.e. of the skin plating, in our case). The damping of the plating, moreover, may be very heavy, introducing problems into the analysis which have not hitherto been significant.

A general theory for calculating the random response has been presented by Powell (12). Here, the response is analysed in terms of the normal modes of vibration of the structure, which must therefore be determined at the outset. The generalised response in each mode is then obtained in terms of the corresponding generalised forces, stiffnesses, masses and damping coefficients.

Consider now the problem of examining the effect on the response of systematically changing, say, the thickness or dynamic properties of a damping layer on (or in) the skin plating. When this change is made, the stiffness and mass of the whole plate are changed. This, in turn, changes the modes of vibration and the corresponding coefficients of stiffness, mass and damping. These coefficients depend in a very complicated way upon the individual stiffnesses and dimensions of the stringers, frames and skin plating. To calculate the total response of one specific structure is a formidable enough computation. To calculate it for a given sub-structure of stringers and frames, but for a range of different damped skin platings is more formidable still. To proceed to investigate the effects of different stringers and frames is out of the question at the present time.

On account of these difficulties, the approach of this report is to consider the damped plate alone, responding in a single mode to a simple random pressure field. Its r.m.s. response must be found in terms of the generalised coefficients, which vary with the different damping treatments and configurations. The response will be compared with that of a plain plate (i.e. with no damping treatment) which has a modal damping ratio equal to that of a typical, real, untreated structure. The effect of replacing this plain plate by the damped plate may then be expressed as a percentage reduction of r.m.s. displacement, stress, transmitted noise, etc.

In representing the skin plating of the real structure by this simple

plate, an idealisation of no mean order is introduced. The approach may be expected to yield estimates of reductions which are approximately correct provided that in the significant modes of the real structure the plate energy is much greater than the energy of the stringers and frames. Whether or not this is satisfied, it can be stated categorically that the reductions found in the simplified approach must be greater than those actually achieved. The reductions found for an optimum configuration of the simplified model will therefore be the greatest possible. They will set an "upper bound" to the effectiveness of the treatment, beyond which no further improvement may be obtained.

For the comparison mentioned above, some typical values are required of the damping ratios of the significant modes of vibration of untreated structures. The sources and nature of this "initial damping" are considered in Chapter II. Some measured and calculated values are also discussed.

In former investigations into the damping of plates, the effectiveness of a damping treatment has always been assessed by the magnitude of the flexural loss factor it produces. (The flexural loss factor is equal to 2 x the damping ratio of a flexural mode). It has been assumed, in effect, that an increase of flexural loss factor means a corresponding reduction in response. Now the responses of randomly excited plates, or of plates excited randomly at resonance, depend not only upon the loss factor but also upon the plate mass and stiffness. Since these latter quantities vary as the damping treatment is changed, it is possible for the changing stiffness (say) to reduce or reinforce the effect of the changing loss factor. The value of the loss factor alone is then no longer a sufficient criterion by which to judge the treatment effectiveness.

On the basis of the "simplified plate approach" to the response calculation, it is possible to derive a new set of criteria for assessing the effectiveness of the damped plate. These take into account the loss factor and a non-dimensional "stiffness ratio" and "mass ratio". Different criteria are required in relation to different response quantities (plate surface stress, plate inertia forces, sound transmitted, etc.) and to random and harmonic excitation. They are developed in Chapter III.

These new criteria are used in Chapter IV to compare the effectiveness of two similar unconstrained layer treatments on a given plate. (The theory of the damping and stiffness of the treated plate is also given in this chapter).

The problem of designing a damped sandwich plate is to determine, for a given weight or stiffness of plate, the ideal damping material and the optimum plate and damping layer thicknesses to minimise the response. In order to do this, it is necessary in the first place to know how the plate stiffness and loss factor depend upon the damping layer thickness and dynamic properties. This is investigated in Chapter V. Also considered is the dependence of the plate surface bending stresses on these quantities, when the plate is

deformed in a given mode. Using these plate characteristics in conjunction with the criteria of Chapter III, the optimum material properties and thickness are found which minimise the response of a plate of given size. The responses of these 'optimised' plates are to be compared with those of untreated plates.

Experimental verification is required for the sandwich plate theory developed. Firstly, a comparison is required between the theoretical values of plate stiffness and loss factor, and values measured in harmonic tests. The measurement of these quantities presents problems which are fully discussed in Chapter VI and which (it is believed) have been overcome by the development of suitable apparatus and testing technique. The apparatus has also been used to measure the damping and stiffness of some commercial sandwich samples. It is shown in Chapter VI how these measured results can be used to compare the effectiveness of each commercial treatment as an aeroplane structural element.

When the damping of a plate is increased to high values (of the order of 10% of critical, or more), the random inertia forces due to the plate motion are no longer very much greater than the random external force exciting the plate. There now exists a significant correlation between the exciting force and the inertia force which is negligible when the damping is light. These features must be included in the analysis of the loads on the supports of a randomly-vibrating, heavily-damped plate. Chapter VII contains the analysis for a damped beam, subject to a non-normal loading.

In this random theory, the concept of the complex stiffness is used assuming its usual frequency-independent character. It is assumed, in effect, that the complex stiffness at the resonant frequency of the system is applicable throughout the frequency range, whereas we know that in fact it varies very considerably. Further, it is assumed that the damping and stiffness measured under harmonic conditions may be used to compute the response under random conditions. The legitimacy of each of these assumptions and the validity of the random theory have been examined experimentally by exciting the same sandwich specimens as before with a randomly varying force. This experiment is described in Chapter VIII.

Chapter II

The Damping of Untreated Structures

II.1 The Sources of the Damping

In this chapter we consider the sources and nature of the damping of untreated structures. This is done in order to understand the significance and magnitudes of some values of damping measured on full-scale and model structures. These values are required in subsequent estimates of the effects of damping treatments.

The sources of the damping of the structural vibration are:

(a) the internal damping of the structural material
(b) the damping of the structural joints
(c) the acoustic radiation from the vibrating surface.

The internal damping capacity of conventional light alloys used in aeroplane structures is very low. At a cyclic stress amplitude of 2000 lb in^{-2}, the cyclic energy dissipation is only 0.1% of the elastic energy at the maximum strain. This increases to about 0.3% at 5000 lb in^{-2}. These rates of energy dissipation cannot contribute more than $\frac{1}{4\pi} \times 0.001$ or $\frac{1}{4\pi} \times 0.003$ to the damping ratio of a structure vibrating with the respective maximum stress amplitude. Measured values of structural damping are orders of magnitude greater than these. Material damping is therefore insignificant by comparison with the other sources, which will now be discussed in greater detail.

II.2 The Damping of Structural Joints

When a structure vibrates in the modes described in Chapter I a number of different and complicated loading actions are imposed upon the riveted joints which exist between the skin plating and the stringers, between the skin and the frames. For example, when a stringer-skin combination bends (as in Figure 3C) the joining rivets undergo a shearing action, arising from the usual shear stresses in a beam. In addition, they undergo a tensile-compressive action perpendicular to the plate surface, arising from the normal plate inertia forces. When the same combination twists (as in Figure 3a) a bending moment or a tensile-compressive loading is applied. The loading actions on the stringer-frame joint are considerably more complicated, consisting of both twisting moments and bending moments, together with shearing and tensile loads. Energy is dissipated at the joints under each of these loading actions.

The mechanism of the dissipation under shear loading is fairly well understood and has been described elsewhere by the author (13). The mechanisms under the other loading actions have not yet been investigated, but the predominant part must be played by slipping and plasticity of the contacting surfaces. The non-linearity of these processes makes it extremely difficult to study the combined effect of different loading actions applied simultaneously.

The damping of shear loaded riveted joints has been investigated experimentally by the author (13). Tests were carried out on $\frac{1}{8}$ in. diameter countersunk rivets joining an 18 S.W.G. joint plate to a 20 S.W.G. Alclad

stringer (see Figure 12). Flexural vibration of the stringer at about 150 cps imposed the oscillating shear load on the joint. Measurements were made of the energy input required to maintain steady vibration of the beam over a wide range of amplitudes. Making due allowance for energy dissipation in various "extraneous" sources, the dissipation at the joint was determined. Its variation with load amplitude is shown by Curve I of Figure 13, where the actual dissipation per cycle has been divided by the square of the joint load amplitude. We shall call this quantity the "energy dissipation coefficient". If the damping mechanism at the joint followed a simple linear viscous or hysteretic law, then the dissipated energy would be proportional to the square of the load. A horizontal straight line would be obtained in Figure 13. It is seen, therefore, that the joint damping mechanism does behave in a sensibly linear manner up to a load amplitude of about one pound in which load region relative slipping of the joint plates probably begins. Thereafter the damping increases more rapidly with load amplitude. Analysis of the rising part of the curve suggests that the cyclic dissipation is proportional (approximately) to the cube of the load amplitude. The increase may be attributed to an increasing annular area over which slip is occurring.

In the early part of the experiment difficulty was found in obtaining a smooth curve over the rising portion, and this was traced to the fact that the dissipation was decreasing quite rapidly with time. This time variation is shown in Figure 14, each section of the curve showing the change of energy dissipation while the joint load amplitude was maintained at a constant value. The experiment was conducted in the sequence indicated, different constant amplitude levels being interspersed with zero-load "rest-periods". The significant features of this curve are

(a) the very rapid drop of energy dissipation with time immediately after the application of a new high load level

(b) the tendency for the dissipation curve to flatten out after a long period of steady loading, and then (it is believed) to approach a constant value.

After this test involving prolonged loading, the dissipation was again measured over the whole range of loads previously covered. Curve II of Figure 13 was then obtained. Comparison with curve I (which is that of the first test, before prolonged loading) indicates that the effect of prolonged loading was effectively to shift the whole curve to the right, i.e. to delay the load at which the slipping process began. The high values of dissipation at large load amplitudes have been reduced, whereas the low value at low loads has remained almost constant and now extends to rather higher load levels.

An explanation for this phenomenon can be found in the inter-surface detericration which occurs when slip takes place. In the slipping process, a welding and tearing action proceeds on the rubbing surfaces. This causes oxidation of the rubbing surfaces (visible to the naked eye after the experiment) and a reduction of the coefficient of friction. At the same time, oxide deposits around the rivet shank increase the degree of fixity of the rivet in its hole, and so increase the stiffness of the joint. These two effects together result in decreased dissipation for a given load amplitude.

The energy dissipation due to a slipping process is obviously

dependent upon the normal pressure between the two surfaces. In riveted joints, this normal pressure is likely to vary considerably from one joint to another. Considerable variation might be expected, therefore, between the measured energy dissipation coefficients of nominally identical joints. This has been investigated by testing a number of jointed beams of identical design to that already considered. Figure 15 shows the variation of the joint energy dissipation coefficients obtained from each of three beams, after they had been subjected to prolonged loading. Over the low load range, the dissipation coefficients are surprisingly close in value. The 'critical' loads at which the values begin to rise are of the same order, and by shifting any curve either to the left or right it may quite accurately be superimposed upon another of the curves. Reproducibility of the energy dissipation of these riveted joints therefore appears to be possible over the lower load range, but differences occur in the loads at which the rise begins.

From these results, some general prognostications may be made in relation to the joint damping of reinforced plate structures:

(a) Harmonic tests at low vibration amplitudes should indicate that the damping is sensibly linear.

(b) As the vibration amplitude increases each of the many joints involved will enter the slipping condition, one after the other. No simple general rule may be deduced to represent the associated increase of damping. This must depend on the relative magnitudes of the loads on the different joints, and on the critical slip loads.

(c) At high vibration amplitudes the damping may decrease with time. This is of serious importance when a constant high-level excitation source is vibrating the structure (e.g. a jet-noise field), as the vibration amplitude will then increase with time.

(d) At low amplitudes, nominally identical structures should have closely similar values of damping ratio for a given mode. At high amplitudes the damping may vary from structure to structure. However, these variations may not be as great (in proportion) as the differences between the dissipation coefficients of similar single joints at high load levels. The presence of many joints in the structure may effectively 'average-out' the effect of these differences.

Acoustic Damping

II.3 Acoustic Damping of Single Panels and Local Modes

In order to understand the nature of the acoustic damping of the local modes of Chapter I, it is convenient first of all to study the acoustic radiation from a single vibrating plate situated in an otherwise rigid, infinite, plane baffle. This plate may be regarded as representing the section of skin plating bounded by two adjacent stringers and frames. Consideration of a plane rather than a cylindrical baffle makes little quantitative difference to the results, so long as the acoustic wavelengths involved are not much greater than the cylinder diameter. The greater part of this theory of acoustic damping was formerly presented by the author in Reference 13.

Each element, dxdy, of the vibrating surface may be considered as an elemental piston vibrating with the local harmonic velocity of the plate, $u_o e^{i\omega t}$. This piston radiates a pressure wave of wavelength λ_a into the surrounding medium of density ρ. At a point distant r from the piston the instantaneous pressure is known from classical acoustic theory to be

$$dp = -\frac{i\rho\omega}{2\pi r} u_o e^{i\omega t} \cdot e^{i2\pi r/\lambda_a} dx dy . \qquad \ldots(2.1)$$

This has components in phase with, and in quadrature with the piston velocity. Another piston, at the distance r from the first and vibrating in phase with it, is subjected to both of these components. The existence of the in-phase component means that the piston has to do work in moving against it, and this then constitutes the damping "mechanism". The existence of the quadrature component stems from the inertia reaction on the piston from the medium, and this gives rise to the "virtual inertia" of the medium, as seen by the vibrating plate.

Extracting the real (in-phase) part of the pressure from Equation 2.1, and replacing the local piston velocity $u_o e^{i\omega t}$ by $\dot{w}$ (it being assumed that the velocity variation is harmonic), the elemental <u>damping</u> pressure is found to be

$$dp = \rho c \frac{2\pi}{\lambda_a^2} \frac{\sin(2\pi r/\lambda_a)}{2\pi r/\lambda_a} \dot{w}\, dx dy \qquad \ldots(2.2)$$

where c is the speed of sound in the medium. The function $\sin(2\pi r/\lambda_a) \div (2\pi r/\lambda_a)$, which represents the variation of pressure with the distance r, behaves in a familiar way, being unity when $r = 0$, zero when $r = \lambda_a/2$, and thereafter oscillating and decaying quite rapidly.

The <u>total</u> damping pressure at the second piston due to all the other elemental pistons is therefore

$$\rho c \frac{2\pi}{\lambda_a^2} \iint_A \frac{\sin(2\pi r/\lambda_a)}{2\pi r/\lambda_a} \cdot \dot{w}\, dx dy \qquad \ldots(2.3)$$

where the integration extends over the whole vibrating surface, r being the distance from the second piston to all the other elements. This is the damping pressure on <u>one</u> side of the plate. If the plate can radiate freely from both sides, the total effective damping pressure will be twice this. In aeroplane structures, it is probably more accurate to assume free radiation from the outside surface only, and the remaining work proceeds on this assumption.

$\dot{w}$ may be written in the form $\dot{q}\, f(x, y)$, where $\dot{q}$ is the generalised velocity of the plate vibrating in the mode $f(x, y)$. Using this in Equation 2.3, and forming the Rayleigh Dissipation Function, the generalised damping coefficient corresponding to $\dot{q}$ is found to be

$$b_{ac} = \rho c \frac{2\pi}{\lambda_a^2} \iint_A f(x,y) \iint_A \frac{\sin(2\pi r/\lambda_a)}{2\pi r/\lambda_a} f(x,y)\, dx dy\, dx dy \ldots(2.4)$$

Inspection of this double integral shows that the greater part of its value must derive from that region of the plate over which the displacement, $f(x, y)$, has its greatest magnitudes. For most practical aircraft plate sizes and natural frequencies the wavelength λ_a will be much greater than the longest dimension of this region. From this it follows that a fair approximation to the integral (2.4) may be obtained by putting

$$\frac{\sin(2\pi r/\lambda_a)}{2\pi r/\lambda_a} = 1$$

Hence

$$b_{ac} \doteq \rho c \frac{2\pi}{\lambda_a^2}\left[\iint_A f(x,y)\,dx\,dy\right]^2$$

or, putting $\lambda_a = 2\pi c/\omega$,

$$b_{ac} \doteq \frac{\rho}{c}\frac{\omega^2}{2\pi}\left[\iint_A f(x,y)\,dx\,dy\right]^2 . \qquad \ldots(2.5)$$

This shows that at low frequencies (i.e. large acoustic wavelengths) the damping coefficient is proportional to the square of the frequency.

At very high frequencies (very small acoustic wavelengths) classical acoustic theory shows that the local damping pressure on a vibrating surface is ρc x the local normal velocity,

i.e. $\rho c\, f(x,y)\, q$.

The generalised damping coefficient is then found to be

$$\rho c \iint_A f^2(x,y)\,dx\,dy . \qquad \ldots(2.6)$$

which is independent of frequency.

From these damping coefficients we may obtain the damping ratios corresponding to the natural frequency of the plate, ω_n i.e. (b_{ac} at ω_n) ÷ critical damping coefficient. The critical generalised damping coefficient of the plate is given by

2 x natural frequency x generalised mass

$$= 2\omega_n \iint_A \mu f^2(x,y)\,dx\,dy$$

where μ is the local plate mass per unit area, and will be taken to be constant over the plate. The damping ratios for low and high natural frequencies are then

$$\delta_{ac} = \frac{\rho}{c}\cdot\frac{1}{4\pi}\cdot\frac{\omega_n}{\mu}\,\frac{\left\{\iint_A f(x,y)\,dx\,dy\right\}^2}{\left\{\iint_A f^2(x,y)\,dx\,dy\right\}^2} \qquad \ldots(2.7)$$

for low frequencies, and

$$\delta_{ac} = \rho c / 2\omega_n \mu \qquad \ldots(2.8)$$

for high frequencies.

At low frequencies, the damping ratio therefore depends on the mode in which the plate vibrates, but this is not so at high frequencies.

If the plate is rectangular, simply supported and vibrates in its fundamental mode ($f(x,y) = \sin \pi x/a \,.\, \sin \pi y/b$), the integrals in Equation 2.7 may be evaluated.

The natural frequency of the plate in this mode is known to be

$$\omega_n = 2\pi\,(t/b^2)\,0.477\,(E_m/\rho_m)^{1/2}\,(1 + 1/n^2)\ ,$$

where E_m is the plate Young's Modulus, ρ_m is the density, t is the thickness and n is the length breadth ratio, a/b. In deriving the constant factor in this expression, Poisson's Ratio was taken to be 0.3. The damping ratio of the plate is then found to be

$$\delta_{ac} = (0.156/c)(\rho/\rho_m)(E_m/\rho_m)^{1/2}(n + 1/n)\ . \qquad \ldots(2.9)$$

For a given plate material and mode of vibration, the acoustic damping ratio is seen to be dependent only upon the air density, the sound velocity and the length : breadth ratio of the plate, provided the plate is not so long as to invalidate the long-acoustic-wavelength assumption.

If the rectangular plate is fully fixed along all four edges, we may obtain an order of magnitude expression for δ_{ac} by assuming $f(x, y) = [\cos(2\pi x/a) - 1]\,[\cos(2\pi y/b) - 1]$. This gives

$$\omega_n = 2\pi\,(t/b^2)\,1.098\,(E_m/\rho_m)^{1/2}(1 + 2/3n^2 + 1/n^4)^{1/2}.$$

(The accurate value involves the constant 1.07 instead of 1.098). The damping ratio is now found to be

$$\delta_{ac} = (0.245/c)(\rho/\rho_m)(E_m/\rho_m)^{1/2}(1 + 2/3n^2 + 1/n^4)^{1/2} \ldots(2.10)$$

Figure 18 shows δ_{ac} plotted against n for an aluminium plate with each of the edge conditions considered. A length : breadth ratio of three is typical of fuselage panels; such a panel on its own may be expected therefore to have an acoustic damping ratio of about 0.004 or 0.005, depending on the edge support.

When allowance is made for the decay of the pressure amplitude with increasing distance from an elemental piston (i.e. including the $\sin(2\pi r/\lambda_a)/(2\pi r/\lambda_a)$ term correctly) the integral of Equation 2.4 can only be evaluated numerically. The acoustic damping pressure over the panel must then be less than that assumed in the above theory, and the damping ratios will therefore be less. This effect will increase with increasing length of plate, i.e. with n. Such a numerical evaluation has been carried out by Maggiarotty (14) under the author's direction. For the special case of an aluminium plate, 5 in. wide and 0.048 in. thick, the damping ratios are presented as points on Figure 16, showing the reduction due to the decaying (or "non-uniform") pressure.

We can now consider qualitatively the acoustic damping of a mode which involves two or more adjacent panels, separated by a flexurally stiff longitudinal stringer. Firstly, suppose that the panels are vibrating in phase with one another in 'fixed-sided' modes (similar to the type C modes of Figure 3). There will be a damping pressure on each panel due to the adjacent panels. If the panel width is small compared with the sound wavelength, and there are two such adjacent panels, the damping pressure will be nearly twice that of a single panel. Likewise, the damping pressure on three narrow, adjacent panels will be nearly three times that of the single panel. The acoustic damping ratio of this mode is therefore likely to be of the order of 0.015.

If the panels are separated by a torsionally flexible stringer, and each vibrates in a 'simply-supported' mode in anti-phase with its neighbouring panels, the damping pressure from one panel will tend to cancel out the pressure on its neighbour, and vice-versa. The acoustic damping of such modes is likely to be negligibly small. Local modes of type A (Figure 3) will therefore have negligible acoustic damping.

If there is a row of several adjacent similar fixed-sided panels, a rough estimate of the acoustic damping may be made assuming the existence of an infinite line of panels. Suppose the radiated sound wavelength is greater than several panel widths. The damping pressure at the centre of the rth panel due to vibration of the sth panel in the mode $q_s f_s(x, y)$ is given approximately by

$$\rho c \frac{2\pi}{\lambda_a^2} \frac{\sin 2\pi(r_r - r_s)/\lambda_a}{2\pi(r_r - r_s)/\lambda_a} \dot{q} \iint_A f_s(x.y)\, dx\, dy$$

(from Equation 2.3), where $r_r - r_s$ is the distance between the centres of panels r and s. If all the panels vibrate in the same mode and with the same amplitude, the total pressure at the centre of the rth panel will be

The summation extends over all the panels.

The damping coefficient will now be calculated assuming that the pressure at all points on any panel is equal to that at the panel centre. We first find an approximate value for the infinite sum, using the integral

$$\int_0^{\infty} \frac{\sin x}{x}\, dx = \frac{\pi}{2}$$

If the panel width is b, this gives

$$\sum_{s=-\infty}^{s=+\infty} \frac{\sin 2\pi (r_r - r_s)/\lambda_a}{2\pi (r_r - r_s)/\lambda_2} \doteqdot \frac{\lambda_2}{2b}$$

and the damping pressure becomes

$$\dot{q}_s\ \rho c \frac{\pi}{\lambda_2 b} \iint_A f_s(x,y)\, dx\, dy$$

The contribution from any panel to the generalised damping coefficient of the whole system is then

$$\rho c \frac{\pi}{\lambda_a b} \left[\iint_A f_s(x,y)\, dx\, dy \right]^2$$

which is λ_a/b times the damping coefficient of a single isolated panel. The damping ratio of the whole system will then be approximately λ_a/b times that of the single panel.

For the Caravelle fuselage, the frequency of the type C modes was approximately 1000 cps ($\lambda_a = 13$ in.), the panel width was about $3\frac{1}{2}$ in. and the length : breadth ratio was 2 . The acoustic damping ratio would therefore be of the order of $(13/3.5) \times 0.004 = 0.015$, if the stringers did not bend or contribute appreciably to the potential energy of the vibration. That they do in fact contribute inevitably means that the value of δ_{ac} calculated above is an <u>over</u>-estimate.

If a second long row of panels exists alongside the first, cancellation of the damping must occur if they vibrate in counter-phase with the first. Reinforcement of the damping must occur if they vibrate in phase with the first. The Caravelle tests gave no indication of any phase-relationships (correlation) across frames, and it was concluded that each row of panels (between frames) was vibrating independently. No reinforcement or cancellation would then occur.

II.4 The Damping of Model Structures

This section reviews some values of the damping of model structures measured by the author and others. The modes represented small sections of a fuselage structure and consisted of stringers, frames and skin plating of normal dimensions, riveted together with standard sized rivets and by standard techniques.

In the first investigation (by the author, with Froud (13)) a top-hat section stringer was tested which had a narrow 18 S.W.G. plate riveted to its flanges (see Figure 17). The rivets were identical to those of para II.2. The stringer was excited in its fundamental bending mode, subjecting the rivets to shear loads together with small normal loads. Values of the "equivalent linear damping ratio" (as defined in reference 15) were measured over a range of beam amplitudes. At the highest amplitude, when the greatest rivet shear load was about 7 lb., the damping ratio of the whole beam was only 0.00025. This is about twice that expected from the material damping. The contribution of the rivet damping to this total was calculated using the method proposed by the author (16), incorporating the rivet damping properties measured on single joints. The rivet contribution came to only 2% of the measured total! A greater contribution would be made if the beam was shorter or if only one line of rivets attached the plate to the stringer. Even under these conditions, the contribution of the stringer-skin rivets to the total damping ratio will still be a very small proportion of the total damping. Damping ratios of the order of 0.004 and more have been measured for "local" modes of larger models (see later paragraphs). We may reasonably conclude, therefore, that the shearing of the stringer-skin rivets does not contribute appreciably to the damping of these modes.

As one part of another project, Mercer(17) under the author's direction, measured the damping of some local modes of a plate which was reinforced by two frames along its long edges (see Figure 18) and by seven equi-spaced stringers across its width. Each panel so formed was 6.75 in. wide, 13.5 in. long and 0.028 in. thick. Attachment rivets were at 1.5 in. pitch. The structure was excited harmonically, using light exciter coils at each panel centre. Modes of Type A (stringer torsion modes of Figure 3) had damping ratios of about 0.006 to 0.007 . These were the same when the model was in free air or in vacuo. i.e. acoustic damping was negligible. Modes of Type C (stringer bending modes of Figure 3) had damping ratios of 0.01 to 0.011, and these were slightly smaller in vacuo than in free air. Acoustic damping would not be large for this model as it was "unbaffled", and pressure cancellation could occur from one side of the model to the other. It is noteworthy that the stringer bending mode had a larger damping ratio than the torsion mode.

A very significant feature of this experiment was that the frequency-response curve from the strain at a panel centre showed groups of peaks centred on the natural frequencies of the Type A and Type C modes. Some of these peaks must correspond with modes in the 'intermediate' class, mentioned in Chapter I, para 1.2, but more peaks existed than could be accounted for in this way. The dominant Type A mode for one specimen occurred at a frequency of 148 cps, but two strong peaks also occurred at 144 cps and 142 cps. A cursory examination indicated that the modes at these frequencies were similar in form to the Type A mode. (They cannot, of course, be 'too' similar without violating the orthogonality condition). The

signifance of this feature will appear in para II.5.

Ford and Clarkson (18) have studied the local modes of a curved reinforced structure measuring 6 ft. by 4 ft. The stringer and frame spacings were 4.5 in. and 9 in. respectively. The skin thickness was 0.028 in. and the rivet pitch was 1 in. The structure was excited harmonically using plane sound waves from a loudspeaker. Strain gauges measured the strain response at the centres of ten adjacent panels between the middle two frames. In the course of the investigation, the following damping ratios were measured from 'vector plots' of the response:

	Frequency c.p.s.	Mode	Damping Ratio
(i)	310	Stringer Torsion, Fig. 3a	0.0046
(ii)	341	Every fourth stringer bending, Others bending and twisting. Fig. 19a	0.0034
(iii)	354	Every third stringer bending, Others twisting and bending. Fig. 19b	0.0036
(iv)	384	Every other stringer bending, Others twisting. Fig. 19c	0.005
(v)	396	Similar to (iv) Fig. 19d	0.0047
(vi)	600	Stringer bending. Fig. 3c	0.008

A full discussion of these results is not possible since very little is really known about the modes of vibration. The modes drawn in Figure 19 were deduced entirely from the measured bending strains at panel centres, so the ratios of stringer displacements to panel centre displacements were not known. Further, the extent to which adjacent rows of panels were participating (a factor on which the acoustic damping depends) was also not known. It may be observed, however, that the damping of the stringer bending mode is again appreciably greater than that of the stringer torsion mode. Also, the damping ratios of modes (ii), (iii), (iv) and (vi) increase progressively as more stringers appear to undergo pure bending loads. This increase could be attributed to a progressive increase in one (or more) particular loading action, e.g. the shear load on the stringer-frame joint, or the normal load on the stringer-skin joint. It is unlikely to be attributable to increasing shear loads on the stringer-skin joints, as this loading action has been shown to make an insignificant contribution to the damping. Inspection of the modes of displacement suggests that acoustic damping should not be significant except in the stringer bending mode at 600 cps. In the absence of information regarding the motion of adjacent rows of panels, no further comment may be made on this point.

II.5 The Damping of Actual Aeroplane Structures

The only damping data relating to actual structures are three values obtained by Clarkson and Ford in their Caravelle and Comet investigations (8). The measurements were made from the random signals from strain gauges on various panel centres as the structure vibrated in a jet-noise field.

The method of measurement depends on the following property of the random response of a single degree of freedom system. If the random exciting force has a flat spectrum in the neighbourhood of the system natural frequency, the auto-correlation function of the response forms a damped cosine curve when plotted against the time delay. The rate of decay of this curve, with respect to time delay, is the same as that of the free damped vibration of the system with respect to real time.

Accordingly, the random strain gauge signals were filtered through a $\frac{1}{3}$ octave band filter centred on the natural frequency of the stringer torsion mode of the structure. This filtering was intended to isolate the response of one mode only. The filtered signal was then auto-correlated and the decay of the auto-correlation curve was measured. The damping ratios derived are shown below:

Location of Panel	Panel Size	Frequency c.p.s.	Damping Ratio
Caravelle Rear Fuselage	7 in. between frames 3.5 in. between stringers	600	0.016
Caravelle Elevator	7 in. stringer to edge 5.6 in. between ribs	300	0.020
Comet Tailplane	11 in. between ribs 6 in. between stringers	400	0.014

These values are considerably greater than anything measured on laboratory specimens. Two reasons may be offered for this:

(i) Shielded leads to the strain gauges were taped or glued to the panels and stringers concerned. This could increase the damping very considerably.

(ii) There is good reason to believe that the filtering did not, in fact, isolate a single mode, but that more than one structural resonance was contained within the frequency band of the filter. Mercer, it will be recalled, found a group of resonant frequencies centred on the stringer torsion frequency, and this could be true of the actual aeroplane structures. The auto-correlation technique used to measure the damping is unable to differentiate between the damping of a single mode and the total damping of two (or more) 'close' modes contained within the filter bandwidth. e.g. the damping ratio 0.016 could imply the existence of two modes, equally excited, with damping ratios of approximately 0.008.

The resolving power of the technique therefore needs to be much improved before the results of such damping measurements can be treated with much confidence. Care must also be taken to ensure that the measuring equipment does not add to the structural damping.

II.6 Concluding Remarks on the Damping of Untreated Structures

Experiments on single joints indicate that the damping of nominally identical structures at low amplitude levels should be sensibly linear and substantially the same from one structure to another. At high amplitudes, non-linearity and time dependence of the damping is to be expected.

Acoustic radiation appears to be capable of developing damping ratios of 0.016 or more for stringer bending modes, but such highly damped modes have not yet been isolated in model work. The magnitude of the acoustic damping depends critically upon the phase-relationship between the motion of adjacent panels or rows of panels. Reinforcement or cancellation of the acoustic damping may occur, depending on whether adjacent panels (or rows) are in-phase or out-of-phase. The acoustic damping of stringer torsion modes should be negligible.

Measured values of the damping of model structures have not been obtained in systematic damping studies, so few general conclusions are warranted. It appears, however, from the work of both Mercer and Ford that stringer bending modes have higher damping than stringer torsion modes. The principal source of the bending mode damping is thought to be in the stringer-frame joint. Mercer's small model with large panels had damping ratios of 0.011 and 0.006 respectively for the two modes, whereas Ford's large model with small panels had damping ratios of 0.008 and 0.005.

Damping ratios measured on actual aeroplane structures were in the region of 0.014 to 0.020. Confidence cannot yet be placed in these results, owing to deficiencies in the resolving power of the measuring technique and also to the possible presence of extraneous damping sources in the experiments.

In subsequent calculations in which are required some values of the damping of untreated structures, we shall therefore take 0.005 as representing the lowest values and 0.0125 for the highest values. There is obviously a considerable degree of arbitrariness about the latter figure.

Chapter III

Criteria for Comparing the Effectiveness of Damping Treatments

III.1 The Need for Criteria

It has been common practice for many years to specify the effectiveness of a damping treatment by the amount by which it increases the loss factor of the system to which it is added. This practice stemmed from early unconstrained layer treatments being soft and adding little to the stiffness of the steel plates to which they were applied. The treatment giving the greatest loss factor increase would also give the greatest attenuation of response, and the efficiency of the treatment could be judged by the "loss factor per given weight of treatment". Now that damping treatments are being used on light, aluminium structures, a reconsideration of this criterion is necessary, since the incorporation of modern treatments changes the system stiffness quite considerably.

Acoustically excited vibration, the associated stresses and the transmitted noise, together with numerous other response quantities depend in different ways upon the damping, stiffness and mass of the system. Some of the quantities increase with increasing stiffness, whereas others decrease. Since the effectiveness of a damping treatment must ultimately be judged by its effect upon the response, it is evident that the loss factor increment alone is an insufficient criterion by which to judge. Furthermore, different criteria are required when considering different response quantities.

In this chapter criteria are derived which provide a basis for comparing the effects of different treatments on a number of response quantities. Expressions are first derived (or quoted) for various response quantities of simple linear systems in terms of the mass, stiffness and damping of the systems. Both random and harmonic excitations are considered. From these expressions the "criteria" are deduced. For the systems under harmonic excitation the derived expressions relate to resonant conditions, and a comparison is sought between their magnitudes before and after the damping treatment is added.

It must be recognised that, in general, the damping treatment will change the resonant frequency of the system. If the frequency of the harmonic exciting force does not change, then a system initially at resonance will be "de-tuned" and the resultant attenuation of the response will not necessarily be due to the damping of the treatment. However, in most systems to which damping treatments are likely to be applied the frequency of excitation changes with changes of operating conditions, and there is bound to be some operating condition, at which resonance of the treated system will occur. The response at this new condition should therefore be compared with the response at the untreated resonant condition, under the assumption that the amplitude of the exciting force is the same at both frequencies. This is, in effect, what is done in section III.2 of this chapter, where consideration is given to the amplitudes of harmonic displacement, velocity acceleration, inertia force and the surface bending stresses of a vibrating. In all cases, the response in one mode of vibration only is considered, it being further assumed that the damping treatment does not change the mode.

Section III.3 considers damping treatments in relation to harmonic

sound transmission through simple structures. Once again, resonant conditions are assumed to pertain both before and after the treatment is applied, it being assumed that changing the operating conditions can always restore the system to a resonant state. Coincidence transmission through plates of infinite length is also considered, the change in the operating conditions required to restore coincidence after the treatment has been added being explained in the text.

In section III.4 random excitation of the system is considered and further criteria relating to displacement, acceleration, inertia force and bending stress are investigated. Here there is no need to consider changing operating conditions when the treatment is added to the system. The only assumption that is necessary is that the power spectral density of the existing force is the same at the resonant frequencies of both the untreated and treated systems, and, furthermore, does not vary appreciably in the region of the resonant frequencies. Finally, this section deals with the effect of a damping treatment upon the sound pressure transmitted through two simple plate structures subjected to random pressure fluctuations.

III.2 Criteria Applicable to Harmonic Vibrations

III.2.1 Characteristics of the Mechanical System

Here we consider the effect of a damping treatment on the response of a system vibrating in a single natural mode of vibration under the action of a harmonic exciting force. Before the damping treatment is added, the generalised mass and stiffness of the system are M and K respectively. Suppose also that there exists a viscous damping mechanism, giving a generalised damping coefficient C. Denoting the exciting force by $P.e^{i\omega t}$ the equation of motion of the system (in terms of the generalised displacement, q) is

$$M\ddot{q} + C\dot{q} + Kq = P e^{i\omega t} \qquad \ldots(3.1)$$

The damping treatment increases the mass and stiffness coefficients to $M\theta$ and $KR(1 + i\eta)$ respectively. If the vibrating system is a uniform flat plate attached to a rigid structure, and the damping treatment is in the form of a uniform layer over the plate, then θ is the factor by which the treatment increases the mass per unit area, and R is the factor by which it increases the flexural stiffness of the plate. The equation of motion after treatment is therefore

$$M\theta\ddot{q} + C\dot{q} + KR(1+i\eta) = P e^{i\omega t} \qquad \ldots(3.2)$$

III.2.2 The Effect of the Treatment on the Resonant Displacement Amplitude

Provided the initial damping (represented by C) is small compared with the added damping, the maximum amplitude of q (denoted by $\bar{q}_{max}$) occurs at the frequency

$$\omega_n = (KR/M\theta)^{1/2} \qquad \ldots(3.3)$$

Then $$\bar{q}_{max} \doteq P/(C\omega_n + KR\eta) \doteq P/KR\eta \qquad \ldots(3.4)$$

Now the maximum displacement of the system in its untreated condition can be expressed in the form $P/K\eta_i$ where η_i is twice the damping ratio (C/C_{crit}) corresponding to the initial damping. The effect of the damping treatment has therefore been to divide the initial resonant displacement amplitude by $K\eta/\eta_i$. The effectiveness, and hence the efficiency, of a treatment used to attenuate vibration displacements is evidently measured by the value of the product $K\eta$. In general, for unconstrained layers, this product increases monotonically with the quantity of treatment added, whereas η approaches an asymptotic value. $K K\eta$ is of course a true measure of the damping added to the system, whereas η is a function of the damping and stiffness. The criterion by which different treatments should be judged when used to attenuate harmonic vibration displacements is therefore the value of $K\eta$ per unit weight of treatment. Similarly, when the effect of increasing the amount of a given treatment is considered, the values of $K\eta$ for the different amounts should be compared. The value of η itself is an insufficient criterion.

III.2.3 The Effect of the Treatment on the Surface Bending Stresses of a Vibrating Plate

The effect of small thicknesses of unconstrained layer treatments on plate bending stresses is virtually the same as the effect on the displacement amplitude. However, the surface stress is proportional to the product of the amplitude of curvature and the distance between the surface and the effective neutral surface of the section, and with large thicknesses this distance may be up to five times that for the untreated plate. Suppose this distance before treatment is y, and after treatment is αy. Since the amplitude of the oscillating curvature is proportional to the displacement amplitude, the surface stress in the untreated state is proportional to $yP/K\eta_i$, and in the treated state to $\alpha yP/KK\eta$. The final stress is therefore equal to the initial stress divided by $K\eta\alpha^{-1}/\eta_i$.

With sandwich plates, the concept of neutral surfaces no longer holds. Suppose now that the surface stress at a point on the untreated plate is σ_u when deformed in a given mode of normal displacement by a given amount. When the sandwich plate is deformed in the same way and by the same amount, the surface stress will be $\alpha_s \sigma_u$, say. (α_s may have values between $\frac{1}{4}$ and 3), Under the harmonic excitation previously assumed, the ratio of the oscillating stresses is evidently $1 : \eta_i/K\eta\alpha_s^{-1}$.

In each case, the factor $K\eta\alpha^{-1}$ represents the effect of the damping treatment, the larger it is the smaller being the bending stress. $K\eta\alpha^{-1}$ is then the criterion by which different treatments should be judged when considering their effects upon surface bending stresses due to harmonic vibration at resonance. We shall call α the "stress ratio". For plates treated with unconstrained layers the above definitions turn out to be the same, so the suffix 's' is not, in fact, required.

III.2.4 The Effect on the Resonant Velocity Amplitude

The amplitude of the generalised velocity of the system is given by $\omega\bar{q}$ where $\bar{q}$ is the displacement amplitude at the frequency ω. This may easily be shown to have a maximum value at the frequency $\omega_n(1+\eta^2)^{\frac{1}{2}}$ when the assumption is made that the viscous damping is small compared with the

hysteretic damping. At this frequency the velocity amplitude is given by

$$|\dot{q}|_{max} = P/K^{\frac{1}{2}} M^{\frac{1}{2}} \kappa^{\frac{1}{2}} \theta^{\frac{1}{2}} [2(1+\eta^2)^{\frac{1}{2}} - 1] , \qquad \ldots(3.5)$$

which, for small values of η reduces to

$$|\dot{q}|_{max} = P/K^{\frac{1}{2}} M^{\frac{1}{2}} \kappa^{\frac{1}{2}} \theta^{\frac{1}{2}} \eta . \qquad \ldots(3.6)$$

The maximum attenuation of harmonic velocity amplitude is obviously obtained when the product $\kappa^{\frac{1}{2}}\theta^{\frac{1}{2}}\eta$ is as large as possible. The mass of the treatment (included in the factor θ) is now important, but when comparing the effectiveness of equal weights of different treatments the significant parameter is the product $\kappa^{\frac{1}{2}}\eta$. The criterion by which different treatments should be judged when used to attenuate vibration velocity amplitudes is therefore the value of $\kappa^{\frac{1}{2}}\eta$ per given weight of treatment. When judging the effect of different quantities of the same treatment the complete expression $\kappa^{\frac{1}{2}}\theta^{\frac{1}{2}}\eta$ must be used as the criterion.

III.2.5 The Effect on the Resonant Acceleration and Inertia Force Amplitudes

The generalised acceleration amplitude under harmonic excitation is given by $\omega^2\bar{q}$. This has a maximum value at the frequency $\omega_n(1+\eta^2)^{\frac{1}{2}}$ making the same assumption as before with regard to the magnitude of the viscous damping. At this frequency the acceleration amplitude is given by

$$|\ddot{q}|_{max} = P/M\theta\eta(1+\eta^2)^{-\frac{1}{2}} \qquad \ldots(3.7)$$

reducing to

$$|\ddot{q}|_{max} = P/M\theta\eta \qquad \ldots(3.8)$$

for small values of η. This is minimised by making θ as large as possible. Considering equal weights of different treatments, the signficant parameter is evidently η itself. Its value is therefore a sufficient criterion by which to judge the efficiency of a given quantity of treatment used to attenuate acceleration amplitudes.

The inertia force amplitude is directly proportional to the product of the generalised mass and the generalised acceleration amplitude. Its maximum value therefore occurs at the same frequency as the maximum acceleration, and is proportional to

$$P/\eta(1+\eta^2)^{-\frac{1}{2}} \qquad \ldots(3.9)$$

reducing to P/η for small η. Again, the value of η for a given weight

of treatment is a sufficient criterion by which to judge the efficiency when attenuating inertia force amplitudes.

It should be noted that as η becomes large, the term $\eta(1+\eta^2)^{-\frac{1}{2}}$ approaches unity. Any attempt to increase the value of η provided by a given treatment when η is already large, is not then accompanied by a worth-while reduction of acceleration or inertia force amplitude. It is probable, however, that when η is large enough for this effect to be important, the problems arising from the accelerations and inertia forces will have already been solved. The criteria developed in the whole of this section are summarised in table 1.

III.3 Criteria Applicable to Harmonic Sound Transmission through Simple Structures

As the addition of damping to a system has little effect upon forced vibrations apart from those occurring at resonance, this section will deal only with sound transmitted under structural resonant conditions and "coincidence" conditions. Two special cases only will be considered but these will serve to show the different ways in which the mass, stiffness and damping properties of the treatment affect the transmitted sound pressure. This implies, of course, that different efficiency criteria are required for judging the merits of different treatments, depending on the nature of the transmission.

Two very simple transmission mechanisms will be considered:

(1) The sound transmitted through a finite flexible plate set in an otherwise rigid and infinite wall (or baffle). An incident field of plane harmonic sound waves impinges on one side of the plate causing resonance in one of its natural modes. The sound wavelength is assumed to be large compared with the plate dimensions.

(2) The sound transmitted through an infinite flexible plate when an infinite field of plane harmonic waves impinges on one side, causing "coincidence" transmission to exist.

III.3.1 The Sound Transmitted Through a Finite Plate

As stated above, the plate is considered to be mounted in an infinite rigid wall. Firstly, it is assumed that free field conditions exist on both sides of the wall, and on one side the incident field exerts an oscillating pressure on the plate. It is further assumed that the wavelength of the sound radiated by the motion of the plate is large compared with the plate dimensions. (This is inevitable if the incident sound wavelength is large, as already assumed).

Now the sound pressure at any distance from the plate is found by integrating Equation 2.1 (Chapter II) over the whole plate surface. If both r and λ_a are large compared with the plate dimensions, the integration yields

$$p(r,t) \simeq -i \frac{\rho\omega}{2\pi r} |\dot{q}| e^{i\omega t} \cdot e^{i2\pi r/\lambda_a} \iint_A f(x,y)\, dx\, dy$$

where $\dot{q}$ is the amplitude of the generalised velocity corresponding to the

mode $f(x,y)$. The sound pressure amplitude is therefore proportional to $\omega^2 q_1$, i.e. to the amplitude of the generalised acceleration . We may therefore use the result of the last section to obtain the criterion relating to resonant harmonic sound pressure transmitted through a simple plate. The sound transmitted is evidently proportional to

$$P/M\theta(1+\eta^2)^{\frac{1}{2}}.\eta \quad ,$$

in which P is now to be interpreted as the generalised force corresponding to the incident sound pressure, and $M\theta$ as the generalised mass of the plate corresponding to the given mode. It is implicit that the acoustic radiation damping is small compared with the treatment damping, an assumption which is justifiable for any conceivable plate. For a given weight of damping treatment, the transmitted pressure is inversely proportional to $\eta(1+\eta^2)^{-\frac{1}{2}}$, which expression is the criterion required.

Now if one side of the plate is enclosed by a reverberant cavity, the natural modes of the plate will couple with standing waves within the cavity. There are, in fact, an infinite number of standing waves with which any one plate mode may couple, implying that there is an infinite set of natural frequencies at which the mode may resonante. (See, for example, refs. 19, 20). It is required to establish, therefore, the relationship between the resonant pressure amplitude within the cavity, corresponding to any one of the standing wave systems, and the generalised plate characteristics (including θ, R and η). A preliminary investigation has been carried out by the author (the work to be published later) considering a rectangular cavity, one wall of which consists of the flexible plate assumed to have simply supported edges. The other walls were considered to be rigid. The results of the analysis suggest the following effects of increasing θ , R and η :

The sound pressure at each of the standing wave resonances is inversely proportional to η . The effect of increasing θ and R may be combined by considering the effect they have on the uncoupled natural frequency of the plate, and then examining the effect of change of frequency. If the coupled standing wave - plate natural frequency is much less than that of the uncoupled plate, then an increase of the plate frequency tends to increase the resonant sound pressure. If, on the other hand, the coupled frequency is considerably greater than the plate frequency, then increasing the plate frequency decreases the resonant sound pressure. When the coupled frequency is close to the plate frequency, no such generalisation may be made and each case must be considered on its own merits.

III.3.2 The Sound Transmitted by Coincidence through an Infinite Plate

We now consider the effect of a damping treatment on the sound pressure transmitted through an infinite plate (or beam), on one side of which is an incident sound field of planeharmonic waves whose wave-fronts are inclined at an angle β to the plate surface. Before the treatment is added, coincidence transmission exists, the trace velocity of the incident field coinciding exactly with the phase velocity of the flexural wave in the plate excited by the incident field. The transmitted pressure is then equal to the incident sound pressur . The massand stiffness of the damping treatment changes the phase velocity of the flexural wave, and if the

incident sound field remains the same, a de-tuning effect will reduce the transmitted pressure. The reduction due to the de-tuning may be considerably greater than that due to the additional damping. If, however, the inclination or the frequency of the incident field is changed (the incident pressure remaining constant) and coincidence conditions are restored, then a measure of the effectiveness of the damping treatment may be found by comparing the transmitted sound pressure under these new coincidence conditions with the pressure under the initial conditions.

In the subsequent analysis, a unit width of the treated plate need only be considered. This has a complex flexural stiffness $R D(1 + i\eta)$ and a mass per unit length $\mu\theta$. The imaginary part of the complex stiffness represents the internal damping due to the damping treatment. D and μ are the flexural stiffness and mass per unit area before the treatment is added. R and θ are the stiffness and mass factors representing the effect of the treatment.

Let the incident pressure amplitude be p_i. Due to reflection of the incident wave and consequent pressure doubling, the incident pressure acting on the plate is given by

$$2p_i \exp i(\omega t + 2\pi x/\lambda_t) \qquad \ldots(3.10)$$

(See Figure 20 for explanation of undefined symbols). If it is assumed already that the flexural wave in the plate is of harmonic form, and of wavelength λ_t, it may be shown that the transmitted (or re-radiated) pressure, p_t, acting on the plate surface is

$$\rho c \sec\phi \cdot \partial w/\partial t \qquad \ldots(3.11)$$

where w is the local transverse bending displacement of the plate. this re-radiation occurs from each side of the plate, the net re-radiation pressure acting on the plate is $2\rho c \sec\phi \cdot \partial w/\partial t$.
The equation for the forced motion of the plate may now be written

$$R D(1+i\eta)\,\partial^4 w/\partial x^4 + \mu\theta\,\partial^2 w/\partial t^2 = -2p_i \exp i(\omega t + 2\pi x/\lambda_t) - 2\,\partial w/\partial t\ \rho c.\sec\phi \qquad \ldots(3.12)$$

Derivatives of w with respect to y are zero, since the sound field consists of infinite plane waves. Putting $w = \bar{w} \exp i(\omega t + 2\pi x/\lambda_t + \varepsilon)$, equating the real and imaginary parts on both sides and eliminating ε, it is found that

$$\bar{w} = 2p_i\left[\left\{R D(2\pi/\lambda_t)^4 - \mu\theta\omega^2\right\}^2 + \left\{R D(2\pi/\lambda_t)^4\eta + 2\rho c\,\omega\sec\phi\right\}^2\right]^{-\frac{1}{2}} \qquad \ldots(3.13)$$

For small η, it is sufficiently accurate to consider coincidence transmission occurring at the frequency ω_c, given by

$$R D(2\pi/\lambda_t)^4 - \mu\theta\omega_c^2 = 0. \qquad \ldots(3.14)$$

The local plate velocity and the incident sound pressure are then exactly in phase and the transmitted sound pressure is close to its maximum value, which actually occurs at a slightly greater frequency.

At the frequency ω_c, the transmitted sound pressure amplitude is $\omega_c \bar{w} \rho c . \cos\phi$. Substitution for $\bar{w}$ and rearrangement yields

$$P_t = P_i \left[1 + \frac{KD\,(2\pi/\lambda_t)^4 \eta}{2\rho c\, \omega_c \sec\phi} \right] \qquad \ldots(3.15)$$

Now the trace wavelength λ_t is related to ω_c by

$$\left.\begin{aligned} \lambda_t \sin\phi &= \lambda = 2\pi c/\omega_c \\ \text{and also by} \quad \omega_c^2 &= (KD/\mu\theta)(2\pi/\lambda_t)^4 \ \text{(from 3.14)} \end{aligned}\right\} \qquad \ldots(3.16)$$

Using these relationships, λ_t and ω_c, or λ_t and ϕ may be eliminated from equation 3.15. We then have

$$P_t = P_i \left[1 + \frac{c^2 \operatorname{cosec}^2\phi}{2\rho c \sec\phi}\, \eta\, (\mu\theta)^{3/2} (KD)^{-\frac{1}{2}} \right]^{-1} = P_i / k_\phi \qquad \ldots(3.17)$$

or

$$P_t = P_i \left[1 + \frac{\omega_c}{2\rho c} \left\{ 1 - (c^2/\omega_c)(\mu\theta/KD)^{\frac{1}{2}} \right\}^{\frac{1}{2}} \mu\theta\eta \right]^{-1} = P_i / k_\omega \qquad \ldots(3.18)$$

Equation 3.17 may be used to indicate the effect of η, θ and K on the transmitted pressure when the inclination of the incident field is kept constant while the frequency is varied to restore coincidence. Equation 3.18 may be used to indicate the effect when the frequency is kept constant and the inclination is changed. It is implied here that coincidence transmission may indeed be restored. This may not always be possible, as suggested, for example, by the term $\{1 - (c^2/\omega_c)(\mu\theta/KD)^{\frac{1}{2}}\}^{-\frac{1}{2}}$ in equation 3.18. If θ/K is such as to make this term vanish, or to be imaginary, coincidence transmission cannot occur at the particular frequency ω_c.

Now when η is zero (no internal damping), $p_t = p_i$. The pressure amplitude transmitted under damped conditions is therefore $1/k_\phi$ or $1/k_\omega$ times that transmitted under undamped conditions. The significant factors involved in k_ϕ and k_ω which must be made as great as possible in order to produce the greatest attenuation of pressure are:

$$\eta\, \theta^{\frac{3}{2}}\, K^{-\frac{1}{2}} \qquad \ldots(3.19)$$

and

$$\eta\, \theta \left[1 - (c^2/\omega_c)(\mu/D)^{\frac{1}{2}} (\theta/K)^{\frac{1}{2}} \right]^{\frac{1}{2}} \qquad \ldots(3.20)$$

It is evident that η should be as great as possible for the greatest

attenuation. Furthermore, expression 3.19 indicates that it is desirable for R to be as small as possible. In this case, an increase of stiffness counteracts, in some measure, the effect of the increased damping.

It may be noted that the term $(\mu/D)^{\frac{1}{2}}(\theta/K)^{\frac{1}{2}}$ in expression 3.20 is inversely proportional to the resonant frequency of a treated finite plate, when vibrating in a flexural mode of wavelength λ_t. The value of expression 3.20 is reduced when this frequency decreases, indicating therefore that it is undesirable for the damping treatment to decrease the resonant frequency of the system if the transmitted sound pressure under constant frequency conditions is to be minimised. If two different damping treatments provide equal loss factors, η, the most effective treatment will be that giving the greatest frequency increase (or smallest decrease).

III.4 Criteria Applicable to Random Vibrations

III.4.1 Random Mechanical Response Quantities

Once again, the response of a single degree of freedom system only will be considered. The system is excited by a force which varies randomly with time, and it is assumed that the power spectrum of the corresponding generalised force does not vary appreciably in the region of the natural frequency of the system. The equation of motion of the system, in terms of the generalised displacement, q, is

$$M\theta\ddot{q} + C\dot{q} + K_R(1 + i\eta)q = P(t) \qquad \ldots(3.21)$$

where $P(t)$ represents the random exciting force. If the power spectral density of $P(t)$ is denoted by $\Phi_p(\omega)$, then it is well known that the power spectral density of the generalised displacement, $\Phi_q(\omega)$, is given by

$$\Phi_q(\omega) = \Phi_p(\omega)/|Z|^2 \qquad \ldots(3.22)$$

$|Z|^2$ is the square of the modulus of the mechanical impedance,

i.e. $$(K_R - \omega^2 M\theta)^2 + (\omega C + K_R\eta)^2 \qquad \ldots(3.23)$$

The mean square value of the generalised displacement, $\langle q^2 \rangle$ is given by $\int_0^\infty \Phi_q(\omega)\, d\omega$. Under the restriction quoted above the variation of $\Phi_p(\omega)$, and assuming small total damping, the integral yields

$$\langle q^2 \rangle = \Phi_p(\omega_n)(\pi/2)/K_R(C + K_R\eta/\omega_n), \qquad \ldots(3.24)$$

where $$\omega_n^2 = K_R/M\theta \qquad \ldots(3.25)$$

We assume now that the initial viscous damping is very much smaller than the added hysteretic damping, and also allow that η may be large (i.e. of the order of 1). The root mean square displacement then becomes

$$q_{rms} = \left[\Phi_p(\omega_n)(\pi/2)\right]^{\frac{1}{2}}\left[M^{\frac{1}{4}} K^{\frac{3}{4}} \theta^{\frac{1}{2}} R^{\frac{3}{4}} \eta^{\frac{1}{2}} F_d(\eta)\right]^{-1} \quad \ldots(3.26a)$$

where $$F_d(\eta) = \left[\frac{2(1+\eta^2)}{1+\sqrt{1+\eta^2}}\right]^{\frac{1}{4}} \quad \ldots(3.26b)$$

Thus the r.m.s. displacement is inversely proportional to $K^{\frac{3}{4}} \theta^{\frac{1}{4}} \eta^{\frac{1}{2}} F_d(\eta)$ and the corresponding efficiency criterion for a damping treatment is the value of $K^{3/4} \eta^{1/2} F_d(\eta)$ per given weight of treatment. It follows, by direct comparison with para III.2.3 that the criterion relating to the surface bending stress of a treated plate is $K^{3/4} \eta^{1/2} F_d(\eta) \kappa^{-1}$ per given weight of treatment.

(When η is very small, $F_d(\eta)$ is very nearly equal to one, and expression 3.26a reduces to that normally quoted for the r.m.s. displacement of a lightly damped, randomly-vibrating system of one degree of freedom. When η is large, $F_d(\eta)$ may be regarded as a 'large damping correction factor' converting the expression for the r.m.s. displacement of the lightly damped system to that of the heavily-damped system. It has the value of 1.14 when $\eta = 1$, and 1.04 when $\eta = 0.5$).

Under the same assumptions as above, the root mean square value of the generalised random velocity is given by

$$\dot{q}_{rms} = \left[\Phi_p(\omega_n)\pi/2\right]^{\frac{1}{2}}\left[M^{\frac{3}{4}} K^{\frac{1}{4}} \theta^{\frac{3}{4}} R^{\frac{1}{4}} \eta^{\frac{1}{2}} F_v(\eta)\right]^{-1} \quad \ldots(3.27a)$$

where $$F_v(\eta) = \left[\frac{2}{1+\sqrt{1+\eta^2}}\right]^{\frac{1}{4}} \quad \ldots(3.27b)$$

The r.m.s. velocity is therefore inversely proportional to $K^{\frac{1}{4}} \theta^{\frac{3}{4}} \eta^{\frac{1}{2}} F_v(\eta)$, and the corresponding efficiency criterion is the value of $K^{\frac{1}{4}} \eta^{\frac{1}{2}} F_v(\eta)$ per given weight of treatment.

Consider now the mean square value of the random generalised acceleration. The power spectral density of the acceleration is given by ω^4 times the power spectral density of the generalised displacement. Integrating this from $\omega = 0$ to $\omega = \infty$, and making the same restrictions as above upon the variation of the power spectrum in the region of the natural frequency, the mean square value of the generalised acceleration is found to be

$$\langle \ddot{q}^2 \rangle = \Phi_p(\omega)\, \pi/2 \left[M^{\frac{5}{2}} K^{-\frac{1}{2}} \theta^{\frac{5}{2}} R^{-\frac{1}{2}} \eta\, F_a(\eta)\right]^{-1} + \langle P^2(t) \rangle M^2 \theta^2 \quad \ldots(3.28a)$$

where $$F_a(\eta) = \left[\frac{2}{1+\sqrt{1+\eta^2}}\right]^{\frac{1}{2}} \left[2 - \sqrt{1+\eta^2}\right] \quad \ldots(3.28b)$$

The first of the two components of this expression may be said to derive from the resonant response of the system, and is therefore dependent upon the damping. The second component is associated with the inertia reaction of the system, depending only upon the mass of the system. The relative magnitudes of the two components are obviously critically dependent upon the shape of the spectrum of the generalised force. If the resonant component is small compared with the other, the effect of the damping treatment will be mainly that of its mass, i.e. "mass law" attenuation will pertain. If the resonant component forms an appreciable part of the total response, then the criterion $K^{-\frac{1}{2}}\eta F_a(\eta)$ may be used to compare the effects on random acceleration of equal weights of different treatments. It is convenient to take the square root of this criterion and since η is often much less than one, it becomes $K^{-\frac{1}{4}}\eta^{\frac{1}{2}}$.

The force exerted by a randomly excited system on its supports consists of the vector sum of the exciting forces and the inertia forces corresponding to the response of the system. If the system is responding primarily in one mode, this total force will be proportional (approximately) to the product of the displacement of the system and the modulus of the generalised complex stiffness of the mode. (This is exact for a single mass-spring-damper oscillator, attached to a rigid base, and having the spring and damper in parallel. A more complete treatment of the forces on the supports of a damped beam is given in Chapter VII). The r.m.s. value of the force is therefore proportional to

$$q_{rms} \quad K R (1+\eta^2)^{\frac{1}{2}}$$

Using equation 3.26a, this becomes

$$\left[\Phi_p(\omega_n)\,\pi/2\right]^{\frac{1}{2}}\left[M^{\frac{1}{4}} K^{-\frac{1}{4}} \theta^{\frac{1}{4}} K^{-\frac{1}{4}} \eta^{\frac{1}{2}} F_r(\eta)\right]^{-1} \qquad \ldots(3.29a)$$

where $$F_r(\eta) = F_a(\eta)/(1+\eta^2)^{\frac{1}{2}} \qquad \ldots(3.29b)$$

Assuming once again that $\eta^2 \ll 1$, the efficiency criterion derived from this expression is evidently $K^{-\frac{1}{4}}\eta^{\frac{1}{2}}$ per given weight of treatment (N.B. for convenience the resultant of the inertia and exciting forces will be referred to simply as the "reaction force" from now on).

It may be noted that the last of the two "square-bracketed" terms of Equation 3.29 becomes $(\eta/\omega_n)^{-\frac{1}{2}}$, if $\eta^2 \ll 1$. Since this quantity must be as large as possible to minimise the random force, ω_n should obviously be as small as possible. It is therefore disadvantageous for a damping treatment to increase the natural frequency of the system, as far as these reaction forces are concerned. Such an increase counteracts, in some measure, the benefits arising from the increased damping.

The criteria and related response expressions derived in this section are summarised in Table 2.

III.4.2 Sound Transmission through a Single Plate Under Random Excitation

Now suppose that the finite plate of para III.3.1 is subjected on one side to random pressure fluctuations which give rise to a generalised force having a spectrum which is flat (or nearly flat), as before. The r.m.s. sound pressure transmitted by one of the plate modes of vibration to the far field on the other side will be proportional to the generalised r.m.s. acceleration of the plate mode. The effectiveness of a damping treatment in attenuating the resonant component of the transmitted pressure is therefore represented by the same expression as derived above for the r.m.s. acceleration. The corresponding efficiency criterion is again the value of $K^{-4}\eta^{-2}$ per given weight of treatment (for small damping).

At this juncture we may look in more detail at the spectrum of the random transmitted noise, which, like the generalised acceleration, is proportional to ω^4 times the spectrum of the generalised displacement, i.e. to

$$\frac{\Phi_p(\omega_n)\ \omega^4}{(K_R - \omega^2 M\theta)^2 + (K_R\eta)^2}$$

With low damping, this has a pronounced peak at (or close to) the resonant frequency $(K_R/M\theta)^{\frac{1}{2}}$. At zero frequency it has the value zero, but at high frequency it approaches the value

$$\Phi_p(\omega) \Big/ M^2\theta^2$$

The high frequency components of the transmitted noise are therefore affected only by the mass of the plate. It is partly due to this feature that the mean square pressure has the two 'components' derived in Equation 3.28. If the second of the components is large compared with the first (and this may be so even if the damping is small, provided $\Phi_p(\omega)$ has high values above the resonant frequency) then the transmitted noise will have a marked resonant peak in its spectrum without being "predominantly resonant". This point was made in section I.4, Chapter I.

III.4.3 Random Sound Transmission through an Array of Plates Subjected to Boundary Layer Pressure Fluctuations

As a further example of the different criteria which must be used for different systems and response quantities, reference will now be made to the work of Kraichnan (11). This considers the acoustic radiation from an array of thin, independent, square plates on one side of which a moving airstream exerts convected boundary layer pressure fluctuations. After certain simplifying assumptions have been made, expressions are developed for the mean square radiated sound pressure (i.e. transmitted pressure) in terms of the mean square incident pressure and plate parameters. Many different modes of plate vibration contribute to the total radiation.

Under longitudinal dipole excitation, which has a distributed convection

velocity, the mean square radiation pressure $\langle p_r^2 \rangle$ is found to be of the form

$$\langle p_r^2 \rangle = \langle p^2 \rangle C_1 \left[(\mu D)^{\frac{1}{2}} (\theta K)^{\frac{1}{2}} \eta \left(\theta \mu + \frac{C_2}{a^2} D K \right) \right]^{-1} \quad \ldots(3.30)$$

$\langle p^2 \rangle$ is the mean square incident pressure, and C_1 and C_2 are constants relating to the pressure distribution only. a is the length of the plate, $\theta\mu$ the mass per unit area, and DK the real part of the flexural rigidity of the plate. The expression is valid only for small values of η. The criterion for judging the efficiency of a damping treatment in attenuating the radiated r.m.s. sound pressure is now the value of

$$\left[K^{\frac{1}{2}} \eta \left(\theta + \frac{C_2}{a} \frac{DK}{\mu} \right) \right]^{\frac{1}{2}}$$

per given value of θ. (The power $\frac{1}{2}$ is introduced to allow for the root mean square value).

When the incident pressure fluctuations derive from transverse dipole excitation and a sharp convection velocity, the mean square radiation pressure is of the form

$$\langle p_r^2 \rangle = \langle p^2 \rangle C_3 \left[\mu^{\frac{3}{4}} D^{\frac{1}{4}} \theta^{\frac{3}{4}} K^{\frac{1}{4}} \eta \right]^{-1} \quad \ldots(3.31)$$

the corresponding efficiency criterion for a damping treatment in relation to the r.m.s. pressure being the value of $K^{\frac{1}{2}} \eta^{\frac{1}{2}}$ per given weight.

One of the assumptions made in the derivation of the above expressions is that the damping (or loss) factor, η, is the same for each of the modes contributing to the radiation. When the damping derives from a visco-elastic damping treatment, this assumption is invalid for two reasons:

(a) The visco-elastic properties of the damping medium are considerably frequency dependent, and will therefore cause variations in η from mode to mode on account of the different natural frequencies involved.

(b) Constrained layer damping treatments give loss factors and flexural stiffnesses which depend on the wavelength of the flexural vibration. The treatments are designed to give optimum damping under certain conditions of geometry and wavelength and these conditions cannot be satisfied by all possible modes. The extension of Kraichnan's analysis to cover variations of damping factor and flexural stiffness with frequency in undoubtedly beset with great difficulties.

III.5 Estimation of Response Reductions from Criterion Values

From the derivations of the expressions for the different criteria, it is evident that for all the harmonic responses

$$\frac{\text{Response after treatment}}{\text{Response before treatment}} = \frac{\eta_i}{\text{Criterion Value}}$$

and for all the random responses

$$\frac{\text{R.M.S. Response after treatment}}{\text{R.M.S. Response before treatment}} = \frac{\eta_i^{\frac{1}{2}}}{\text{Criterion Value}}$$

Denoting the value of these fractions by R, the percentage reduction of the response due to the addition of the treatment is clearly $100(1 - R)\%$.

Chapter IV

A Comparison of Two Different Unconstrained Layer Treatments

The criteria deduced in Chapter III will now be used as a basis for comparing two different unconstrained layer treatments, applied uniformly to one side of an aluminium plate undergoing flexural vibration. It will be shown that whereas one treatment may be superior in its effect when judged by one of the criteria, another treatment may be superior when judged by another criterion. Furthermore, one of the criteria may indicate that a given treatment is most effective when a certain optimum quantity is used, whereas another criterion may indicate that a different optimum quantity is required.

First of all, it is necessary to derive the equations of flexural motion of the treated plate in terms of the normal co-ordinates, from this analysis, expressions must be derived for the loss factors and stiffness ratios corresponding to the modes of vibration, in terms of the plate dimensions and material properties.

IV.1 The Loss Factor and Stiffness Ratio of a Flat Plate with an Unconstrained Layer Treatment, Vibrating in Flexural Modes

For the sake of simplicity at this stage, we shall consider a long narrow plate of unit width and constant thickness, vibrating in a flexural mode essentially as a beam (see Figure 21). The damping treatment forms a uniform layer of thickness h_3 on one side of the basic (metal) plate of thickness h_1. The Young's Moduli of the two materials are $E_d(1 + i\eta_d)$ and E_m respectively. The damping of the basic plate will be ignored.

If η_d was zero, there would exist a neutral surface of bending, in the plane of which no direct strain would exist at any time during a cycle of flexural vibration. The position of this surface may be found by the usual composite beam theory. Although it no longer exists in the same physical sense when the non-zero η_d is admitted, it still forms a convenient datum (or origin) for the transverse co-ordinate, z, and will still be referred to as "the neutral surface".

It will be assumed that when the plate bends, transverse sections of the plate which were initially plane and perpendicular to the neutral surface remain plate and perpendicular. If the curvature $\partial^2 w/\partial x^2$ is now imposed upon the neutral surface without straining the surface itself, the x-wise strain at any point z_n below the surface is

$$\varepsilon_x = -z_n \frac{\partial^2 w}{\partial x^2} \qquad \ldots(4.1)$$

The corresponding direct stresses in the two layers are respectively

$$\sigma_x = -E_d(1 + i\eta_d) z_n \frac{\partial^2 w}{\partial x^2} \quad \text{and} \quad \sigma_x = -E_m z_n \frac{\partial^2 w}{\partial x^2} \qquad \ldots(4.2)$$

Integrating these stresses over the whole cross-sectional area to find the

total direct load on the section, it is found that the real part vanishes (by definition of the neutral surface and the use of z_n), but the imaginary part

$$- E_d \eta_d \int_d z_n \, dA \; \frac{\partial^2 w}{\partial x^2}$$

does not vanish. (The symbol 'd' or 'm' in the lower limit position of the integral implies integration over the sectional area of the damping or metal layer respectively). Now if there are no externally applied direct loads nor significant longitudinal inertia forces, there can at no time exist any resultant direct load on the section, real or imaginary. There must therefore exist another strain and stress system, superimposed upon that due to $\partial^2 w/\partial x^2$ above, which annuls the non-zero imaginary load. This other strain system is, of course, that associated with longitudinal vibration of the plate. By virtue, therefore, of the unsymmetric distribution of the damping treatment, damping coupling exists between the flexural and longitudinal plate motion. Following Oberst (21), however, we shall first assume that the effect of this coupling on the plate flexural stiffness and damping is negligible. The justification for this will be seen later when the coupling effects are included.

Next, take moments of the stresses of Equation 4.2 about the neutral surface and equate the total (integrated) moment to the externally applied moment, M(x, t). This yields

$$M(x,t) = - \frac{\partial^2 w}{\partial x^2} \left[- \int_m E_m z_n^2 \, dA - \int_d E_d (1 + i\eta_d) z_n^2 \, dA \right]$$

or

$$M(x,t) = (EI)_t (1 + i\eta) \frac{\partial^2 w}{\partial x^2} \qquad \ldots(4.3)$$

in which $(EI)_t$ is the total flexural rigidity of the plate as given by the composite beam theory. i.e.

$$(EI)_t = E_m I_m + E_d I_d = E_m \int_m z_n^2 \, dA + E_d \int_d z_n^2 \, dA \qquad \ldots(4.4)$$

η is the "flexural loss factor" of the plate and is given by

$$\eta = \frac{E_d I_d}{(EI)_t} \cdot \eta_d \qquad \ldots(4.5)$$

When the plate vibrates under the action of the time-dependent transverse loading $p(x)e^{i\omega t}$, there also exists the transverse inertia loading $-\mu\theta \, \partial^2 w/\partial t^2$, $\mu\theta$ being the mass per unit area of the treated plate. The

equation of motion of the plate becomes

$$(EI)_t(1+i\eta)\frac{\partial^4 w}{\partial x^4} + \mu\theta\frac{\partial^2 w}{\partial t^2} = p(x)\,e^{i\omega t} \qquad \ldots(4.6)$$

We shall consider the displacement of the plate in terms of its normal modes of undamped flexural motion, i.e. those modes which satisfy the homogeneous equation 4.6 with $\eta = 0$. Hence we write

$$w = \sum_{n=1}^{\infty} q_n f_n(x) \qquad \ldots(4.7)$$

where the f_n's are the non-dimensional normal modes and the q_n's the corresponding normal co-ordinates. The equations for the q_n's may now be obtained in the usual way by substituting Equation 4.7 into 4.6, multiplying throughout by f_n and integrating over the whole length, a, of the plate. Provided there are no concentrated springs attached to the plate, the orthogonal properties of the modes may be used to show that the equation of motion corresponding to the nth co-ordinate is independent of any other co-ordinate. i.e. no damping coupling exists between the flexural modes, and we have

$$\ddot{q}_n\int_0^a \mu\theta f_n^2\,dx + q_n(EI)_t(1+i\eta)\int_0^a (f_n^{iv})^2\,dx = \int_0^a p(x) f_n\,dx.\,e^{i\omega t} \qquad \ldots(4.8)$$

The generalised stiffness of the plate corresponding to the nth mode and co-ordinate is therefore

$$K_n = (EI)_t\int_0^a (f_n^{iv})^2\,dx \qquad \ldots(4.9)$$

and the generalised hysteretic damping coefficient is

$$H_n = \eta(EI)_a\int_0^a (f_n^{iv})^2\,dx \qquad \ldots(4.10)$$

The "generalised modal loss factor", H_n/K_n, is simply η (the plate flexural loss factor) and is <u>independent of the mode of transverse vibration</u>.

Now consider the plate before being treated, vibrating in the same mode. The flexural rigidity is $(EI)_u$ and the mass per unit length is μ. The equation of motion in the nth co-ordinate is

$$\ddot{q}_n\int_0^a \mu f_n^2\,dx + q_n(EI)_u\int_0^a (f_n^{iv})^2\,dx = \int_0^a p(x) f_n\,dx.e^{i\omega t} \qquad \ldots(4.11)$$

The ratio of the generalised stiffnesses in this mode of the treated and

untreated plates is then

$$K = (EI)_t / (EI)_u \qquad \ldots(4.12)$$

which again is <u>independent of the mode of transverse vibration</u> , and is simply the ratio of the flexural rigidities of the two plates.

Explicit expressions for K and the modal loss factor for the flat plate may now be derived using Equations 4.4 and 4.5. Writing $h_2/h_1 = \tau$, and $E_d/E_m = e$, we find

$$E_m I_m = \frac{E_m h_1^3}{12}\left\{1 + \frac{3(e\tau)^2(1+\tau)^2}{(1+e\tau)^2}\right\} \; ; \; E_d I_d = \frac{E_m h_1^3}{12}\left\{e\tau^3 + \frac{3(e\tau)(1+\tau)^2}{(1+e\tau)^2}\right\}.$$

Since $(EI)_u = E_m h_1^3/12$ the stiffness ratio becomes

$$K = \frac{E_m I_m + E_d I_d}{(EI)_u} = 1 + \frac{3e\tau(1+\tau)^2}{(1+e\tau)^2} + e\tau^3 \qquad \ldots(4.13)$$

Likewise, using Equation 4.5 and the above expressions, we find

$$\eta = \eta_d \frac{E_d I_d}{E_m I_m + E_d I_d} = \eta_d \left\{e\tau^3 + \frac{3e\tau(1+\tau)^2}{(1+e\tau)^2}\right\} K^{-1} \ldots(4.14)$$

In addition to the modal loss factor and stiffness ratio, the stress ratio is also required in some of the criteria (see para III.2.3). For the unconstrained layer treatment this is simply the ratio of the distances between the free plate surface and the neutral surface after and before treatment. Before treatment, the distance is $h_1/2$. After treatment it is

$$\frac{h_1}{2}\left\{\frac{1 + 2e\tau + e\tau^2}{1+e\tau}\right\}$$

The stress ratio is evidently.

$$\alpha = \frac{1 + 2e\tau + e\tau^2}{1+e\tau}$$

We now return to consider the effect of the coupling between the flexural&longitudinal motion of the damped plate. The longitudinal displacement will be represented by the term u_o , which is the x-wise displacement of the neutral surface, is a function of x, and is constant across the section. The total strain at the point z_n is now

$$\varepsilon_x = \frac{\partial u_o}{\partial x} - z_n \frac{\partial^2 w}{\partial x^2} \qquad \ldots(4.15)$$

Corresponding to this strain distribution is the total load on the cross-section

$$E_m \int_m [\partial u_o/\partial x - z_n \partial^2 w/\partial x^2]\,dA + E_d(1+i\eta_d)\int_d [\partial u_o/\partial x - z_n \partial^2 w/\partial x^2]\,dA.$$

This reduces to

$$\{E_m A_m + E_d A_d (1+i\eta_d)\}\partial u_o/\partial x - i\eta_d E_d A_d \bar{z}_d \partial^2 w/\partial x^2 \qquad \ldots(4.16)$$

since

$$E_m \int_m z_n\,dA + E_d \int_d z_n\,dA = 0$$

A_m and A_d are the total cross-sectional areas of the metal and damping layers, and $\bar{z}_m$, $\bar{z}_d$ are the distances from their centroids to the neutral surface.

If longitudinal inertia forces are present, the x-wise derivative of this load must be equated to the sum of the longitudinal inertia loading, $\mu_0 \partial^2 u_o/\partial t^2$, and a term associated with the angular acceleration of the section, $\partial^3 w/\partial x \partial t^2$. This term is present since the centre of gravity of the section does not coincide with the neutral surface. Now the natural frequencies of the flexural vibration of practical aeroplane plates are relatively so low that both of these longitudinal inertia loadings are negligible. Proceeding on this assumption, and equating the total direct load to zero, we obtain the relationship between $\partial u_o/\partial x$ and $\partial^2 w/\partial x^2$:

$$\frac{\partial u_o}{\partial x} = \frac{i E_d \eta_d A_d \bar{z}_d}{E_m A_m + E_d A_d (1+i\eta_d)} \frac{\partial^2 w}{\partial x^2} \qquad \ldots(4.17)$$

Substituting this into Equation 4.15, multiplying by the appropriate E and integrating the moment of the stresses over the whole sectional area, we obtain the new relationship between the bending moment and the curvature. After some reduction, this becomes

$$M(x,t) = \left\{ (EI)_t (1+i\eta) + \frac{\eta_d^2 E_d^2 A_d^2 \bar{z}_d^2}{E_m A_m + E_d A_d (1+i\eta_d)} \right\} \frac{\partial^2 w}{\partial x^2} \qquad \ldots(4.18)$$

The general form of this is similar to that of Equation 4.3, in that the bending moment is still proportional to the curvature, and that the constant of proportionality (the complex flexural rigidity) depends on the dimensions of the cross-section only together with the material properties. The equations of motion of the plate may then be set up as before, using the same normal co-ordinates and modes. The stiffness ratio for each mode will still be proportional to the flexural rigidity of the plate, and the modal loss factors will still be proportional to the plate flexural loss factor.

The first term in the large brackets of Equation 4.18 is the complex flexural rigidity of Equation 4.3, obtained by ignoring the coupling. The second term therefore represents the effect of the coupling. If we now put $A_d/A_m = \tau$, (the ratio of the thicknessess of the two layers) and $E_d/E_m = e$, this second term becomes

$$E_d A_d \bar{z}_d^2 \left\{ \frac{\eta_d^2 (1 + 1/e\tau)}{(1 + 1/e\tau)^2 + \eta_d^2} - i\eta_d \frac{\eta_d^2 (e\tau)^2}{(1 + 1/e\tau)^2 + \eta_d^2} \right\} \qquad \ldots(4.19)$$

We may now compare the magnitude of this term with the first term of Equation 4.18, using some typical values of τ and e. A stiff damping treatment may have $E_d = 10^6$ lb. in.$^{-2}$, and $\eta_d = 0.35$. Applied to an aluminium plate, this gives e = 0.1. Taking $\tau = 10$ (a very large value), the bracketed term of expression 4.19 becomes $0.06 - i\eta_d 0.03$. It will be smaller than this for smaller values of e or τ. Now the term outside the bracket, $E_d A_d \bar{z}_d^2$, may be regarded as being one "part" of the total flexural

rigidity $(EI)_t$, and can never be greater than the total. With $e = 0.1$ and $\tau = 10$, it is approximately one third of $(EI)_t$. The second term of Equation 4.16 is therefore approximately $(EI)_t(0.02 - i\,0.01)$. The effect of the coupling on the real part of the flexural stiffness is therefore to increase it by only 2% , when the large values are given to e and τ .

Considering the imaginary part of Equation 4.16 , and using the expanded form of $(EI)_t\eta$ from Equations 4.5 and 4.4 , it can be shown that the effect of the coupling is to reduce it by about 1½% when the same values of e and τ are used as above. It is evident, therefore, that for the practical conditions to be dealt with in subsequent parts of this chapter, we may use the results of the theory in which the coupling was ignored.

IV.2 A Comparison of the Effects of Equal Weights of Different Treatments

The treatments to be considered are two different grades of Aquaplas, and will be referred to as Treatment A and Treatment B . They both consist of filled resins, different fillers being used in each case. Their properties, as deduced from laboratory tests on simple treated specimens at a given temperature and frequency, are:

	Treatment A	Treatment B
E_d	860,000 lb.in.$^{-2}$	1,080,000 lb.in.$^{-2}$
η_d	0.19	0.33
Specific Gravity	1.20	1.68

Using this data, values have been obtained for the loss factor η and the stiffness ratio R for a uniform plate covered uniformly with different quantities of the treatments. An aluminium plate has been considered, having $E_m = 10.8\times10^6$ lb in^{-2} and a specific gravity of 2.84 . R and η are plotted in Figures 22 and 23, the abscissae being the weight of the treatment as a fraction of the weight of the plate. The highest value of the weight ratio (10) is not intended to represent a practical configuration, but is included to indicate the ultimate trends.

From these values of R and η the values have been calculated of selected criteria from the preceding chapter and these are plotted in Figures 22 to 25. It should be noticed that at this stage the mass ratio term, θ^m , has been omitted from the criteria as the comparison between the two treatments is being carried out on an equal weight basis. The effect of the mass term will therefore be the same for both treatments and need not be included. In section IV.4 the mass effect is included in order to compare the effectsof different amounts of the same treatment.

The criterion relating to harmonic displacement amplitude $(R\eta)$ is shown in Figure 23, together with the loss factor, η , which is the criterion relating to harmonic sound pressure transmitted at resonance through a finite plate. Figure 24 shows the criteria relating to random vibration amplitude $(R^{\frac{1}{2}}\eta^{\frac{1}{2}})$, random reaction force $(R^{\frac{1}{4}}\eta^{\frac{1}{2}})$ and random transmitted boundary layer noise $(R^{\frac{1}{8}}\eta^{\frac{1}{2}})$. ($\eta$ is small enough here to justify putting $F_d(\eta) = F_r(\eta) = 1$. Figure 25 shows the criteria relating to the bending stress at thefree surface of the plate when vibrating under harmonic resonant or random conditions ($R\eta\alpha^{-\frac{1}{2}}$ and $R^{\frac{3}{4}}\eta^{\frac{1}{2}}\alpha^{-\frac{1}{2}}$ respectively).

Before comparing the curves for the two treatments, it is useful to

observe the nature of the curves for R and η . Since small amounts of treatment add little to the plate stiffness, R is little greater than unity at low weight ratios. As the treatment weight increases to very large values, the flexural stiffness of the treatment about its own principal axis becomes the dominant part of the total flexural stiffness. This is therefore then approximately proportional to the cube of the thickness (and weight) of the treatment, which is also evident from equation 4.13. The stiffness ratio therefore increases monotonically with the treatment weight.

The loss factor, η , increases linearly with treatment weight with small amounts of treatment but passes through a maximum as the weight becomes larger. After this, it oscillates slightly and approaches the asymptotic value of η_d . The flexural loss factor cannot exceed the loss factor of the material providing the damping, as equation 4.14 shows.

Comparing now the curves for treatments A and B , it will be seen from Figure 22 that treatment A , with the smaller value of E_m, nevertheless provides a higher stiffness ratio R than treatment B . This is due to the lower density of treatment A , which therefore has a greater thickness for a given weight of material and a correspondingly greater second moment of area about the neutral surface of the composite plate. This has an important bearing upon the criteria $R\eta$ and $R^{\frac{2}{3}}\eta^{\frac{1}{2}}$, which are shown in Figures 23 and 24. At low treatment weights the value of each of these criteria is higher for treatment B (with the superior material loss factor and Young's Modulus) than for A . At higher treatment weights this superiority is reversed due to treatment A providing the higher stiffness ratio. At the low treatment weights, where the stiffness ratio is little greater than unity, the two criteria approach the values of η and $\eta^{\frac{1}{2}}$ respectively, and the treatment providing the highest loss factor η is automatically superior.

Consider now the criterion $R^{-\frac{1}{4}}\eta^{\frac{1}{2}}$ (Figure 24), relating to random reaction forces, or to the resonant component of random transmitted sound pressure. Since the stiffness ratio is raised to a negative power in this criterion, the treatment providing the lower stiffness ratio but the higher loss factor (treatment B) is inevitably superior over the whole weight range. It may be seen that equation 3.19 giving the criterion relating to one form of coincidence transmission, contains $\eta R^{-\frac{1}{2}}$, i.e. $(R^{-\frac{1}{4}}\eta^{\frac{1}{2}})^2$. The criterion $R^{-\frac{1}{4}}\eta^{\frac{1}{2}}$ may therefore be used in relation to both random reaction forces and this form of coincidence transmission.

The criterion $R^{\frac{1}{8}}\eta^{\frac{1}{2}}$ (Figure 24) also shows treatment B to be superior up to, and beyond, a weight ratio of 10 on account of the higher loss factor and the very small power to which σ is raised. A maximum appears to occur at the weight ratio of about 10, but the curves will inevitably rise at higher (very impracticable) weight ratios on account of the positive power of R and the asymptotic nature of η .

The criteria relating to the surface bending stresses (Figure 25) follow a generally similar trend to the criteria relating to vibration displacement amplitudes. Over the lower weight range, treatment B is superior to A under both random and harmonic conditions, but treatment A is superior under random conditions above a weight ratio of about 0.5 . This superiority derives from the larger values of $R^{3/4}\eta^{\frac{1}{2}}$ for treatment A above this weight, which implies smaller vibration amplitudes. The superiority of A over B does not, however, become more marked as the weight increases

in the same manner as exhibited by $K^{\frac{2}{4}}\eta^{\frac{1}{2}}$. This is due to the distance between the free plate surface and the composite plate neutral surface being greater for the lower density treatment A than for B. As the weight of treatment increases, this distance with treatment A becomes increasingly greater than that with B. It is this latter effect that causes $K\eta\alpha^{-1}$ for treatment A to be slightly inferior to that for B throughout the weight range despite the superiority of $K\eta$ for A above a weight ratio of about 0.75.

IV.3 A Comparison of Different Amounts of the Same Treatment

The criteria considered in the previous section did not contain the mass ratio term θ. This was omitted since equal weights of different treatments were being compared. Now a damping treatment may add considerably to the weight of the thin plating of aeroplane structures. When considering the effect on the response of varying the quantity of a given treatment, the mass effect must therefore be included in the criterion used. Figure 26 shows some of the criteria considered in the other figures, but with the appropriate mass ratio term included.

The criteria relating to both boundary layer noise and the noise transmitted through a single plate increase steadily throughout the range of weights considered, but comparison with Figure 24 shows that over the upper part of the range the increase is due mostly (if not entirely) to the increasing mass. The random reaction force criterion shows that the treatments have a maximum effect upon random reaction forces at optimum treatment weights of about 0.6 and 0.75 of the weight of the plate for treatments A and B respectively. These compare with optimum weights of about 1.5 and 2.0 required to give maximum values to η for these treatments.

The criterion relating to harmonic sound pressure transmitted through a finite plate ($\theta\eta$) will not exhibit the maximum shown by η alone for these treatments, but will rise steadily above a relative treatment weight of about 1, roughly in proportion to θ.

Equation 3.4 shows that the harmonic displacement amplitude, and therefore the corresponding surface bending stress are independent of θ; the relevant curves of Figures 23 and 25 may therefore be considered in the present discussion. Each of these curves is monotonically increasing, implying that increasing the amount of the treatment will always provide a further reduction in the amplitude of resonant vibration and stress. The r.m.s. (random) displacement and stress are dependent upon the mass ratio θ, the corresponding criteria for the damping treatment being $\theta^{\frac{1}{4}}R^{\frac{2}{4}}\eta^{\frac{1}{2}}$ and $\theta^{\frac{1}{4}}K^{\frac{2}{4}}\eta^{\frac{1}{2}}\alpha^{-1}$. Since θ is raised to a positive power, these expressions will still increase monotonically with increasing weight of treatment.

IV.4 Response Reductions Obtainable Using the Treatments

We now use the calculated values of the criteria in conjunction with the initial (untreated) structural damping values of section II.6 in order to estimate response reductions. For this we require the expressions quoted in section III.5, in which the mass ratio term must be included in the criteria. The initial loss factor, η_i, to be taken in these expressions is 2 x the initial damping ratio, and will therefore have the minimum value of 0.01 and the maximum value of 0.025. η_i^2 will then be 0.1 and 0.16 respectively.

The responses having criterion values which increase monotonically can obviously be reduced by any required amount if sufficient treatment is added. We shall therefore consider the reductions of these responses when the weight of the treatment is 50% of the plate weight. The random reaction force criterion, however, passes through a maximum value. The response reduction corresponding to this value will be quoted.

The following table sets out the percentage reductions of selected responses under the above conditions:

Response	Treatment A		Treatment B	
	Low η_i	High η_i	Low η_i	High η_i
Random Surface Stress	34%	71%	84%	74%
Random Reaction Force	64%	43%	74%	59%
Boundary Layer Noise	80%	68%	82%	72%
Harmonic Displacement	96%	90%	96.5%	91%

These reductions have been obtained from the stiffness ratios and loss factors of a simple plate with no reinforcing such as stringers and frames. When the plate forms part of a stringer reinforced structure, the stringers may contribute considerably to the total potential energy of the coupled plate-stringer modes of vibration. If the plate stiffness is now increased by the addition of the damping treatment to K times its initial stiffness, the overall modal stiffness will increase by a smaller factor. The stiffness ratios used above are therefore overestimates of those to be expected in reinforced structures. Likewise, the modal loss factor increments arising from the addition of the treatment to the plate must be less than the plate loss factors calculated above, since the loss factor of the whole system cannot under any circumstances be greater than that of its sub-system with the greatest loss factor.

It follows therefore that the response reductions quoted above for the surface stress, boundary layer noise and harmonic displacement are certainly over-estimates of the reductions to be obtained on real structures. The random inertia force reduction is also most probably overestimated, but being proportional to the fourth root of the stiffness, a stiffness reduction will cause a slight response reduction. Since the fourth root is involved, however, this is a small effect in the present argument and will not compare with the effect of the over-estimated loss factor. The reductions quoted in the "Low η_i" columns are therefore greater than those which may be obtained with real reinforced structures, and therefore set an upper bound to the response reductions which can be achieved with these treatments.

IV.5 Concluding Remarks

In comparing the effectiveness of the two treatments, it has been shown that with relatively small weights of damping treatment, the treatment giving the greatest loss factor to the whole system is superior as judged by each

of the criteria. This follows from the fact that at small relative weights the stiffness and mass increases are negligible for the particular damping configurations considered. The loss factor is then the only parameter which changes appreciably when the treatment is added. At greater relative weights, it has been shown that one treatment having a lower density, a lower stiffness and a lower material loss factor than another can nevertheless be more efficient (on an equal weight basis) in attenuating vibration displacement amplitudes and plate surface bending stresses.

The criteria relating to harmonic and random reaction forces show that there are optimum quantities of treatment to give the greatest effects, but the optimum quantities differ for the harmonic and random conditions. If the amount actually used is mid-way between two values, (the geometric mean, say) the reduction in effectiveness below the maximum realizeable is very slight. The other criteria considered are all monotonically increasing with increase of treatment weight, implying that increasing the amount of treatment used will always further reduce the response.

The implications of these results are that when damping treatments are being considered for use on light aluminium structures, their effectiveness cannot be sufficiently defined by stating only the loss factor obtainable from a given amount of the treatment. The factor by which the stiffness of the structure is increased must also be given. This implies that the results of the standard Geiger test, whereby the time rate of decay of a treated steel plate is given as the measure of the effectiveness of the treatment, is also insufficient. This time rate of decay is (in effect) but an alternative form of presenting the value of the loss factor (see Kerwin (29)).

The fact that a poorer quality treatment has been shown to have a superior effect, in some instances, than one of higher quality, suggests that the optimum design or compounding of a treatment will be different depending on the particular vibration response quantity it is required to attenuate. It may be that damping treatments can be developed further along these lines, a different treatment being designed and recommended for different applications.

The inclusion of the mass and stiffness effects into the criteria for assessing damping treatments will be more than ever important when "space" damping techniques are being considered. In these techniques, the damping layer is separated from the plate by a shear-stiff, light spacer layer. Very large stiffness increases can then be expected for relatively small weights of treatment.

Chapter V

The Damped Sandwich Plate

V.1 Scope of Chapter V

This chapter presents the theory of the response to external pressure fluctuations of a flat, rectangular sandwich plate with a damped core and simply-supported edges. The equations of motion of the plate are derived, and their solutions are found in terms of a series of sinusoidal modes of transverse displacement. Expressions are derived for the displacement in each mode and also for the surface stresses in the face-plates. From these are developed expressions for the loss factor and stiffness ratio for each mode.

Consideration is then given to the dependence of the modal loss factor and the resonant and random response criteria upon the wavelength, core thickness and core dynamic shear modulus. The optimum design of damped plates is sought. Comparisons are made between the responses of damped sandwich plates with different core thicknesses of optimum stiffness, and the response of a solid plate of equal weight. A comparison is also made between the stiffness at high and low frequencies of the two plates. It appears that maximum damping and minimum response can only be obtained at the expense of the static (i.e. very low frequency) stiffness. The sensitivity of the response to effects of temperature on the core properties is also considered.

V.2 Review of Former Investigations

A theoretical analysis of the damping of a sandwich plate was first conducted by Plass (23), who considered the face plates to be thin membranes and restricted the work to a one-dimensional problem. In effect, therefore, a sandwich beam was considered. No optimum design of the plate was sought.

Ross, Kerwin and Dyer (24) considered the damped sandwich beam with finite thickness face-plates, but the core thickness was taken to be small compared with the face-plates. The flexural loss factor was the only damping 'parameter' discussed and was shown to be dependent on both flexural wavelength and core thickness. The core damping was introduced by ascribing to the core the complex shear modulus, $G(1 + i\beta)$. The equation of motion of the beam was not derived in this analysis.

Kurtze and Watters (25) have analysed the acoustic transmission loss characteristics of sandwich beams and have shown that higher flexural loss factors can be obtained with this arrangement than with unconstrained layers. They show, however, that the sandwich configuration is inferior to the unconstrained treatment as far as frequency response is concerned. This follows from the dependence of the loss factor on the flexural wavelength.

More recently, Yu (26) has analysed the the damping of two dimensional flat plates, including hysteretic damping (complex moduli) in both core and face-plates. Deriving the equations of motion of the plate, he proceeds to discuss the damping of the plate in terms of the logarithmic decrement for which he obtains expressions involving the (different) loss factors of each of the three layers. The actual response of the plate to time-dependent loading is not considered.

Freudenthal and Bienick (27) have analysed the forced vibrations of flat and curved damped sandwich plates, considering the displacement amplitudes excited by harmonic loading. A general response theory is presented based on the 'normal mode' approach, whereby the total response is expressed as the infinite series of the responses in the individual normal modes. No optimum configurations are investigated, nor are the effects of varying the core thickness or dynamic properties.

V.2 The Response of a Damped Sandwich Plate to Normal Fluctuating Pressures

V.2.1 Derivation of the Differential Equations of Motion

The sandwich plates to be considered in this chapter are flat and rectangular, simply supported along all four edges. Acting on the plate are harmonic pressures which may vary in amplitude over the surface. The two face-plates are of uniform and equal thickness h_1, and have a Young's Modulus of E. The soft core has a constant thickness h_2 and is considered to be isotropic with the complex shear modulus $G_c = G(1 + i\beta)$. The following restrictions are made upon the strains and stresses within the plate:

(i) There is no significant direct strain in the core face-plates perpendicular to the plane of the face-plates. Both the plates and the core therefore deflect by the same amount normal to the plate surface.

(ii) There is no significant shear strain across the depth of the face-plates i.e. τ_{xz} and τ_{yz} in the face-plates are ignored. (See Figure 25 for the notation used).

(iii) Direct stresses in the soft core parallel to the plate surface are very much smaller than the stresses in the face-plates, and may therefore be ignored.

Inertia forces associated with both normal and in-plane accelerations are initially included, but the in-plane inertia forces (corresponding to the usual 'rotatory' inertia effects) are subsequently dropped for simplicity. Figure 25 shows the complete system of co-ordinate axes, displacements, stresses and moments used in the analysis. It will be noticed that τ_{xy} is the shear stress in the plate, whereas τ_{xz} and τ_{yz} are the shear stresses in the core. No further distinction need be made here between core and face-plate shear stresses as neither τ_{xy} in the core nor τ_{xz} and τ_{yz} in the face-plates are referred to.

Consider now the equilibrium of the moments, shears and normal loading on the element $h_1.dx.dy$ of the upper face-plate. The normal loading derives from the normal tensile (or compressive) stress in the core together with the externally applied pressure on the outside surface. Denote the total downward acting loading on the upper plate element by q_1. Acting on the lower surface of this element are shear tractions of magnitude $\tau_{xz}\,dx.dy$ and $\tau_{yz}\,dx.dy$. For equilibrium of these tractions and the loading with the M_x, M_y, and M_{xy} moments on the edges of the element, it is necessary that

$$\frac{\partial^2 M_x}{\partial x^2} - 2\frac{\partial^2 M_{xy}}{\partial x \partial y} + \frac{\partial^2 M_y}{\partial y^2} = -q_1 - \frac{h_1}{2}\left\{\frac{\partial \tau_{xz}}{\partial x} + \frac{\partial \tau_{yz}}{\partial y}\right\} \quad \ldots(5.1)$$

Now

$$\tau_{xz} = G_c\left\{\frac{\partial w}{\partial x} + \frac{\partial u}{\partial z}\right\}_{core} \quad \& \quad \tau_{yz} = G_c\left\{\frac{\partial w}{\partial y} + \frac{\partial v}{\partial z}\right\}_{core} \qquad \ldots(5.2)$$

and since the core direct stresses, σ_x and σ_y, and the core x and y inertia forces are to be neglected, τ_{xz} and τ_{yz} will not vary over the depth of the core. Further, w does not vary over the core depth. It follows that $\partial u/\partial z$ is constant across the depth and is given by

$$\frac{\partial u}{\partial z} = \frac{\left\{u_2 - \frac{h_1}{2}\frac{\partial w}{\partial x}\right\} - \left\{u_1 - \frac{h_1}{2}\frac{\partial w}{\partial x}\right\}}{h_3} \qquad \ldots(5.3)$$

where u_1 and u_2 are the x-wise displacements of the mid-surfaces of the top and bottom plates respectively. Hence

$$\tau_{xz} = G_c\left\{\left(1 + \frac{h_1}{h_3}\right)\frac{\partial w}{\partial x} + \frac{u_2 - u_1}{h_3}\right\} \qquad \ldots(5.4)$$

Similarly, it is shown that

$$\tau_{yz} = G_c\left\{\left(1 + \frac{h_1}{h_3}\right)\frac{\partial w}{\partial y} + \frac{v_2 - v_1}{h_3}\right\} \qquad \ldots(5.5)$$

where v_1 and v_2 are the y-wise displacements of the top and bottom plate mid-surfaces. Substituting from Equations 5.4 and 5.5 into Equation 5.1, and replacing M_x, M_y, and M_{xy} by the usual expressions involving w and D (the face-plate flexural rigidity) the face-plate equation becomes

$$D\left\{\frac{\partial^4 w}{\partial x^4} + 2\frac{\partial^4 w}{\partial x^2 \partial y^2} + \frac{\partial^4 w}{\partial y^4}\right\} = q_1 + \frac{G_c h_1}{2h_3}\left\{(h_1 + h_3)\left(\frac{\partial^2 w}{\partial x^2} + \frac{\partial^2 w}{\partial y^2}\right) - 2\left(\frac{\partial u_1}{\partial x} + \frac{\partial v_1}{\partial y}\right)\right\} \qquad \ldots(5.6)$$

in which have been used the relationships $u_2 = -u_1$, $v_2 = -v_1$. These are readily shown to be true (28) for the flexural modes to be considered in this chapter. An equation similar to 5.6 holds for the bottom plate, subjected to the total normal loading q_2.

Next consider the equilibrium of the plate element under the action of the surface shear tractions, the edge direct stresses and the in-plane inertia forces. The direct stresses on the edges may be considered as consisting of uniform stresses σ_{x1}, σ_{y1} (the 'mid-plane' stresses) upon which are superimposed plate bending stresses deriving from M_x, M_y and varying linearly across the plate depth from zero at the mid-plane surface. Likewise, the shear stresses on the edges consist of mid-plane shear stresses τ_{xy1}, together with linearly varying shear stresses deriving from the M_{xy} moment which are zero at the mid-plane surface. For equilibrium of the forces in the x and y directions, only the mid-plane

stresses need be considered. For equilibrium in the x-direction:

$$h_1\left\{\frac{\partial \sigma_{x1}}{\partial x} + \frac{\partial \tau_{xy1}}{\partial y}\right\} = \rho_p h_1 \frac{\partial^2 u_1}{\partial t^2} - \tau_{xz} \qquad \ldots(5.7)$$

and in the y-direction

$$h_1\left\{\frac{\partial \sigma_{y1}}{\partial y} + \frac{\partial \tau_{xy1}}{\partial x}\right\} = \rho_p h_1 \frac{\partial^2 v_1}{\partial t^2} - \tau_{yz} \qquad \ldots(5.8)$$

The stress-strain relationships for the plates are

$$\sigma_{x1} = \frac{E}{(1-\nu^2)}\left\{\frac{\partial u_1}{\partial x} + \nu \frac{\partial v_1}{\partial y}\right\}$$

$$\sigma_{y1} = \frac{E}{(1-\nu^2)}\left\{\frac{\partial v_1}{\partial x} + \nu \frac{\partial u_1}{\partial y}\right\}$$

$$\tau_{xy1} = \frac{E}{2(1+\nu)}\left\{\frac{\partial v_1}{\partial x} + \frac{\partial u_1}{\partial y}\right\}$$

Using these together with Equations 5.4 and 5.5, the equilibrium equations 5.7 and 5.8 become

$$\frac{E}{(1-\nu^2)}\frac{\partial^2 u_1}{\partial x^2} + \frac{E}{2(1+\nu)}\frac{\partial^2 u_1}{\partial y^2} - \frac{2G_c}{h_1 h_3} u_1 - \rho_p \frac{\partial^2 u_1}{\partial t^2} + \frac{E}{2(1-\nu)}\frac{\partial^2 v_1}{\partial x \partial y}$$

$$= -\frac{G_c}{h_1 h_2}(h_1 + h_3)\frac{\partial w}{\partial x} \qquad \ldots(5.9)$$

and

$$\frac{E}{(1-\nu^2)}\frac{\partial^2 v_1}{\partial y^2} + \frac{E}{2(1+\nu)}\frac{\partial^2 v_1}{\partial x^2} - \frac{2G_c}{h_1 h_3} v_1 - \rho_p \frac{\partial^2 v_1}{\partial t^2} + \frac{E}{2(1-\nu)}\frac{\partial^2 u_1}{\partial x \partial y}$$

$$= -\frac{G_c}{h_1 h_3}(h_1 + h_3)\frac{\partial w}{\partial y} \qquad \ldots(5.10)$$

Next consider the equilibrium of the direct and shear stresses normal to the plate surface. Suppose the core exerts a tensile stress σ_{z1} on the bottom surface of the top plate, and a tensile stress of σ_{z2} on the upper surface

of the bottom plate. The normal inertia force per unit area on each of the face plates is

$$-\rho_p h_1 \frac{\partial^2 w}{\partial t^2}$$

(i.e. acting in the negative z-direction). In addition to these loadings, there will in general be an external pressure $p_1(x,y,t)$ acting on the outer surface of the upper plate and a pressure $p_2(x, y, t)$ acting on the bottom surface of the lower plate. The total downward acting pressure, applied externally, is therefore

$$p_1(x,y,t) - p_2(x,y,t) = p(x,y,t)$$

The total loadings on each plate are then

$$q_1 = p_1(x,y,t) - \rho_p h_1 \frac{\partial^2 w}{\partial t^2} + \sigma_{z1} \qquad \ldots(5.11)$$

$$q_2 = -p_2(x,y,t) - \rho_p h_1 \frac{\partial^2 w}{\partial t^2} - \sigma_{z2} \qquad \ldots(5.12)$$

An element of the core, $h_3.dx.dy$ is subjected to the normal tensile stresses σ_{z1} and σ_{z2} on its top and bottom faces, and to the transverse inertia force

$$-\rho_c h_3 \frac{\partial^2 w}{\partial t^2} dx\,dy$$

For equilibrium of this element, we must have

$$-h_3\left\{\frac{\partial \tau_{xz}}{\partial x} + \frac{\partial \tau_{yz}}{\partial y}\right\} = -\rho_c h_3 \frac{\partial^2 w}{\partial t^2} - \sigma_{z1} + \sigma_{z2} \qquad \ldots(5.13)$$

Adding Equations 5.11, 5.12 and 5.13, and putting $2\rho_p h_1 + \rho_c h_3 = \mu$ (the total mass per unit area of the whole plate), yields

$$q_1 + q_2 = p(x,y,t) - \mu \frac{\partial^2 w}{\partial t^2} + h_3\left\{\frac{\partial \tau_{xz}}{\partial x} + \frac{\partial \tau_{yz}}{\partial y}\right\}$$

Since the two face plates deflect transversely by the same amount it is necessary that $q_1 = q_2$. Hence

$$q_1 = \frac{p(x,y,t)}{2} - \frac{\mu}{2}\frac{\partial^2 w}{\partial t^2} + \frac{h_3}{2}\left\{\frac{\partial \tau_{xz}}{\partial x} + \frac{\partial \tau_{yz}}{\partial y}\right\} \qquad \ldots(5.14)$$

Substituting this into Equations 5.6 and using Equations 5.4 and 5.5 yields

$$D\left\{\frac{\partial^4 w}{\partial x^4} + 2\frac{\partial^4 w}{\partial x^2 \partial y^2} + \frac{\partial^4 w}{\partial y^4}\right\} - \frac{G_c(h_1+h_3)}{2h_3}\left\{(h_1+h_3)\left(\frac{\partial^2 w}{\partial x^2} + \frac{\partial^2 w}{\partial y^2}\right) - 2\left(\frac{\partial u_1}{\partial x} + \frac{\partial v_1}{\partial y}\right)\right\} + \frac{\mu}{2}\frac{\partial^2 w}{\partial t^2} = \frac{p(x,y,t)}{2} \qquad \ldots(5.15)$$

Equations 5.9, 5.10 and 5.15 constitute the differential equations of motion which must be satisfied by the displacement components u_1, v_1 and w when the plate is vibrating under the action of the fluctuating pressure $p(x,y,t)$.

V.2.2 Solution of the Differential Equations for a Simply Supported Rectangular Plate under Harmonic Excitation

The modes of free vibration of an undamped sandwich plate with these edge conditions are represented by

$$\left.\begin{aligned} u_1 &= U_{mn}\cos\frac{n\pi x}{a}\sin\frac{m\pi y}{b}\,e^{i\omega t} \\ v_1 &= V_{mn}\sin\frac{n\pi x}{a}\cos\frac{m\pi y}{b}\,e^{i\omega t} \\ w &= W_{mn}\sin\frac{n\pi x}{a}\sin\frac{m\pi y}{b}\,e^{i\omega t} \end{aligned}\right\} \qquad \ldots(5.16)$$

where a is the length and b is the breadth of the plate. The ratios $U_{mn} : V_{mn} : W_{mn}$ have specific (real) values for each mode. The forced motion of a damped plate may be represented by an infinite series of modes of the type of Equations 5.16, but the ratios $U_{mn} : V_{mn} : W_{mn}$ will not be the same as for the natural undamped modes, and will be complex, indicating that the displacements are not in phase with one another.

In order to find the coefficients W_{mn} (i.e. the amplitudes of transverse motion of the modes), first represent the pressure distribution on the plate by the infinite series

$$p(x,y,t) = \sum_m \sum_n A_{mn}\sin\frac{n\pi x}{a}\sin\frac{m\pi y}{b} \qquad \ldots(5.17)$$

where the coefficient A_{mn} varies harmonically if $p(x,y,t)$ varies harmonically. If Equations 5.16 and 5.17 are substituted into Equation 5.15, it is seen that the U's, V's and W's are independent of the B's, C's and D's and the A's are the only coefficients of the pressure series that are required. These are easily shown to be given by

$$A_{mn} = \frac{4}{ab}\int_0^b\int_0^a p(x,y,t)\sin\frac{n\pi x}{a}\sin\frac{m\pi y}{b}\,dx\,dy \qquad \ldots(5.18)$$

Furthermore, the substitution of Equations 5.16 and 5.17 into Equations 5.9, 5.10 and 5.15 yields a set of equations for U_{mn}, V_{mn}, W_{mn} which are completely independent of the set for U_{rs}, V_{rs} and W_{rs}, etc. i.e. there is no coupling between the modes of transverse displacement, damping or otherwise.

Attention will now be restricted to harmonic pressure fluctuations, so that $A_{mn} = |A_{mn}| e^{i\omega t}$. Equations 5.9 and 5.10 are now used to obtain U_{mn} and V_{mn} in terms of W_{mn}. Notice that the third and the fourth terms on the left hand sides of Equations 5.9 and 5.10 become

$$\left\{\frac{2G_c}{h_1 h_3} - \rho_p \omega^2\right\} U_{mn} e^{i\omega t} \quad \& \quad \left\{\frac{2G_c}{h_1 h_3} - \rho_p \omega^2\right\} V_{mn} e^{i\omega t}$$

The terms $\rho_p \omega^2$ in these will be neglected from now on. i.e. we ignore the inertia forces in the planes of the face-plates, and so suppress the appearance of "thickness-shear" modes in the final results. This is justifiable so long as

$$\omega^2 \ll \frac{2G_c}{\rho_p h_1 h_3} \quad (= \omega_{ts}^2)$$

ω_{ts} is the frequency of the 'pure thickness-shear mode' in the absence of any coupling with the transverse motion. It will almost certainly always be well above the frequency of the fundamental plate flexural mode for any practical damped plate configuration, but a check should always be made to ensure that this condition is being satisfied when calculations are made on the basis of the subsequent theory.

Introducing the symbols $r = \left(\frac{b}{m}\right)\Big/\left(\frac{a}{n}\right)$

and
$$\Psi_{mn} = \frac{r^2+1}{1-\nu^2} \cdot \frac{\pi}{2} \cdot \frac{E}{G_c} h_1 h_3 \left(\frac{m}{b}\right)^2 \qquad \ldots(5.19)$$

Equations 5.9 and 5.10 yield

$$U_{mn} = + W_{mn} \frac{\pi m r (h_1 + h_3)}{2b (1 + \Psi_{mn})} \qquad \ldots(5.20)$$

and
$$V_{mn} = + W_{mn} \frac{\pi m (h_1 + h_3)}{2b (1 + \Psi_{mn})} \qquad \ldots(5.21)$$

Now using these together with Equations 5.16 and substituting into Equation 5.15, it is found that

$$W_{mn}\left\{2D\frac{\pi^4}{b^4} m^4 (r^2+1)^2 \left[1 + \frac{3(1+\tau)^2}{1+\Psi_{mn}}\right] - \mu\omega^2\right\} = |A_{mn}| \qquad \ldots(5.22)$$

where $\tau = h_3/h_1$

For a visco-elastic (high-polymer) core material, G_c will be complex and equal to $G(1 + i\beta)$, and Ψ_{mn} will therefore also be complex. Furthermore E for the plates may be complex, but when light alloy face plates are considered, the imaginary component may be neglected. The term within the brackets on the left hand side of Equation 5.22 may therefore be written in the form

$$\left[1 + \frac{3(1+\tau)^2}{1 + \Psi_{mn}} \right] = 4 K_{mn} (1 + i\eta_{mn}) \qquad \ldots(5.23)$$

which equation defines the symbols K_{mn} and η_{mn}. The explicit forms of K_{mn} and η_{mn} will be considered later, and they will be identified as the modal stiffness ratio and loss factor respectively.

Equation 5.22 permits the evaluation of all the 'generalised co-ordinates' W_{mn}, representing the transverse displacements of the plate in its different modes. The resonant frequency, ω_{mn}, of the mode mn is given by the vanishing of the real part of the left hand side of Equation 5.22. i.e.

$$\omega_{mn}^2 = \frac{2D\pi^4}{\mu b^4} m^4 (r^2+1)^2 4 K_{mn} \qquad \ldots(5.24)$$

The term

$$\frac{2D\pi^4}{\mu b^4} m^4 (r^2+1)^2 4 K_{mn}$$

is proportional to the generalised stiffness of the mn^{th} mode; μ is proportional to the generalised mass, and

$$\frac{2D\pi^4}{\mu b^4} m^4 (r^2+1)^2 4 K_{mn} \eta_{mn}$$

to the generalised hysteretic damping coefficient.

Now consider a single, solid plate of thickness $2h_1$ and of Young's Modulus E, subjected to the same harmonic pressure loading $p(x,y,t)$. In the absence of damping, the response of this plate in the mn^{th} mode is given by

$$W_{mn} \left\{ 8D \frac{\pi^4}{b^4} m^4 (r^2+1)^2 - \mu\omega^2 \right\} = |A_{mn}| \qquad \ldots(5.25)$$

in which

$$8D \frac{\pi^4}{b^4} m^4 (r^2+1)^2$$

(to be denoted by k_{mn}) is proportional to the generalised stiffness of the solid plate. (D still corresponds to the plate of thickness h_1). It is now evident that the factor K_{mn} is the ratio of the generalised stiffness of the damped sandwich plate in the mn^{th} mode to that of the solid plate of thickness $2h_1$ in the same mode, and is therefore the "stiffness ratio" corresponding to the mn^{th} mode.

Equation 5.22 may now be written in the form

$$W_{mn} = \frac{|A_{mn}|}{k_{mn} K_{mn} (1 + i\eta_{mn}) - \mu\omega^2} \qquad \ldots(5.26)$$

which shows clearly that η_{mn} is the modal loss factor corresponding to the mn^{th} mode. The total transverse deflection of the plate at any point and instant is

$$w(x,y,t) = \sum_{m=1}^{\infty}\sum_{n=1}^{\infty} \frac{|A_{mn}| e^{i\omega t} \sin\frac{n\pi x}{a} \sin\frac{m\pi y}{b}}{k_{mn} K_{mn}(1+i\eta_{mn}) - \mu\omega^2} \qquad \ldots(5.27)$$

V.2.3 The Expressions for the Stiffness Ratio and the Loss Factor

The stiffness ratio K_{mn} and the loss factor η_{mn} are defined by Equation 5.23. When the complex shear modulus $G(1 + i\beta)$ is used in $\bar{\Psi}_{mn}$ (Equation 5.19), we may write

$$\bar{\Psi}_{mn} = \frac{\Psi_{mn}}{(1 + i\beta)} \qquad \ldots(5.28)$$

in which Ψ_{mn} is real and contains the real part only of the core shear modulus. i.e.

$$\Psi_{mn} = \frac{(r^2+1)}{(1-\nu^2)} \cdot \frac{\pi^2}{2} \cdot \frac{E}{G} \left(\frac{h_1}{b/m}\right)^2 \tau \qquad \ldots(5.29)$$

This is one of the most important parameters on which the sandwich plate stiffness and damping depend. It represents, in effect, the ratio of the direct stiffness of a length b/m of unit width of a face plate to the real part of the shear stiffness of the same length and width of the core. Substituting Equation 5.28 into Equation 5.23 and separating the left hand side into real and imaginary parts, it is found that

$$K_{mn} = \frac{1}{4}\left\{1 + \frac{3(1+\tau)^2(1 + \Psi_{mn} + \beta^2)}{(1+\Psi_{mn})^2 + \beta^2}\right\} \qquad \ldots(5.30)$$

$$\eta_{mn} = \frac{\beta \Psi_{mn} \{3(1+\tau)^2\}}{(1+\Psi_{mn})^2 + \beta^2 + 3(1+\tau)^2(1 + \Psi_{mn} + \beta^2)} \qquad \ldots(5.31)$$

This expression for the loss factor is of the same form as that derived by Ross, Kerwin and Dyer (26), with $1/\Psi_{mn}$ equivalent to their "shear parameter". However, the factor $(r^2 + 1)/(1 - \nu^2)$ included in Ψ_{mn} converts their "beam" shear parameter to a two-dimensional finite plate shear parameter. Detailed consideration of R_{mn} and η_{mn} will be given later.

V.2.4 The Surface Bending Stresses in the Sandwich Plate

The total direct stress at the outer surface of one of the face-plates consists of the sum of the mid-surface stress, σ_{x1} or σ_{y1}, together with the bending stress, σ_{bx} or σ_{by}, due to the face-plate bending about its own neutral plane. At the outer surface of the top plate the bending stress in the x direction is

$$\sigma_{bx} = \frac{Eh_1}{2(1-\nu^2)}\left\{\frac{\partial^2 w}{\partial x^2} + \nu\frac{\partial^2 w}{\partial y^2}\right\}$$

$$= \sum_{m=1}^{\infty}\sum_{n=1}^{\infty} -\frac{Eh_1}{2(1-\nu^2)}\frac{\pi^2 m^2}{b^2}\left\{\nu + r^2\right\} W_{mn} \sin\frac{n\pi x}{a} \sin\frac{m\pi y}{b}$$

At the mid-surface of the top plate

$$\sigma_{x1} = \frac{E}{(1-\nu^2)}\left\{\frac{\partial u_1}{\partial x} + \nu\frac{\partial v_1}{\partial y}\right\}$$

which, from Equations 5.16, 5.20 and 5.21 becomes

$$\sigma_{x1} = \sum_{m=1}^{\infty}\sum_{n=1}^{\infty} -\frac{Eh_1}{2(1-\nu^2)}\frac{\pi^2 m^2}{b^2}(\nu + r^2)\left\{\frac{(1+\tau)}{1+\Psi_{mn}}\right\} W_{mn} \sin\frac{n\pi x}{a} \sin\frac{m\pi y}{b}$$

Hence

$$\sigma_{x1} + \sigma_{bx} =$$

$$\sum_{m=1}^{\infty}\sum_{n=1}^{\infty} -\frac{Eh_1}{2(1-\nu^2)}\frac{\pi^2 m^2}{b^2}(\nu + r^2)\left\{1 + \frac{(1+\tau)}{1+\Psi_{mn}}\right\} W_{mn} \sin\frac{n\pi x}{a} \sin\frac{m\pi y}{b}$$

Notice that the stress σ_{x1} is not in phase with σ_{bx}, since Ψ_{mn} is a complex quantity. Now it is the amplitude of the total stress which is of greatest importance, rather than its two components. If only one mode of vibration (the mn^{th}) is being excited signficantly, the amplitude of the corresponding total stress becomes (using Equation 5.28)

$$- |\sigma_{total}| =$$

$$\frac{Eh_1}{2(1-\nu^2)} \frac{\pi^2 m^2}{b^2} (\nu + r^2) \left\{ \frac{(2 + \psi_{mn} + \tau)^2 + \beta^2 (2+\tau)^2}{(1+\psi_{mn})^2 + \beta^2} \right\}^{\frac{1}{2}} W_{mn} \sin \frac{n\pi x}{a} \sin \frac{m\pi y}{b}$$

...(5.32)

The amplitude of the surface stress in a solid plate of thickness $2h_1$, vibrating in the mode

$$W_{mn} \sin \frac{n\pi x}{a} \sin \frac{m\pi y}{b}$$

is

$$\frac{Eh_1}{(1-\nu^2)} \frac{\pi^2 m^2}{b^2} (\nu + r^2) W_{mn} \sin \frac{n\pi x}{a} \sin \frac{m\pi y}{b}$$

Hence, given a sandwich plate having face plates of thickness h_1 and a solid plate of thickness $2h_1$, each vibrating in the same mode and with the same amplitude of transverse motion, the ratio of the amplitudes of the surface stresses is given by

$$\alpha_{mn} = \frac{|\sigma_{sandwich}|}{|\sigma_{solid}|} = \frac{1}{2} \left\{ \frac{(2 + \psi_{mn} + \tau)^2 + \beta^2 (2+\tau)^2}{(1+\psi_{mn})^2 + \beta^2} \right\}^{\frac{1}{2}} \quad ...(5.33)$$

which is the modal "stress ratio" required in certain response criteria.

V.3 The Dependence of the Plate Dynamic Properties on the Wavelength, Core Thickness and Core Damping Properties

V.3.1 The Stiffness Ratio and Plate Loss Factor

It has been shown in section V.2.3 that κ_{mn} and ψ_{mn} depend upon τ, β and ψ_{mn}. Variation of the core shear modulus, G, changes ψ_{mn} (see Equation 5.29), an increase of G reducing ψ_{mn}. ψ_{mn} also depends on the ratio of the plate thickness to the semi-wavelength ($h_1.m/b$) and on the ratio of the lateral to longitudinal wavelength, r. A change of the value of ψ_{mn} may therefore be interpreted as a change of G, or of the lateral or longitudinal wavelengths. From now on, the suffix mn will be dropped for convenience.

Figures 28 and 29 show κ and η plotted against ψ for three different values of β, the value of τ being chosen arbitrarily at 1.0.

The variation of the stiffness ratio with the extreme values of ψ may be explained in the following way:

As ψ decreases, the core shear stiffness increases relative to the plate direct stiffness and for a given transverse displacement the core shear strain is reduced. In the limit as $\psi \rightarrow 0$ the core shear strain vanishes and the bending strain distribution across a plate section corresponds with the two-dimensional equivalent of "plane sections remaining plane and normal to the neutral surface". (See Figure 30a). The neutral surface in this limiting case is the mid-plane of the whole sandwich. This accounts for the upper asymptotic behaviour of K . This upper value of K may be derived very simply by using for the sandwich plate flexural rigidity the expression for

$$\frac{E}{(1 - \nu^2)} \times \text{second moment of area of unit width of both face-plates about the mid-surface of the sandwich.}$$

As ψ increases, the relative core shear stiffness decreases and for a given transverse displacement the core shear stress is reduced. This is accompanied by a reduced direct stress in the mid-plane of the face-plates. In the limit as $\psi \rightarrow \infty$, the core shear stress vanishes altogether and so also do the mid-plane stresses and direct displacements (u and v) in the face-plates. The two face-plates may then be said to be bending "independently by the same amount", each plate bending about its own mid-plane as the neutral surface. (See Figure 30b). The flexural rigidity of the sandwich plate is now equal to the sum of the flexural rigidities of the two face-plates on their own, and the lower asymptotic value of K may be calculated on this basis.

The explanation may be presented in an alternative form using a simple spring-damper analogue model of the plate. The plate flexural stiffness derived from the two parallel systems:

(a) The low flexural stiffness of each plate about its own mid-plane neutral surface, involving no mid-plane strain in the plates.

(b) The high flexural stiffness of both plates about the sandwich mid-plane surface, involving mid-plane strains in the plates.

The two systems are coupled by the complex shear stiffness of the core. The analogue of the system is shown in Figure 30c, in which k_a represents the total stiffness of (a) above, k_b represents (b) and $k_c(1 + i\beta)$ represents the complex stiffness of the core. The displacement of point X represents W_{mn} and that of point Y represents U_{mn} or V_{mn} . Now an increase of ψ is represented by an increase of k_c. With very high k_c , therefore, $(k_c \gg k_b)$ the total stiffness at point X is nearly equal to $k_a + k_b$. With very low k_c , the total stiffness hardly exceeds k_a .

This simple analogue shows that the true nature of the mechanism of the plate stiffness and damping centres on the coupling of one stiff system with another flexible system by means of an elementary spring damper unit. The mass at X represents the transverse inertia of the plate, whereas a mass at Y may be included to represent the (omitted) longitudinal inertia of the plates.

Turning now to the loss factor η , Figure 31 shows that it increases in direct proportion to low values of ψ , but in inverse proportion to high values of ψ . Maximum values of η occur in the range of $\psi = 5$ to 8 . Plotting K and η against ψ for other values of τ , similar sets of curves are obtained, but η has different maximum values occurring at

different values of ψ . Differentiating equation 5.31 with respect to ψ shows that the maxima occur when

$$\psi = (1 + 3(1+\tau)^2)^{\frac{1}{2}} (1+\beta^2)^{\frac{1}{2}} = \psi_{opt.\eta} \qquad \ldots(5.34)$$

and the corresponding maximum values of the plate loss factors are

$$\eta_{max} = \frac{\beta . 3(1+\tau)^2}{2(\psi_{opt.\eta}+1) + 3(1+\tau)^2} \qquad \ldots(5.35)$$

Figure 31 shows these values of η_{max} plotted against the thickness ratio τ. Within the practical range of τ , η_{max} increases with increasing τ . At very high values of τ , η_{max} approaches the value of β .

To explain the manner in which η varies with ψ , it is convenient to use the fact that the plate loss factor is proportional to the cyclic energy dissipation divided by the maximum amount of potential energy stored in the course of one cycle. (There are certain problems of interpretation of "maximum potential energy" when the strains in the face-plates are not all in phase with one another, but the general argument that follows is unaffected by this). At high values of ψ , when the two plates bend almost independently, the shear strain is almost equal to

$$\left[1 + \frac{h_1}{h_3}\right] \frac{\partial w}{\partial x} = \gamma$$

(from equations 5.2 and 5.3) and is almost independent of the low core stiffness. The energy stored in the core is porportional to $G\gamma^2$, so that increasing G(decreasing ψ) is accompanied by a proportionate increase in the energy stored in the core, but by a negligible change in the face-plate energy and total energy stored. Since the core energy dissipated is proportional to the core energy stored, it follows that as ψ decreases, η increases in inverse proportion to ψ . On the other hand, at low values of ψ when the shear strain in the core is very small, the shear stress is almost independent of G and equal to that predicted by the plate theory from which shear deformation effects have been ignored. Since the core potential energy is proportional to $(\text{stress})^2/G$, the cyclic dissipation is inversely proportional to G and directly proportional to ψ . The maximum loss factor occurs in the "transition region" between the two extreme forms of plate bending. With very deep cores, the contribution of the face-plates to the total plate energy in this transition region is very small. The total plate energy is nearly equal to the core energy, and the plate loss factor is therefore nearly equal to the core loss factor.

V.3.2 <u>The Harmonic Displacement Criterion, and the Random Surface Stress and Reaction Force Criteria</u>

The expressions for these criteria are, respectively,

$$K\eta \;, \quad K^{\frac{2}{4}} \eta^{\frac{1}{2}} \theta^{\frac{1}{4}} \alpha^{-1} F_d(\eta) \quad \& \quad K^{-\frac{1}{4}} \theta^{\frac{1}{4}} \eta^{\frac{1}{2}} (1+\eta^2)^{-\frac{1}{2}} F_d(\eta)$$

in which the stiffness ratio K_{mn} , of Equation 5.30 is to be used. The

mass ratio, θ, is the ratio of the mass per unit area of the sandwich plate to that of a solid plate of thickness $2h_1$ and depends on the plate and damping layer densities. Materials which could be used for damped sandwich cores have densities in the region of 40% of aluminium alloy plates. The mass of a plate having a core of thickness τh_1 between face-plates of thickness h_1 is then $(1 + 0.20\tau)$ times that of a solid plate of thickness $2h_1$. A mass ratio of $(1 + 0.20\tau)$ is therefore used.

Plotting these criteria against ψ, sets of curves are obtained similar to those of Figure 29. Each curve displays the characteristic maximum and characteristic asymptotic behaviour at high and low values of ψ. The harmonic displacement criterion,

$$K\eta = \frac{\beta \psi 3(1+\tau)^2}{4[(1+\psi)^2 + \beta^2]}$$

(from Equations 5.30 and 5.31) has a maximum value of

$$(K\eta)_{max} = \frac{\beta 3(1+\tau)^2}{8[1 + (1+\beta^2)^{\frac{1}{2}}]} \qquad \ldots(5.36)$$

at the value of ψ given by

$$\psi_{opt.K\eta} = (1+\beta^2)^{\frac{1}{2}} \qquad \ldots(5.37)$$

It may be noted here that as β gets very large, $K\eta_{max}$ approaches the value $\frac{3}{8}(1+\tau)^2$ which is the maximum possible value obtainable for a given τ, assuming that a material is available having the required value of G and the high value of β. If $\beta = 4$, the value of $(K\eta)_{max}$ is 80% of its maximum possible value.

Maximum values of the random stress and reaction force criteria are not readily obtained in the same way, owing to unwieldy algebra involved in the differentiation. Instead, it is sufficiently accurate to assume that the maximum values occur at the value of ψ corresponding to the intersection of the high-ψ and low-ψ asymptotes of the criteria. (This technique actually gives the exact values of ψ_{opt} for η and $K\eta$. See Section V.6 for the derivation of the equations of the asymptotes). Using this approach, it is found that the maximum values of the random stress criterion occur when

$$\psi_{opt.rs} = (1+\beta^2)^{\frac{1}{2}}(1+3(1+\tau)^2)^{-\frac{1}{4}}(2+\tau)^2 \qquad \ldots(5.38)$$

and the maximum values of the random reaction force criterion occur when

$$\psi_{opt.rf} = (1+\beta^2)^{\frac{1}{2}}(1+3(1+\tau)^2)^{\frac{3}{4}} \qquad \ldots(5.39)$$

Figure 32 shows $\psi_{opt}(1+\beta^2)^{-\frac{1}{2}}$ for the different criteria (from Equations

5.34, 5.37, 5.38 and 5.39) plotted against τ, and shows a widely diverging requirement for the optimum value of ψ as τ increases. If the core properties are such as to give the maximum value to one of the criteria, another criterion will not have its maximum value. Although at low values of τ the values of ψ_{opt} are nearly constant, it must be remembered that since ψ is proportional to τ (Equation 5.29), the value of G to maximize the criteria must decrease as τ decreases.

The maximized values of $K\eta$ and the random stress and reaction force criteria are shown by the "increasing weight" curves of Figures 33 to 35. Here it has been considered that as the core depth increases, the weight of the whole sandwich plate increases, the face-plate thickness remaining constant.

As the core thickness decreases, each of the maximized criteria evidently approach constant values. As the core thickness increases, the random stress criterion and $K\eta$ increase monotonically. The random reaction force criterion increases with increasing τ over the range indicated, but at higher values of τ it reaches a maximum and then decreases. These curves indicate that if weight is no problem, the minimum response is obtained with the thickest core and with the material having the highest loss factor, β. High material loss factors, however, are usually only obtained at the expense of some other desirable property, e.g. a wide range of temperature and frequency over which the high values are maintained. Further, the material with the highest loss factor may not have the high value of G required to give the optimum value of ψ in the high τ range, where the criteria have their highest values. It is possible, therefore, that a material with a low loss factor and high G may give greater criterion values at high τ than a material with a high loss factor but with a lower G, if the latter material is being used under non-optimum conditions.

V.4 The Optimum Design of Damped Sandwich Plates

V.4.1 The 'Constant Weight' Theory

In section V.3, it was assumed that as τ increased, the face-plate thickness remained constant and the total weight of the plate therefore increased. The problem facing the designer of an aeroplane plate structure which must withstand intense random pressure fluctuations may be formulated thus:

"For a given weight of plate, obtain the configuration which has the minimum random stresses, consistent with a satisfactory static stiffness".

If damped sandwich plates are to be considered here, the approach must therefore be to consider the variation of the response criteria as τ increases at the same time as h_1 decreases to maintain a constant total weight. Decreasing the face-plate thickness implies a reduction of the flexural stiffness of the whole plate and in considering now the variation of the criteria with τ, the stiffness ratio to be used must include this effect. Suppose the weight of the whole sandwich plate is to be equal to that of a solid plate of thickness h and density ρ. When the thickness of each of the face-plates is h_1 and of the core th_1^p, the weight

per unit area of the plate is

$$\rho_c \tau h_1 + 2\rho_p h_1 = \rho_p h$$

Hence

$$h_1 = \frac{h/2}{(1 + \tau \rho_c / 2\rho_p)} \qquad \ldots(5.40)$$

The stiffness ratio to be used in the criteria for comparing plates of equal weight and different τ is given by

$$\frac{\text{Flexural stiffness of the sandwich plate}}{\text{Flexural stiffness of the solid plate of equal weight}}$$

which is readily shown to be equal to

$$\frac{K_{mn}}{(1 + \tau\rho_c/2\rho_p)^3} = K_{cw} \qquad \ldots(5.41)$$

The stress ratio, α_{mn}, must also be modified for the same reason. The new stress ratio to be used is given by:

Surface bending stress in the sandwich plate ÷ Surface bending stress in the solid plate of equal weight, undergoing the same transverse displacement.

This is easily seen to be

$$\frac{\alpha_{mn}}{(1 + \tau\rho_c/2\rho_p)} = \alpha_{cw} \qquad \ldots(5.42)$$

The criteria derived in the last section must therefore be divided by

$$(1 + \tau \rho_c / 2\rho_p)^{3x+y+z}$$

x, y and z are the powers to which the stiffness ratio, the stress ratio and the mass ratio, respectively, are raised in the criteria. Note that this has the effect of removing the mass ratio from the criteria since $\theta = (1 + \tau \rho_c/2\rho_p)$. Since this divisor does not contain ψ or β, the values of ψ at which the 'constant weight' criteria pass through their maximum values (for a given τ) are the same as derived in the last section. The corresponding maximum values of the constant weight criteria (with $\rho_c/\rho_p = 0.4$) are shown by the "Constant Weight" curves of Figures 33, 34 and 35. The plate loss factor, η_{max}, is unaffected by the decreasing skin thickness, being dependent only upon the thickness ratio τ, and the parameters ψ and β.

Each of the constant weight criteria differ negligibly from the increasing weight criteria at low values of τ, since the face-plate thicknesses scarcely differ. At higher values of τ, the constant weight random stress and harmonic displacement criteria are less than the corresponding increasing weight criteria, due to the reduced values of K. These criteria pass through maximum values when τ is approximately 5 and 8 respectively. On the other hand, the random reaction force criterion, having K raised to a negative power, benefits from the reduction of the stiffness associated with the decreasing face-plate thickness. The constant weight criterion values are therefore greater than the increasing weight values, and, moreover, do not pass through a maximum as τ increases. From the point of view of this

criterion alone, it is beneficial to have τ as large as possible.

Since the stiffness of the plate may well be of equal importance to the dynamic response characteristics embodied in the above criteria, the values of the stiffness ratio $K_{mn}/(1 + \tau\rho_c/2\rho_p)^3$ corresponding to the maximum values of the criteria are plotted in Figure 36. These show that below a core thickness ratio of 1, the stiffness of a sandwich plate designed to maximize any of the criteria is less than the stiffness of a solid plate of equal weight. At low frequencies, or under static loading conditions, the stiffness of these modes of displacement (on which the buckling stress depends) will be considerably less than indicated by Figure 36, since the frequency dependent shear modulus of the core, G , is always much less at low frequencies than at high frequencies. Indeed, if the low static value of G gives a high enough value of ψ , the static stiffness ratio for the plate with a very thin core becomes $\frac{1}{4}$ (from Equations 5.30 and 5.41) while for the plate with $\tau = 5$ it becomes 1/32. It is evident, therefore, that the minimum dynamic response of the sandwich plate can only be obtained at the expense of the static stiffness if no increase of weight is permitted.

V.4.2 The Constant Stiffness Theory

If the plate must withstand appreciable static loads in addition to the fluctuating loads, a certain minimum static stiffness is automatically specified by the known static loading and the degree of transverse deflection or buckling permitted in the plate. Suppose that this static stiffness is to be maintained as the core thicknesses is varied and the response criteria are examined.

Now under static (or low frequency) loading conditions, the shear moduli of damping materials are usually very small, and creep readily occurs. Under these conditions, therefore, ψ is likely to be very high and Equation 5.30 shows that the stiffness ratio K_{mn} is virtually independent of τ , ψ and β , approaching the value $\frac{1}{4}$. The static stiffness then depends only upon the thickness of the face-plates, and is twice the flexural stiffness of one of the face-plates. In order to maintain a constant value of the static stiffness, therefore, it is necessary only to maintain a constant thickness of the face plates. The total thickness of the face-plates will be 4^3 times the thickness of the solid plate having the required static stiffness.

Maximized criterion values for sandwich plates having face-plates of constant thickness are shown by the "increasing weight" curves of Figures 33, 34 and 35. These have been discussed in Section V.3.2, the theory of which may be regarded as the "Constant Static Stiffness Theory". The conclusions reached relate to the optimum design of plates for a given static stiffness.

V.4.3 The Choice of the Optimum Core Material (Constant Weight Theory)

If a damped sandwich plate is to be used for the skin plating of an aeroplane structure, and is to be designed for minimum random stresses and/or reaction forces, it will be necessary in the first place to know the mode (or modes) which are likely to contribute most significantly to the total response. This is necessary since the plate dynamic properties depend on the modal wavelength. Clarkson and Ford (9), have found from tests on jet-excited aeroplane fuselages and tail surfaces that the significant modes are those in which adjacent panels of stiffened plate structures vibrate in anti-phase, the semi-

wavelength (b/m) being approximately equal to the stringer or rib pitch. Modes with effective semi-wavelengths of one half of this may also be important. The semi-wavelength in the other direction (a/n) is of the order of the spacing of the stiffening in that direction. The values of r and (b/m) required in the sandwich plate theory may therefore be determined. Now the mode of vibration of the stiffened plate, with adjacent panels vibrating in anti-phase, is not the pure sinusoidal mode assumed in the foregoing theory, due to the restraint offered by the stiffeners. The effect of this is discussed briefly in section V.5, but the optimum core properties should not be appreciably different from those required for the sinusoidal mode.

Suppose that the mass per unit area of the plate has been fixed at μ by purely weight considerations. Minimum random stresses are obtained when τ is approximately 5, so that the face-plate thickness h_1 must be $\mu/4\rho_p$, assuming that $\rho_c/\rho_p = 0.40$. It has already been shown that $\psi_{opt.rs}$ is considerably different from $\psi_{opt.ef}$, so that some compromise is necessary if both random stresses and reaction forces are to be made as small as possible. As a compromise, therefore, the value of ψ_{opt} will be taken to be the geometric mean of these two quantities, i.e.

$$(1+\beta^2)^{\frac{1}{2}}\left\{1+3(1+\tau)^2\right\}^{\frac{1}{4}}(2+\tau) \qquad \ldots(5.43)$$

With $\tau = 5$, this becomes $\psi_{opt} = 22.6\,(1+\beta^2)^{\frac{1}{2}}$. The corresponding expression for the stiffness ratio is then

$$K \doteq \frac{1}{4}\left\{1 + \frac{4.58}{(1+\beta^2)^{\frac{1}{2}}}\right\} \qquad \ldots(5.44)$$

Now suitable materials can usually be manufactured with $\beta \doteq 1$, whence $K \doteq 1.06$ and $\psi_{opt} = 32$. From Equations 5.29, therefore,

$$G = \frac{(r^2+1)}{(1-\nu^2)}\frac{\pi^2}{2}\frac{E}{\psi_{opt}}\left(\frac{h_1}{b/m}\right)^2\tau$$

$$\doteq 0.77\,\frac{(r^2+1)}{(1-\nu^2)}\,E\left(\frac{h_1}{b/m}\right)^2 \qquad \ldots(5.45)$$

The core material must possess this value of G at the resonant frequency of the mode. When the plate modes are coupled with the stiffener torsion and bending modes, this frequency must be found by the method of Lin (2), (see also Clarkson (4)) adapted for sandwich plates. As a first approximation, however, the plate flexural stiffness could be taken to be $K D$, where K has the

value deduced above, and Lin's method for solid plates could be used. If there is negligible coupling with the stiffeners (a very extreme case) the resonant frequency will be given by

$$\omega = \left(\frac{k_{mn} K_{mn}}{\mu}\right)^{\frac{1}{2}} \quad \text{(from Equation 5.24)}$$

which, with $K_{mn} = 1.06$ gives

$$f = 1.33 \left(\frac{E h_1^3}{\mu(1-\nu^2)}\right)^{\frac{1}{2}} \frac{(r^2+1)}{(b/m)^2} \quad \text{c.p.s.}$$

V.4.4 The Optimum Design of a 6 in. Square Plate with Given Core Materials

We now consider the application of the constant weight theory to the design of a simply supported 6 in. square sandwich plate, the total weight of which must be equal to that of a single 18 S.W.G. (0.048 in.) plate. This is representative of a skin panel on the tail-plane of a certain jet-transport aeroplane. The use of two different damping materials is to be investigated, and the optimum core and face-plate thicknesses determined. The two different materials to be used are

(A) a broad temperature band material developed for sandwich plates
(B) a soft, pressure sensitive material, as used for damping tapes.

We shall consider the response criteria at one temperature only (10°C), at which the materials have the following properties:-

Frequency (c.p.s)		100	200	400	600	1000
Material A: ($lb.in^{-2}$)	G	4640	6820	9900	11900	15400
	β	0.96	0.87	0.80	0.76	0.68
Material B: ($lb.in^{-2}$)	G	180	260	380	480	660
	β	1.20	1.23	1.20	1.17	1.10

The specific gravity of the two materials has been taken to be 1.0 and of the face plates, 2.80. The Young's Modulus of the plates is 10^7 lb. in^{-2} and Poisson's Ratio, ν, is 0.3. The fundamental mode of vibration only is to be considered. Values of the stiffness ratio and the plate loss factor have been computed for a range of values of τ, the face plate thickness varying with τ to maintain constant weight. The calculation necessarily involves a method of successive approximation, for at each value of τ the natural frequency of the plate is initially unknown. A frequency is therefore guessed, and the corresponding values of G and β are used to calculate K. With this values, the resonant frequency is estimated and then used to find improved values of G and β and then an improved value of K. This process is continued until it converges on a steady value of K. Values of η, $K\eta$, and the random

reaction force and random surface stress criteria are then calculated. These values are shown in Figures 37 and 38.

Each of the criteria increases with increasing τ until τ lies between 5 and 10. Here, the criteria approach or reach maximum values. Plate B has superior criterion values throughout since the values of ψ are much closer to the optimum values than those of plate A. Furthermore, the loss factor of material B is consistently greater than that of material A. For plate A, ψ reaches a maximum value of about 0.24 at $\tau = 6.0$ as τ increases. This value is about one seventieth of the value required to maximize η. On the other hand for plate B, ψ reaches a maximum of about 11 at $\tau = 6.0$, which is about one half of $\psi_{opt.\eta}$.

The existence of the maximum values of the criteria in the region $\tau = 5$ to 10 stems mainly from the effect of the decreasing face-plate thickness, as τ increases. Equation 5.29 shows that ψ is proportional to $h_1^2 \tau / G$, where h_1 is the thickness of the face-plates. Putting

$$h_1 = \frac{h/2}{(1 + \tau \rho_c / 2\rho_p)}$$

(as in section V.4.1) it is found that $h_1^2 \tau$ has its maximum value when $\tau = 2\rho_p/\rho_c$. i.e. 5.50 in the above case. Although G also changes with τ (due to the change of natural frequency), this was a small effect in the above calculation and ψ still passed through a maximum value close to $\tau = 5.50$. Now the equation for the low-ψ asymptote for η (see section V.6) shows that when ψ is much below the optimum value and τ is greater than, say, 1.0, then the plate loss factor η is almost independent of τ and is proportional to ψ. Under these conditions, η passes through a maximum as ψ passes through a maximum.

Although material A does not appear in the above example to be as effective as material B, at a shorter modal wavelength or with a greater total weight its effectiveness will improve. Also, if steel face-plates are used ($E = 2 \times 10^7$ lb. in.$^{-2}$) with material A, the value of ψ will be further increased and will come closer to the optimum value, giving increased effectiveness. With these same changes, the plate with material B will have a value of ψ considerably greater than the optimum value, and the effectiveness of material B will decrease. It is evident, therefore, that each material must be examined on its merits in conjunction with the configuration in which it is to be used, and considering also the frequency of operation.

V.5 Stress and Reaction Force Reductions Obtainable Using Damped Sandwich Plates

A comparison is now made between the random surface stresses and the random reaction forces in two similar plates, one of them being a damped sandwich plate and the other being a solid plate damped only by the 'extraneous' mechanisms of rivet, acoustic and material damping. The plates are subjected to a random loading which is assumed to excite significantly only one mode, the same mode for each plate. The power spectral density of the corresponding generalised force is assumed to be the same at the natural frequency of each plate and is assumed not to vary appreciably in the neighbourhood of these

frequencies.

The percentage reduction of the stress and reaction force will be found using the criterion values in conjunction with η_i, as described in Chapter III, section III.5. The values of η_i used in Chapter IV, section IV.4 will again be used. Taking $\eta_i = 0.025$ in conjunction with the maximized low-τ criteria values from Figures 34 and 35 with $\beta = 1.0$, it is found that the random surface stresses are reduced by 65% and the random reaction forces by 73% when the solid plate is replaced by a damped sandwich plate of equal weight and of optimum design. Taking $\eta_i = 0.01$ in conjunction with maximized criteria values at $\tau = 5$ and $\beta = 1.0$, the reductions become 90% and 92% for the "constant weight" condition, and 96% and 88% for the "increasing weight" condition.

It should be remembered that the maximum reduction of the random stress does not occur at the same value of ψ (or G) as the maximum reduction of random reaction force, i.e. the maximum reductions will not be obtained at the same temperature or frequency. If the plate is designed such that the value of ψ is between the optimum values for the random stress and reaction force criteria, the values of the criteria themselves may be reduced by no more than about 20%, and the reduction quoted above will be slightly less.

When a sandwich plate is incorporated in a real structure with stringers and frames, these flexible stiffening members will cause the stiffness ratio and loss factor of the whole structural mode to be different from those of a simply-supported plate vibrating in a sinusoidal mode. The overall loss factor is likely to be less than that of the simple sandwich plate. The stiffness ratio is likely to be greater than κ of Equation 5.30 if this is less than unity, and less than κ if this is greater than unity. Since the mode of plate vibration is no longer sinusoidal, it is probable that an iterative technique will be required to determine the actual mode of vibration in the first place, before the values of κ and η for the whole vibrating configuration can be determined. This is to be the subject of future work.

If more than one mode participates in the total motion, it will not be possible to minimize the response in more than one mode. However, it is possible that if two modes adjacent in the frequency spectrum are excited, the values of their response criteria could lie on either side of the peak of the criterion: ψ curve. Both values could then be close to the maximum and the total response arising from both modes could then be minimised.

V.6 Off-Peak Values of the Criteria; Temperature Bandwidth Factors

Mention has already been made of the asymptotes which the criteria values approach as ψ becomes very large or very small. Figure 24 (and similar curves for other criteria) show that these asymptotes give good approximations to the actual criterion values provided ψ is about ten times greater than the optimum value, or less than one tenth of it. Now in a multi-modal response calculation, the loss factor and flexural stiffness (and also some of the response criteria) corresponding to several different modes will be required. No more than one or two low-order modes can have criteria values close to the maximum. The loss factors and stiffness ratios for the remaining modes could be taken to be those given by the relevant asymptote.

Equations 5.30, 5.31 and 5.33 show that at low values of ψ

$$\left.\begin{aligned} K &\to \tfrac{1}{4} + \tfrac{3}{4}(1+\tau)^2 \\ \eta &\to \frac{\psi\beta}{1+\beta^2}\cdot\frac{3(1+\tau)^2}{1+3(1+\tau)^2} \\ \alpha &\to 1 + \frac{\tau}{2} \end{aligned}\right\} \qquad \ldots(5.46)$$

At high values of ψ

$$\left.\begin{aligned} K &\to \tfrac{1}{4} \\ \eta &\to \frac{\beta}{\psi}\,3(1+\tau)^2 \\ \alpha &\to \tfrac{1}{2} \end{aligned}\right\} \qquad \ldots(5.47)$$

From these expressions, equations for the criterion asymptotes may be obtained. Note that at low values of ψ, the greatest loss factor is obtained when $\beta = 1$ but at high values of ψ, η increases in proportion to β. Note, further, that there will be a lower limit to the value of η, set by the existence of hysteretic damping in the face plates and at the plate boundary attachments. The effect of these damping sources has not been included in the analysis of this chapter. The above values of η are therefore only of use if they are considerably greater than the value deriving from these other sources.

Off-peak values of the criteria have also to be considered in relation to the sensitivity of the plate response to changes of temperature. Suppose, in the first place, that the plate vibrates in a single mode, at the frequency and temperature at which ψ has the optimum value for a specified criterion. Variation of the temperature changes G and β and hence changes ψ. The criterion value changes, following a curve similar to that of Figure 24. Sufficient change of temperature, up or down, will bring the criterion value down to one half of the maximum value at ψ_{opt}. Now in order to find the exact range of temperature over which a particular configuration with a particular core material has criterion values greater than the half-peak values,

it is necessary to have a complete set of curves of G and β vs. frequency and temperature for the material. In the paragraphs which follow, the temperature bandwidth is investigated in qualitative terms without such information for a range of configurations (different values of τ), optimised according to different criteria. Instead of an actual temperature bandwidth being found (no specific core material being considered) an alternative "bandwidth factor" has been postulated, and its dependence on τ and β has been investigated. Despite its limitations, this work is sufficient to show that some configurations must have a markedly superior temperature bandwidth than others.

Supoose, firstly, that β does not change as G changes. Denote by ψ_u and ψ_ℓ the values of ψ corresponding to the half-peak criterion values. (ψ_u and ψ_ℓ are the upper and lower values respectively). Now the quotient ψ_u/ψ_ℓ (or "bandwidth factor") is also the quotient of the two values of G giving the half-peak criterion values. Using the relevant curves of G vs. temperature, such as Figure 11, this quotient can be interpreted as a temperature bandwidth. Clearly, therefore, the greater the value of ψ_u/ψ_ℓ , the greater is the actual temperature bandwidth between which the criterion values exceed the half-peak values.

Exact expressions for ψ_u/ψ_ℓ corresponding to the plate loss factor, η , can be obtained from Equation 5.31 by equating this to $\eta_{max}/2$ from Equation 5.35, and solving the quadratic equation for ψ . We then find

$$\left[\frac{\psi_u}{\psi_\ell}\right]_\eta = \frac{1 + \sqrt{1 - \dfrac{\psi^2_{opt.\eta}}{\left[2\psi_{opt.\eta} + \frac{3}{2}(1+\tau)^2 + 1\right]^2}}}{1 - \sqrt{1 - \dfrac{\psi^2_{opt.\eta}}{\left[2\psi_{opt.\eta} + \frac{3}{2}(1+\tau)^2 + 1\right]^2}}} \qquad \ldots(5.48)$$

where $\psi^2_{opt.\eta} = (1 + \beta^2)(1 + 3(1 + \tau)^2)$.

Similarly, for the criterion $R\eta$, we find

$$\left[\frac{\psi_u}{\psi_\ell}\right]_{R\eta} = \frac{1 + \sqrt{1 - \dfrac{\psi^2_{opt.R\eta}}{\left[2\psi_{opt.R\eta} + 1\right]^2}}}{1 - \sqrt{1 - \dfrac{\psi^2_{opt.R\eta}}{\left[2\psi_{opt.R\eta} + 1\right]^2}}} \qquad \ldots(5.49)$$

where $\psi^2_{opt.R\eta} = (1 + \beta^2)$.

Exact expressions for ψ_u/ψ_ℓ for the other criteria are not obtainable in the same way, owing to the unwieldy algebra involved. However, from curves of the criteria plotted against ψ for different values of τ and β , the bandwidth factors may be determined graphically.

Figures 39 and 40 show the bandwidth factors for four different criteria

plotted against the core thickness ratio for three different (constant) values of β . The curves for η and the random reaction force criterion show that there is a definite advantage in having large core thicknesses, as the bandwidth factors increase considerably with thickness. The bandwidth factor for u_η is insensitive to core thickness, and that for the random stress criterion tends to be slightly less at high core thicknesses than at low. In general, the effect of having higher core loss factors is to reduce the bandwidth factor.

Considering now the effect of a change of both loss factor, β , and G , it will be shown that the conclusions just drawn are still valid. We may suppose that G changes first (β remaining constant and equal to β_i , say) followed by the change of β (G remaining constant). If the combined effect is to bring the criterion down to the half-peak value, the corresponding values of ψ will differ from those above. Denote the new values by ψ_{un} and $\psi_{\ell n}$, corresponding to which are the new values of the core loss factor β_u and β_ℓ . We shall now assume that in the region ψ_u to ψ_{un} , and ψ_ℓ to $\psi_{\ell n}$, the criterion asymptotes are sufficiently close to the actual curves to permit deductions to be made from them with regard to the bandwidth factors. Under this assumption, the harmonic and random criteria in the region of ψ_u are proportional to η and η^2 respectively. i.e. to

$$\frac{\beta}{\psi} 3(1+\tau)^2 \qquad \& \qquad \left\{\frac{\beta}{\psi} 3(1+\tau)^2\right\}^{\frac{1}{2}}$$

For either of these to have the same (half-peak) values at ψ_{un} and β_u as at ψ_u and β_i (= the initial value of β at ψ_{opt}), we must have

$$\frac{\beta_i}{\psi_u} = \frac{\beta_u}{\psi_{un}} \qquad \text{i.e.} \qquad \psi_{un} = \psi_u \frac{\beta_u}{\beta_i}$$

Similarly, in the region of ψ_ℓ , the harmonic and random criteria are proportional to

$$\psi \frac{\beta}{1+\beta^2} \qquad \text{and} \qquad \left\{\frac{\psi\beta}{1+\beta^2}\right\}^{1/2} \qquad \text{respectively.}$$

For either of these to have the same (half-peak) values at $\psi_{\ell n}$ and β_ℓ as at ψ_ℓ and β_i , we must have

$$\psi_{\ell n} \cdot \frac{\beta_\ell}{1+\beta_\ell^2} = \psi_\ell \cdot \frac{\beta_i}{1+\beta_i^2}$$

i.e. $$\psi_{\ell n} = \psi_\ell \cdot \frac{\beta_i}{\beta_\ell} \frac{1+\beta_\ell^2}{1+\beta_i^2}$$

Hence $$\frac{\psi_{un}}{\psi_{\ell n}} = \frac{\psi_u}{\psi_\ell} \left\{ \frac{\beta_u \beta_\ell}{\beta_i^2} \frac{(1+\beta_i^2)}{(1+\beta_\ell^2)} \right\} \qquad \ldots(5.50)$$

This differs from ψ_u/ψ_ℓ by a factor which depends only upon the β's and not upon τ. The new bandwidth factor, $\psi_{un}/\psi_{\ell n}$, must therefore vary with τ in the same manner as the previous factor ψ_u/ψ_ℓ. The deduction already made with regard to the effect of τ on the bandwidth factor is therefore still valid, within the limits of the validity of the assumptions of the argument.

It must be remembered that as G and β change with temperature so also does the stiffness ratio K, and the resonant frequency of the mode. This frequency change causes a further change of G and β. However, the effect of this on G and β (and hence also on the response criteria) is certainly much less than the effect of temperature alone.

V.7 Conclusions Drawn from Chapter V

The theory of the response of two-dimensional flat plates with damped cores has been developed. The results re-emphasize the conclusions of Ross, Kerwin and Dyer (24) who showed in a one-dimensional analysis that the loss factors of the transverse modes of vibration depend on the modal wavelength and core thickness, as well as on the core dynamic properties. The other criteria upon which the plate response depends have been found in this paper to show a similar dependence.

For any given mode and core thickness, there exists an optimum core shear stiffness to maximize the loss factor of the mode, but different optimum stiffnesses are required to minimize different response quantities (e.g. random surface bending stresses, harmonic resonant displacement amplitudes, etc.). With very thin cores having a material loss factor of 1, the maximum modal loss factor is about 0.3 but this is obtained at the expense of the high

frequency stiffness of the plate which is then about one half of that of a solid plate of equal weight. The static (i.e. low frequency) stiffness of the sandwich plate is about one quarter of that of the solid plate, owing to the shear modulus of the core being low under static or low frequency loading conditions. With thick cores (core thickness five times that of the face-plate) having a material loss factor of 1, maximum plate loss factors of about 0.8 can be achieved. With a given face-plate thickness, the minimum plate response is obtained with the thickest optimized core.

Comparisons have been made between the random responses of plates of equal weights vibrating in the same (single) mode, but having different core thickness: face-plate thickness ratios. The minimum response occurs when this ratio is about 5 : 1. The high frequency stiffness of the plate, in the given mode, is then nearly equal to that of the solid plate of equal weight, but the static stiffness may be as low as 1/32 nd of that of the solid plate. Although it appears that maximum damping and minimum response can only be obtained at the expense of static stiffness, a satisfactory static stiffness might be obtainable if lower damping could be accepted and non-optimum core shear stiffnesses were used.

With the large core thicknesses under optimum conditions, a rough estimate suggests that the r.m.s. stresses and reaction forces in a randomly excited sandwich plate may be about 10% of those in a solid plate of equal weight. With the small core thicknesses this figure becomes 30 - 40% .

The sensitivity of the minimized plate response to changes of the core dynamic properties (and hence to changes of temperature) has been investigated. Random reaction forces and the plate loss factor are less sensitive to these changes when the core thickness is high than when it is low. Harmonic resonant displacements and random surface stresses are equally sensitive, or nearly so, at high and low thicknesses.

Chapter VI

Harmonic Experiments on Damped Sandwich Specimens

VI.1 Scope of Chapter VI

This chapter describes some experiments carried out on a number of different damped sandwich specimens to measure their modal loss factors and stiffness ratios. Some of the specimens were commercial products which were to be assessed and others were specially made in order to check systematically certain aspects of the theory of Chapter V. This check was confined to an examination of the variation of $\aleph$ and η with respect to both core thickness and wavelength, for small core thicknesses only.

The measurements were made with the specimens vibrating in different sinusoidal modes over a wide frequency range. Ensuring that the modes were sinusoidal presented problems in the design of the apparatus. The heavy damping encountered with some of the strips presented problems of measurement not hitherto encountered. These problems are discussed and their solutions are described.

It has been concluded (with some qualification) that the results of the 'systematic check' confirm the theory of Chapter V relating to plate loss factors and stiffness ratios.

As the commercial specimens were all of different thickness and weight, there was little point in assessing and comparing them directly. A more useful comparison may be made between specimens of equal weight, it being assumed that the specimens can be manufactured in "scaled-up" or "scaled-down" forms. For this purpose, it was necessary to deduce the loss factors and stiffness ratios of the scaled specimens from the values measured on the specimens supplied. A relatively rapid method has been derived for this deduction process and is described in a later section. Finally, the scaled-up specimens are compared on the basis of values of the reaction force criterion.

VI.2 The Design of the Apparatus

The apparatus in which the sandwich specimen loss factors and stiffness ratios were to be measured had to satisfy the following requirements:

(a) The specimens had to be easily inserted and removed.
(b) The specimens had to vibrate in sine-modes. This was desirable for the purposes of comparing one specimen with another, as comparisons would have little meaning if the modes of vibration were different. It was necessary if the results were to be used in conjunction with the theory of Chapter V, and if stiffness ratios were to have any meaning.
(c) It had to be possible to excite and measure modes of vibration having frequencies as high as 1000 c.p.s. and as low as 50 c.p.s.

Requirement (a) was most readily satisfied by using narrow strips of the sandwiches rather than two-dimensional plates which would need to be carefully attached all round their four edges. Accordingly, specimens were tested which were 0.30 in. wide, and about 11 in. long. Further, to satisfy both (a) and (b) the specimens had to be effectively simply-supported at the ends and no masses

could be attached to the strip between these ends. This introduced problems of exciting the vibration, the normal method of which is to add a light coil to the strip and to excite electro-dynamically. Likewise, a problem of measuring the vibration arose, as suitable non-contacting vibration transducers were not available.

To provide effectively simple supports at the ends, the specimens were suspended from the "cradles" illustrated in Figure 41(a). These consisted of two vertical shim steel strips (A), 0.002 in. thick, 0.10 in. wide and about 0.5 in. long. At the top of these was soldered the brass bridge piece (B) to which the specimen was attached by a 10 B.A. screw (c). One of the specimen face-plates was tapped to receive this screw. The mid-surface of the specimen intersected the vertical strips half-way up their free length. In this way, the vertical strips imposed the minimum of rotational restraint upon the specimen. At their bottom ends, the vertical strips were soldered into brass support rods which were tightly screwed into a heavy base of 3 in. by 3 in. steel. One of the supports incorporated a crystal force transducer (see later paragraph) and certain necessary insulated sections. The whole assembly was bolted on to a massive base-plate.

To excite the specimen without adding exciting coils, the metal face-plates themselves were used as "exciting elements". Permanent magnets bolted to the steel base created a magnetic field which cut across the specimen in the direction perpendicular to the required direction of vibration. An alternating current was passed through the length of the specimen, as a result of which an oscillating loading acted on the specimen and excited the vibration. The permanent magnets could easily be moved and "reversed" in order to change the direction of the magnetic field. In this way it could be arranged that some regions of the specimen were excited in counter-phase with others, and the excitation could be arranged to suit the particular mode of vibration required. The alternating supply current entered the specimen via the vertical support strips.

Measurement of the vibration was accomplished by incorporating a piezo-electric crystal in one of the end supports, (Figure 41b) and measuring its voltage output as the oscillating load from the specimen was imposed upon it. This oscillating load derived from the inertia loading on the specimen and the exciting loading. The two components had to be separated in order to measure the required quantities. The technique used is explained later.

A photograph of the whole assembly is shown in Figure 42. Some of the pole pieces have been removed from the permanent magnets for clarity.

VI.3 The Problems of Measuring the Stiffness Ratios and High Modal Loss Factors

As some of the specimens were very highly damped (modal loss factors of nearly 1.0), several problems arose in measuring the loss factors and stiffness ratios. The stiffness ratio is defined (as in chapterV, section V.2.2) as the ratio of the generalised stiffness of the sandwich plate vibrating in a given mode to that of a solid plate of thickness $2h_1$ vibrating in the same mode. Its experimental determination is most readily achieved by measuring the "displacement resonant frequency" $(\aleph K/M\Theta)^{\frac{1}{2}}$ and deducing it from this. Accurate identification of this frequency was therefore required.

High modal loss factors imply low response (inertia forces) at resonance

and the possibility of a large proportion of the total response at resonance deriving from non-resonant modes. Further, the inertia force exerted on the support of the simply supported specimen by vibration in the resonant mode may not greatly exceed the force due to the excitation loading. These factors completely prohibit the use of the simple 'frequency-response' curve method to measure either the loss factor or the resonant frequency. However, the Nyquist diagram technique of Kennedy and Pancu (29) is well suited to the problem and has been adopted. The problem of the presence of unwanted modes of vibration was further overcome by arranging the magnets of the exciting system to produce the distribution of excitation loading which best suited the required mode (see Figure 43). The generalised exciting forces in the unwanted modes were then very small, if not zero.

The theory of the adaptation of the Kennedy and Pancu method to the present problem is presented in section V.4. The in-phase and quadrature components of the force transducer output (relative to the exciting force) were plotted against one another to form an arc of a circle in the region of the resonant frequency. Ideally, the larger the arc of measured points, the greater should be the accuracy with which the circle can be drawn. Now with a modal loss factor of nearly one, the two quadrants on either side of the resonant frequency cover a total frequency range of about 90% of the resonant frequency. Over a range as wide as this (especially with resonant frequencies in the 500 c.p.s. region) the frequency dependence of the core dynamic shear modulus might be expected to cause some variation of the modal stiffness and loss factor. Arising from this might be some distortion of the Nyquist diagram from the usual circular form and use of the distorted diagram will result in errors of estimating the resonant frequency and the loss factor. In the present investigation however this problem has been ignored, as the errors are certainly quite small. Justification for ignoring the problem comes from the results of the random experiments to be described later. The random behaviour was first predicted on the basis of the harmonically measured values of stiffness ratio and loss factor, and satisfactory agreement with experimental results was obtained.

VI.4 The Theory of the Measurement of the Resonant Frequency and Loss Factor

The method of Kennedy and Pancu for analysing vibration data centred on the vectorial representation of the displacement of the harmonically vibrating system. In the present work, the force exerted by the vibrating system on its support was measured. Accordingly, we require an analysis of this force vector, in order to relate the modal loss factor and resonant frequency to the properties of the force vector diagram. (Since the force exerted on the support is equal and opposite to the reaction at the support, from now on we shall refer to this force as "the reaction").

Consider a beam of length b which is excited by the harmonically varying loading $p(y)\, e^{i\omega t}$; y is the lengthwise co-ordinate. $p(y)$ is entirely real, so all points are being excited in-phase with, or in counter-phase with one another. Let the transverse displacement of the beam at any point be $w(y)\, e^{i\omega t}$, where $w(y)$ may be a complex quantity. Denoting the mass per unit length of the beam by μ, the local harmonic inertia loading is $\omega^2 w(y) \mu\, e^{i\omega t}$, giving the total loading at a point of

$$\left\{ p(y) + \omega^2 \mu\, w(y) \right\} e^{i\omega t}$$

The support reaction is now

$$\int \{ p(y) + \omega^2 \mu w(y) \} dy \qquad \ldots(6.1)$$

in which the limits (or constants) of integration must be adjusted according to the boundary conditions of the beam.

We now expand $w(y)$ as an infinite series of the normal modes of vibration of the beam, i.e.

$$w(y) = \sum_{n=1}^{\infty} W_n f_n(y)$$

The generalised displacement, $W_n = \bar{W}_n e^{i\omega t}$, corresponding to the nth normal mode satisfies the generalised equation of motion

$$M_n \ddot{W}_n + K_n (1 + i\eta_n) W_n = \int_o^b p(y) f_n(y) dy \cdot e^{i\omega t}$$

$$= P_n \cdot e^{i\omega t} \quad \text{say.}$$

From this we have

$$\bar{W}_n = \frac{P_n}{(K_n - \omega^2 M_n) + i K_n \eta_n} = \frac{P_n}{Z_n(\omega)} \qquad \ldots(6.2)$$

and the total support reaction is

$$\left\{ \int p(y) dy + \sum_{n=1}^{\infty} \frac{\int \mu f_n dy \cdot P_n \omega^2}{Z_n(\omega)} \right\} e^{i\omega t} \qquad \ldots(6.3)$$

The amplitude of the component of this which is in-phase with the exciting loading is

$$R = \int p(y) dy + \sum_{n=1}^{\infty} \int \mu f_n dy \cdot P_n \frac{\omega^2 (K_n - \omega^2 M_n)}{(K_n - \omega^2 M_n)^2 + K_n^2 \eta_n^2} \qquad \ldots(6.4)$$

Likewise, the quadrature component amplitude is

$$Q = - \sum_{n=1}^{\infty} \int \mu f_n dy \cdot P_n \cdot \frac{\omega^2 K_n \eta_n}{(K_n - \omega^2 M_n)^2 + K_n^2 \eta_n^2} \qquad \ldots(6.5)$$

Consider now the Argand diagram obtained by plotting R against ϕ for different values of ω . The existence of the frequency independent term $\int p(y)dy$ in the expression for R shows immediately that there must be a 'displaced origin' from which the frequency dependent components of the vectors radiate, even if thereis only one significant term in the infinite series. The total reaction vector consists, therefore, of a constant component deriving from the externally applied loading together with the frequency dependent components from the inertia forces.

Following Kennedy and Pancu, we examine next the frequency-dependent vector corresponding to just one of the modes, the rth,say. Now it is known that if the stiffness and damping do not vary with frequency, then the tip of the vector of the generalised displacement

$$P_r \left\{ \frac{(K_r - \omega^2 M_r) - i K_r \eta_r}{(K_r - \omega^2 M_r)^2 + K_r^2 \eta_r^2} \right\}$$

traces out a circle of diameter $P_r/K_r\eta_r$, with the centre on the imaginary axis. At any frequency, ω , the amplitude of the corresponding inertia force vector is $\omega^2 \int \mu f_r dy$ times this. The argument of the vector is unchanged. It can easily be shown that the tip of the inertia force vector still traces out a circle, but the axis of the circle (i.e. the diameter which passes through the origin of the inertia force axes) is inclined to the imaginary axis by $\tan^{-1}\eta$ (see Figure 44) . The diameter of the circle is

$$d_r = (1+\eta_r^2)^{\frac{1}{2}} \omega_r^2 \int \mu f_r dy \frac{P_r}{K_r \eta_r} = \frac{(1+\eta_r^2)^{\frac{1}{2}}}{\eta_r} \cdot \frac{\int \mu f_r dy}{M_r} P_r \quad \ldots(6.6)$$

which is the maximum amplitude of the inertia force corresponding to the rth mode, and occurs at the frequency

$$\omega_{ri} = \omega_r (1 + \eta_r^2) \quad \ldots(6.7)$$

ω_r is the "displacement resonant frequency", $(K_r/M_r)^{\frac{1}{2}}$.

Suppose it is possible in a practical investigation to arrange the loading, $p(y)$, such that the generalised forces in all but one preferred mode (the rth) are small. In the neighbourhood of ω_r the inertia forces from all modes but the rth will be very small. In this region the tip of the total measured reaction vector then traces out a circular arc,and a circle can be drawn through the measured points.

For various practical reasons, the magnitude of $\int p(y)dy$ will probably not be known. As it is not possible in drawing the circle to rely upon measured values of the reaction at very low frequencies, (down to zero), the precise location of the origin O_i will not be known. This means that neither of the frequencies ω_r and ω_{ri} can readily be identified from the circle

that has been drawn. Kennedy and Pancu overcame their similar problem of identifying ω_r by considering the derivative $ds/d(\Omega^2)$. (s = length of arc, $\Omega^2 = (\omega/\omega_r)^2$). This had a maximum value at $\omega = \omega_r$. The same property holds for the reaction vector diagram. Denoting the length of its arc by s_r, we can show that

$$\frac{ds_r}{d(\Omega^2)} = P_r \frac{\int \mu f_r dy}{M_r} \frac{(1+\eta_r^2)^{\frac{1}{2}}}{(1-\Omega^2)^2+\eta_r^2} \qquad \ldots(6.8)$$

which has a maximum value at $\Omega = 1$, i.e. at ω_r. Inspection of this expression, and practical experience, show that with large values of η_r this derivative does not change sufficiently in the neighbourhood of ω_r to permit an accurate identification of the frequency ω_r. An alternative method of determining ω_r is therefore required.

The frequency which can be determined most accurately from the vector diagram is ω_m, at which the imaginary component of the inertia force vector of one mode has its maximum value. The corresponding point in the circle lies on the diameter which is parallel to the imaginary axis, and is therefore very easily located. Differentiating the rth term of the series for $\bar{q}$ with respect to ω^2 and equating the derivative to zero shows that

$$\omega_m = \omega_r (1+\eta_r^2)^{\frac{1}{4}} \qquad \ldots(6.9)$$

When η_r has been determined, ω_r is quickly found from ω_m. η_r can be found from the vector diagram in several different ways. Each of these depends essentially on the relationship between η_r and the angle subtended at the circle centre by certain pairs of points on the circle. Consider first the rate of change with respect to ω of the real part of the inertia force vector at the frequency ω_m. The real part of the vector is given by

$$R_r = \frac{\int \mu f_r dy \cdot P_r \cdot \omega^2 K_r \eta_r}{(K_r - \omega^2 M_r)^2 + K_r^2 \eta_r^2} \qquad \text{(from Eqn. 6.4)} \qquad \ldots(6.10)$$

from which we find

$$\left[\frac{dR_r}{d\omega}\right]_{\omega=\omega_m} = \frac{\int \mu f_r dy \cdot P_r \cdot \omega_m}{K_r} \frac{1}{(1+\eta_r^2)^{\frac{1}{2}} - 1}$$

Dividing this by the diameter of the circle, d_r, from equation 6.6 and using 6.9, we have

$$\frac{[dR_r/d\omega]_{\omega=\omega_m}}{d_r} = \frac{\eta_r}{(1+\eta_r^2)^{\frac{1}{2}} - 1} = f_1(\eta_r) \qquad \ldots(6.11)$$

Now each of the terms comprising the left hand side are very easily obtained from the vector diagram, once a good circle has been drawn. Evaluating the left hand side using the measured data, the corresponding value of η_r may be found from the further relationship:

$$\eta_r = \frac{2 f_1(\eta_r)}{f_1^2(\eta_r) - 1} \qquad \ldots(6.12)$$

Alternatively, the curve of $f_1(\eta_r)$ vs. η_r on Figure 45 may be used.

Notice that when η_r is small, $f_1(\eta_r) \doteq 2/\eta_r$. Using this approximation, the error in estimating η_r is no greater than 6% when η_r is 0.5.

This method of determining η_r depends, in effect, upon the relationship between η_r and the angle subtended at the centre of the circle by an element of arc of "length" $d\omega$, situated at the point corresponding to ω_m. Alternatively, it may be recognised as an adaptation of the "phase-change method" of measuring damping, described elsewhere by the author (16).

The other methods to be used all depend on measuring the frequencies corresponding to certain pairs of points on the circle which subtend right angles at the centre. The points concerned are indicated on Figure 44. Three pairs of points are considered since the vector diagrams from different experiments had their best-defined arcs in different positions. Some of the experiments yielded arcs which extended beyond the quadrants on both sides of point M, but this was not always the case.

Point M corresponds to the frequency ω_m. The points are to be paired as follows:

Point A ($\omega_a < \omega_m$) together with point M; $\omega_m - \omega_a = \Delta\omega_{am}$.
Point B ($\omega_b > \omega_m$) together with point M; $\omega_b - \omega_m = \Delta\omega_{bm}$.
Point C ($\omega_c < \omega_m$) together with point D ($\omega_d > \omega_m$);

$$\omega_d - \omega_c = \Delta\omega_{cd}$$

Notice that both D and C together with point M subtend an angle of 45° at the centre.

The following relationships can be established between η_r and the above frequency intervals:

$$\frac{\Delta\omega_{am}}{\omega_m} = 1 - \left\{ \frac{\eta_r + 1 - (1+\eta_r^2)^{\frac{1}{2}}}{\eta_r - 1 + (1+\eta_r^2)^{\frac{1}{2}}} \right\}^{\frac{1}{2}} \qquad \ldots(6.13)$$

$$\frac{\Delta\omega_{bm}}{\omega_m} = \left\{ \frac{\eta_r + 1 + (1+\eta_r^2)^{\frac{1}{2}}}{\eta_r + 1 - (1+\eta_r^2)^{\frac{1}{2}}} \right\}^{\frac{1}{2}} - 1 \qquad \ldots(6.14)$$

$$\frac{\Delta\omega_{cd}}{\omega_m} = \frac{1}{(1+\eta_r^2)^{\frac{1}{4}}} \left\{ (1 - \eta_r \cot\phi_d)^{\frac{1}{2}} - (1 - \eta_r \cot\phi_c)^{\frac{1}{2}} \right\} \qquad \ldots(6.15)$$

where $\phi_c = \frac{3}{8}\pi + \frac{1}{2}\tan^{-1}\eta_r$ & $\phi_d = \frac{5}{8}\pi + \frac{1}{2}\tan^{-1}\eta_r$

These functions are plotted against η_r in Figure 45, and may be used directly to find η_r corresponding to known values of $\Delta\omega/\omega_m$.

We have now established methods of measuring the (high) modal loss factor, η_r, and the displacement resonant frequency ω_r. The use of these methods is described in the next sections of this chapter.

VI.5 Details of the Specimens and Electronic Apparatus

VI.5.1 The Specimens

Three different commercial sandwich specimens were tested and also four other specimens which had been made in the laboratory. The commerical specimens were:

(a) "Hycadamp", manufactured by Fireproof Tanks, Ltd., having a core of tough nitrile rubber.

(b) "Dynadamp", manufactured by the Lord Manufacturing Co. (U.S.A.). This had a core of soft synthetic rubber which had been specially developed to have a broad temperature and frequency range over which it maintained its damping properties.

(c) An experimental sample manufactured by Farbwerke Hoechst (Germany) with a soft, broad-temperature band core material of unspecified composition. This material was developed by Dr. H. Oberst. The specimen will therefore be referred to as 'Oberst's Specimen'.

Each specimen had aluminium alloy face-plates. Dimensions of the cores and face plates are given in Table III together with measured values of the face-plate Young's Modulus.

The other specimens had cores built up from layers of an adhesive damping film manufactured by the 3M's Co. for use in damping tape configurations. These layers were sandwiched between strips of 20 S.W.G. aluminium alloy plate. Specimens were made with one, two, three and four layers of the film. They

will therefore be referred to as 3M1, 3M2 etc. The manufacturers supplied some data concerning the dynamic shear modulus, and this is given in Table III together with measured values of the face-plate Young's Moduli.

VI.5.2 The Electronic Apparatus

The apparatus required for exciting the specimens consisted of a Solartron L.F. Oscillator which was connected to a power amplifier via a variable attenuator. The current output from the amplifier was passed through a step-down transformer the secondary winding of which was then connected to the ends of the specimen. In this way an alternating current of up to 10 amps could be passed through the specimen, which was thereby subjected to an oscillating loading proportional to and in phase with the current flowing.

The oscillator frequency could be varied in increments of 0.1 c.p.s. up to 100 c.p.s., and of 1 c.p.s. up to 1110 c.p.s. The accuracy of the signal frequency was stated to be within 2% of the indicated value.

The supply current to the specimen was measured by measuring the voltage drop across one of the supply leads to the specimen. A Solartron Valve Voltmeter was used for this purpose. This voltage was also required as the phase reference with respect to which the components of the reaction transducer signal were to be measured. These components were directly indicated on a Solartron "Resolved Components Indicator" when both of the voltage signals were supplied to it.

Considerable care had to be taken to avoid picking up mains hum on the lead from the high impedance reaction transducer to the Resolved Components Indicator. Careful shielding of the transducer and connections in the lead were required, together with the use of low-noise shielded cable.

VI.6 Details of the Experiments Conducted

VI.6.1 Phase Calibration of the Reaction Transducer

The accurate determination of the frequency ω_m from the response diagram of the measured points depends on the accurate knowledge of the phase relationship between the exciting force and the support reaction. It therefore had to be verified that the reaction transducer signal was in phase with the force exerted on the support. If not, the phase relationship had to be measured. Phase shift here can be minimised by having a very high input impedance in the apparatus to which the reaction transducer was connected. The Resolved Components Indicator had an input impedance of more than 50 Megohms, but this was insufficient to prevent some measurable phase shift at frequencies below 200 c.p.s.

The phase calibration was carried out as follows:

An aluminium strip was inserted in the testing apparatus and was

excited at its resonant frequency by means of a very small coil attached to its mid-span position. The coil was free to move in a magnetic field and carried an alternating current. An oscillating inertia force now acted on the support, together with one half of the exciting force. Since the damping ratios of the modes of vibration were very low (less than 0.001) the inertia force greatly exceeded the half of the exciting force.

The magnets on the apparatus which were normally used for excitation purposes now provided a magnetic field which could be used for velocity measuring purposes. Since the specimen was vibrating in their magnetic field, an alternating voltage was developed across the ends of the specimen which was proportional to and in phase with the harmonic velocity of the specimen. The inertia force exerted on the support was in quadrature with this signal. Since the inertia force greatly exceeded the exciting force the harmonic force applied to the support was in almost exact quadrature with the voltage signal. The output signal from the reaction transducer was then compared (phase-wise) with this other signal, using the Resolved Components Indicator. The measured phase difference was attributed to the phase difference between the force applied to the reaction transducer and the voltage output.

Four different strips were used, each having different thicknesses. They were excited in their fundamental and second overtone modes, permitting phase measurements to be made at eight frequencies from 28 c.p.s. to 850 c.p.s.

VI.6.2 Tests on the Specimen Supports

The supports were required to provide end conditions as close to "simply-supported" as possible. This was checked by mounting a 20 S.W.G. strip in the apparatus and measuring the natural frequencies of the first five flexural modes. As the damping of the strip was very low, the natural frequency was taken to be equal to the frequency for maximum amplitude of the reaction signal.

The measured frequencies were compared with the frequencies calculated for the first five modes of a truly simply-supported strip of the same dimensions and mechanical properties as the tested strip.

VI.6.3 Tests on the Sandwich Specimens

Each specimen was tested in the same way. Having been fixed into the testing apparatus, the oscillating current was supplied and kept at a constant level while the frequency was changed. At each frequency setting, the two components of the reaction transducer output signal were measured.

To excite the specimens in their fundamental modes, the five magnets along the length were arranged to give magnetic fluxes in the same direction. To excite the first overtone, only four magnets were used. Two adjacent magnets acted in the same direction, opposite to that of the other pair. The second, third and fourth overtones were also excited in turn with the appropriate magnet arrangement. Where possible, the magnets were fixed as close as possible to the modal anti-nodes.

With each new magnet arrangement, the frequency range was quickly scanned in order to locate approximately the appropriate resonance. That the mode excited was the required mode could be ascertained by running a pencil tip along the

vibrating specimen. The number and locations of the nodes could then easily be identified by touch. Detailed measurements of the reaction transducer signal were then taken and the response diagram was plotted immediately. In this way, the necessary frequency increments could be gauged and taken at once.

A record was kept of the ambient temperature throughout the tests which were carried out between 21°C and 23°C.

VI.6.4 Measurement of E of the Face-Plates

Some spare specimens were split apart and one of the face-plates from each was tested to measure the Young's Modulus. This was carried out either in a standard tensile testing machine, with an extensometer attached to the specimen, or by supporting the specimen on knife-edges at its ends, placing small weights on the beam at the centre and measuring the central deflection with a travelling microscope. In each case, E was deduced from the slope of the load-deflection curve.

The results of these tests have already been presented in Table III of specimen data.

VI.7 Results

VI.7.1 The Phase Calibration

The phase lag of the reaction transducer signal behind the applied force is shown on Figure 46. Above 200 c.p.s., this is less than 2° and was found to have no substantial effect upon the resonant frequencies and loss factors subsequently measured from the response diagrams.

Below 200 c.p.s., the phase lag increases steadily in the manner characteristic of piezo-electric transducers. At 30 c.p.s., however, the phase lag is still only 10°.

VI.7.2 The Support Conditions

The measured and calculated natural frequencies of the 20 S.W.G. strip are shown below.

Mode	Fundamental	First Overtone	Second Overtone	Third Overtone	Fourth Overtone
Measured Frequency c.p.s.	28.35	113	246	446	678
Calculated Frequency c.p.s.	28.4	113.6	255	454	710

If any significant rotational restraint had existed at the supports, the measured natural frequencies would have been greater than the calculated values and the frequency of the fundamental mode would have been affected more than the frequencies of the other modes. It is evident, therefore, that there was virtually no rotational restraint at the end of the strip, and that one of the design requirements for the supports was satisfied.

That the measured frequencies of the higher modes were lower than the calculated frequencies may be attributed in part to the effect of the rotational inertia of the end-support, but most (it is thought) to the effect of slight flexibility of the supports in their longitudinal direction.

VI.7.3 The Response Diagrams

Some typical response diagrams obtained from the tests are shown in Figures 47 and 48. It will be noticed that very good circular diagrams were obtained over the whole frequency range considered, from 40 c.p.s. to over 1000 c.p.s. A unique circular arc could usually be drawn through the measured points from each test, the arc sometimes extending over a semi-circle or more. Some of the sets of measurements, however, yielded only very small arcs (e.g. Figure 48a), but it was usually possibly to identify clearly a frequency ω_m and to measure a corresponding modal loss factor.

The Dynadamp specimen yielded a "compressed" circular diagram, characteristic of systems having non-linear damping which increases with amplitude (Figure 48b). A loss factor can be deduced from the circular arc drawn through the points closest to ω_m, but it is difficult to place much confidence in its exact value or signficance. The results would have had more physical signficance (but little more practical value) had the test been conducted at constant amplitude of displacement, the components of the exciting force (current) being measured at different frequencies with reference to the reaction signal. The reciprocal of the new "complex" exciting force should be taken, and its real and imaginary parts plotted against one another. This should yield a circular diagram from which may be obtained a loss factor and frequency ω_m which correspond with the particular amplitude of vibration of the test.

Another observed pecularity in the measured diagrams was the "secondary" mode at about 196.6 c.p.s. on Figure 48c. This was a very lightly damped mode which was detected at, or close to this frequency on most of the specimens. Its origin could not be traced, but it was <u>not</u> associated with flexural distortion of the specimens as its damping was much too low. The measured loss factor for the "primary" mode at 170 - 180 c.p.s. was measured by both the "$dR/d\omega$ method" and the "$\Delta\omega_{am}$ method". Identical results were obtained from both methods, giving confidence that the presence of the secondary mode did not affect the measurement of the loss factor of the primary mode.

VI.7.4 Derived Results

The methods of section VI.4 were used to deduce from the response diagrams the values of ω_r for each resonant mode and the corresponding modal loss factors. The values of ω_r were then used to calculate the modal stiffness ratios in the following simple manner:

A solid plate of thickness $2h_1$ vibrates in the r^{th} mode. Denote the corresponding generalised stiffness and mass by K and M. The corresponding displacement resonant frequency $(\omega_r)_{solid}$, is equal to $(K/M)^{\frac{1}{2}}$. When the sandwich plate vibrates in the same mode, the generalised stiffness and mass are given by $\mathcal{R}K$ and ΘM (by definition of the stiffness and mass ratios). Corresponding to these is the displacement resonant frequency, ω_r, given by

$$\omega_r^2 = \mathcal{R}K/\Theta M = (\mathcal{R}/\Theta).(\omega_r)^2_{solid} \qquad \ldots(6.16)$$

From this, we have

$$K = \frac{\theta (\omega_r)^2}{(\omega_r)^2_{solid}} \qquad \ldots(6.17)$$

θ was derived from the known weight of the specimen. $(\omega_r)_{solid}$ was calculated using the known expressions for the natural frequencies of a simply supported uniform beam of thickness $2h_1$. The value of h_1 taken was the face-plate thickness of the particular specimen being considered. The stiffness ratio evaluated was therefore that defined in Chapter V, section V.2.2. These stiffness ratio may be described as being "relative to" the stiffness of a plate having twice the thickness of the face-plate of the particular specimen.

The values of K and η derived from the response diagrams are tabulated in Table V and are plotted on Figures 49-52 with the frequency ω_r as the abscissa. The frequency abscissa has been chosen as it is a near equivalent to a ψ abscissa. Since ψ is a function of both G and wavelength, it is also a function of frequency. As the frequency increases, so also does ψ. The frequency abscissa is also convenient for purposes to be described in Section VI.9.

From any one specimen, values of K and η can be found only at the discrete, resonant frequencies. The values of K and η indicated by the curves between these frequencies therefore appertain to specimens of other lengths.

The modal loss factors and stiffness ratios obtained as above may be used to deduce the corresponding values of G and β for the core material. Equations 5.30 and 5.31 (Chapter V) were first solved simultaneously to give ψ ($\propto G^{-1}$) and β in terms of K and η. Substituting the measured values of K and η into these relationships yielded the corresponding values of G and β. These values were assigned to the frequency ω_r, but it is clearly an arbitrary matter as to whether they should be assigned to ω_m, ω_r or to any other intermediate frequency. Further, since K and η_m were obtained from data covering a fairly wide frequency range, the values of G and β computed from them must be of the nature of "weighted average" values over that range. They should not, however, differ significantly from the true values. The computed values of G and β are plotted on Figures 54-56.

VI.8 Discussion of Results

VI.8.1 The Results from the 3M's Specimens

The experimental values of K and η are shown on Figures 49 and 50 together with theoretical values that were calculated using the damping material properties listed in section VI.5.1. In calculating the theoretical values, the expressions for K and η of Equations 5.30 and 5.31 (Chapter V) were used. These expressions, which were derived for the two-dimensional plate theory, were adapted to the one-dimensional strip conditions by using

$$\psi = \frac{\pi^2}{2} \frac{E}{G} \left(\frac{h_1}{b/m}\right)^2 \tau \qquad \ldots(6.18)$$

This is the limiting value of ψ as $r \rightarrow \infty$, the constrained modulus $E/(1 - \nu^2)$ being replaced by the unconstrained modulus E.

Comparison of the experimental and theoretical values shows good agreement in the general trends and orders of magnitude, but the experimental values are mostly greater than the theoretical values. This is more pronounced with the larger thicknesses of the core.

In seeking an explanation for this discrepancy, consideration must first be given to the assumptions of the theory and to the conditions of the tests. The most important approximation in the theory that could influence the results is the neglecting of inertia forces in the planes of the face-plates. However, it was shown that this was justified provided a certain inequality was satisfied (see Section V.2.2), and this was, in fact, adequately satisfied by each of the specimens at all the frequencies of test. The conditions of the tests that could cause the experimental and theoretical results to differ are the conditions at the supports. However, the results of the tests on the supports (Section VI.7.2) suggested that measured frequencies, and hence measured stiffness ratio, should be slightly less that theoretical values, whereas the stiffness ratios of the sandwich specimens were greater than the theoretical values.

The most significant clue to the root of the discrepancy lies in the fact that some of the measured loss factors exceed the maximum values that can theoretically be achieved with the particular core thicknesses and with the values of β given by the manufacturer. (See Equation 5.35 for the maximum loss factor). This can only be explained by admitting the possibility that the properties of the material used in the tests differed from the data supplied. The same explanation was offered by Ross, Kerwin and Dyer (26) who found discrepancies between their measured and theoretical loss factors of thick bars treated with damping tape. They pointed out that there can be a wide scatter in the measured values of G and β of nominally identical specimens of the material selected from different batches. This, it was believed, was sufficient to account for their discrepancies which were greater in proportion than those found in our sandwich tests.

Consider now the measured and theoretical values of η shown on Figure 53, where η is plotted against the core thickness for each of the modes. It is to be noticed that the maximum measured values of η are greater than the theoretical maximum values, that they occur at greater values of τ, and that the values of η for mode I are slightly less than the theoretical values. Each of these characteristics can be attributed to the values of G and β for the core in the tested specimens being greater than the values assumed in the calculation of the theoretical values. Justification for this statement has been found from a study of the extensive calculations undertaken for Chapter V, in which values of K and η were computed for wide ranges of G, β and τ.

The values of G and β which were derived from the measured values of K and η (as described in Section VI.7.4) were found to be consistently greater than the manufacturer's data, further confirming the validity of the explanation offered above.

It may be concluded that the experimental results discussed in this

section confirm the theory of Chapter V for small core thicknesses (in particular the theory of Sections V.2.2 and V.2.3), after due allowance has been made for the core properties differing from the manufacturer's data.

VI.8.2 The Results from the Commercial Specimens

At this stage there is little point in comparing the values of K and η for the different specimens, as the weights of each were different. Some comments are warranted, however, on the variation of K and η with frequency.

Figure 52 shows that the maximum loss factor of Oberst's specimen occurs at about 400 c.p.s., and over the frequency range covered in the tests does not drop by more than 10% below its maximum value. If the loss factor alone was the criterion for judging the damping effectiveness of the specimen, we could conclude that the specimen was ideal for use in aeroplane structures, since the peak in the jet noise spectrum usually occurs near the 400 c.p.s. peak in the loss factor curve. On the other hand, the stiffness ratio drops quite rapidly with increasing frequency over the whole range, and at 700 c.p.s. is about one sixth of the value at 60 c.p.s. Arising from this, it is found that the criterion $K\eta$ has its maximum value below 60 c.p.s. and drops by about 25% over the frequency range, whereas the reaction force criterion, $K^{-\frac{1}{4}}\eta^{\frac{1}{2}}(1+\eta^2)^{-\frac{1}{2}}f_d(\eta)$, has its maximum value above 800 c.p.s. and drops by about 40% over the range. These results further emphasize that caution must always be exercised when considering claims made for a damping treatment which are based solely on the magnitude of the loss factor.

The loss factor of the Hycadamp specimen is seen to increase steadily with increasing frequency, and there is little indication of the approach of a maximum value. The inertia force criterion increases even more rapidly with frequency. So far as is known to the author, the Hycadamp configuration was reached by guesswork rather than by systematic analysis and design. Using a systematic approach, as outlined in Chapter V, higher loss factors and criterion values could be obtained, having maximum values closer to the regions of most intense excitation. In its present form, Hycadamp appears to be quite suitable for the attenuation of high frequency transmitted boundary layer noise.

The Dynadamp loss factors vary very little over the frequency range covered. The values indicated on Figure 52 were measured at low amplitudes of vibration, and different values could be obtained at larger amplitudes. A comprehensive study of the non-linearity was not undertaken. The results that are indicated therefore give only an order of magnitude for the Dynadamp loss factors, but this is sufficient to show that they are considerably smaller than those of the other specimens.

VI.9 Methods of Comparing the Commercial Specimens

VI.9.1 Direct Comparison of the Existing Specimens

The different specimens may be compared after values of the criteria have been determined from the measured values of K and η. The stiffness ratios must first be modified since the values quoted for each specimen are relative to the stiffness of a plate having twice the thickness of the face-plate (h_1) of the particular specimen. When used in criteria for comparing one specimen with another, they must all be relative to the stiffness of a "standard" plate of a given thickness ($= h_r$, say). The quoted stiffness ratios

must therefore be multiplied by $(2h_1/h_r)^3$. Since the specimens have different weights per unit area, the mass ratio term must be included in the criterion expressions.

Comparisons can only be made between criterion values corresponding to the same mode (i.e. the same wavelength) of vibration. Otherwise, they have no meaning.

VI.9.2 Comparison of Specimens of Equal Weight

We shall not proceed with the details of a comparison along the above lines, as the differences between the weights of the various specimens were so large as to deprive the comparison of practical value. A more useful comparison can be ma[illegible]ween the specimens if their thicknesses are all scaled to make them of e[illegible] weight, or as near to equal weight as possible, bearing in mind that the [illegible]-plates are only obtainable in S.W.G. sizes. New values must first be estimated for K and η of these new specimens. These new values can be calculated using the method outlined and used in Chapter V, section V.4.4. G and β must be known over the frequency range of interest, so the values deduced from the harmonic test results (Section VI.7.4) may be used.

The successive approximation method of section V.4.4 can be a tedious process if K and η are required for a number of modes and different specimens. A much more rapid method may be used if approximate values of K and η are sufficient and if the scaled specimens have the same core thickness ratios as the originals. Briefly, the method consists of taking the curves of K and η vs. frequency for the original specimen and translating them laterally (in the frequency direction) by an amount which depends on the thickness scaling factor. The loss factor curve is also translated vertically. In these new positions, the curves give the values of the stiffness ratio and loss factor for the scaled specimen. The details of the method and its justification will now be developed.

Two sandwich specimens, A and B, have the same core material and core thickness ratios but different face-plate thicknesses, (h_a and h_b, say). The dynamic flexural stiffnesses are proportional to $K_a(f)h_a^3$ and $K_b(f)h_b^3$ respectively, the $K(f)$'s being the frequency dependent stiffness ratios. Suppose that values of $K_a(f)$ are known for a range of frequencies, and values of $K_b(f)$ are required.

The stiffness ratios are functions of the non-dimensional quantities τ, ψ and β (see Equation 5.30). ψ is a function of frequency, since it depends on the modal wavelength and on the frequency dependent shear modulus. Suppose that it has the value ψ_a when specimen A vibrates at the resonant frequency f_a in the corresponding mode of wavelength λ_a. At this stage of the argument we permit the lengths of the two specimens to be different, such that there exists for specimen B a mode of wavelength λ_b and resonant frequency f_b for which $\psi_b = \psi_a$.

We now suppose that β is not signficantly different at the two frequencies f_a and f_b. Since τ is the same for both plates, and so also is ψ, it follows that the two plates have the same stiffness ratios at the frequencies f_a and f_b.

Let the values of G at these two frequencies be G_a and G_b.

Equating the values of ψ for the two specimens at the two frequencies, and cancelling out the equal terms, we have

$$\frac{1}{G_a}\left[\frac{h_a}{\lambda_a}\right]^2 = \frac{1}{G_b}\left[\frac{h_b}{\lambda_b}\right]^2$$

or

$$\left[\frac{\lambda_a}{\lambda_b}\right]^2 = \frac{G_b}{G_a}\left[\frac{h_a}{h_b}\right]^2 \qquad \ldots(6.19)$$

We shall now express λ_a/λ_b and G_a/G_b in terms of the frequency ratio f_a/f_b. The resonant frequencies are proportional to

$$\sqrt{\frac{\text{Flexural stiffness}}{\text{Mass x Wavelength}^4}}$$

Since the mass is proportional to the faceplate thickness, we have

$$f_a \propto \frac{h_a}{\lambda_a^2}\sqrt{K_a(f_a)} \quad \& \quad f_b \propto \frac{h_b}{\lambda_b^2}\sqrt{K_b(f_b)}$$

At these two frequencies $K_a(f_a) = K_b(f_b)$. Hence

$$\frac{f_a}{f_b} = \frac{h_a}{h_b}\cdot\frac{\lambda_b^2}{\lambda_a^2}, \text{ or } \frac{\lambda_a^2}{\lambda_b^2} = \frac{h_a}{h_b}\cdot\frac{f_a}{f_b} \qquad \ldots(6.20)$$

which relates the wavelength ratio to the frequency ratio.

Over limited frequency ranges, it is possible to relate the shear modulus, G, and the frequency by the simple law

$$G \propto f^n$$

n usually has a fractional value, and is easily found from a log-log plot of G vs. frequency. We therefore have

$$\frac{G_a}{G_b} = \left[\frac{f_a}{f_b}\right]^n \qquad \ldots(6.21)$$

which relates the G ratio to the frequency ratio.

Substituting equations 6.21 and 6.20 into equation 6.19 now yields

$$\frac{f_b}{f_a} = \left[\frac{h_a}{h_b}\right]^{\frac{1}{1-n}} \qquad \ldots(6.22)$$

This equation relates the frequencies of the two specimens at which their stiffness ratios are equal. The ratio is seen to be independent of the absolute frequency and depends only upon the ratio of the thicknesses of the two specimens (i.e. the "scaling factor"). If $K_a(f)$ is plotted against log(frequency), the curve for $K_b(f)$ is obtained simply by "laterally translating" the whole curve of $K_a(f)$ "rigidly" in the frequency direction.

Consider now the loss factors η_a and η_b of the two specimens at the two frequencies f_a and f_b. The expression for the loss factor (Equation 5.31) may be written in the form

$$\frac{\eta}{\beta} = \frac{\psi\, 3(1+\tau)^2}{(1+\psi)^2 + \beta^2 + 3(1+\tau)^2(1+\psi+\beta^2)} \qquad \ldots(6.23)$$

If τ, ψ and β have the same values for plate A at frequency f_a as for plate B at frequency f_b, then clearly $\eta_a = \eta_b$. The same lateral translation rule may then be used as before to derive the curve of η_b vs. frequency from the curve of η_a.

Now allow β to change slightly from β_a at f_a to β_b at f_b. If the change is small, we can ignore its effect in the denominator of the right hand side of Equation 6.23, and assume that the whole right hand side still has the same value for the two plates at the two frequencies f_a and f_b. We then have

$$\frac{\eta_a}{\beta_a} = \frac{\eta_b}{\beta_b} \qquad \text{i.e.} \quad \eta_b = \frac{\beta_b}{\beta_a}\cdot\eta_a \qquad \ldots(6.24)$$

This implies that not only is a lateral translation of the η_a curve required to obtain η_b, but also a vertical translation corresponding to the factor β_b/β_a. This factor is not necessarily the same for all frequencies, f_b.

These translation rules have been used to obtain the curves of K and η for a scaled-up specimen of Hycadamp from the curves for the original specimen. The value of the scaling factor, h_b/h_a, was taken to be 1.81, which meant that the scaled specimen had the same weight as the Dynadamp specimen. The values of G derived from the experimental results showed G to be proportional to $f^{0.21}$. The curves obtained by the method are shown on Figure 55 together with those for the scaled specimen calculated by the accurate successive

approximation method described in section V.4.4.

There is very good agreement between the curves of K obtained by the two methods. The curves for η do not agree so well, but are sufficiently close for practical purposes. The differences here have been traced to the accumulation of errors due to the approximations in the lateral translation method.

The values of K found in this way are still relative to the stiffness of a plate having twice the thickness of the face-plate of the scaled specimen, and must be modified (as described in section VI.9.1) before being used for comparing one specimen with another. For comparison purposes it is most convenient if the "standard" plate (of thickness h_r) has the same weight as the scaled specimens. The stiffness ratios relative to this plate are then the "Constant Weight" ratios, K_{cw}, defined in section V.4.1. Values of these for the three commercial specimens are plotted vs. frequency on Figure 56.

The next stage of the comparison process must be to determine the values of K_{cw} and η for specimens of equal weight, vibrating in modes of the same wavelength. As the resonant frequencies corresponding to these modes will (in general) be different for each specimen, the values of K_{cw} cannot be read directly off the curves of Figure 56 as they stand. However, a simple graphical construction may be devised to do this, as follows.

Suppose the resonant frequency of the standard plate is f_r when vibrating in the given mode. The resonant frequency of a scaled specimen in this mode is $f_r K_{cw}^{\frac{1}{2}} = f$. i.e. $K_{cw} = f^2/f_r^2$. If the curve of f^2/f_r^2 vs. f is now superimposed on the curves of K_{cw} vs. f of Figure 56, the intersection points will give both the resonant frequencies and stiffness ratios of the scaled specimens. If the K_{cw} vs. f curves are plotted on a log-log scale, then the curve of f^2/f_r^2 vs. f is simply a straight line of slope = 2 passing through the point $K_{cw} = 1$ and $f = f_r$.

VI.9.3 Comparison of the Reaction Force Criteria for the Scaled Commercial Specimens

The values of K_{cw} and η found from Figure 56 can now be used to compare the three commercial specimens, scaled to be equal in weight to the Dynadamp specimen and vibrating with the same wavelength. Values of the random reaction force criterion, $K^{-\frac{1}{2}} \eta^{\frac{1}{2}}(1 + \eta^2)^{-\frac{1}{2}} f_d(\eta)$, have been calculated and are shown on Figure 57.

There is evidently little to choose between Mycadamp and Oberst's specimen at small wavelengths, but as the wavelength increases, so also does the superiority of Oberst's specimen. The Dynadamp specimen is markedly inferior to the other two over the whole wavelength range. It must be remembered, however, that the Dynadamp specimen showed non-linear characteristics in the harmonic tests and that higher loss factors and lower stiffness ratios might have been obtained at higher amplitude levels. Even so, the random reaction force criterion values would not be expected to increase sufficiently to approach those of the other two specimens.

The random vibration theory, which was used to derive the expressions for the criteria, assumed that the vibrating system was essentially linear. The non-linearity of the Dynadamp specimen means that the significance of its random criterion values is therefore open to doubt. However, the results of

the random experiments to be described in Chapter VIII suggest that the specimen is by no means greatly misrepresented by quoting 'linear' criterion values based on harmonically measured loss factors and stiffness ratios.

VI.10 Conclusions Drawn from Chapter VI

It is considered that the apparatus developed for testing the specimens has adequately satisfied the requirements laid down in Section VI.2, viz. ease of insertion of specimens, sinusoidal modes of vibration, and frequency range of testing from 50 c.p.s. to 1000 c.p.s. The different techniques of measuring the damping have given results consistent amongst themselves, which fact suggests their reliability.

The loss factors and stiffness ratios measured on the laboratory-made specimens were found to vary with core thickness and wavelength in the manner predicted by the theory of Chapter V. There were small magnitude differences between the measured values and the values predicted by the theory incorporating the manufacturer's data for the core properties. The differences were consistent with the given data having lower values than realised by the core material in the specimens.

The loss factor of Oberst's specimen had a maximum value of nearly 1.0 at a frequency of 400 c.p.s., and did not drop by more than 10% of this between 80 c.p.s. and 1000 c.p.s. A thinner specimen of the same proportions would have its maximum loss factor at a higher frequency. The loss factor of the Hycadamp specimen increased steadily over the frequency range from 0.06 at 60 c.p.s. to 0.5 at 900 c.p.s. The loss factor of the Dynadamp specimen varied between 0.04 and 0.06 over the frequency range from 80 c.p.s. to 1200 c.p.s.

The stiffness ratios of each specimen dropped steadily with increasing frequency, Oberst's specimen showing the most marked variation of from 3 to 0.54 between 60 c.p.s. and 700 c.p.s. The effect of this was to move the peak values of some criteria to low frequency regions and of others to high frequency regions.

A quick method has been devised whereby the measured loss factors and stiffness ratios of one specimen may be used to deduce the values for another specimen having the same core thickness ratio but different face-plate thickness. By way of illustrating the method, the three commercial specimens have been compared on the assumption that two of them can be scaled-up to make them equal in weight to the Dynadamp specimen. Under the scaled conditions, Oberst's specimen maintained its superiority over the others when judged by the random reaction force criterion. The maximum value of this criterion occurred at a much higher frequency than that corresponding to the former maximum loss factor.

Chapter VII

The Random Vibration of a Heavily-Damped Beam

VII.1 The Purpose and Scope of the Chapter

The random vibration theory on which parts of chapter III were based was essentially a small-damping theory. Since the last chapter has shown that plate loss factors of up to 1.0 are now realizable, the random theory needs to be re-examined to include the effects of large damping. It is the purpose of this chapter, therefore, to initiate such a re-examination. A comprehensive study is not undertaken, as this chapter (and the next) are intended rather as appendices to the main body of the report. For this reason, the different stages of the theory that is presented are not all discussed and developed as fully as possible, but lines for future investigation are pointed out.

The theory is confined to the evaluation of the total force exerted on one of the supports of a randomly-excited, heavily-damped beam. Certain restrictions are made which effectively limit the applicability of the results obtained to the simplest of vibrating beams, but these restrictions could be removed to generalise the analysis. The important features of the method and the important parameters governing the response are nevertheless clearly shown. Also disclosed are the conditions under which the reaction force criterion is valid, in the form in which it was derived in chapter III.

The approach that is used may be developed to study the randomly-varying bending moments and bending stresses in the beam. Ultimately it may be used to deal with the random vibrations of plates and reinforced structures.

VII.2 Approaches to the Problem

The usual method of analysing the response of a finite beam or plate to random loading is that of Powell (12). In this, the motion of the system is analysed in terms of the normal modes of flexural vibration. To find the force exerted at a point within the system, (say, on a support) it is necessary firstly to find the force exerted when the system is displaced by unit amount in each normal mode in turn. When the actual magnitudes of the modal displacements are known, the total force on the support can be found by summing the "modal" components of force.

So far, of course, this is the accepted method of dealing with harmonically-excited vibration. When the excitation is random, the problem is to find the spectrum of the total force. Powell shows that this consists of the sum of the spectra of the modal components of force, together with certain "cross-spectrum" terms which must be included to allow for the correlation between the modal components. The cross-spectra are difficult terms to evaluate, and appear to become increasingly important as the damping increases.

The number of normal modes that needs to be considered in the analysis depends, of course, upon the accuracy with which the final answer is required. It depends on the damping (the higher the damping, the more modes are required), on the spectrum of the exciting loading (the broader the spectrum, the more modes are excited) and on the ability of the different modes to accept energy from the exciting loading.

An alternative method of analysing the random response may be developed from Williams' method of calculating the transient response of aeroplane structures to gust and landing loads (30). In this, the force within the system is expressed as the sum of two sets of forces:

(a) the force produced at the point by the instantaneous system of external forces, assuming these had built up slowly to their instantaneous values

(b) the force produced at the point by the instantaneous system of inertia forces acting on the system.

Set (a) can be found by the usual methods of static stress analysis. Set (b) can be found in terms of a series of "modal inertia forces", the dynamic response of each mode again having to be analysed. Williams showed that using this approach fewer modes had to be considered in the analysis than in the former method for the same degree of accuracy.

It is a straightforward step to apply to this method the mathematical techniques used by Powell to solve the general random problem. In this way it will be shown in this chapter than the spectrum of the force on a support is equal to the sum of the spectra of the forces exerted there by the external forces and the modal inertia forces, together with cross-spectral terms deriving from the correlation between the inertia and external forces. These cross-spectra terms are of a slightly simpler form than those of Powell's analysis.

Williams' method has been adopted as it still appears to offer more rapid convergence (i.e. requires consideration of fewer modes) than the method of Powell when the damping is high and the loading is continuous and random. A proof of this statement is not given in this chapter, being one of the features scheduled for future investigation. However, there should be no essential problem in using Williams' original proof, almost as it stands.

VII.3 The Reaction at a Support of a Randomly Vibrating Beam with Heavy Damping

VII.3.1 The Power Spectral Density under a General Loading

The beam considered in Section VI.4 is now excited by a distributed loading, $p(y,t)$, which varies randomly with respect to both space and time. It is required to estimate the power spectral density, and hence the mean square value of the total force exerted on the support by the external loading together with the inertia forces of the response.

In the analysis of the random loading and response we shall use the method of generalised harmonic analysis as used by Powell and others. To find the power spectral density of a randomly varying quantity, $q(t)$, we first find its Fourier Transform, $\mathcal{F}_q(i\omega)$, which is defined by the relationship

$$\mathcal{F}_q(i\omega) = \frac{1}{2\pi}\int_{-T}^{T} q(t)\, e^{-i\omega t}\, dt \qquad \ldots(7.1)$$

The power spectral density is then given by the relationship

$$\Phi_q(\omega) = \lim_{T\to\infty} \frac{2\pi}{T} \left|\mathcal{F}_q(i\omega)\right|^2 \qquad \ldots(7.2)$$

and the mean square value of the quantity by

$$\langle q^2(t) \rangle = \int_0^\infty \Phi_q(\omega)\, d\omega \qquad \ldots(7.3)$$

Let the local transverse acceleration of the beam at the point y be $\ddot{w}(y, t)$. The local inertia loading is $-\mu\ddot{w}(y, t)$. Together with the externally applied loading, this gives a total force on a support of

$$L(t) = \int_y \{ p(y,t) - \mu \ddot{w}(y,t) \}\, dy \qquad \ldots(7.4)$$

in which the limits of integration depend on the boundary conditions of the beam. As before, we shall call this total force "the reaction". Let the part of it deriving from $p(y,t)$ be denoted by $P_o(t)$, i.e.

$$P_o(t) = \int_y p(y,t)\, dy \qquad \ldots(7.5)$$

The displacement of the beam, $w(y,t)$, will now be expressed by the series of normal modes of vibration of the beam, as in section VI.4, i.e.

$$w(y,t) = \sum_{n=1}^{\infty} W_n f_n(y)$$

so that the local acceleration may be written in the form

$$\ddot{w}(y,t) = \sum_{n=1}^{\infty} \ddot{W}_n f_n(y) \qquad \ldots(7.6)$$

The generalised displacement and acceleration satisfy the equation

$$M_n \ddot{W}_n + K_n(1+i\eta_n) W_n = \int_o^\ell p(y,t)\, f_n(y)\, dy = P_n(t) \qquad \ldots(7.7)$$

Damping coupling of the normal modes is therefore excluded.

The Reaction now becomes

$$L(t) = P_o(t) - \sum_{n=1}^{\infty} \ddot{W}_n \int \mu f_n(y)\, dy \qquad \ldots(7.8)$$

and its Fourier transform is

$$\mathcal{F}_L(i\omega) = \mathcal{F}_{P_o}(i\omega) - \sum_{n=1}^{\infty} \mathcal{F}_{\ddot{W}_n}(i\omega) \int \mu f_n(y)\, dy \qquad \ldots(7.9)$$

Here $\mathcal{F}_{P_o}(i\omega)$ and $\mathcal{F}_{\ddot{W}_n}(i\omega)$ are the transforms of $P_o(t)$ and $\ddot{W}_n$ respectively.

Now the transforms of the generalised displacement ($\mathcal{F}_{W_n}(i\omega)$), generalised acceleration, ($\mathcal{F}_{\ddot{W}_n}(i\omega)$), and generalised force ($\mathcal{F}_{P_n}(i\omega)$) are related by

$$\mathcal{F}_{\ddot{W}_n}(i\omega) = -\omega^2 \mathcal{F}_{W_n}(i\omega) = \frac{-\omega^2 \mathcal{F}_{P_n}(i\omega)}{(K_n - M_n\omega^2) + iK_n\eta_n} \qquad \ldots(7.10)$$

Putting $$(K_n - M_n\omega^2) + iK_n\eta_n = Z_n \qquad \ldots(7.11)$$

into equation 7.10 and then substituting into equation 7.9 yields

$$\mathcal{F}_L(i\omega) = \mathcal{F}_{P_0}(i\omega) + \sum_{n=1}^{\infty} \frac{\omega^2}{Z_n} \mathcal{F}_{P_n}(i\omega) \int \mu f_n(y)\,dy \qquad \ldots(7.12)$$

To find the power spectral density of L(t), we now use equation 7.2, which gives

$$\Phi_L(\omega) = \lim_{T\to\infty} \frac{2\pi}{T} \left|\mathcal{F}_L(i\omega)\right|^2$$

$$= \lim_{T\to\infty} \frac{2\pi}{T} \mathcal{F}_L(i\omega)\,\mathcal{F}_L^*(i\omega) \qquad \ldots(7.13)$$

the asterisk denoting the complex conjugate.

On substituting $\mathcal{F}_L(i\omega)$ into this from equation 7.12, and denoting the power spectral densities of $P_0(t)$ and $P_n(t)$ by $\Phi_{P_0}(\omega)$ and $\Phi_{P_n}(\omega)$, we find

$$\Phi_L(\omega) = \Phi_{P_0}(\omega) + \sum_{n=1}^{\infty} \frac{\omega^4}{|Z_n|^2} \Phi_{P_n}(\omega) \left[\int \mu f_n(y)\,dy\right]^2$$

$$+ \lim_{T\to\infty} \frac{2\pi}{T} \sum_{n=1}^{\infty} \omega^2 \int \mu f_n(y)\,dy \left\{ \frac{\mathcal{F}_{P_0}^*(i\omega)\mathcal{F}_{P_n}(i\omega)}{Z_n} + \frac{\mathcal{F}_{P_0}(i\omega)\mathcal{F}_{P_n}^*(i\omega)}{Z_n^*} \right\}$$

$$+ \lim_{T\to\infty} \frac{2\pi}{T} \sum_{\substack{n=1 \\ (n\neq m)}}^{\infty} \sum_{m=1}^{\infty} \omega^4 \int \mu f_n\,dy \int \mu f_m\,dy \left\{ \frac{\mathcal{F}_{P_m}(i\omega)\mathcal{F}_{P_n}^*(i\omega)}{Z_m Z_n^*} + \frac{\mathcal{F}_{P_m}^*(i\omega)\mathcal{F}_{P_n}(i\omega)}{Z_m^* Z_n} \right\} \ldots(7.14)$$

The first term on the right hand side is simply the power spectral density of the force, $P_0(t)$, exerted on the support by the external loading. The second term (the first series) is the sum of the individual power spectral densities of the modal inertia forces acting on the support. The third term (the second series) represents the contribution to the total power spectrum due to the fact that the inertia forces in each mode are correlated to some degree with the force exerted by the external loading. The final, double series represents the contribution due to the fact that the inertia forces in one mode are correlated to some degree with those in another mode.

As this chapter is intended mainly to be an introduction to the method of analysis but also to be sufficient to deal with the simple vibrating system of Chapter VIII, we shall now restrict attention to vibration in which the inertia forces in one mode are very much greater than those in all other modes. This would occur in practice, for example, if a plate were excited under coincidence conditions in one of its modes. The expression for the power spectral density of the reaction is now greatly simplified. From the first two series, only the terms corresponding to the significant mode are required, and the final double series may be disregarded altogether. This is not to say, of course, that in general the final series can be ignored. It will certainly be important when there are significant inertia forces present from each of two modes which have close natural frequencies. The higher the damping, the less-close need the frequencies be for the series to be important. However, a detailed study of it must be left to a later date, using the ideas of Lin (31) who has studied a similar series, without the ω^4 term, and with light damping.

We now consider in detail the terms which remain in the equation for the power spectral density of the reaction:

$$\Phi_L(\omega) = \Phi_{P_o}(\omega) + \frac{\omega^4}{|Z_n|^2}\Phi_{P_n}(\omega)\left[\int \mu f_n(y)\,dy\right]^2$$

$$+ \omega^2 \int \mu f_n(y)\,dy \cdot \lim_{T\to\infty}\frac{2\pi}{T}\left\{\frac{\mathcal{F}^*_{P_o}(i\omega)\mathcal{F}_{P_n}(i\omega)}{Z_n} + \frac{\mathcal{F}_{P_o}(i\omega)\mathcal{F}^*_{P_n}(i\omega)}{Z_n^*}\right\} \quad \ldots(7.15)$$

General expressions will first be obtained for the spectral densities $\Phi_{P_o}(\omega)$, $\Phi_{P_n}(\omega)$ and for a cross-spectral density which emerges from the third term. Owing to their complicated nature when the excitation is of the most general kind, these general expressions will then be reduced to a much simpler form corresponding to a special, simple loading.

The first term in Equation 7.15 is given by

$$\Phi_{P_o}(\omega) = \lim_{T\to\infty}\frac{2\pi}{T}\,\mathcal{F}_{P_o}(i\omega)\mathcal{F}^*_{P_o}(i\omega)$$

$$= \lim_{T\to\infty}\frac{1}{2\pi T}\int_{-T}^{+T}\int_y p(y,t)e^{-i\omega t}\,dy\,dt \int_{-T}^{+T}\int_y p(y,t)e^{i\omega t}\,dy\,dt \quad \ldots(7.16)$$

Multiplying the integrals together to form a quadruple integral, re-arranging the order of integration and introducing the variables y_1, y_2, t_1, t_2 to indicate the order of integration, this becomes

$$\Phi_{P_o}(\omega) =$$

$$\lim_{T\to\infty}\frac{1}{2\pi}\int_y\int_y\int_{-T}^{+T} e^{-i\omega(t_1-t_2)}\,\frac{1}{T}\int_{-T}^{+T} p(y_1,t_1)\,p(y_2,t_2)\,dt_1\,dt_2\,dy_1\,dy_2 \ldots(7.17)$$

Now put $t_1 - t_2 = \tau$. The inner integral

$$\lim_{T\to\infty} \frac{1}{T}\int_{-T}^{+T} p(y_1,t_1)\, p(y_2, t_1+\tau)\, dt_1 = \phi_p(y_1, y_2, \tau) \quad \ldots(7.18)$$

is recognised as the cross-correlation function between the pressures at the points y_1, y_2 with the time delay τ .

The power spectral density of $P_o(t)$ now reduces to

$$\Phi_{P_o}(\omega) = \int_y\int_y \lim_{T\to\infty} \frac{1}{2\pi}\int_{-T}^{+T} e^{-i\omega\tau}\, \phi_p(y_1, y_2, \tau)\, d\tau\, dy_1 dy_2 \quad \ldots(7.19)$$

in which

$$\lim_{T\to\infty} \frac{1}{2\pi}\int_{-T}^{+T} e^{-i\omega\tau}\, \phi_p(y_1, y_2, \tau)\, d\tau = \Phi_{pc}(\omega) - i\Phi_{ps}(\omega) \quad \ldots(7.20)$$

is the important "cross power spectral density" of the pressures at y_1 and y_2 . The above equation, (which defines $\Phi_{pc}(\omega)$ and $\Phi_{ps}(\omega)$) shows that in general it is a complex quantity. When $y_1 = y_2$, the imaginary term vanishes and leaves a real term which is the power spectral density of the local pressure. The real part of the cross power spectral density is the "cosine transform" of the cross-correlation function and the imaginary part is (-i) times the sine transform.

The cross power spectral density can be non-dimensionalised by dividing it by the square root of the product of the power spectral densities of the pressures at y_1 and y_2 . Denote these (spectral densities) by $\Phi_p(y_1,\omega)$ and $\Phi_p(y_2,\omega)$. There is no need for a suffix "c" or "s", as the sine transform is now identically zero. Non-dimensionalising in this way, we get:

$$c_c(y_1, y_2, \omega) = \frac{\Phi_{pc}(y_1, y_2, \omega)}{\sqrt{\Phi_p(y_1,\omega).\,\Phi_p(y_2,\omega)}} \quad \ldots(7.21)$$

and

$$c_s(y_1, y_2, \omega) = \frac{\Phi_{ps}(y_1, y_2, \omega)}{\sqrt{\Phi_p(y_1,\omega).\,\Phi_p(y_2,\omega)}} \quad \ldots(7.22)$$

$(c_c - ic_s)$ has been called the "correlation spectrum" of the pressures at the two points. The real part of it is identical to th narrow-band correlation coefficient between the pressures at the two points.

Using the above notation, it can be shown than Equation 7.19 reduces

finally to the form

$$\Phi_{P_o}(\omega) = \int_y \Phi_p^{\frac{1}{2}}(y_1,\omega)\int_y \Phi_p^{\frac{1}{2}}(y_2,\omega).\, c_c(y_1,y_2,\omega)\,dy_2\,dy_1 \quad \ldots(7.23)$$

The imaginary term does not appear as it vanishes in the double y-wise integration - as it must do, for $\Phi_{P_o}(\omega)$ is essentially a real quantity.

Consider now the second term in Equation 7.15. The same type of analysis as above may be used to show that the power spectral density of the generalised force, $\Phi_{P_n}(\omega)$, is given by

$$\Phi_{P_n}(\omega) = \int_0^b \Phi_p^{\frac{1}{2}}(y_1,\omega)\, f_n(y_1)\int_0^b \Phi_p^{\frac{1}{2}}(y_2,\omega)\, f_n(y_2).c_c(y_1,y_2,\omega)\,dy_2\,dy_1 \ldots(7.24)$$

The third term in Equation 7.15 is the most complicated of them all. Whereas only the cosine transform of the cross-correlation function contributes to $\Phi_{P_oo}(\omega)$ and $\Phi_{P_n}(\omega)$, the sine transform and the cosine transform contribute to the third term. It can be shown that

$$\lim_{T\to\infty} \frac{2\pi}{T}\, \mathcal{F}^*_{P_o}(i\omega)\,\mathcal{F}_{P_n}(i\omega) =$$

$$\int_0^b \Phi_p^{\frac{1}{2}}(y_1,\omega)\, f_n(y_1)\int_y \Phi_p^{\frac{1}{2}}(y_2,\omega)\left\{c_c(y_1,y_2,\omega) - i\,c_s(y_1,y_2,\omega)\right\}dy_2\,dy_1 \quad \ldots(7.25)$$

A similar expression holds for $\lim_{T\to\infty} \frac{2\pi}{T}\, \mathcal{F}_{P_o}(i\omega)\,\mathcal{F}^*_{P_n}(i\omega)$.

Evaluating the whole of the third term of Equation 7.15 yields:

$$\frac{2\omega^2}{|Z_n|^2}\int \mu f_n\,dy\left\{(K_n - M_n\omega^2)\int_0^b \Phi_p^{\frac{1}{2}}(y_1,\omega)\, f_n(y_1)\int_y \Phi_p^{\frac{1}{2}}(y_2,\omega)\, c_c(y_1,y_2,\omega)\,dy_2\,dy_1\right.$$

$$\left. + K_n\eta_n\int_0^b \Phi_p^{\frac{1}{2}}(y_1,\omega)\, f_n(y_1)\int_y \Phi_p^{\frac{1}{2}}(y_2,\omega)\, c_s(y_1,y_2,\omega)\,dy_2\,dy_1\right\} \quad \ldots(7.26)$$

We have now obtained detailed expressions for each of the component terms of the power spectral density of the beam reaction, as given by Equation 7.15. For general loading distributions, the evaluation of these expressions for the whole frequency range poses a problem of great complexity. Fortunately, some (but not all) of them need only be evaluated over limited frequency regions, outside which their magnitudes are not important.

In the remainder of this chapter attention will be concentrated on particularly simple loading distributions.

VII.3.2 The Power Spectral Density with a Special Loading Distribution

Suppose now that the external loading is of the form

$$p_o(t) : \ell(y) \qquad \ldots(7.27)$$

where $p_o(t)$ is the instantaneous pressure at the point y_o, and $\ell(y)$ is a non-dimensional pressure distribution function. Crudely speaking, the pressures at all points are now in phase with one another but the amplitudes at all points can be different.

The overall correlation coefficient between pressures at any two points is unity, and the correlation spectrum is entirely real with unit value for all frequencies and pairs of points. This effects great simplifications in the loading dependent terms of the reaction power spectrum.

Equation 7.23 reduces to

$$\Phi_{p_o}(\omega) = \Phi_p(y_o,\omega)\left[\int_y \ell(y)\,dy\right]^2 = \Phi_p(y_o,\omega)\,Y_{oo}^2 \qquad \ldots(7.28)$$

Equation 7.24 reduces to

$$\Phi_{p_n}(\omega) = \Phi_p(y_o,\omega)\left[\int_o^b \ell(y)\,f_n(y)\,dy\right]^2 = \Phi_p(y_o,\omega)\,Y_{nn}^2 \qquad \ldots(7.29)$$

The double integral in Equation 7.26 that contains $c_s(y_1,y_2,\omega)$ vanishes, while the other reduces to

$$\Phi_p(y_o,\omega)\int_o^b \ell(y)\,f_n(y)\,dy\int_y \ell(y)\,dy = \Phi_p(y_o,\omega)\,Y_{no} \qquad \ldots(7.30)$$

Notice that $Y_{\omega} = Y_{oo}\,.\,Y_{nn}$

Each of these terms is now proportional to the power spectral density of the pressure at y_o. As derived above, they will be used for the calculations involved in Chapter VIII.

The loading distribution assumed above is one extreme form in which unit correlation is maintained over the whole beam. At the other extreme is the condition when the correlation falls off to zero in a very short length compared with that of the wavelength of the mode $f_n(y)$. The analysis with this distribution can be dealt with quite simply (though not as simply as the unit correlation case) but will not be considered here. This is another feature to be left for future study.

With the loading distribution of the form given by Equation 7.27, the

power spectral density of the reaction (Equation 7.15) becomes

$$\Phi_L(\omega) = \Phi_p(y_o,\omega)\left\{ Y_{oo}^2 + Y_{nn}^2 \frac{\omega^4}{|Z|^2}\left[\int \mu f_n(y)dy\right]^2 + Y_{no}\frac{2\omega^2(K_n - M_n\omega^2)}{|Z|^2}\int \mu f_n(y)dy\right\} \quad \ldots(7.31)$$

In this, all the Y's are independent of frequency. This is only true for the particularly simple loading distribution with unit correlation over the beam.

VII.3.3 The Mean Square Reaction at the Support due to the Special Loading

The mean square reaction is found by integrating the power spectral density over the whole frequency range from $\omega = 0$ to infinity (see Equation 7.3).

On integrating the first term of Equation 7.31 we obtain Y_{oo} times the mean square value of the loading at y_o

$$\int_o^\infty \Phi_p(y_o,\omega)\, Y_{oo}\, d\omega = Y_{oo}\langle p_o^2\rangle \quad \ldots(7.32)$$

in which $\langle p_o^2\rangle$ is the mean square value of the loading at the point y_o.

Integrating the second and third terms of Equation 7.31 yields integrals of the form

$$\int_o^\infty \Phi_p(y_o,\omega)\frac{\omega^4}{|Z_n|^2}\, d\omega$$

The integration of this has been discussed by the author in a previous paper (32), but only for the case of small damping. However, irrespective of the size of the damping, it can be shown to be identical to

$$\frac{K_n^2}{M_n^2}\left\{\frac{2}{\omega_n^2}\int_o^\infty \Phi_p(y_o,\omega)\frac{\omega^2}{|Z_n|^2}\, d\omega - (1+\eta_n^2)\int_o^\infty \frac{\Phi_p(y_o,\omega)}{|Z_n|^2}\, d\omega\right\} + \frac{\langle p_o^2\rangle}{M_n^2} \quad \ldots(7.33)$$

To evaluate the integrals contained within this expression, we now made the usual assumption that $\Phi_p(y_o,\omega)$ does not vary appreciably with ω in the region of the resonant peak of $1/|Z_n|^2$; and that the greater part of each integral comes from this region of the resonant peak. There is

ample justification for this when the damping is light, but much less when the damping is heavy. However, we shall concern ourselves only with the orders of magnitude of the integrals and the assumption then becomes reasonable. Suppose the value of $\Phi_p(y_o, \omega)$ at the resonant frequency $\omega_n = (K_n/M_n)^{\frac{1}{2}}$ is $\Phi_p(\omega_n)$ (dropping the "y_o" for convenience). On the above assumption we can now say

$$\int_o^\infty \Phi_p(y_o,\omega)\frac{\omega^2}{|Z_n|^2}\,d\omega \;\doteq\; \Phi_p(\omega_n)\int_o^\infty \frac{\omega^2}{|Z_n|^2}\,d\omega \qquad \ldots(7.34)$$

and

$$\int_o^\infty \Phi_p(y_o,\omega)\frac{1}{|Z_n|^2}\,d\omega \;\doteq\; \Phi_p(\omega_n)\int_o^\infty \frac{1}{|Z_n|^2}\,d\omega \qquad \ldots(7.35)$$

The integrals in this final form can be evaluated exactly, provided that K_n and η_n (contained within Z_n) do not vary with frequency. If they do, numerical integration is the only method of evaluation.

The exact integrals are found to be

$$\int_o^\infty \frac{\omega^2}{|Z_n|^2}\,d\omega \;=\; \frac{\pi}{2}\frac{\omega_n^3}{K_n^2\eta_n}\left\{\frac{1+\sqrt{1+\eta_n^2}}{2}\right\}^{\frac{1}{2}} \qquad \ldots(7.36)$$

and

$$\int_o^\infty \frac{1}{|Z_n|^2}\,d\omega \;=\; \frac{\pi}{2}\frac{\omega_n}{K_n^2\eta_n}\left\{\frac{1+\sqrt{1+\eta_n^2}}{2(1+\eta_n^2)}\right\}^{\frac{1}{2}} \qquad \ldots(7.37)$$

These now enable us to find the total mean square reaction, $\langle L^2\rangle = \int_o^\infty \Phi_L(\omega)\,d\omega$, from Equation 7.31. Putting $K_n = M_n\omega_n^2$, we finally obtain

$$\begin{aligned}\langle L^2\rangle \;=\; & \langle p_o^2\rangle\, Y_{oo}^2 \;+\\ & + \langle p_o^2\rangle Y_{nn}^2\frac{\left[\int \mu f_n(y)\,dy\right]^2}{M_n^2}\left\{1 + \frac{\Phi_p(\omega_n)}{\langle p_o^2\rangle}\cdot\frac{\pi}{2}\cdot\frac{\omega_n}{\eta_n}\sqrt{\frac{1+\sqrt{1+\eta_n^2}}{2}}\left(2-\sqrt{1+\eta_n^2}\right)\right\}\\ & + \langle p_o^2\rangle 2Y_{no}\frac{\int \mu f_n(y)\,dy}{M_n}\left\{-1 + \frac{\Phi_p(\omega_n)}{\langle p_o^2\rangle}\cdot\frac{\pi}{2}\cdot\frac{\omega_n}{\eta_n}\sqrt{\frac{1+\sqrt{1+\eta_n^2}}{2}}\left(\sqrt{1+\eta_n^2}-1\right)\right\}\end{aligned} \qquad \ldots(7.38)$$

The first term on the right hand side of this equation is simply the mean square value of the force exerted on the support by the external loading. The second term is the mean square value of the inertia force exerted on the support by virtue of the motion of the beam in the nth mode. The third term allows for the fact that these two forces are correlated with one another and <u>increases</u> with increasing damping.

The necessity for this third "correlation term" may be seen by recognising the total reaction as the sum of two randomly varying <u>vector</u> quantities. The mean square value of the total vector is the mean square value of the <u>modulus</u> of the vector. This, of course, is not equal just to the sum of the moduli of the individual vectors, but to this sum together with another quantity which depends on the phase (i.e. degree of correlation) between the two vectors.

To assess the relative magnitudes of the different terms of Equation 7.38, it is convenient to re-arrange it into the form

$$\langle L^2 \rangle = \langle p_o^2 \rangle \left\{ \left[Y_{oo} - Y_{nn} \frac{\int \mu f_n(y)\,dy}{M_n} \right]^2 + \right.$$

$$+ \frac{\Phi_p(\omega_n)}{\langle p_o^2 \rangle} \cdot \frac{\pi}{2} \cdot \frac{\omega_n}{\eta_n} \sqrt{\frac{1+\sqrt{1+\eta_n^2}}{2}} \cdot \frac{Y_{nn} \int \mu f_n(y)\,dy}{M_n} \times \left[\right.$$

$$\left. \left. \times \left[\frac{Y_{nn} \int \mu f_n(y)\,dy}{M_n} \left(2 - \sqrt{1+\eta_n^2}\right) + 2 Y_{oo} \left(\sqrt{1+\eta_n^2} - 1\right) \right] \right\} \qquad \ldots(7.39)$$

in which Y_{n0} does not appear, having been replaced by $Y_{nn} \cdot Y_{oo}$ in the course of the re-arrangement.

Now the part of Equation 7.39 which is independent of the spectral density, $\Phi_p(\omega_n)$, can be shown to vanish identically when the excitation constitutes a "normal loading". (See Section VII.3.4). The spectrum-dependent term then becomes all-important. Under other loading conditions the term will not vanish, and the magnitude of the non-dimensional factor

$$\frac{\Phi_p(\omega_n)}{\langle p_o^2 \rangle} \cdot \frac{\pi}{2} \cdot \omega_n = \chi \qquad \ldots(7.40)$$

in the other term then plays an important part in establishing the relative importance of the two terms. As this factor frequently appears in random vibration theory of this type (e.g. as in reference 32) some typical values of it are considered below in section VII.4. Without considering specific modes and loading distributions, no more conclusions can be drawn about the relative values of the terms in Equation 7.39. In the next chapter, calculations are carried out on the basis of this theory for a special system, and the relative importance of the terms is seen.

Another non-dimensional term may be identified in Equation 7.39 after dividing through by Y_{oo}^2, viz.

$$\frac{Y_{nn}}{Y_{oo}} \frac{\int \mu f_n(y)\,dy}{M_n} = y \qquad \text{say.} \qquad \ldots(7.41)$$

This term is probably peculiar to the present particular problem and will not be discussed here.

Using the symbols $\mathcal{Y}$ and χ permits Equation 7.38 to be written in the form:

$$\langle L^2 \rangle = \langle p_o^2 \rangle Y_{oo}^2 \left\{ 1 + \mathcal{Y}^2 \left[1 + \chi \frac{1}{\eta_n} \sqrt{\frac{1+\sqrt{1+\eta_n^4}}{2}} \left(2 - \sqrt{1+\eta_n^2} \right) \right] + \right.$$

$$\left. + 2\mathcal{Y} \left[-1 + \chi \frac{1}{\eta_n} \sqrt{\frac{1+\sqrt{1+\eta_n^4}}{2}} \left(\sqrt{1+\eta_n^2} - 1 \right) \right] \right\} \quad \ldots(7.42)$$

or in the alternative form corresponding to Equation 7.39:

$$\langle L^2 \rangle = \langle p_o^2 \rangle Y_{oo}^2 \left\{ (1-\mathcal{Y})^2 + \chi \mathcal{Y} \frac{1}{\eta_n} \sqrt{\frac{1+\sqrt{1+\eta_n^4}}{2}} \left[2(\mathcal{Y}-1) + \sqrt{1+\eta_n^2} (2-\mathcal{Y}) \right] \right\} \quad \ldots(7.43)$$

VII.3.4 Excitation by a Random "Normal" Loading

A "normal" loading is one which at all points on the structure is proportional to the inertia loading corresponding to one of the normal modes of the structure, i.e.

$$\ell(y) = \text{Constant} \times \mu f_n(y) \quad \ldots(7.44)$$

Using this to find the Y's, and remembering that

$$M_n = \int_o^b \mu f_n^2(y)\, dy$$

it is found that $\mathcal{Y} = 1$, and that the whole of Equation 7.39 or 7.43 reduces to the form

$$\langle L^2 \rangle = \left[\int_o^b \ell(y) f_n(y)\, dy \right]^2 \Phi_p(\omega_n) \frac{\pi}{2} \frac{(1+\eta_n^2)}{M_n^{\frac{1}{2}} K_n^{-\frac{1}{2}} \eta_n} \left\{ \frac{1+\sqrt{1+\eta_n^2}}{2(1+\eta_n^2)} \right\}^{\frac{1}{2}} \quad \ldots(7.\ldots)$$

which is actually identical to the square of Equation 3.29 (Chapter III) from which the reaction force criterion was derived. The derivation in this chapter serves to emphasize the conditions under which the reaction force criterion for assessing damping treatments is strictly reliable, viz. when the excitation constitutes a normal loading, when the inertia forces of just one mode predominate and when the power spectral density of the loading does not vary appreciably in the region of the resonant peak of the excited mode.

VII.4 Typical Values of the Parameter χ

Attention was drawn in section VII.3.3 to the non-dimensional parameter χ, defined by

$$\chi = \frac{\Phi_p(\omega_n) \cdot \omega_n}{\langle p_o^2 \rangle} \cdot \frac{\pi}{2}$$

Its magnitude can be visualised by considering a typical spectrum, $\Phi_p(\omega)$, such as that illustrated in Figure 5, or in the diagram below:

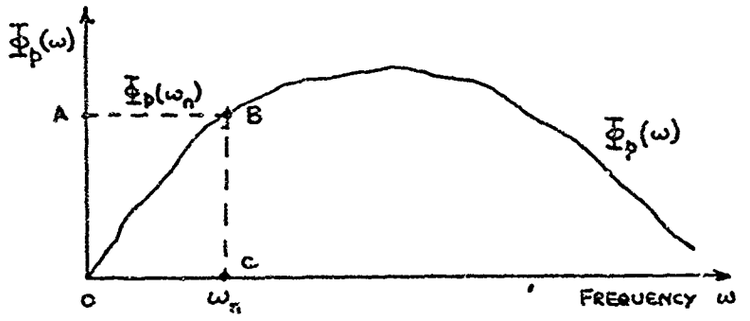

The mean square pressure, $\langle p_o^2 \rangle$, is proportional to the total area under the curve, while the term $\Phi_p(\omega_n).\omega_n$ is proportional to the area within the rectangle OABC. If the spectrum is fairly smooth (i.e. if it has no sharp, high peaks) it is evident that χ will be small if ω_n is at the low frequency end. If the spectrum does contain high peaks, one of which occurs at ω_n, then χ can have a high value. Some typical values of this parameter are quoted below, having been derived from the (smooth) spectra of the noise pressures from an Avon jet engine. Some of these values are used in Chapter VIII.

f_n $(= 2\pi\omega_n)$	χ	Condition
200	0.14	Minimum value, close to jet
200	1.21	Maximum value, close to jet
500	0.15	Minimum value, close to jet
500	0.60	Maximum value, far from jet
1000	0.30	Minimum value, close to jet
1000	0.54	Maximum value, far from jet

The maximum and minimum values were found from data relating to several different jet speeds and locations around the jet.

In the near-field of a jet engine, the noise pressure distribution does not conform to the simple form of Equation 7.27, so that some doubt may be expressed as to the validity of quoting these values of χ in the present context. However, over distances which are representative of fuselage panel dimensions, the narrow-band pressure correlation coefficients do not drop much below a value of 1. This suggests that the quoted values of χ can justifiably be considered here.

Less justification can be offered for quoting values of χ corresponding to boundary layer pressure fluctuations, but it is useful to bear in mind the values which it can take. In view of the nature of the boundary layer pressure spectrum, (see section 1.3.2), it is evident that

$$\chi \doteqdot \frac{\pi}{2} \cdot \frac{f_n}{f_{cut-off}}$$

With f_n = 500 c.p.s, and $f_{cut-off}$ = 6000 c.p.s. (as in Figure 6), this gives χ = 0.13.

VII.5 Concluding Remarks

The first part of the analysis of this chapter has re-emphasized the complexity of calculating the response spectrum of even the simplest beam subjected to a general random loading. However, if the loading distribution is of a simple form, a relatively simple expression may be derived for the mean square response. The expression for this that has been developed in this chapter has disclosed the importance of

(a) a contributory term to the mean square response which <u>increases</u> with increasing damping, and which derives from the correlation between the random excitation and the random inertia forces,

(b) the loading parameter, $\chi = \frac{\Phi_b(\omega_n) \cdot \omega_n}{\langle p_o^2 \rangle} \cdot \frac{\pi}{2}$

The expression for the mean square response was derived on the assumption that:

(i) the power spectral density of the exciting loading did not vary appreciably in the region of the resonant frequency of the system

(ii) that the damping and stiffness of the system were not frequency dependent.

The extent of the region referred to in (i) depends on the damping. The higher the damping, the wider is the region, and the less is the likelihood of assumption (i) being satisfied. Further, if the high damping has been achieved by incorporating a polymeric material in the system, its presence and nature will ensure that the stiffness and damping <u>are</u> frequency dependent, so violating assumption (ii). The error incurred in the theoretical mean square response due to the violation of these two assumptions can only be investigated in particular cases, but it is conceivable that it will be of the same order as that incurred by omitting the large damping correction factors discussed in para. III.4.1.

Chapter VIII

Experiments on Sandwich Beams Under Random Excitation

VIII.1 Purpose and Scope of the Chapter

As several important assumptions have been made in the random vibration theory of Chapter VII, it is to be expected that the theory can only give approximate values of the mean square response. It is therefore desirable to investigate the accuracy with which the theory can in fact predict the random response under real conditions. It is the purpose of this chapter to describe such an investigation in which the sandwich specimens and the test rig of Chapter VI were used with random excitation. The r.m.s. reaction at the support was measured and its value is compared in this chapter with values predicted by the random theory of Chapter VII, using the loss factors and resonant frequencies measured in the harmonic tests of Chapter VI. A comparison of the specimens on the basis of the simple random reaction force criterion is itself to be compared with a comparison based on the measured values of the random reaction.

VIII.2 The General Method of the Investigation

Each of the specimens of Chapter VI was excited in the same test rig as before by a randomly varying current. The response of the specimens was arranged to be predominantly in the second mode by the appropriate disposition of the magnets on the rig. The spectrum of the exciting current (force) was adjusted such that the values of χ (Equation 7.40) corresponding to the frequencies of the second modes were of the order of 0.7, i.e. approximately mid-way between the two values quoted on Section VII.4 for $\omega_2 = 200$ c.p.s. Under these conditions the r.m.s. value of the random reaction signal was measured for a given r.m.s. value of the exciting current.

The theoretical prediction of the random reaction may legitimately be based on the theory of Chapter VII as the specimen test conditions satisfied the loading condition of Equation 7.27 (unit correlation of loading all over the beam) and the "uni-modal condition" of Section VII.3.1. The quantities which must be known for the prediction are shown in Equation 7.38 to be:

(a) η_n and ω_n ; these are to be taken from the harmonic test results of Chapter VI.

(b) $\langle p_o^2 \rangle$; this was proportional to the mean square exciting current.

(c) $\Phi_p(\omega_n)$; this was proportional to the spectral density of the exciting current.

(d) $\ell(y)$, implicit in the Y's ; this was proportional to the distribution along the specimen length of the magnetic flux cutting the specimen.

(e) $f_n(y)$; this has been assumed to be of the form $\sin 2\pi y/b$.

Measurements of (b), (c) and (d) had therefore to be made. Further, the constants of proportionality between the exciting current and the local

loading and also between the reaction force and the reaction voltage signal had to be determined.

In actual fact, the theoretical prediction in this chapter yields the r.m.s. value of the random reaction signal produced by known excitation conditions. This quantity is compared with the measured r.m.s. reaction signal.

VIII.3 Details of the Experiments

VIII.3.1 The Apparatus

The sandwich specimens and the test rig have been fully described in Chapter VI. In these random tests four magnets were stationed at approximately $\frac{1}{8}$ and $\frac{3}{8}$, 5/8 and 7/8 of the beam length from one end. The flux due to each of the first pair acted in the same direction, opposite to that due to the second pair.

The exciting current was supplied by a power amplifier driven by a random-noise signal generator. As the spectrum of this signal was virtually flat up to and beyond 30 kc/s, it had to be shaped to concentrate the signal energy in the lower audio-frequency range. Accordingly, a Cawkell adjustable filter was used, set to pass frequencies between 2 c.p.s. and 700 c.p.s. With this setting, the value of χ for the exciting current had the prescribed value of 0.7 (approximately) at 200 c.p.s.

The r.m.s. value of the exciting current was measured on a Solartron True R.M.S. Voltmeter, using the same voltage signal as in Chapter VI to monitor the exciting current. The spectral density of the current was measured by passing the same voltage signal through a Muirhead L.F. Analyser, and measuring the r.m.s. value of the resultant filtered output. The equivalent pass-bandwidth of the analyser was 3% of the frequency setting. As the analysing filter did not possess by any means an ideal "steep-sided" characteristic, the spectral density measurements may have been subject to small errors.

VIII.3.2 The Experimental Procedure for the Random Tests

Each specimen was tested in the same way at a temperature of 21.5°C, although some tests were conducted at temperatures closer to 24°C. The exciting current was first adjusted to give an r.m.s. voltage of 100 mV across the "measuring resistance" in the circuit (see section VI.5.2). The r.m.s. voltage output from the reaction transducer was then recorded.

Also recorded was the 'residual noise' output signal from the reaction transducer which was present when no exciting current was flowing. This derived principally from mains hum pick-up. Although its r.m.s. value was found to be nearly 10% of the total reaction transducer output for some of the specimens, the true signal due to the reaction force differed negligibly from the measured total. This was due to the residual noise being altogether uncorrelated with the true reaction signal.

VIII.3.3 The Measurement of the Spectrum of the Exciting Current

The voltage signal from the current measuring resistance was passed through the L.F. Analyser which was set in turn at a number of different

frequencies over the range 20 - 700 c.p.s. The r.m.s. value of the output from the analyser was measured on the r.m.s. voltmeter. The spectral density was then given by the square of the indicated r.m.s. value ÷ (0.03 x the frequency setting).

The indicated r.m.s. voltage suffered from long-period fluctuations which were an inevitable consequence of the narrow (3%) bandwidth of the analyser and the finite integrating time of the voltmeter. Although the integrating time constant of the voltmeter was set to about 400 secs., over longer periods than this the r.m.s. indication could vary by as much as ± 15% about a mean value. To estimate the mean value therefore involved a prolonged period of observation and recording for each frequency setting of the analyser.

The measured spectrum is shown in Figure 58.

VIII.3.4 The Determination of the Loading Distribution Function, $\ell(y)$

Since the same current flowed along the whole length of a specimen, the corresponding loading at any point was proportional to the local magnetic flux. To measure the distribution of this flux along the specimen, a short wire conductor, $\frac{1}{4}$ in. long, was placed in the magnetic field in place of the specimen and the force exerted on it was measured when it carried a known direct current. The force was measured with a cantilever beam on which a strain-gauge bridge sensed the bending strains at the root. (The beam was originally used as a vibration displacement transducer). A force on the tip of the beam produced a proportional out-of-balance voltage across the bridge which could be measured on a galvanometer.

Accordingly, the wire conductor was fixed to the end of the beam and placed in position in the magnetic field. A known direct current was passed through it and the galvanometer deflection was recorded. Readings were taken with the conductor at about forty different stations along the magnetic field. The flux distribution, and hence $\ell(y)$, is shown in Figure 59.

Absolute values of the force exerted were not deduced, as the distribution function was only required in a non-dimensional form.

VIII.3.5 The Determination of the Relationship between Loading and Current, Reaction Force and Reaction Transducer Output

The instantaneous loading on the specimens was proportional to the instantaneous current, and hence also to the instantaneous value of the voltage, $V_p(t)$, across the current measuring resistance. We may therefore write:

$$p(y,t) = p_o(t).\ell(y) = k_p.V_p(t).\ell(y) \qquad \ldots(8.1)$$

Similarly, the instantaneous reaction force, $L(t)$, and the reaction transducer output voltage, $V_r(t)$, may be related by

$$V_r(t) = k_r.L(t) \qquad \ldots(8.2)$$

Using k_p and k_r in conjunction with Equations 7.42 or 7.43, it is seen that the mean square value of the reaction transducer voltage is given by

$$\langle V_r^2 \rangle = k_r^2 k_p^2 Y_{oo}^2 \langle V_p^2 \rangle \times \text{Function of } \chi, \mathcal{Y} \text{ and } \eta_n \qquad \ldots(8.3)$$

The prediction of $\langle V_r^2 \rangle$ therefore requires the product $k_r k_p Y_{oo}$; k_r and k_p are not required individually.

The product $k_r k_p Y_{oo}$ was determined from a test on a lightly-damped, solid aluminium specimen (16 SWG) mounted in the test rig and excited harmonically at the resonant frequency of its second mode. Being lightly damped ($\eta_n = 0.002$), the total force exerted on the support was virtually equal to the inertia force alone. The amplitude of this is easily shown to be given by

$$\frac{|p_o(t)|}{\eta_n} \frac{\int_o^b \ell(y) f_n(y)\,dy \int f_n(y)\,dy}{M_n} = \frac{|p_o(t)|\, Y_{oo}\, \mathcal{Y}}{\eta_n} \qquad \ldots(8.4)$$

The amplitudes of the harmonic signals $V_p(t)$ and $V_r(t)$ under this resonant condition were therefore related by

$$|V_r| = k_r \frac{|p_o(t)|}{\eta_n} Y_{oo}\, \mathcal{Y} = k_r k_p \frac{Y_{oo}\, \mathcal{Y}}{\eta_n} \cdot |V_p|$$

or
$$k_r k_p Y_{oo} = \frac{\eta_n |V_r|}{\mathcal{Y}\, |V_p|} \qquad \ldots(8.5)$$

Hence, the product was evaluated from measured values of $|V_r|$ and $|V_p|$ at the resonant frequency of the aluminium specimen. The modal loss factor of the specimen, η_n, was measured from the width of the frequency response curve near resonance and was found to have the value 0.00176. The value of $\mathcal{Y}$ was found using $f_n(y) = \sin 2\pi x/b$, together with the distribution function, $\ell(y)$, found in section VIII.3.4 above. These yielded $\mathcal{Y} = 1.34$.

VIII.4 Details of the Theoretical Prediction of the Random Reaction

The mean square voltage from the reaction transducer has been shown in the last section to be given (theoretically) by:

$$\langle V_r^2 \rangle = k_r^2 k_p^2 Y_{oo}^2 \langle V_p^2 \rangle \left\{ 1 + \mathcal{Y}^2 \left[1 + \frac{\chi}{\eta_n} \sqrt{\frac{1+\sqrt{1+\eta_n^2}}{2}} \left(2 - \sqrt{1+\eta_n^2} \right) \right] + \right.$$
$$\left. + 2\mathcal{Y} \left[-1 + \frac{\chi}{\eta_n} \sqrt{\frac{1+\sqrt{1+\eta_n^2}}{2}} \left(\sqrt{1+\eta_n^2} - 1 \right) \right] \right\} \qquad \ldots(8.6)$$

which has been derived from Equation 7.42. For the mode and loading distribution being considered, $\mathcal{Y}$ has the value 1.34 (as in the last section).

The value of χ has to be evaluated at the frequency ω_n corresponding to the second mode of each specimen. These frequencies are taken from the results of Chapter VI. The value of $\Phi_p(\omega_n)$ required in χ has been taken from the measured spectrum shown in Figure 58. The values of η found in Chapter VI for the second modes have been used.

In the evaluation of $\langle V_r^2 \rangle$, it is of interest to compare the relative magnitudes of its three component parts, viz. that part deriving from the force exerted by the external loading, that part deriving directly from the modal inertia forces, and that part deriving from the correlation between these two forces. These parts are represented non-dimensionally within the large bracket of Equation 8.5 by the unit term, the $\mathcal{Y}^2$ term and the $2\mathcal{Y}$ term, respectively. The values taken by each of these terms for the different specimens are shown in Table VI , in which are also shown the values of $f_n (= \omega_n/2\pi)$, η_n , and finally $\langle V_r^2 \rangle^{\frac{1}{2}}$, i.e. $(V_r)_{rms}$. The values of these latter quantities correspond to $(V_p)_{rms} = 0.100$ volts, at which value the experiments were conducted.

VIII.5 Experimental and Theoretical Results

The measured and predicted values of the r.m.s. reaction transducer output are shown together in Table VI.

VIII.6 Discussion of Results

Before comparing the predicted and the experimental results it is worthy of note that the values in set B of the experimental results are approximately 1.50 times those in set A. Set A were measured first and set B were measured some time later after some of the apparatus had been calibrated. In the course of the calibration the stability of some of the measuring apparatus was suspected. It is possible, therefore, that the values of set B were measured after the apparatus had drifted away from its calibrated state.

If the value of set B are divided by 1.5, it can be seen that both these and set A agree very well with the predicted values.

If these factored set B values and the set A values are correct, the validity and accuracy of the theoretical approach are amply confirmed and the assumptions on which the theory is based are justified - at least, when the theory is applied to the particular specimens and conditions of the tests.

Also justified by the agreement of the results is the use we have made of the harmonically measured values of ω_n and η_n in predicting the response. In Chapter VI (section VI.7.4) some discussion took place on the effect of the frequency dependence of η and R on the apparent values of ω_n and η_n measured from the vector response curves. It was concluded that the effect was likely to be very small. Confirmation for this now comes from the fact that the measured values of ω_n and η_n can be used to predict the random response quite accurately.

The terms in Table VI which contribute to the total predicted response show the relative importance of the correlation term ($\propto 2\mathcal{Y}$), the direct inertia term ($\propto \mathcal{Y}^2$) and the term due to the external loading (the unit term). With low damping (as for the Dynadamp specimen), the direct inertia term predominates in the expected way, and the correlation and external loading

terms are of little signficance. On the other hand, with high damping (as for Oberst's specimen), all three terms are of similar magnitude and the exclusion of any one of them cannot be justified.

That the correlation term should be negative in each case follows from the values of χ being relatively small. On account of this, it can be shown that the correlation effect derives mainly from the correlation of the frequency components of the inertia force and excitation which lie above the natural frequency. Speaking in terms of harmonic motion, these components are known to be in anti-phase with each other, i.e. the correlation between them is negative. The high frequency inertia force components then balance (or "cancel out") the high frequency excitation components.

VIII.7 Comparisons of the Specimens by the Random Reaction Force Criterion and the Measured Force

In this section, by using the foregoing experimental results, we shall investigate the validity of using the random reaction force criterion as a basis for comparing the specimen under the given particular conditions.

Chapter III shows that the magnitudes of the criteria are inversely proportional to the responses to which they relate, i.e. within the assumptions that were stated, the response should be proportional to the reciprocal of the criterion value. Hence, to test the validity of using the inertia force criterion, the reciprocal of its values for each of the seven tested specimens should be compared with the measured values of the random reaction forces. If the ratios of the two sets of values are consistent, the validity of the criterion is demonstrated for the particular conditions under consideration.

In section III.4.1, the random reaction force criterion was derived and this is easily seen to be proportional to $[\eta_n r_i(\eta_n)/\omega_n]^{\frac{1}{2}}$. In this expression the mass and stiffness ratios are included implicitly in ω_n. For the purpose of this section, these expressions have been evaluated as they stand, using the measured values of ω_n and η_n for the second modes of the different specimens. The reciprocals of the values so obtained have then been normalised, for convenience, to make the value for Oberst's specimen equal to 1.0.

To compare these values with the measured values, the same normalising process has been applied to the measured values. They are all presented in Table VII.

Exact agreement between the different rows of this table is not to be expected, bearing in mind that the expression for the criterion was developed after making certain assumptions which were not realised in the experiment (e.g. a flat spectrum of excitation). It would be possible to give an improved semblance of agreement by normalising the values such that another specimen had the unit value. This is a detail which will not be pursued here. It can be stated with confidence, however, that the use of the criterion indicates correctly the order (i.e. the "sequence") in which the "damping effectivenesses" of the different specimens lie. The marginally different values for the 3M3 and 3M4 specimens are the only exceptions to this.

VIII.8 Conclusions drawn from Chapter VIII

Close agreement has been found to exist between the measured and predicted values of the random reaction at the support of the damped sandwich specimens. This appears to confirm the theory of Chapter VII and shows (in particular) that even with high damping ($\eta \doteqdot 0.9$) we have been justified in calculating the response on the assumption that there is little or no variation in the spectral density of the excitation in the region of the system resonance.

The part of the random response deriving from the correlation between the inertia force and the external loading has been found to be very significant for the highly damped specimens but negligible for the more lightly damped specimens. It appears to become significant when η is greater than about 0.15.

It has been found that the values of the resonant frequencies and loss factors of the specimens measured by the methods of Chapter VI may be used with confidence in the theory for predicting the random response.

The random reaction force criterion has been found to be a reliable guide as the order (i.e. the sequence) of the effectivenesses of the different sandwich specimens in damping random reaction forces.

Chapter IX

General Conclusions

Detailed conclusions from the different stages of this report have been included at the end of most of the chapters (chapters II and IV to VIII). Only the most important conclusions will be reported here.

The study of the damping of reinforced plate structures (without any damping treatment) has shown that the damping ratios may vary from 0.005 for stringer torsion modes of a large model to 0.011 for stringer bending modes of a smaller model. Measurements made on full scale aeroplane structures cannot yet be treated with much confidence, but the apparent values of the damping ratios were 0.014 to 0.02 for stringer torsion modes, or modes of similar nature. These values could be over-estimates of the true values. Acoustic radiation can yield damping ratios of up to 0.016 for some modes, but for other modes it could yield nothing.

It has next been shown that in order to judge the relative effectiveness of different damping treatments and configurations, a comparison of the magnitudes of the loss factors of the configurations is generally insufficient. Alternative criteria have therefore been derived, based on a number of simplifying assumptions relating to the system response. These criteria have then been used to compare two different unconstrained layer treatments. It has thereby been shown that for some applications one treatment is superior to the other, but for other applications this superiority is reversed. According to some criteria there exists an optimum thickness of damping treatment to minimise the response of a given plate, but according to other criteria the response continually decreases with increase of treatment thickness.

The theory of the response of a two-dimensional flat sandwich plate with a damped core has next been developed. The modal loss factors and stiffnesses have been found to depend on the modal wavelength, as well as on the core thickness and core dynamic properties. Using the criteria, the optimum core thicknesses and/or core properties have been found which minimise the random and harmonic response of the plate. For a sandwich plate of given total weight, the minimum plate response is obtained when the core is about five times as thick as one of the face-plates, but the static stiffness of such a plate is much lower than that of a solid plate of the same weight; this may not be important in areas of an aeroplane structure which are designed primarily from acoustic fatigue considerations.

If the solid skin plating of a real aeroplane structure is replaced by a sandwich plate having a thick core of optimum properties, a rough estimate suggests that the r.m.s. stresses and reaction forces due to random excitation will be reduced by no more than 90%. If the sandwich plate has a thin core, the reduction is no more than 60-70%.

Comparing the criterion values for the sandwich plates of optimum design with those of the plate treated with an unconstrained layer indicates that the sandwich damping mechanism is more effective all round in reducing random or harmonic response. In particular, if the treatment weight is 50% of the weight of the metal plate(s) and β for the sandwich core is 1.0,

the random stress and reaction force criterion values for the sandwich are about twice those for the other treated plate. i.e. the response is about one half.

The theory for the sandwich plate loss factor and modal stiffness has been partially confirmed by the results of harmonic specimens on small sandwich specimens. The special apparatus that had to be designed and the techniques of measurements that had to be developed have proved to be satisfactory for conducting assessment tests on different damping treatments and configurations.

The theoretical study of the random vibration of a heavily damped beam has disclosed the importance in calculating its response of allowing for the response component deriving from the correlation between the external loading and the inertia forces excited by it. This term can be ignored, however, if the loss factor of the system is less than about 0.15.

In an experimental investigation of the random response of heavily damped beams, close agreement was found to exist between the response predicted by the theory and the measured values. Besides confirming the general validity of the theory, this also showed that values of the loss factors and resonant frequencies measured in the harmonic tests could be used with confidence to predict the random response. For the particular specimens and conditions of test, the random reaction force criterion was found to be a reliable guide to the relative effectiveness of the different specimens in attenuating the random reaction force.

Further work in this field of damping studies should deal with the damping and stiffness of sandwich plates with boundary conditions other than the simple supports dealt with in this report. The one-dimensional, fully-fixed sandwich plate should be amenable to exact theoretical treatment, but approximate methods will probably be required for plates reinforced by flexible stiffeners. Systematic experimental studies of the harmonic and random vibration of stiffened damped plates will also be required.

List of References

1. Miller, P.R. — "Free Vibrations of a Stiffened Cylindrical Shell" Aeronautical Research Council Reports and Memoranda No. R & M 3154.

2. Lin, Y.K. — "Free Vibrations of Continuous Skin Stringer Panels" Journal of Applied Mechanics, December, 1960.

3. Ford, R.D. — "The Response of a Model Structure to Noise - Part I" University of Southampton Report No. A.A.S.U. 181.

4. Clarkson, B.L. — "The Design of Structures to Resist Jet Noise" Jour. Roy. Aero. Soc., October 1962.

5. Middleton, D. — "Near Field Noise Tests on an Avon R.A.26 Engine fitted with Conical Nozzle" Rolls Royce Tech. Report. April, 1959.

6. Callaghan, E.E. Howes, W.L. Coles, W.D. — "Near Field of a Jet-engine Exhaust. II - Cross Correlation of Sound Pressures" N.A.C.A. Technical Note 3764. September, 1956.

7. Bull, M.K. — "Boundary Layer Noise" Ch. VIII in "Noise and Acoustic Fatigue in Aeronautics" - Lecture notes compiled by the staff of the Institute of Sound and Vibration Research, University of Southampton. April, 1963.

8. Clarkson, B.L. Ford, R.D. — "The Response of a Typical Aircraft Structure to Jet Noise" Jour. Roy. Aero. Soc., January 1962.

9. Dyer, I. — "Sound Radiation into a Closed Space from Boundary Layer Turbulence" BBN Report No. 602, December 1958.

10. Corcos, G.M. Liepmann, H.W. — "On the Transmission through a Fuselage Wall of Boundary Layer Noise" NASA T.M. 1420 (1956).

11. Kraichnan, R.H. — "On the Fatigue Failure of Structures due to Vibrations Excited by Random Pressure Fields" Jour. Acoust. Soc. of America, January 1957.

12. Powell, A. — "On the Fatigue Failure of Structures due to Vibrations Excited by Random Pressure Fields" Jour. Acoust. Soc. of America , December 1958.

13. Mead, D.J. "The Damping Stiffness and Fatigue Properties of Joints and Configurations Representative of Aircraft Structures"
Papers presented at the WADC - University of Minnesota Conference in Acoustical Fatigue, September 1959. Reported in WADC Tech. Report 59 - 676.

14. Mangiarotty, R.A. "The Acoustic Radiation Damping of Vibrating Panels"
M.Sc. Thesis submitted to University of Southampton, 1960.

15. Mead, D.J. "The Effect of a Damping Compound on Jet-Efflux Excited Vibrations - Part I"
Aircraft Engineering, March 1960.

16. Mead, D.J. "The Internal Damping Due to Structural Joints and Techniques for General Damping Measurement"
Aeronautical Research Council, Current Paper No. 452, 1959.

17. Mercer, C.A. "Optimum Design of Damped Structures for Acoustic Fatigue"
Thesis submitted to University of Southampton for degree of B.Sc.(Eng.) with Honours, May, 1962.

18. Clarkson, B.L.
Ford, R.D. "The Response of a Model Structure to Noise"
Part II - Curved Panel
University of Southampton Report No. AASU 206, April, 1962.

19. Foxwell, J.H.
Franklin, R.E. "Acoustic Effects in the Vibrations of Structures"
Aeronautical Research Council Report No. ARC 19,743, 1957.

20. Foxwell, J.H.
Franklin, R.E. "The Vibrations of a Thin-Walled Stiffened Cylinder in an Acoustic Field"
Aeronautical Quarterly, Vol.10, 1959.

21. Oberst, H.
Frankenfeld, K. "Uber die Dämpfung der Biegeschwingungen dünner Bleche durch fest haftende Beläge, I"
Acustica, Akustische Beihafte, 4. 1952.

22. Kerwin, E.M. "Damping of Flexural Waves by a Constrained Visco-elastic Layer".
Journ. Acoustical Soc. America Vol. 31, No.7, July, 1959.

23. Plass, H.J. "Damping in Elastic Rods and Sandwich Structures by Incorporation of Additional Visco-Elastic Material" Proceedings of the Third Midwestern Conference on Solid Mechanics, pp.48-71, 1957.

24. Ross, D. Kerwin, E.M. Dyer, I. "Flexural Vibration Damping of Multiple-Layer Plates" Bolt, Beranek and Newman Report No. 564, July, 1958.

25. Kurtze, G. Watters, B.G. "New Wall Design for High Transmission Loss or Damping" Journal of the Acoustical Society of America, Vol. 31, No. 6, June, 1959, pp. 739-748.

26. Yu, Y.Y. "Damping of Flexural Vibrations of Sandwich Plates" Report submitted to U.S. Air Force Office of Scientific Research under Contract AF49(638)-453, TN No. 10, May, 1961.

27. Freudenthal, A.M. Bieniek, M.P. "Forced Vibrations of Sandwich Structures" WADD Tech. Report 60-307 (USAF)

28. Mead, D.J. Pretlove, A.J. "On the Vibrations of Cylindrically Curved Elastic Sandwich Plates: Part I, with the Solution for Flat Plates" University of Southampton Report No. AASU 186, August, 1961.

29. Kennedy, C.C. Pancu, C.D.P. "Use of Vectors in Vibration Measurement and Analysis" J.Ae.Sc., November 1947.

30. Williams, D. "Displacements of a Linear System under a Given Transient Load" Aero. Quarterly, August 1949.

31. Lin, Y.K. "Stresses in Continuous Skin Stiffener Panels under Random Loading" J. Aero. Space Sci., June 1962.

32. Mead, D.J. "A Note on the Use of Sandwich Structures in Severe Acoustic Environments" University of Southampton Report No. AASU 145, 1960.

Response Quantity	Frequency For Maximum Response	Maximum Value of Response	Value of Response at ω_n	Treatment Criterion (small η)	Equation No.
Vibration Displacement	ω_n	$P/KR\eta$	$P/KR\eta$	$R\eta$	3.4
Plate Bending Stress	ω_n	$P\alpha/KR\eta$	$P\alpha/KR\eta$	$R\eta\alpha^{-1}$	
Velocity	$\omega_n(1+\eta^2)^{\frac{1}{4}}$	$P/K^{\frac{1}{2}}M^{\frac{1}{2}}R^{\frac{1}{2}}\theta^{\frac{1}{2}}[2(1+\eta^2)^{\frac{1}{2}}-1]^{\frac{1}{2}}$	$P/K^{\frac{1}{2}}M^{\frac{1}{2}}R^{\frac{1}{2}}\theta^{\frac{1}{2}}\eta$	$R^{\frac{1}{2}}\theta^{\frac{1}{2}}\eta$	3.5, 3.6
Acceleration and Sound Pressure Transmitted by Finite Plate	$\omega_n(1+\eta^2)^{\frac{1}{2}}$	$P/M\theta\eta(1+\eta^2)^{-\frac{1}{2}}$	$P/M\theta\eta$	$\theta\eta$	3.7, 3.8
Inertia Force	$\omega_n(1+\eta^2)^{\frac{1}{2}}$	$P/\eta(1+\eta^2)^{-\frac{1}{2}}$	P/η	η	3.9

Table 1 Summary of Expressions for the Maximum Values of Harmonic Response and the Corresponding Treatment Criteria

Response Quantity	r.m.s. Response	Treatment Criterion	Equation No.
Displacement	$[\Phi_p(\omega_n)\frac{\pi}{2}]^{\frac{1}{2}}\,[M^{\frac{1}{4}}K^{\frac{3}{4}}\theta^{\frac{1}{4}}R^{\frac{3}{4}}\eta^{\frac{1}{2}}F_d(\eta)]^{-1}$	$\theta^{\frac{1}{4}}R^{\frac{3}{4}}\eta^{\frac{1}{2}}F_d(\eta)$	3.26
Velocity	$[\Phi_p(\omega_n)\frac{\pi}{2}]^{\frac{1}{4}}\,[M^{\frac{3}{4}}K^{\frac{1}{4}}\theta^{\frac{3}{4}}R^{\frac{1}{4}}\eta^{\frac{1}{2}}F_v(\eta)]^{-1}$	$\theta^{\frac{3}{4}}R^{\frac{1}{4}}\eta^{\frac{1}{2}}F_v(\eta)$	3.27
Acceleration ($\propto$ Sound Pressure through plate, III.4.2)	$\left\{\Phi_e(\omega_n)\frac{\pi}{2}(1-\eta^2)(M^{\frac{5}{4}}K^{-\frac{1}{2}}\theta^{\frac{5}{2}}R^{-\frac{1}{2}}\eta F_a(\eta))^{-1}\right\}^{\frac{1}{2}}$ $+\ \langle F^2(t)\rangle / M^2\theta^2$	$\theta^{\frac{5}{4}}R^{-\frac{1}{4}}\eta^{\frac{1}{2}}F_a(\eta)$	3.28
Reaction Force	$\text{Const.}[\Phi_p(\omega_n)\frac{\pi}{2}]^{\frac{1}{2}}[M^{\frac{1}{4}}K^{-\frac{1}{4}}\theta^{\frac{1}{4}}R^{-\frac{1}{4}}\eta^{\frac{1}{2}}F_r(\eta)]^{-1}$	$\theta^{\frac{1}{4}}R^{-\frac{1}{4}}\eta^{\frac{1}{2}}F_r(\eta)$	3.29
Boundary layer Sound Pressure Transmitted	$\text{Const.}\langle p^2\rangle[m^{7/8}B^{1/8}\theta^{7/8}R^{1/8}\eta^{1/2}]^{-1}$	$\theta^{7/8}R^{1/8}\eta^{1/2}$	3.31

Table II Summary of Expressions for r.m.s. Random Response and the Corresponding Treatment Criteria

Specimen	Hycadamp	Dynadamp	Oberst's	3M's
Face-plate thickness, in.	0.0188	0.0388	0.025	0.0348
Core thickness ratio, τ	1.72	0.204	2.90	0.055 , 0.117 0.166 , 0.222
Width, in	0.30	0.30	0.30	0.30
Length between supports, in.	10.54	10.54	10.54	10.54
Face-plate E, lb. in^{-2}.	9.70 $x10^6$	10.05 $x10^6$	10.0 $x10^6$	10.25 $x10^6$

Table III Dimensions and E's of Specimens

Temperature \ Frequency c.p.s.		30	100	300	1000
0°C	G	224	492	990	2170
	β	1.28	1.11	1.00	0.97
23°C	G	32	58	103	216
	β	1.13	1.30	1.37	1.25

Table IV Maker's Data on 3M's Adhesive Damping Film
(G is in $lb.in^{-2}$ units)

Specimen	Mode No.	Frequency (f_m, c.p.s.)	η	K
HYCADAMP	1	56	0.074	4.59
	2	192	0.20	3.32
	3	374	0.34	2.39
	4	582	0.42	1.78
	5	832	0.53	1.43
DYNADAMP	1	76	0.048	1.66
	2	272	0.041	1.34
	3	533	0.052	1.01
	4	830	0.057	0.78
	5	1180	0.060	0.64
OBERST	1	60	0.55	2.99
	2	178	0.86	1.42
	3	322	0.97	0.87
	4	487	0.95	0.63
	5	690	0.88	0.54
3M1	1	55	0.16	0.94
	2	199	0.31	0.78
	3	425	0.31	0.67
	4	700	0.33	0.57
	5	1056	0.31	0.53
3M2	1	53	0.28	0.87
	2	193	0.40	0.69
	3	386	0.43	0.52
	4	664	0.44	0.51
	5	975	0.44	0.44
3M3	1	51	0.39	0.79
	2	175	0.52	0.55
	3	374	0.45	0.51
	4	618	0.42	0.43
3M4	1	53	0.40	0.86
	2	185	0.50	0.64
	3	390	0.52	0.54
	4	605	0.50	0.46
	5	935	0.44	0.42

Table V Values of $f_m (= \omega_m/2\pi)$, K and η from experiments on the Sandwich Specimens

Specimen	Oberst	Dynadam	Hycadamp	3M1	3M2	3M3	3M4	
f_n	154	272	190	195	187	165	175	
η_n	0.86	0.041	0.20	0.30	0.38	0.51	0.52	
λ	0.65	0.90	0.75	0.75	0.73	0.69	0.70	
Unit term	1	1	1	1	1	1	1	
η^2 term	2.94	41.2	8.36	6.09	5.10	3.97	3.98	
2η term	-2.01	- 2.63	-2.48	-2.38	-2.31	-2.22	-2.21	
Total	1.93	39.6	6.88	4.71	3.79	2.75	2.77	
Predicted $(V_r)_{rms}$, mV	1.0	4.51	1.88	1.56	1.40	1.19	1.19	
Measured $(V_r)_{rms}$, mV	1.0 (23°)	4.62 (24°)	1.42 (24°)	1.64 (21°)	1.29 (21°)	-	1.15 (21°)	Set "A"
and Temp. (°C)	1.50 (21.5°)	6.3	2.7	2.18	1.95	1.85	1.80	Set "B"

Table VI Measured and Predicted Values of r.m.s. Reaction Transducer Output

Specimen	Oberst	Dyna.	Hyca.	3M1	3M2	3M3	3M4
Criterion Reciprocals Small Damping	1.0	5.25	2.04	1.70	1.49	1.24	1.27
Criterion Reciprocal Large Damping	1.0	5.9	2.22	1.85	1.61	1.31	1.35
Normalised Response, Set A	1.0	4.62	1.42	1.64	1.29	-	1.15
Normalised Response, Set B	1.0	4.2	1.8	1.45	1.3	1.23	1.20

Table VII Comparison of Normalised Values of Measured Response with Normalised Criterion Reciprocals

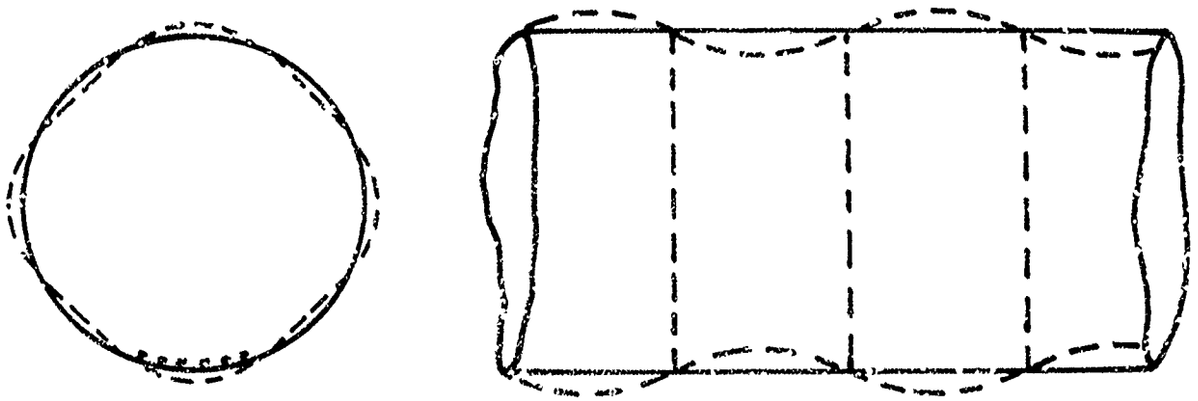

FIG.1 'OVERALL' MODE OF CYLINDER (FUSELAGE) VIBRATION

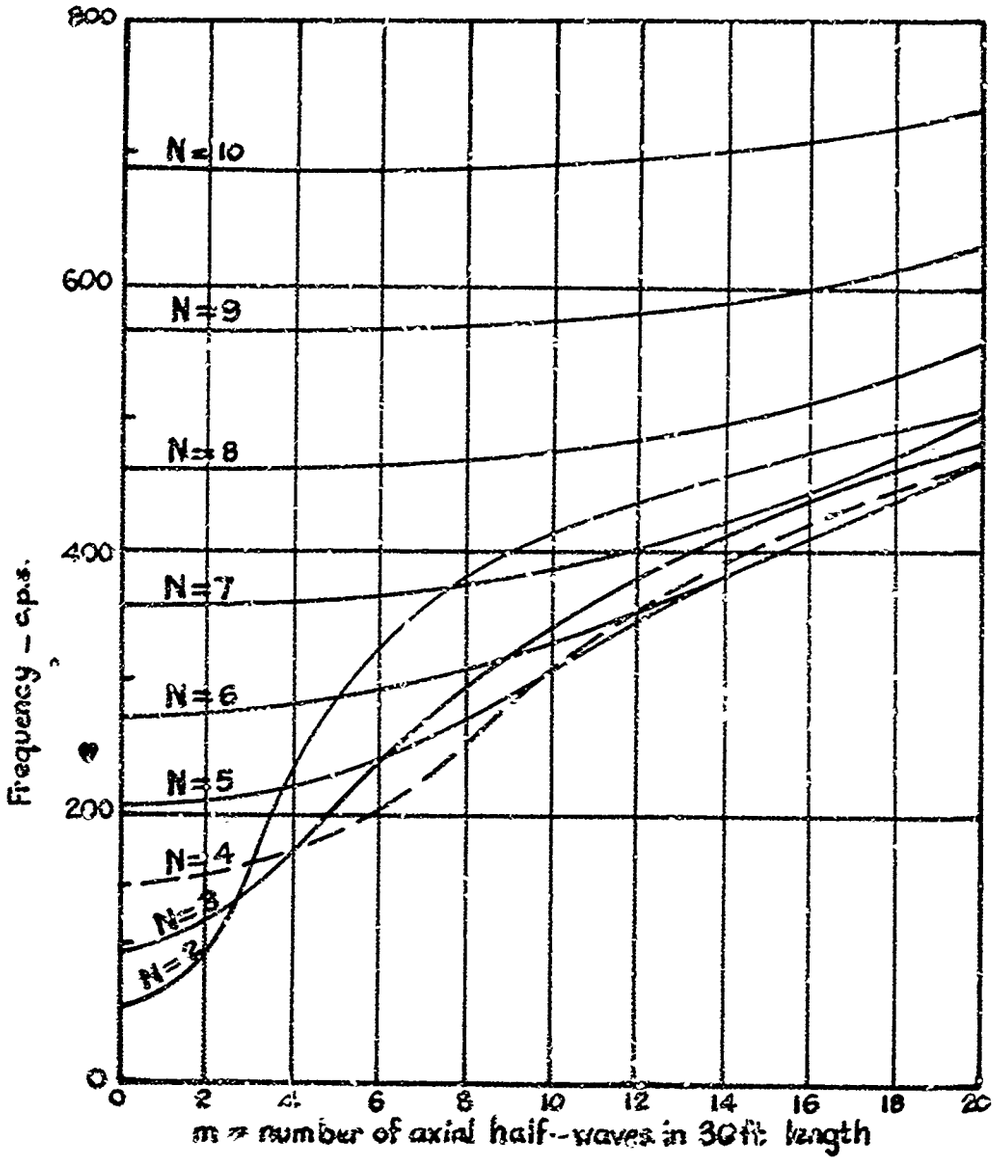

N = number of full-waves around circumference

FIG. 2 NATURAL FREQUENCIES OF OVERALL MODES OF A FUSELAGE STRUCTURE

Diameter = 10 ft. Length = 30 ft.
Stringer Pitch = 7½ in. Frame Pitch = 20 in.

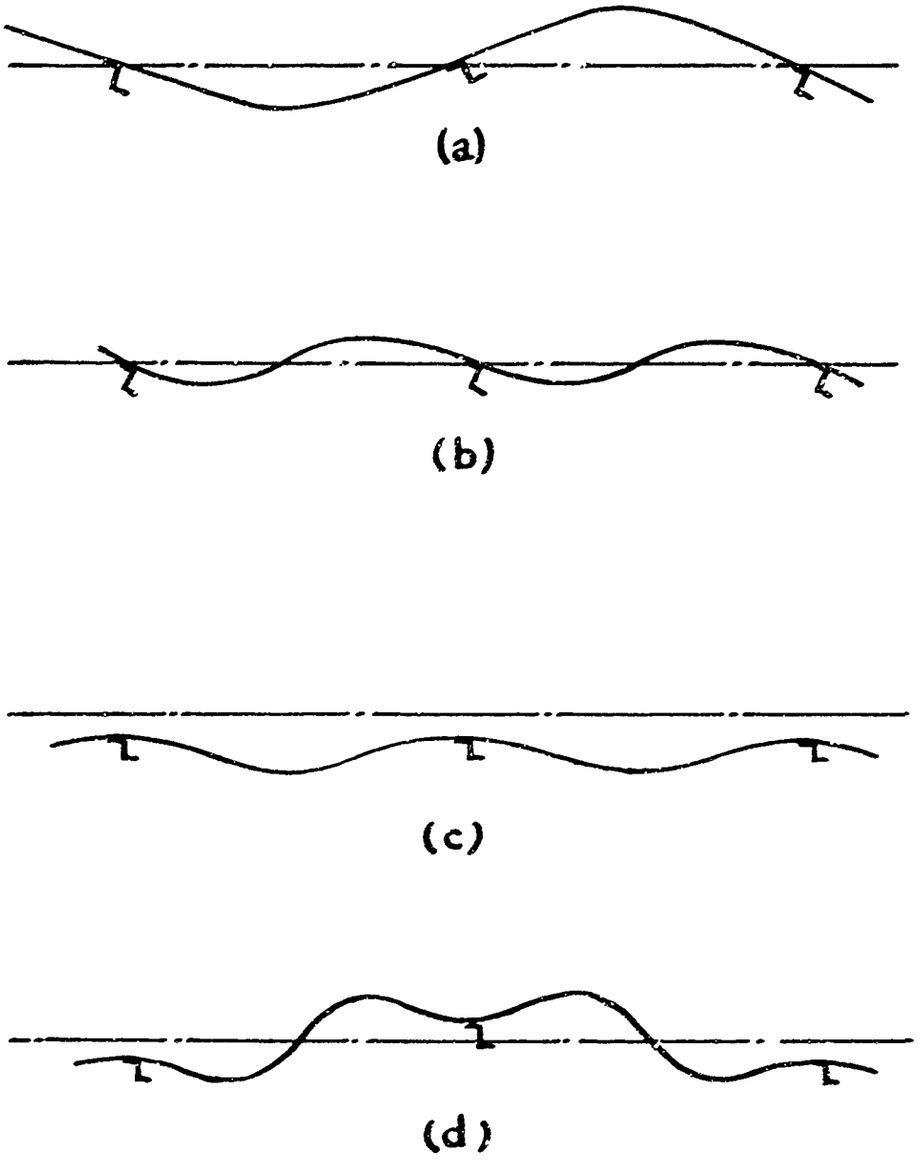

FIG.3 THE FOUR BASIC 'LOCAL' MODES OF A STIFFENED PLATE

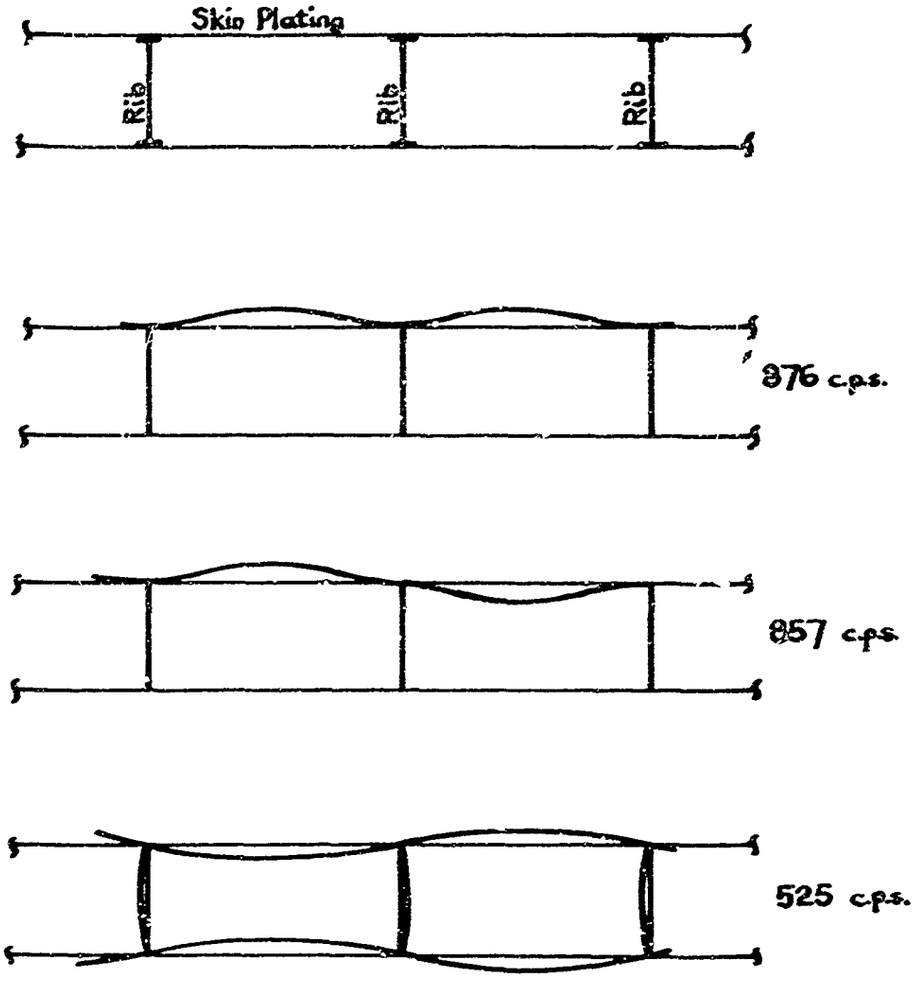

Frequencies quoted were measured on an actual tail-plane

FIG.4 RIB-SKIN MODES OF TAIL-PLANE STRUCTURE

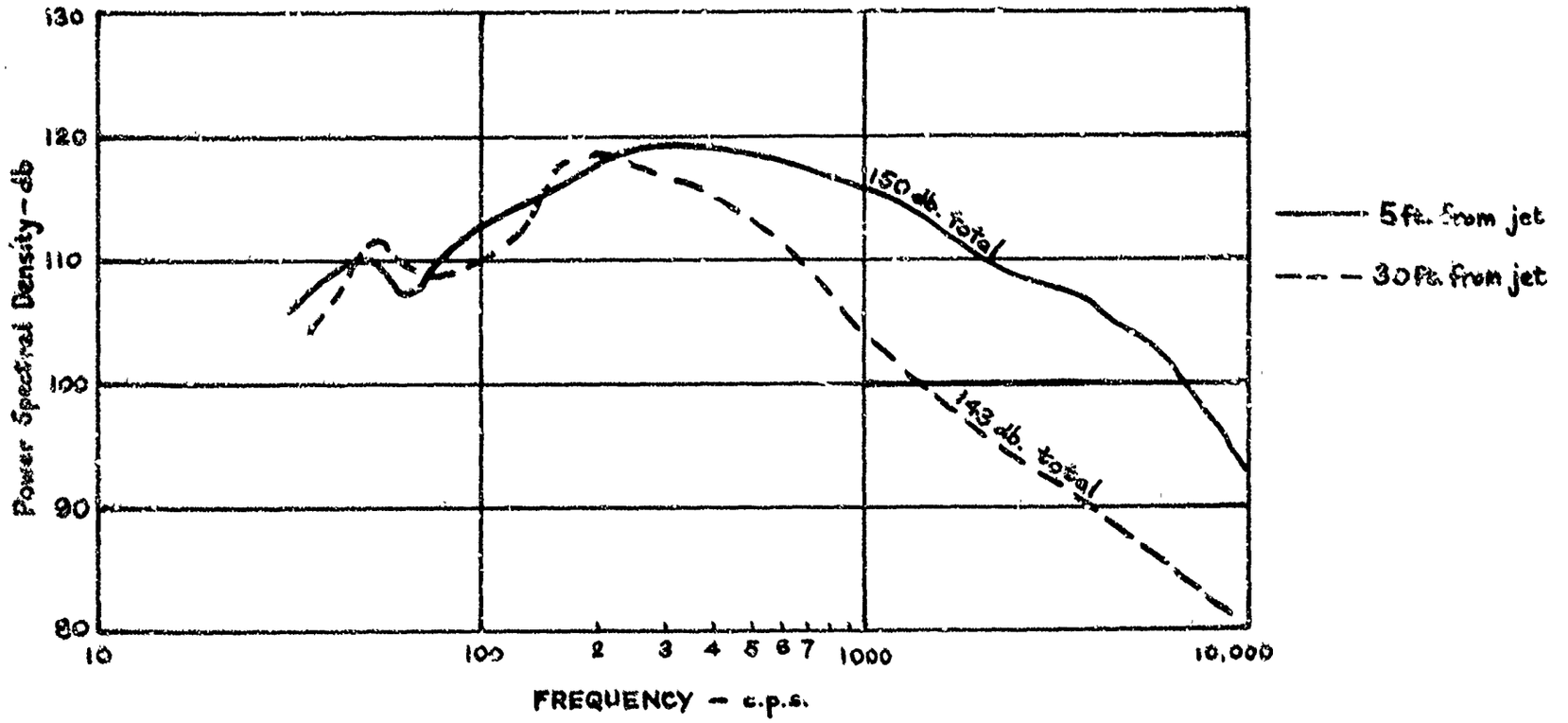

FIG. 5 NOISE SPECTRA FROM R.R. 'AVON' JET ENGINE

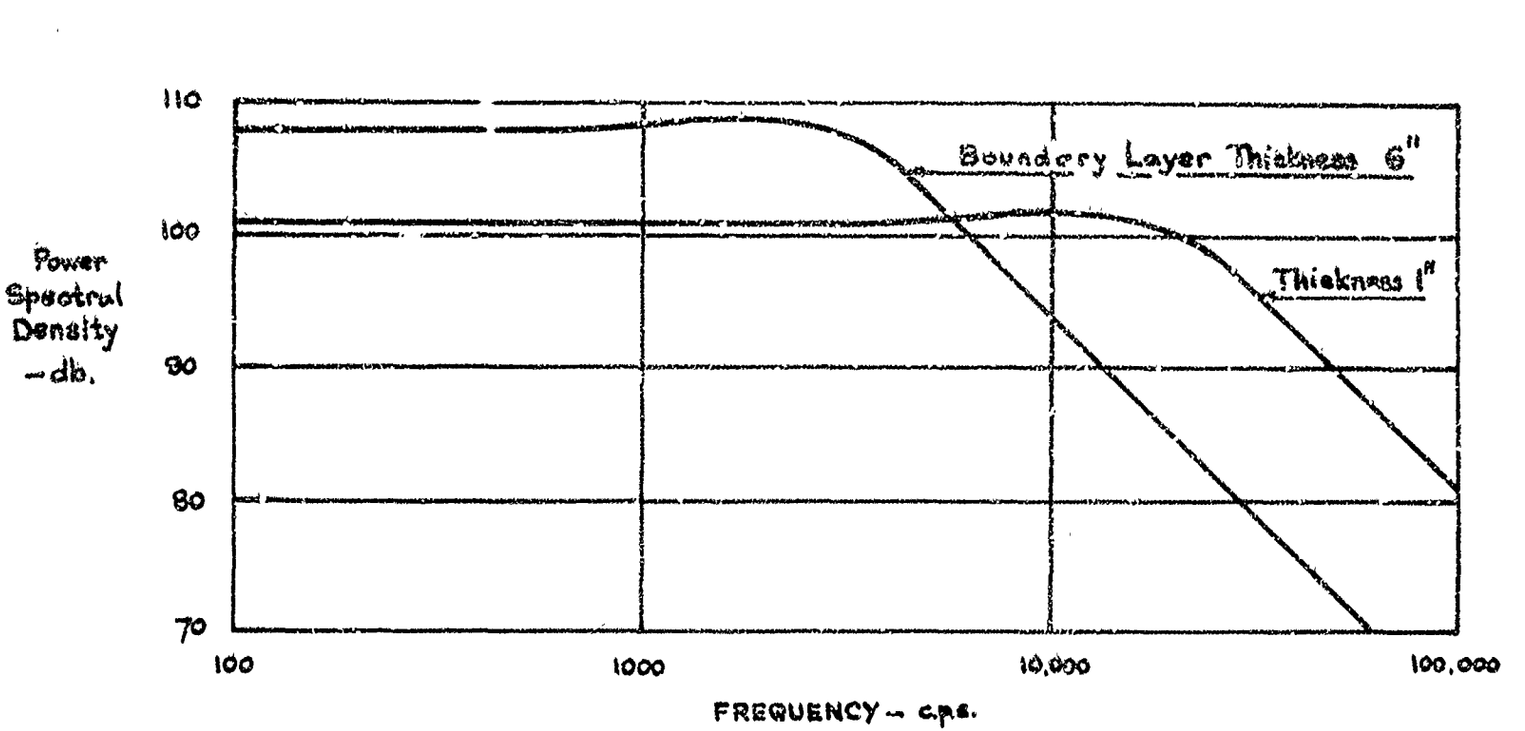

FIG. 6 TYPICAL BOUNDARY LAYER PRESSURE SPECTRA

AIR SPEED 600 m.p.h. AT SEA LEVEL ; OVERALL PRESSURE LEVEL 143 db. APPROX.

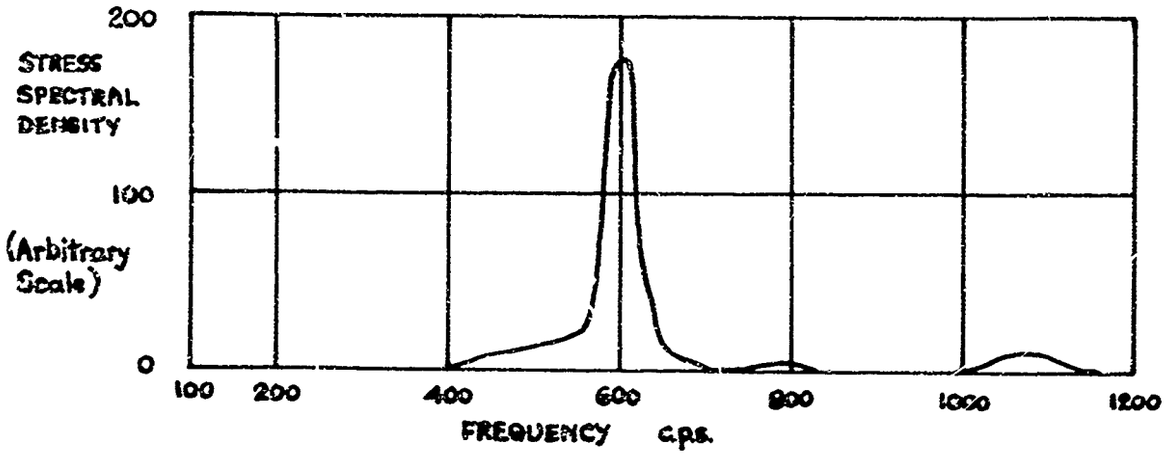

FIG. 7 SPECTRUM OF RANDOM STRESS IN A FUSELAGE PANEL

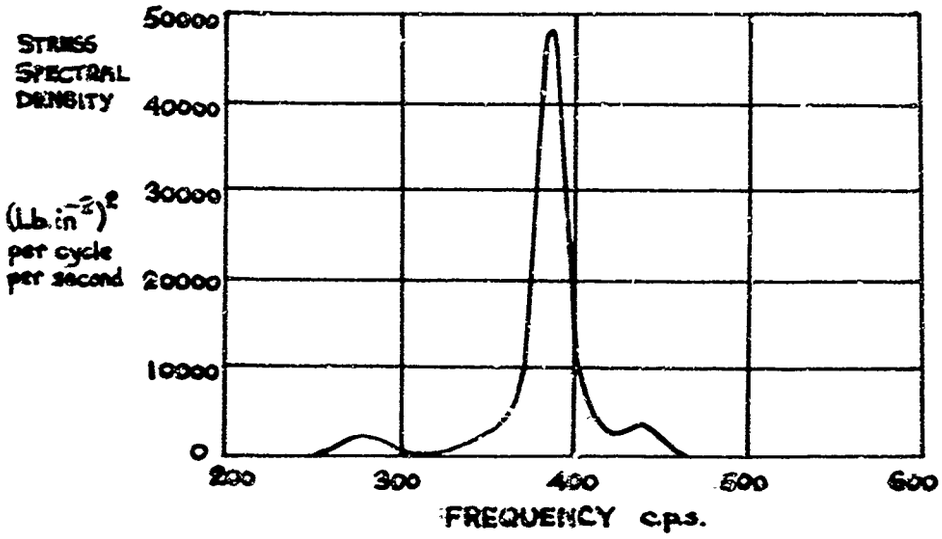

FIG. 8 SPECTRUM OF RANDOM STRESS IN TAILPLANE SKIN

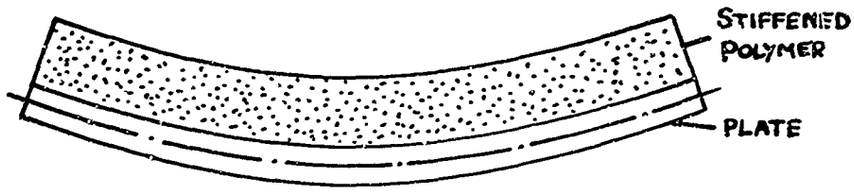

9a 'UNCONSTRAINED LAYER' CONFIGURATION
(e.g. AQUAPLAS)

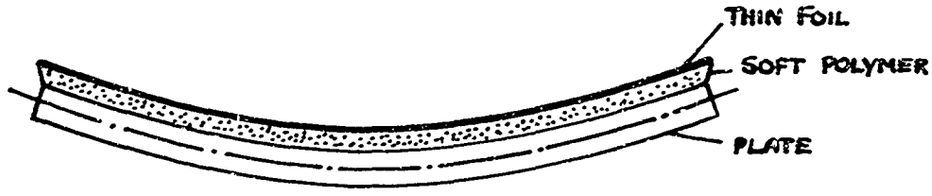

9b 'DAMPING TAPE' CONFIGURATION

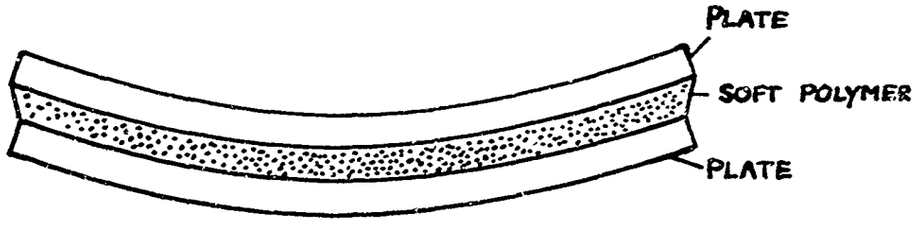

9c 'DOUBLE-SKIN' CONFIGURATION

FIG. 9 ENERGY DISSIPATING MECHANISMS OF CONSTRAINED AND UNCONSTRAINED LAYER TREATMENTS

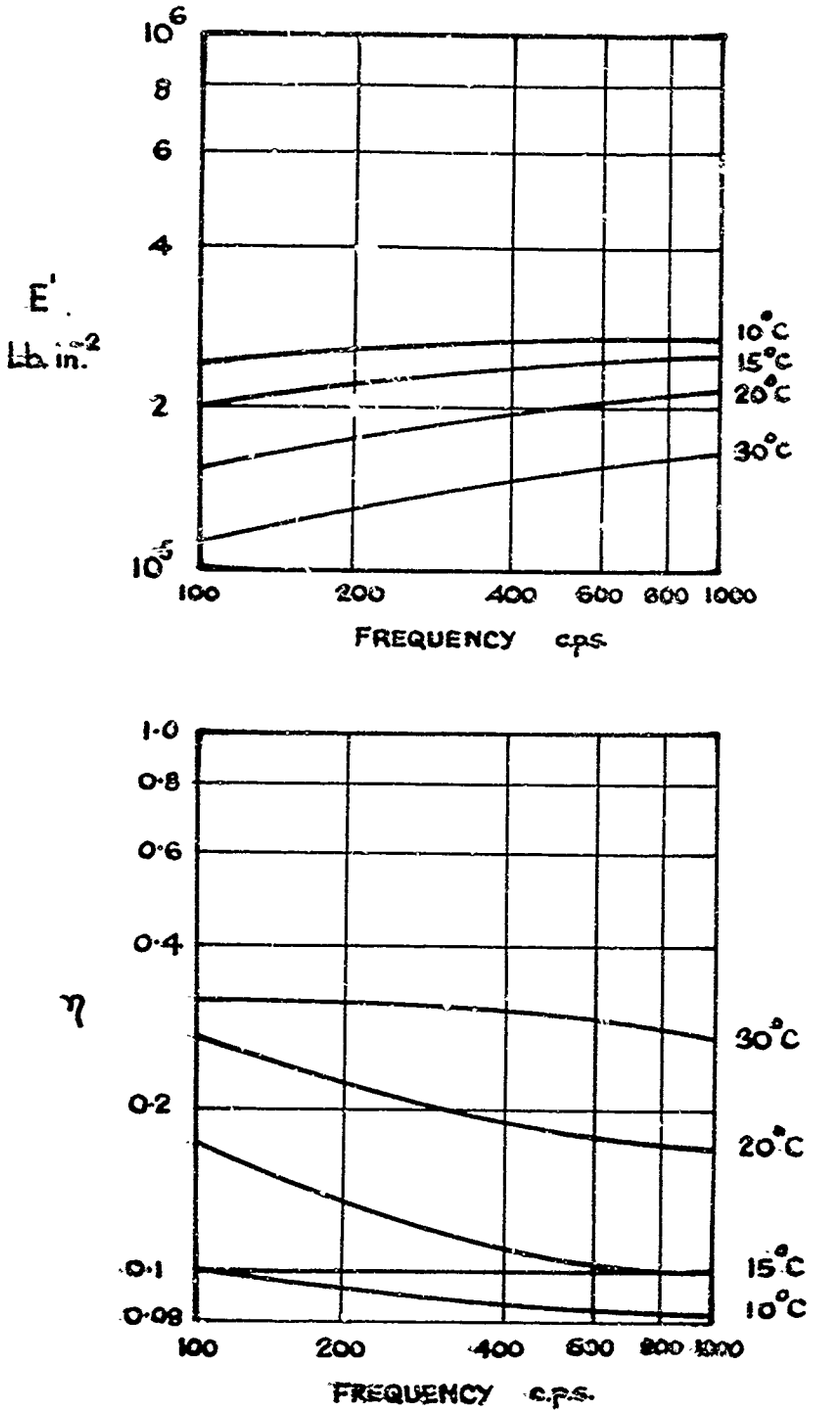

FIG. 10 YOUNG'S MODULUS E' AND LOSS FACTOR η OF AN EARLY UNCONSTRAINED LAYER TREATMENT

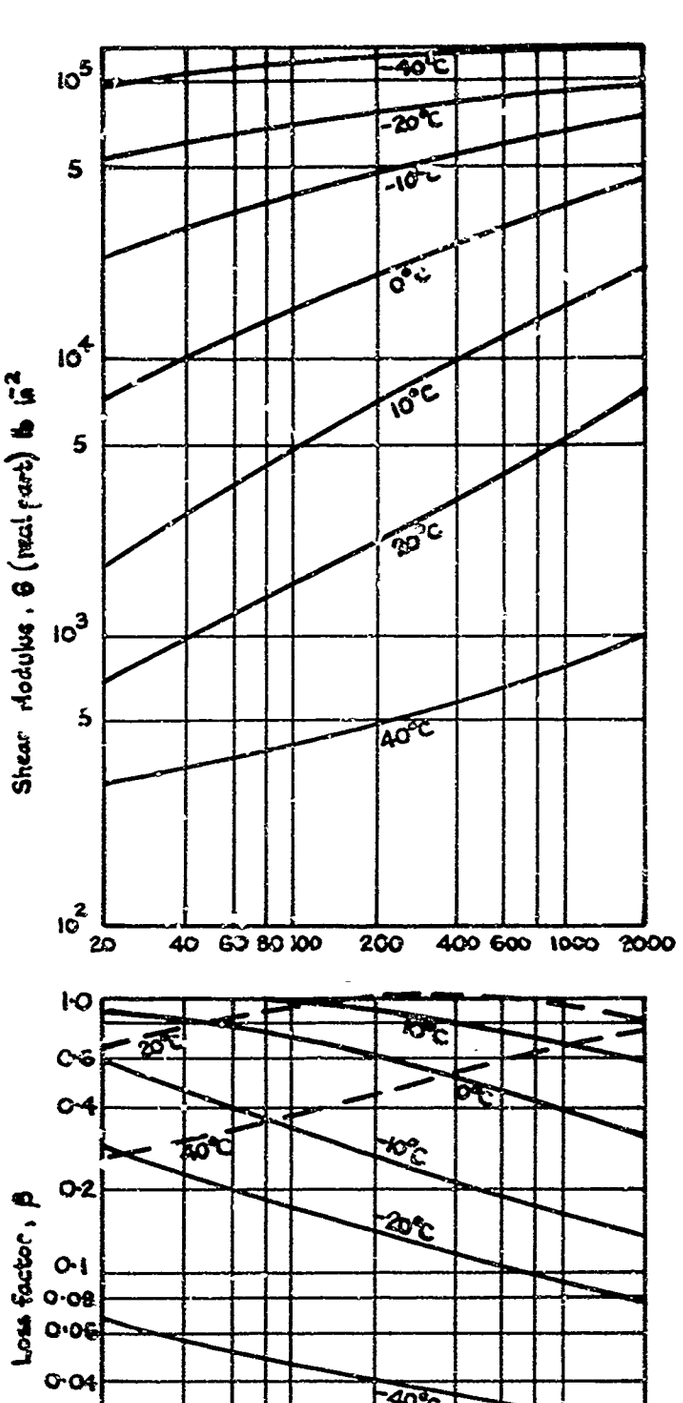

FIG. 11 THE COMPLEX SHEAR MODULUS, $G(1 + i\beta)$ OF A HIGH DAMPING MATERIAL vs. FREQUENCY

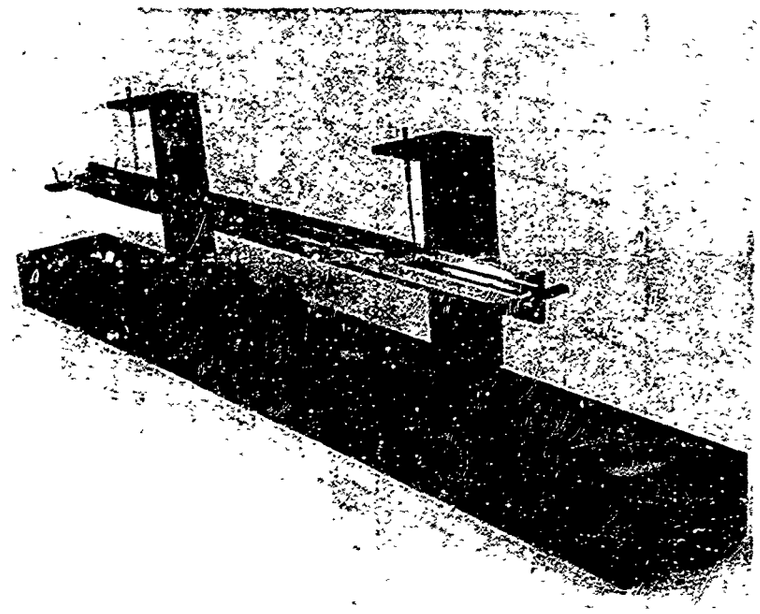

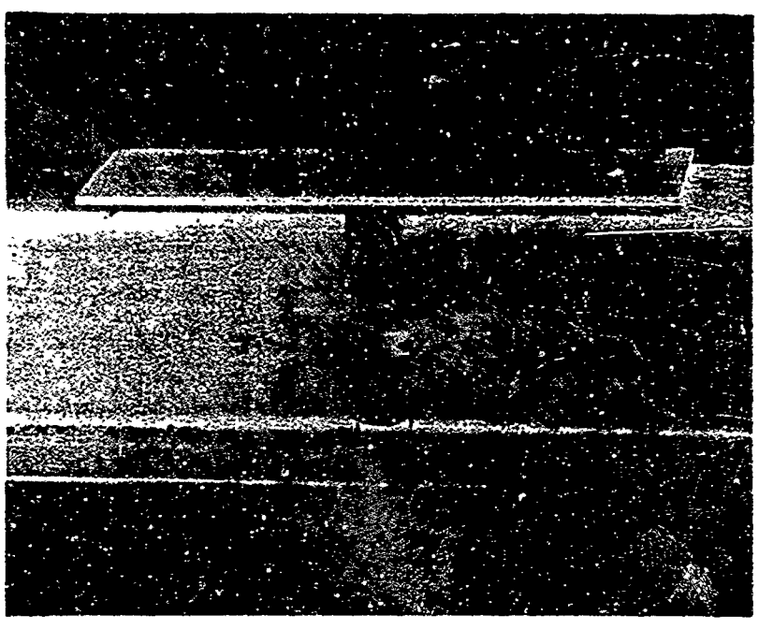

FIG. 12 THE BEAM AND JOINT USED IN THE RIVET DAMPING INVESTIGATION

CURVE I : BEFORE PROLONGED LOADING

CURVE II : AFTER PROLONGED LOADING

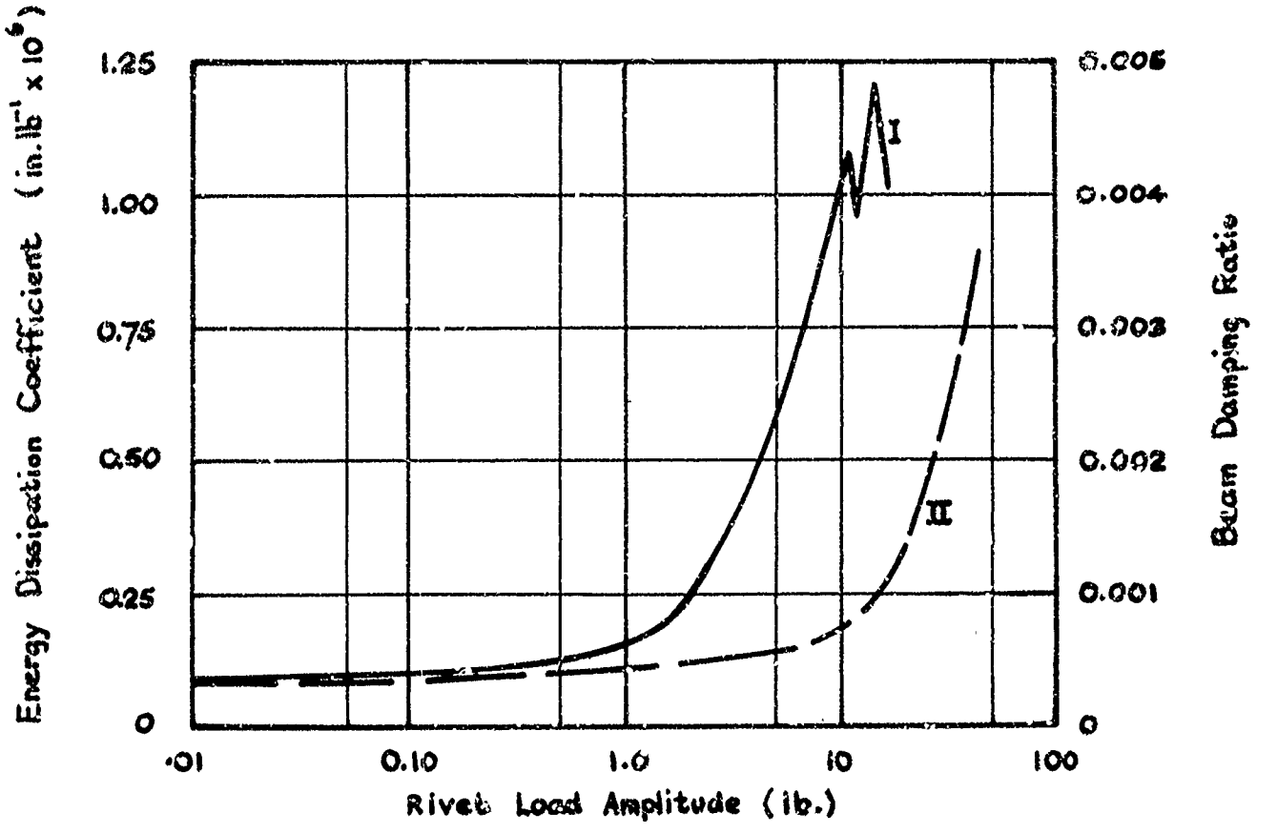

FIG. 13 THE ENERGY DISSIPATION COEFFICIENT, $\Delta E/P^2$, FOR A SINGLE $\frac{1}{8}$" DIA. COUNTERSUNK RIVET IN ALCLAD PLATES, BEFORE AND AFTER PROLONGED LOADING

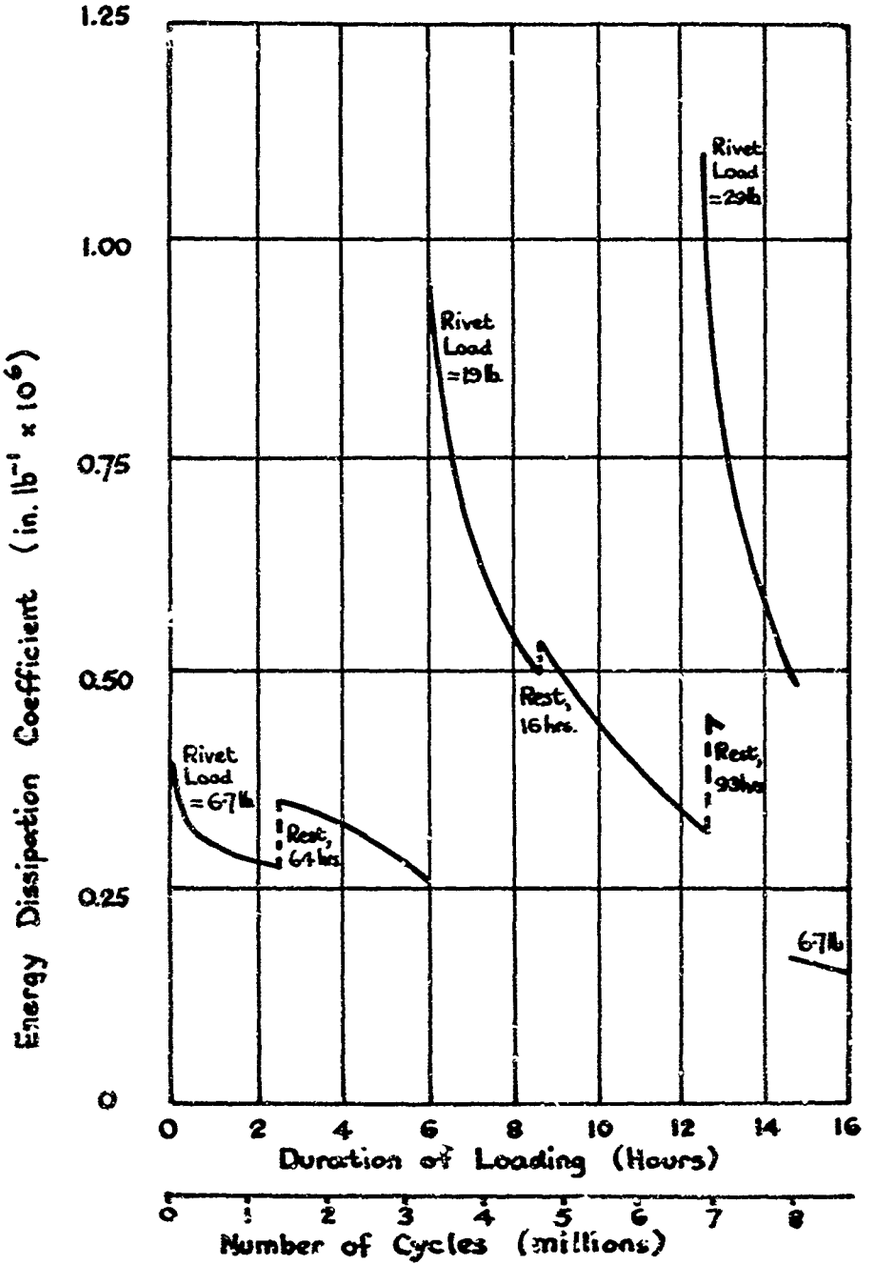

FIG. 14 THE VARIATION OF THE ENERGY DISSIPATION COEFFICIENT WITH DURATION OF LOADING

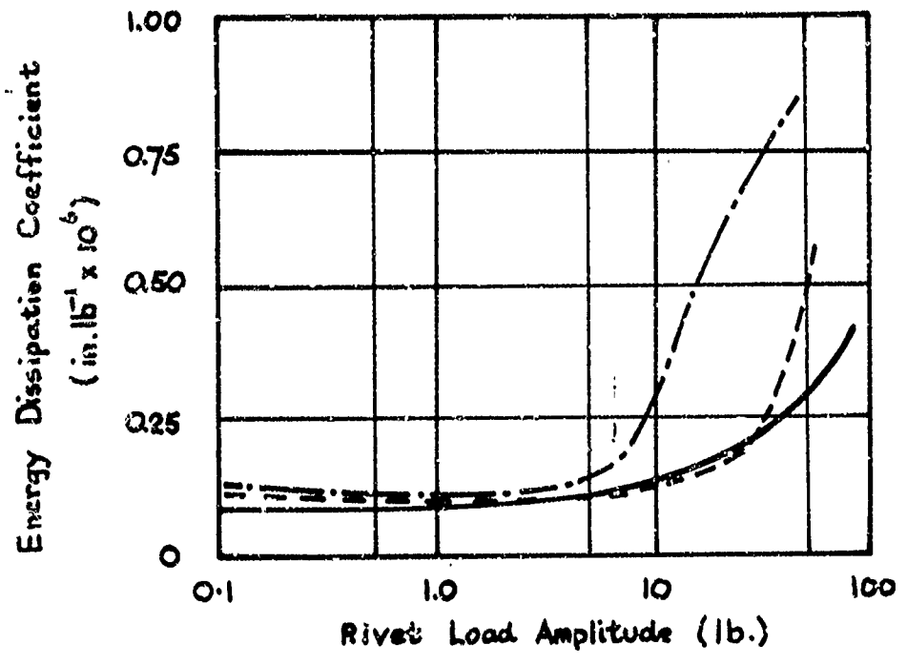

FIG. 15 COMPARISON OF THE ENERGY DISSIPATION COEFFICIENTS OF NOMINALLY IDENTICAL JOINTS

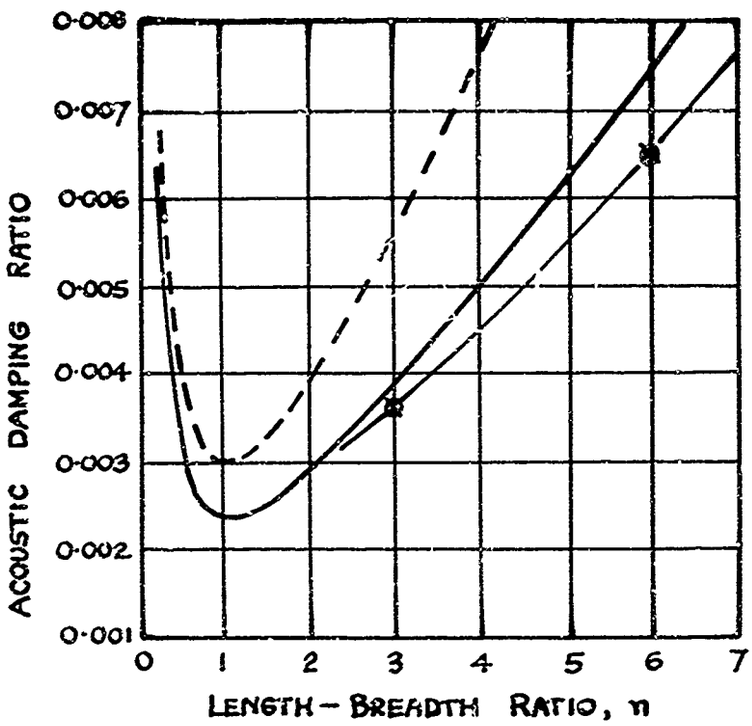

– – – – – Fully-fixed plate – Uniform Pressure Theory

——— Simply-supported plate – * * *

—⊕— Simply-supported plate, 5" wide, 0·048 in. thick, non-uniform pressure theory.

FIG. 16 ACOUSTIC DAMPING RATIOS OF RECTANGULAR PLATES VIBRATING IN FUNDAMENTAL MODES

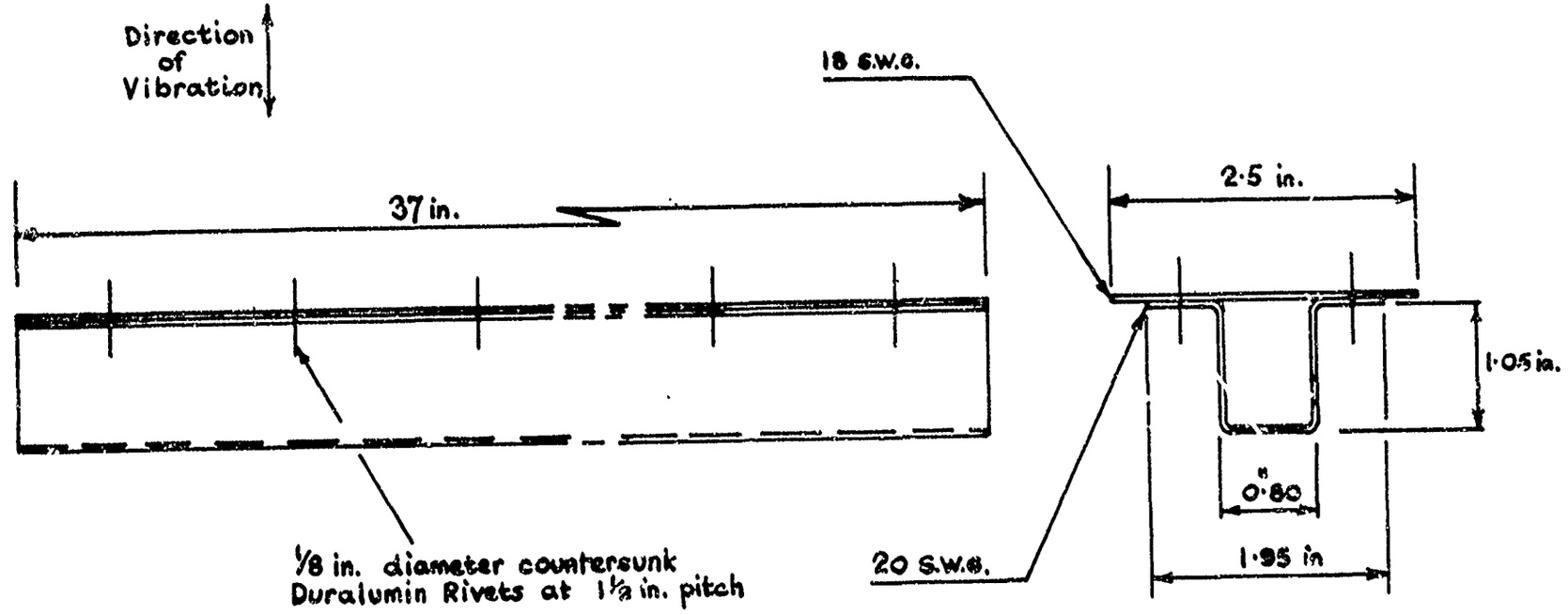

FIG.17 SKIN-STRINGER BEAM FOR MULTI-JOINT STUDY (ALCLAD, DTD 546)

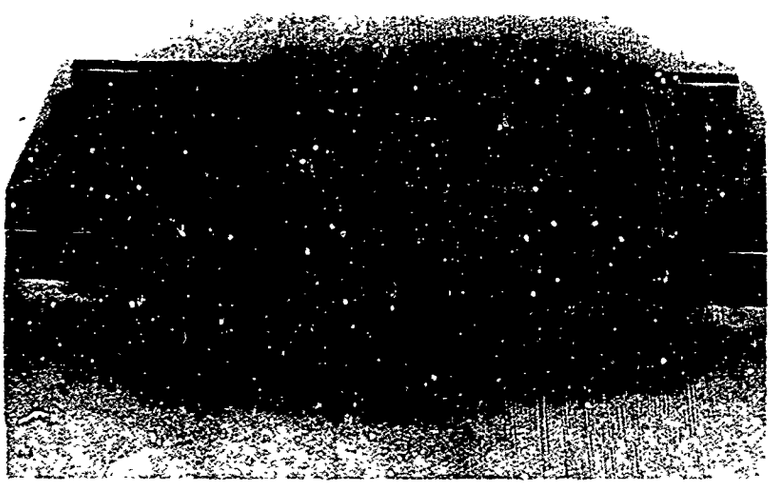

FIG. 18 MODEL USED FOR MODAL DAMPING INVESTIGATION

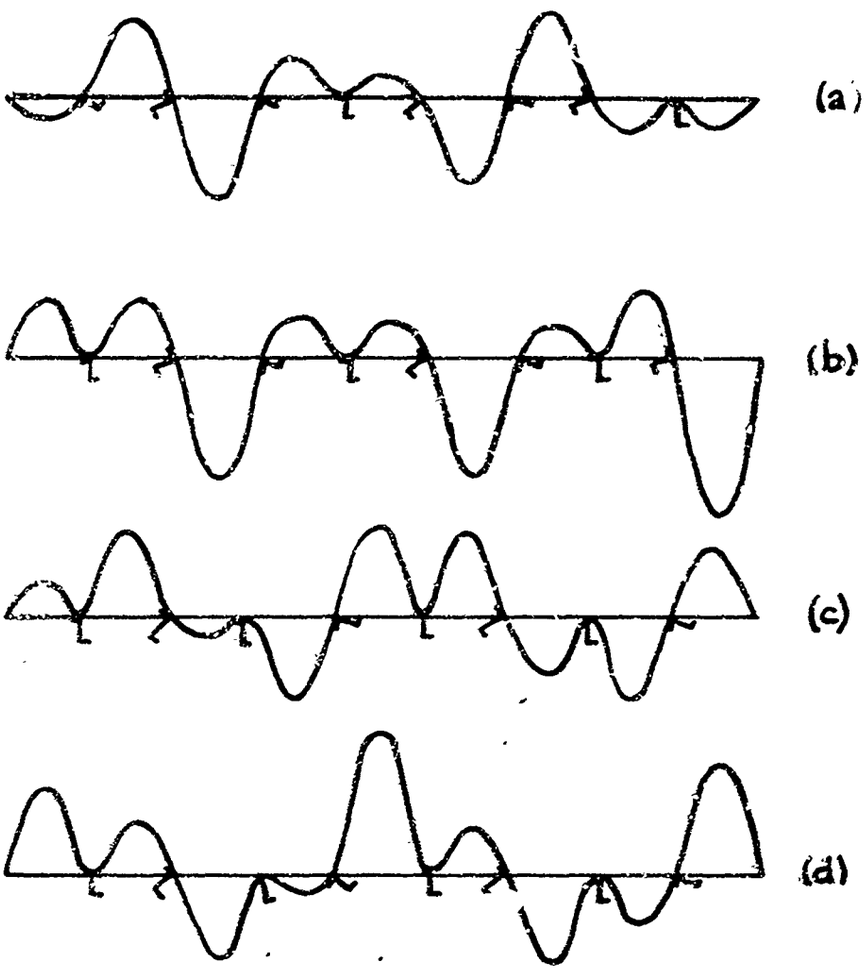

FIG. 19 MODE OF PLATE DISTORTION BETWEEN STRINGERS

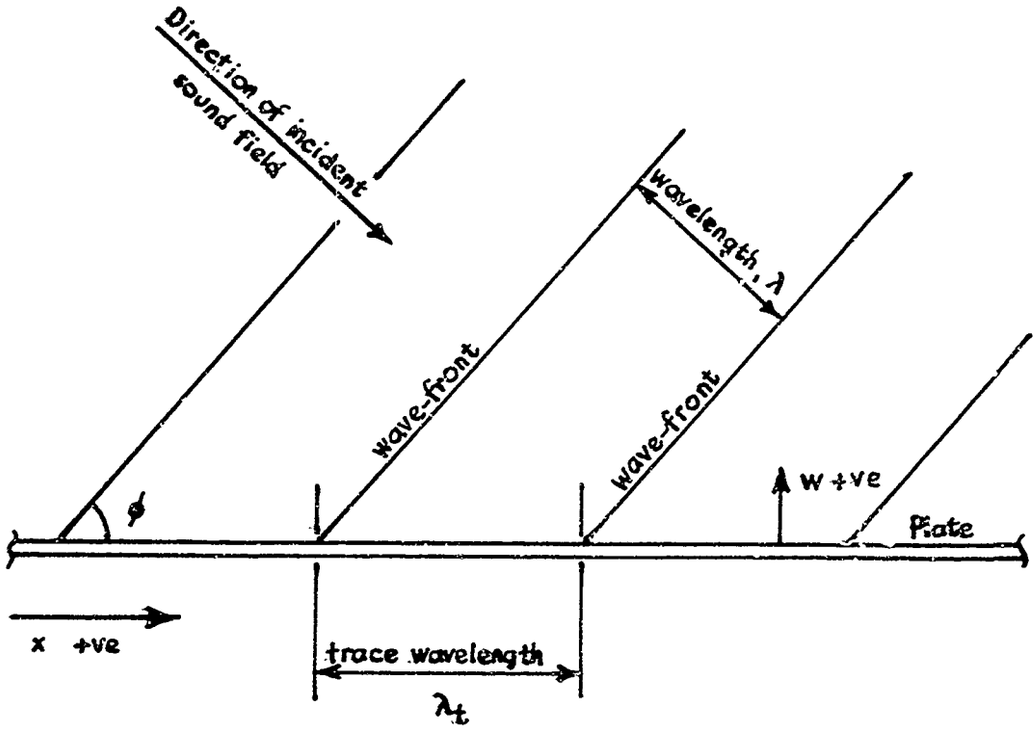

FIG. 20 DIAGRAM ILLUSTRATING SYMBOLS USED IN CHAPTER III

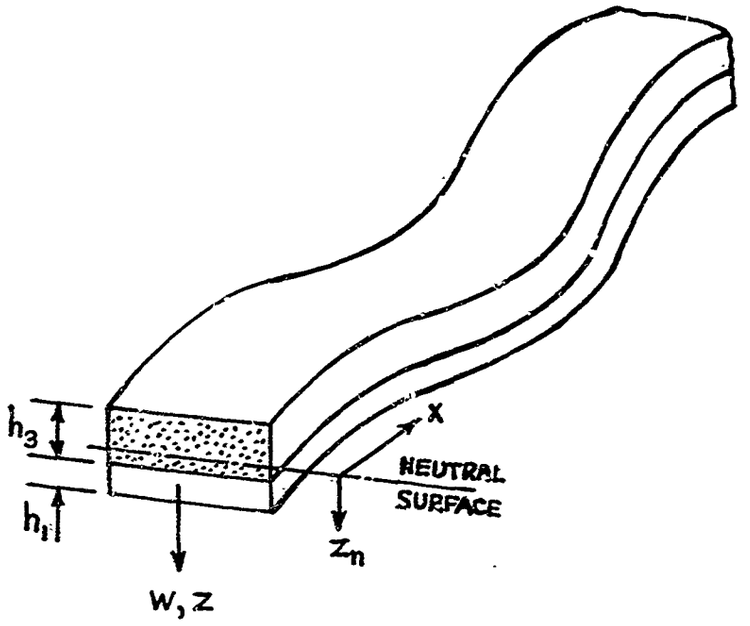

FIG. 21 DISPLACEMENT AND CO-ORDINATE SYSTEM USED IN CHAPTER IV

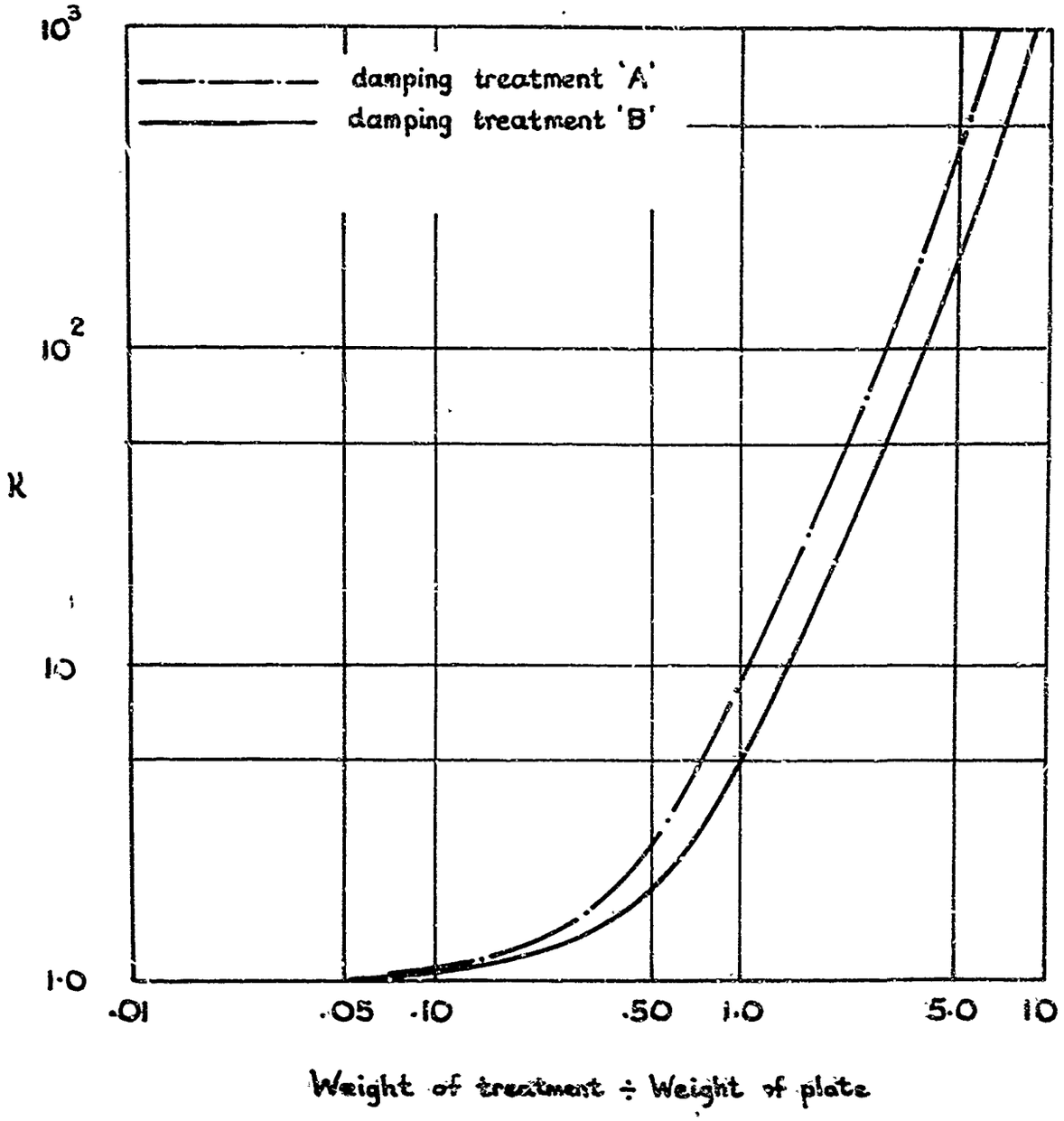

FIG.22 THE STIFFNESS RATIO R AS A FUNCTION OF RELATIVE WEIGHT OF TREATMENT

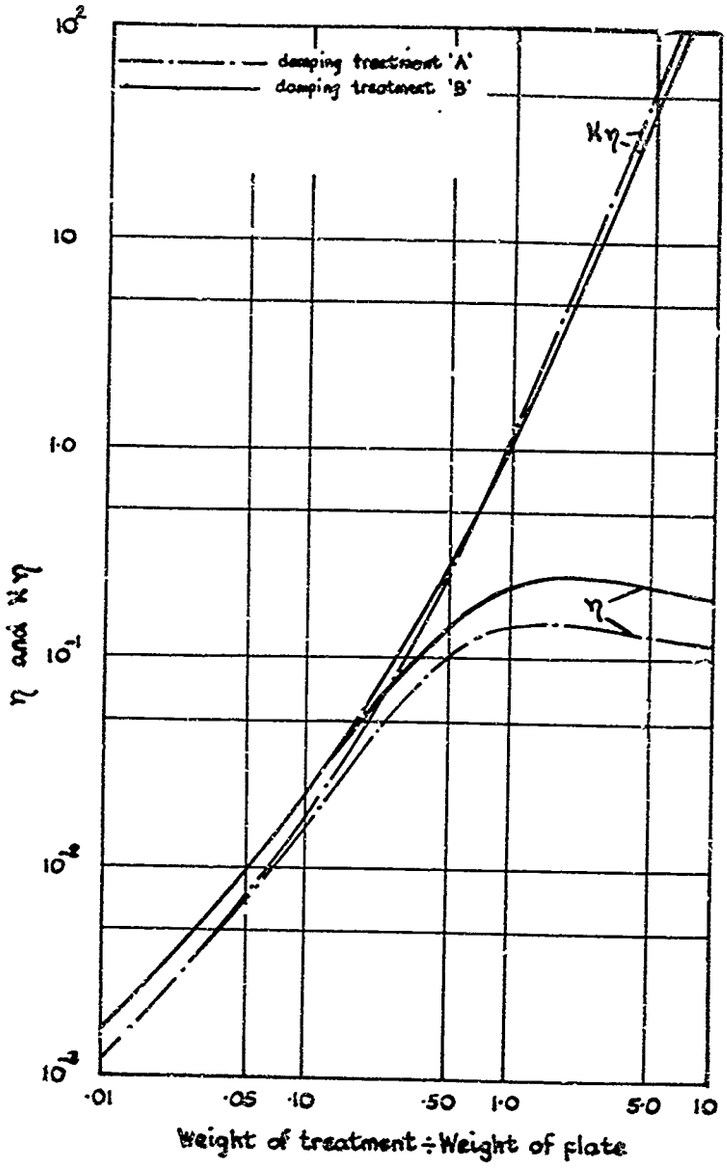

FIG. 23 THE LOSS FACTOR η AND THE CRITERION $K\eta$ FOR THE TREATED PLATE AS A FUNCTION OF RELATIVE WEIGHT OF TREATMENT

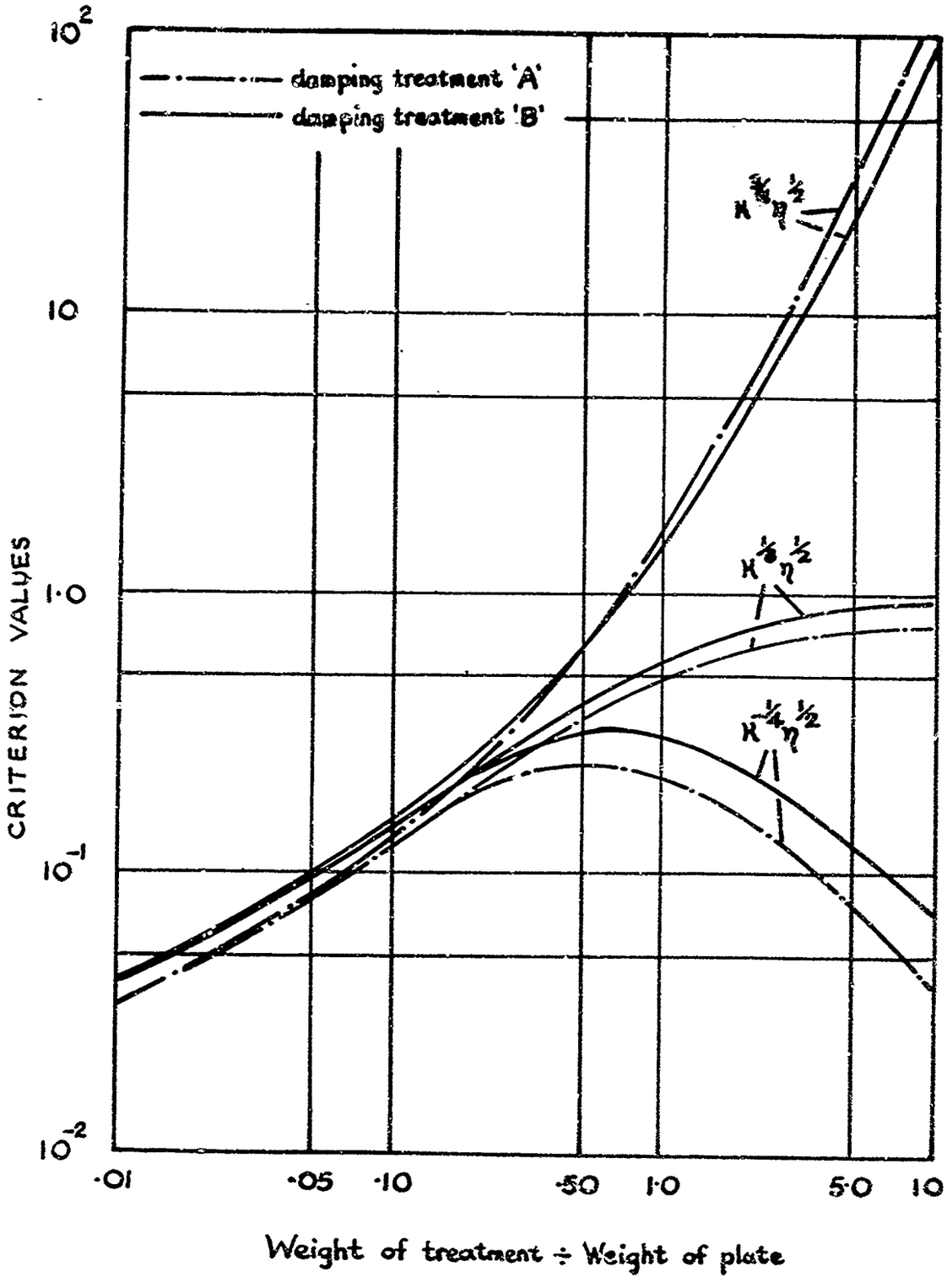

FIG. 24 CRITERIA RELATING TO RANDOM DISPLACEMENT ($K^{3/4}\eta^{1/2}$) SOUND PRESSURE TRANSMITTED ($K^{1/8}\eta^{1/2}$) AND REACTION FORCE ; MASS EFFECT NOT INCLUDED

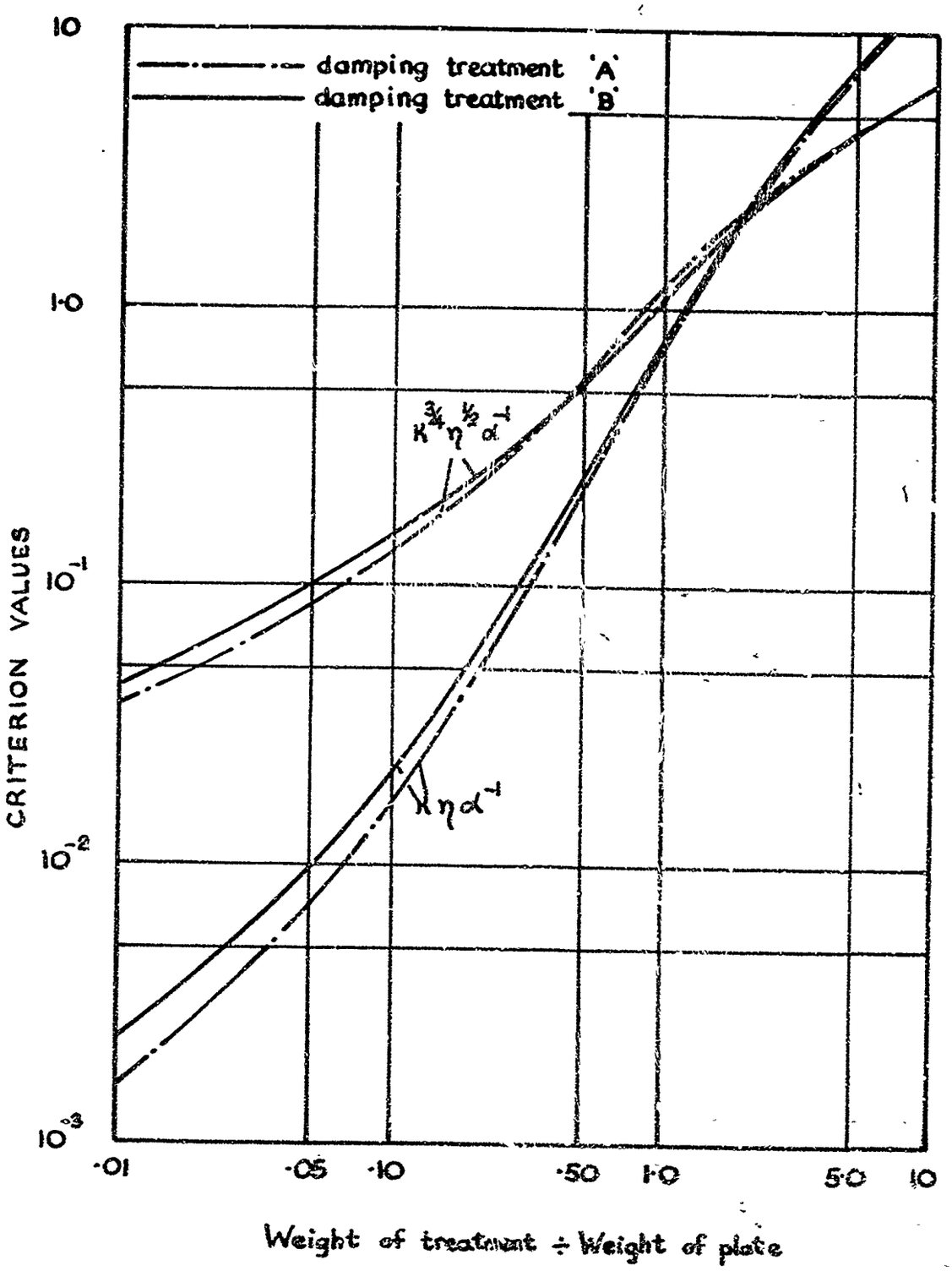

FIG. 25 CRITERIA RELATING TO RANDOM AND HARMONIC PLATE BENDING STRESSES; MASS EFFECT NOT INCLUDED

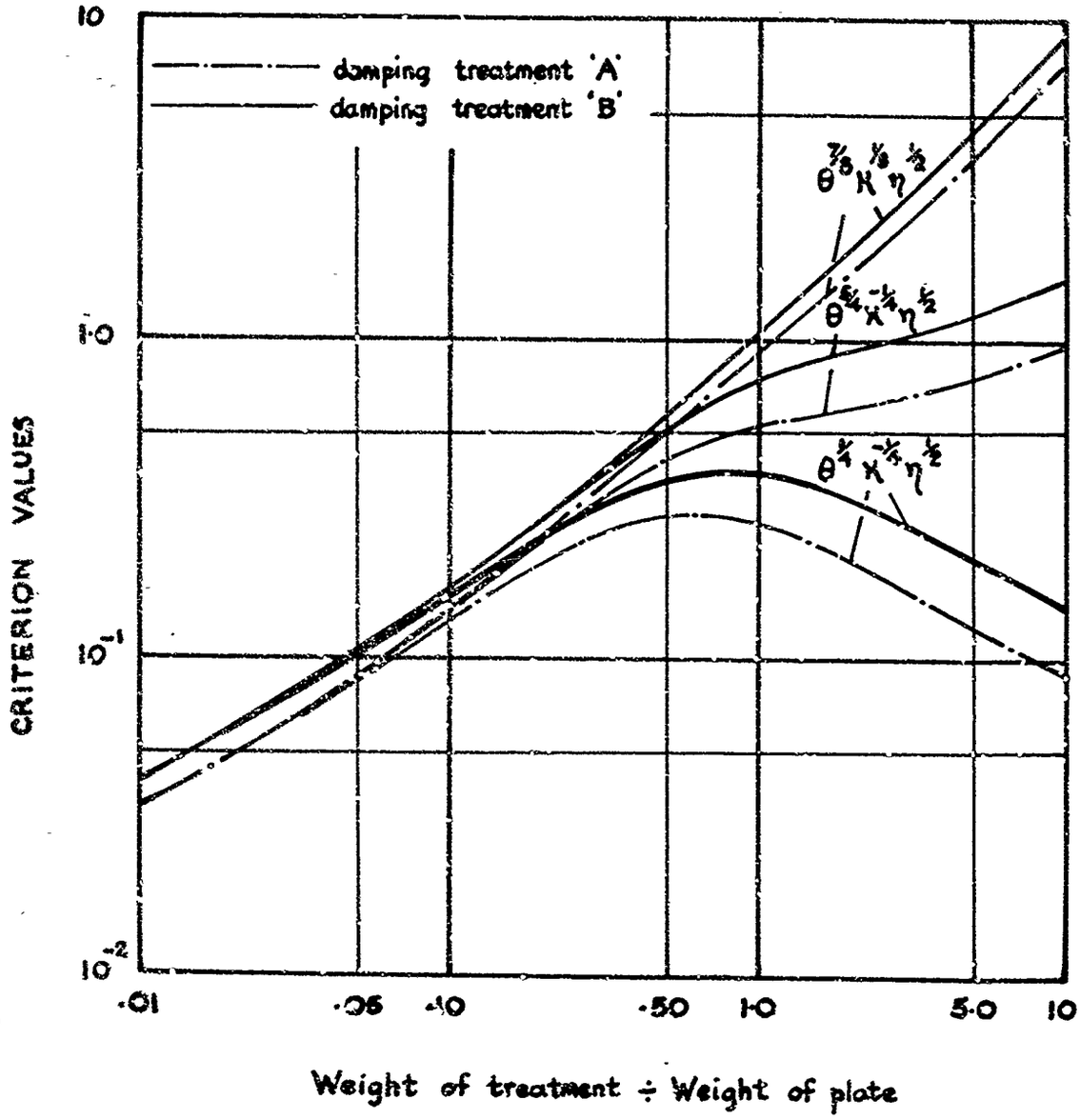

FIG. 26 CRITERIA RELATING TO RANDOM TRANSMITTED SOUND PRESSURE ($\theta^{2/3}K^{1/3}\eta^{1/2}$), RANDOM ACCELERATION ($\theta^{5/4}K^{-1/4}\eta^{1/2}$), AND RANDOM INERTIA FORCE ($\theta^{1/4}K^{-1/4}\eta^{1/2}$). MASS EFFECT INCLUDED.

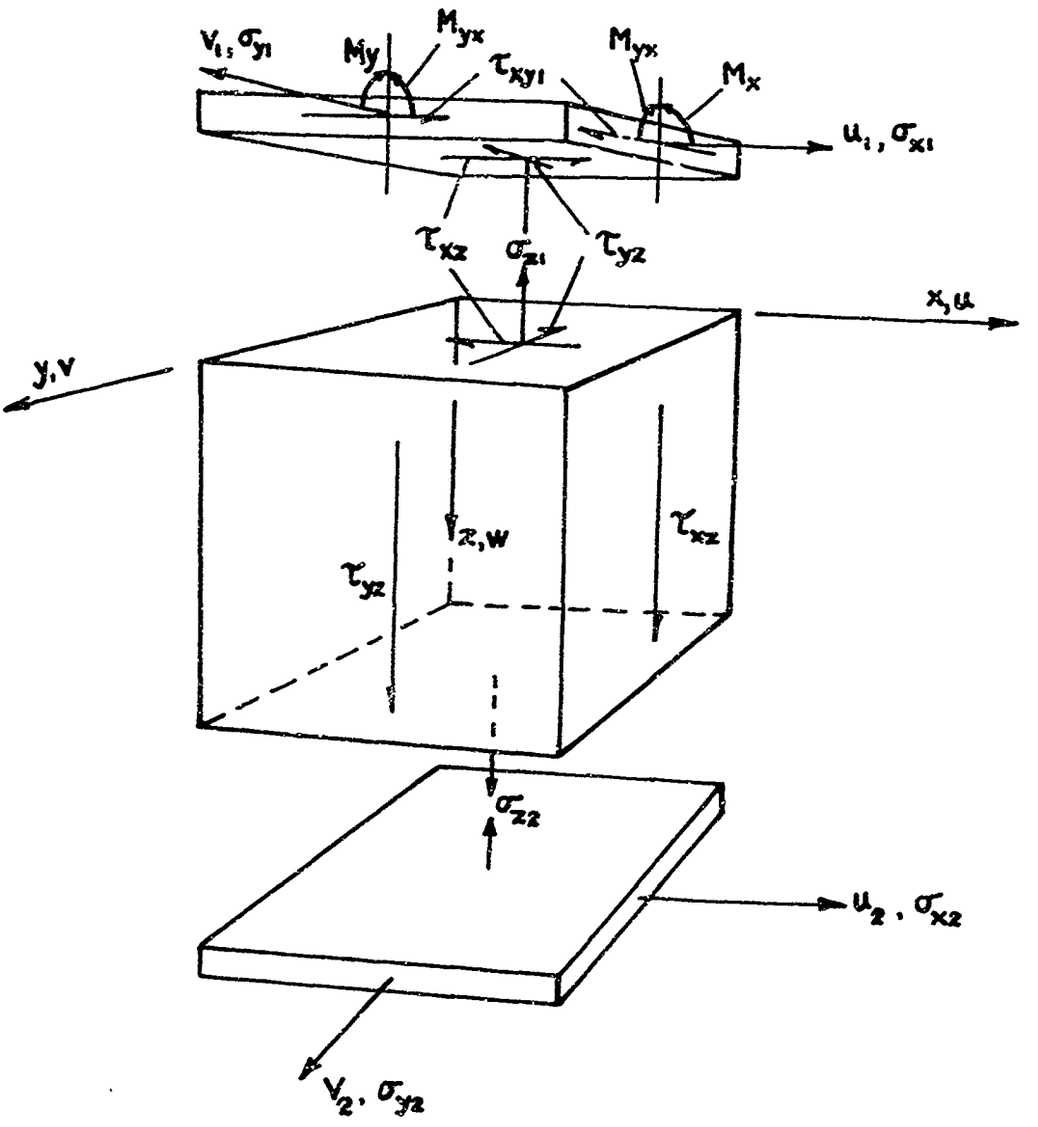

FIG. 27 CO-ORDINATE AXES AND NOTATION FOR DISPLACEMENTS AND STRESSES

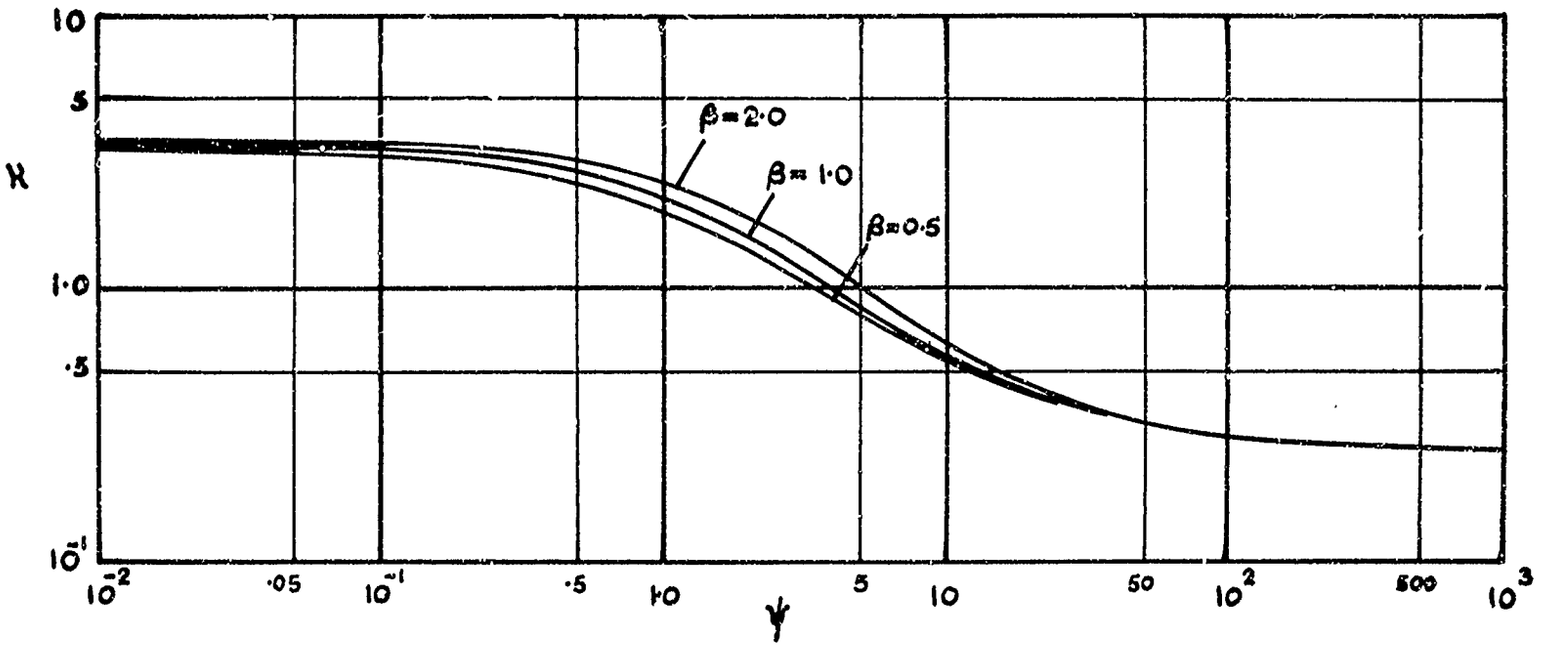

FIG.28 VARIATION OF THE SANDWICH PLATE STIFFNESS RATIO χ WITH ψ AND CORE LOSS FACTOR β

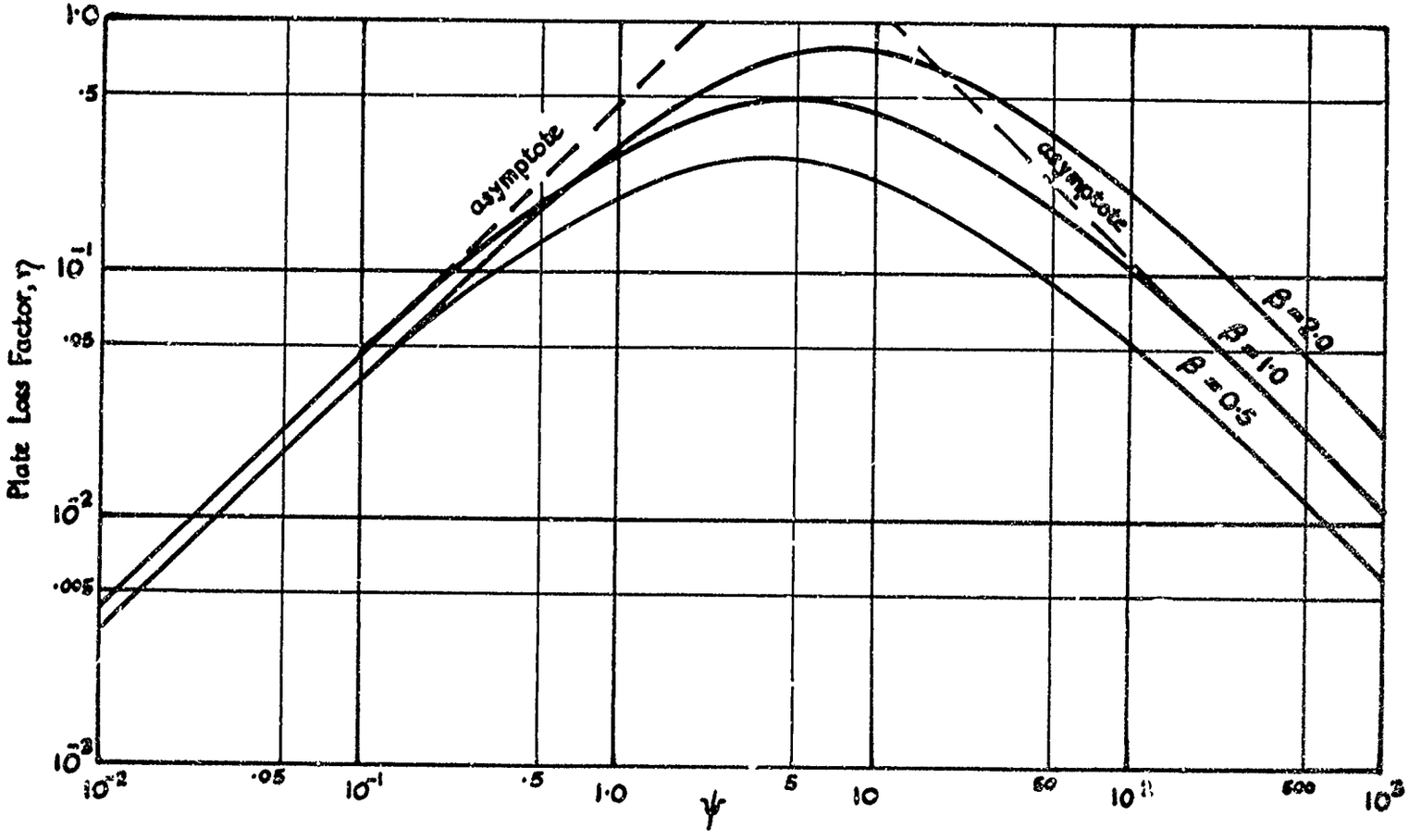

FIG. 29 VARIATION OF THE SANDWICH PLATE LOSS FACTOR, η, WITH ψ AND CORE LOSS FACTOR, β ($\tau = 1{\cdot}0$)

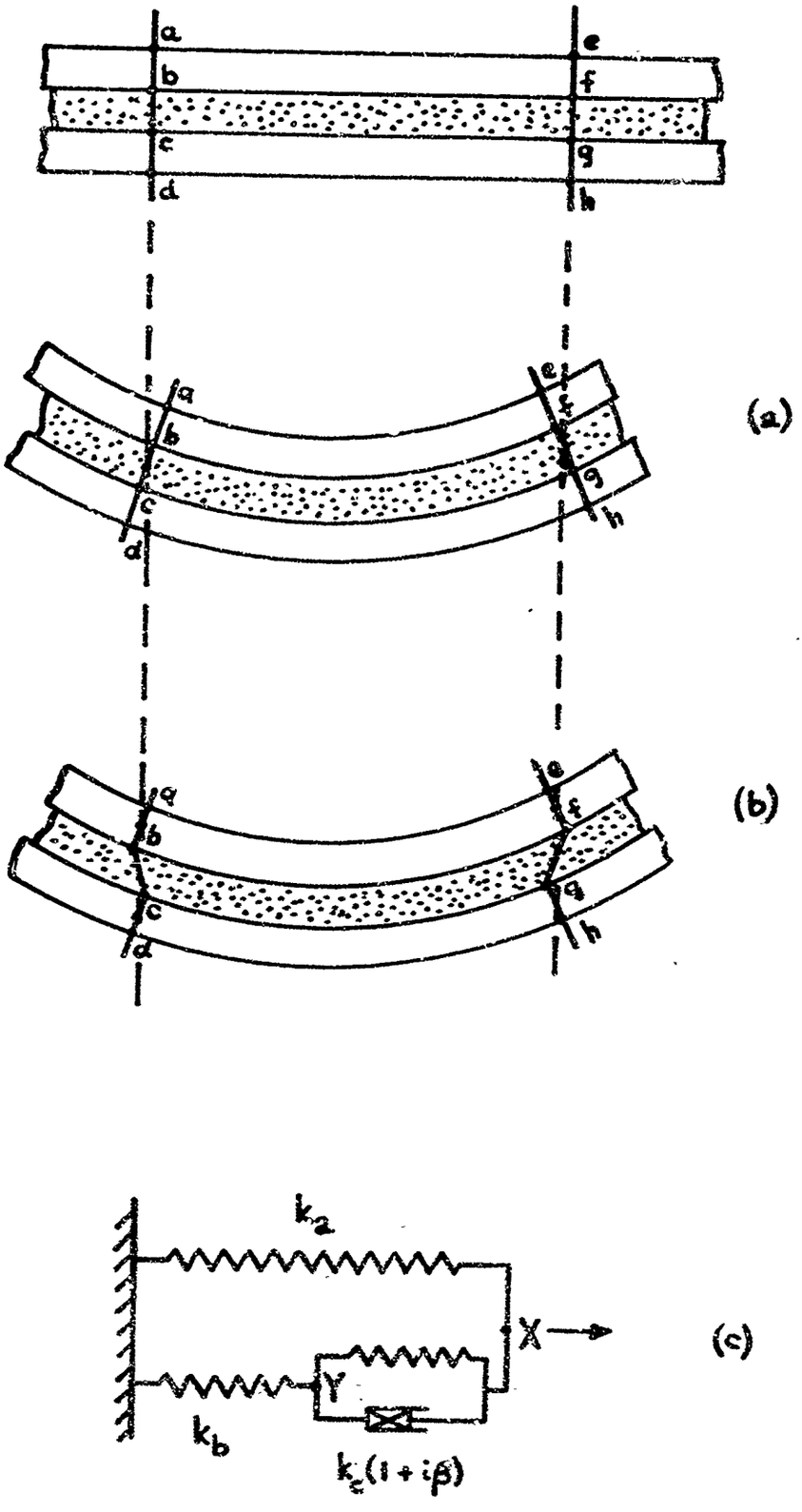

FIG.30 DIAGRAMS ILLUSTRATING BENDING DISPLACEMENTS OF A SANDWICH PLATE

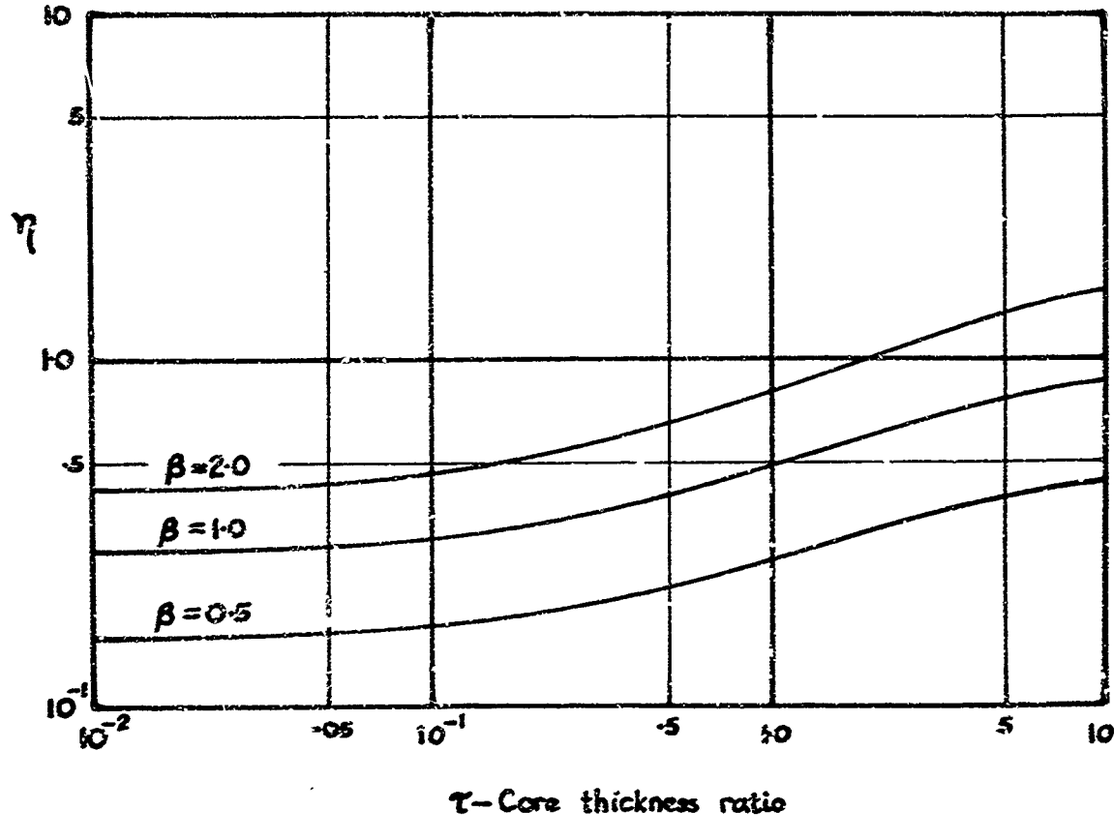

FIG.31 MAXIMIZED VALUES OF η

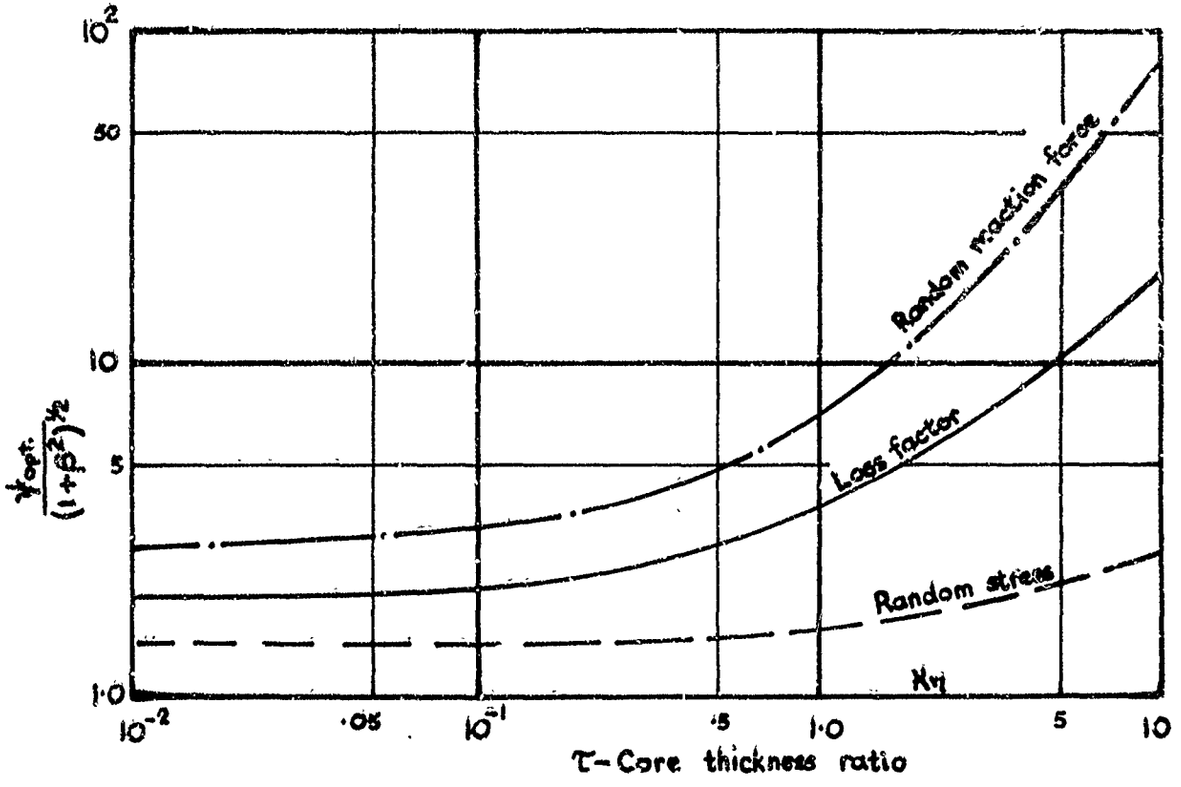

FIG. 32 OPTIMUM VALUES OF $\psi \div (1+\beta^2)^{1/2}$ TO MAXIMIZE VARIOUS RESPONSE CRITERIA

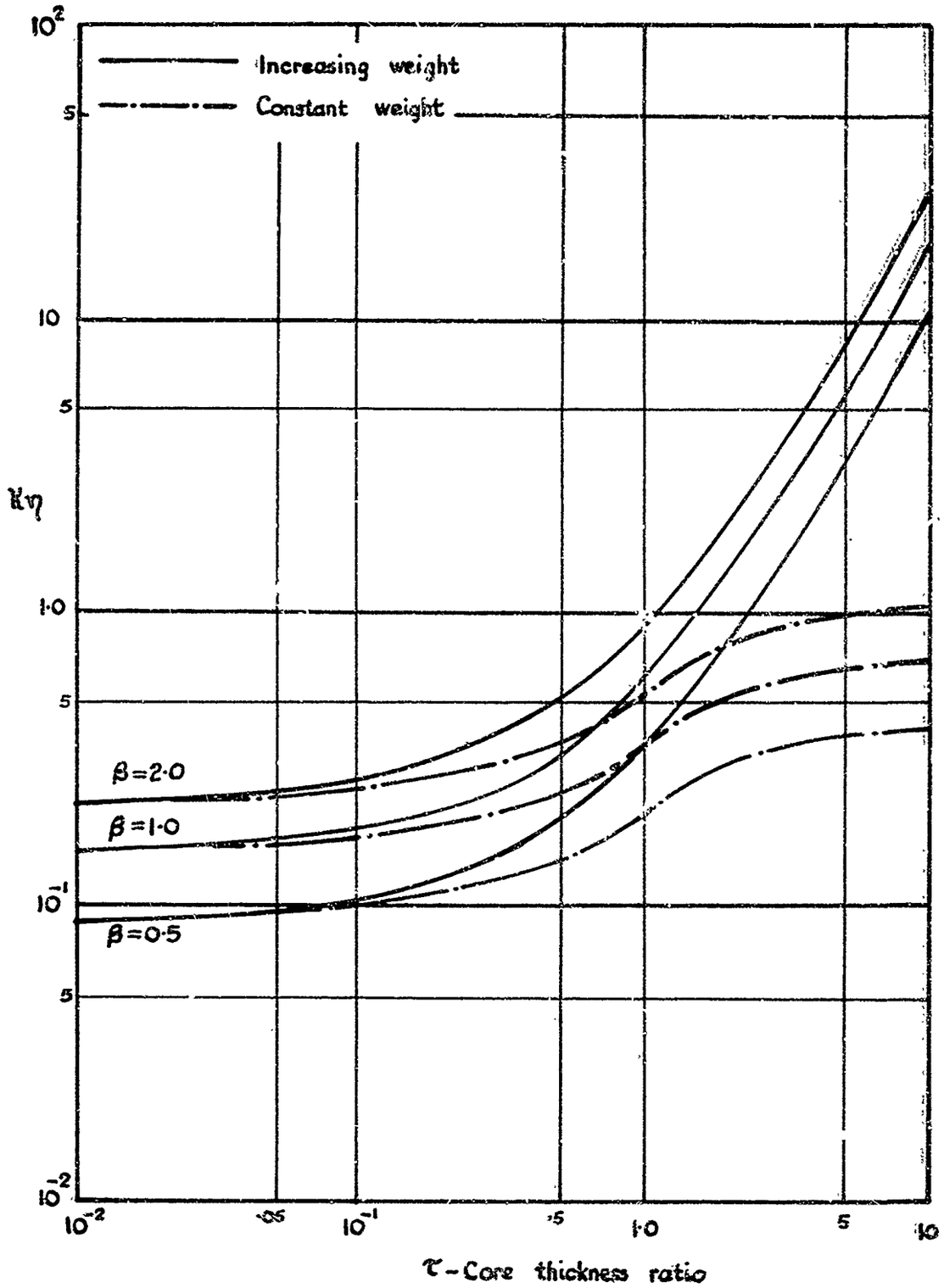

FIG. 33 MAXIMIZED VALUES OF $K\eta$

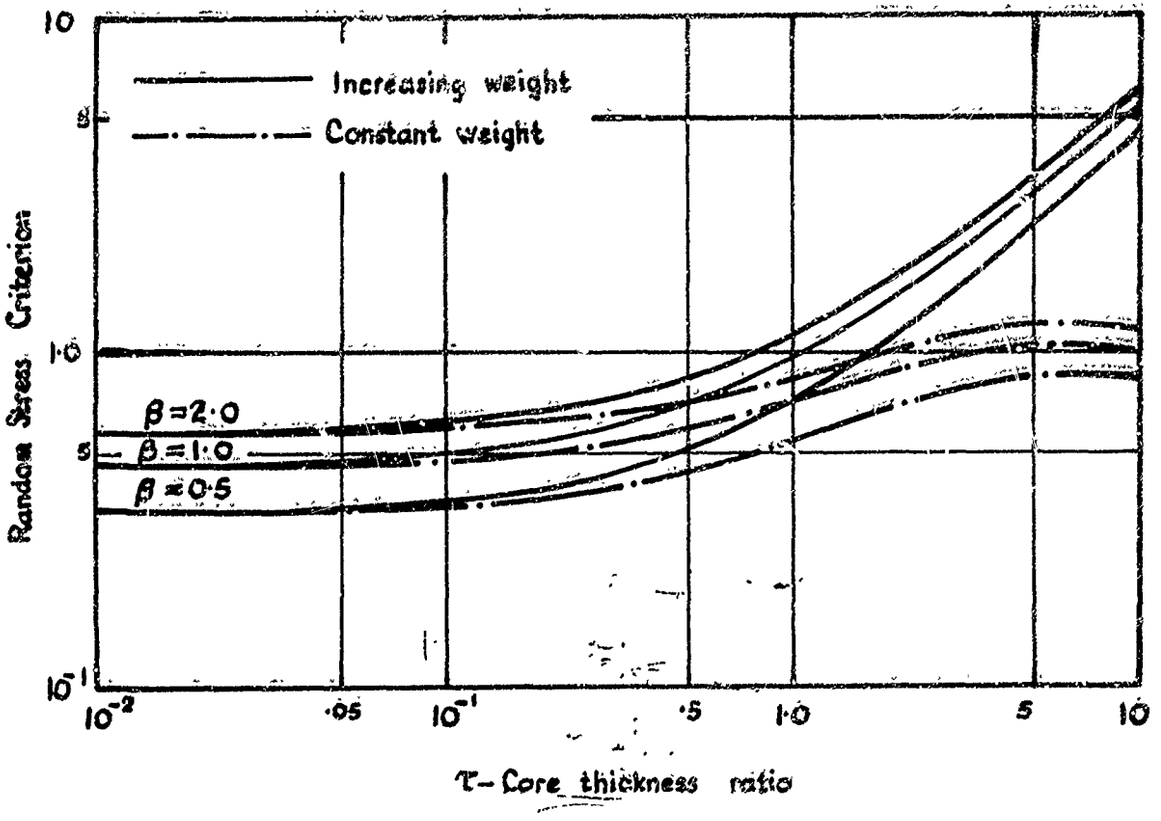

FIG. 34 MAXIMIZED VALUES OF THE RANDOM STRESS CRITERION

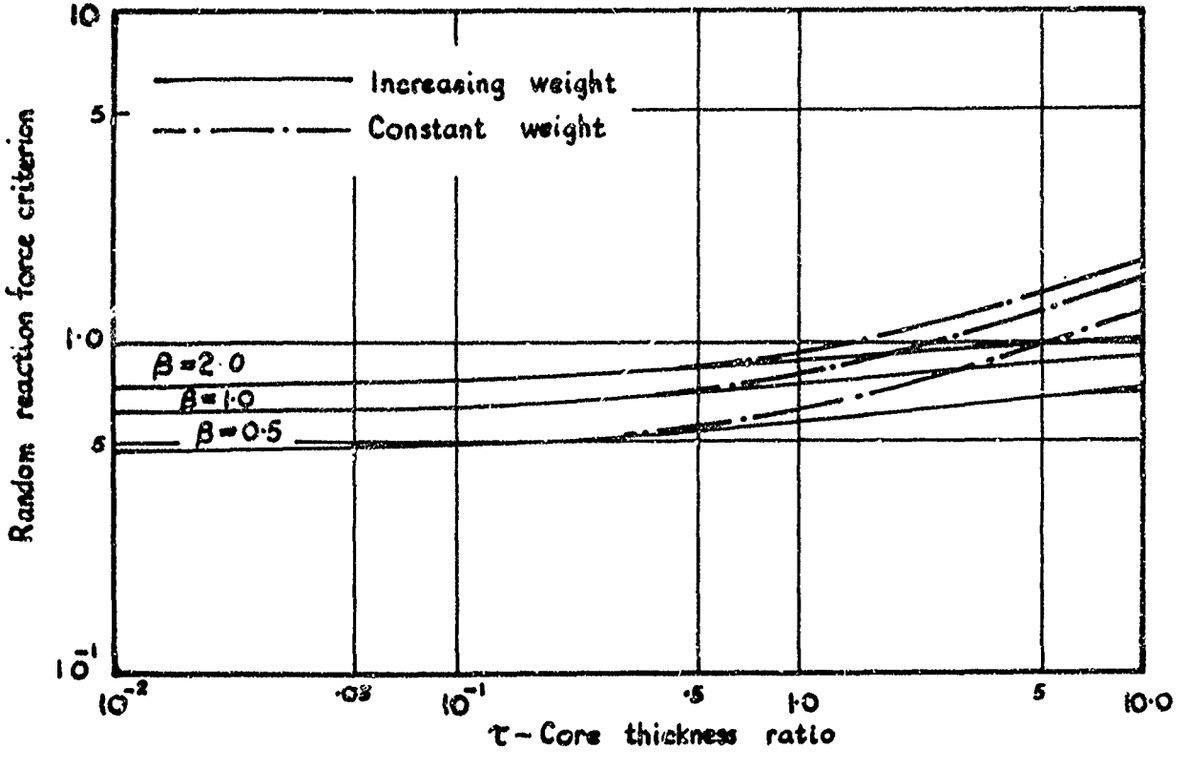

FIG. 35 MAXIMIZED VALUES OF THE RANDOM REACTION FORCE CRITERION

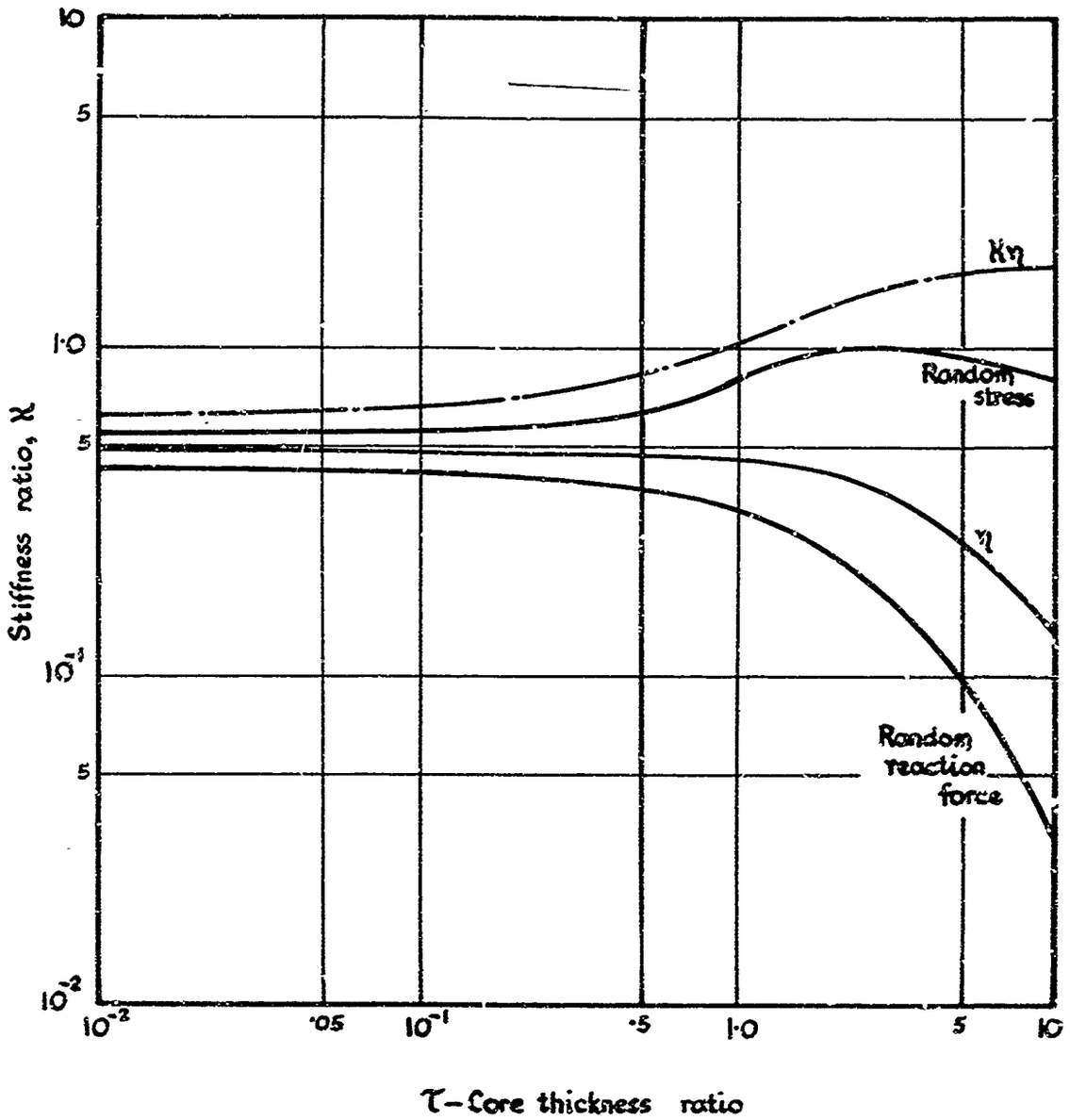

FIG. 36 THE STIFFNESS RATIOS OF PLATES OF CONSTANT WEIGHT, CORRESPONDING TO ψ_{opt} FOR THE DIFFERENT CRITERIA

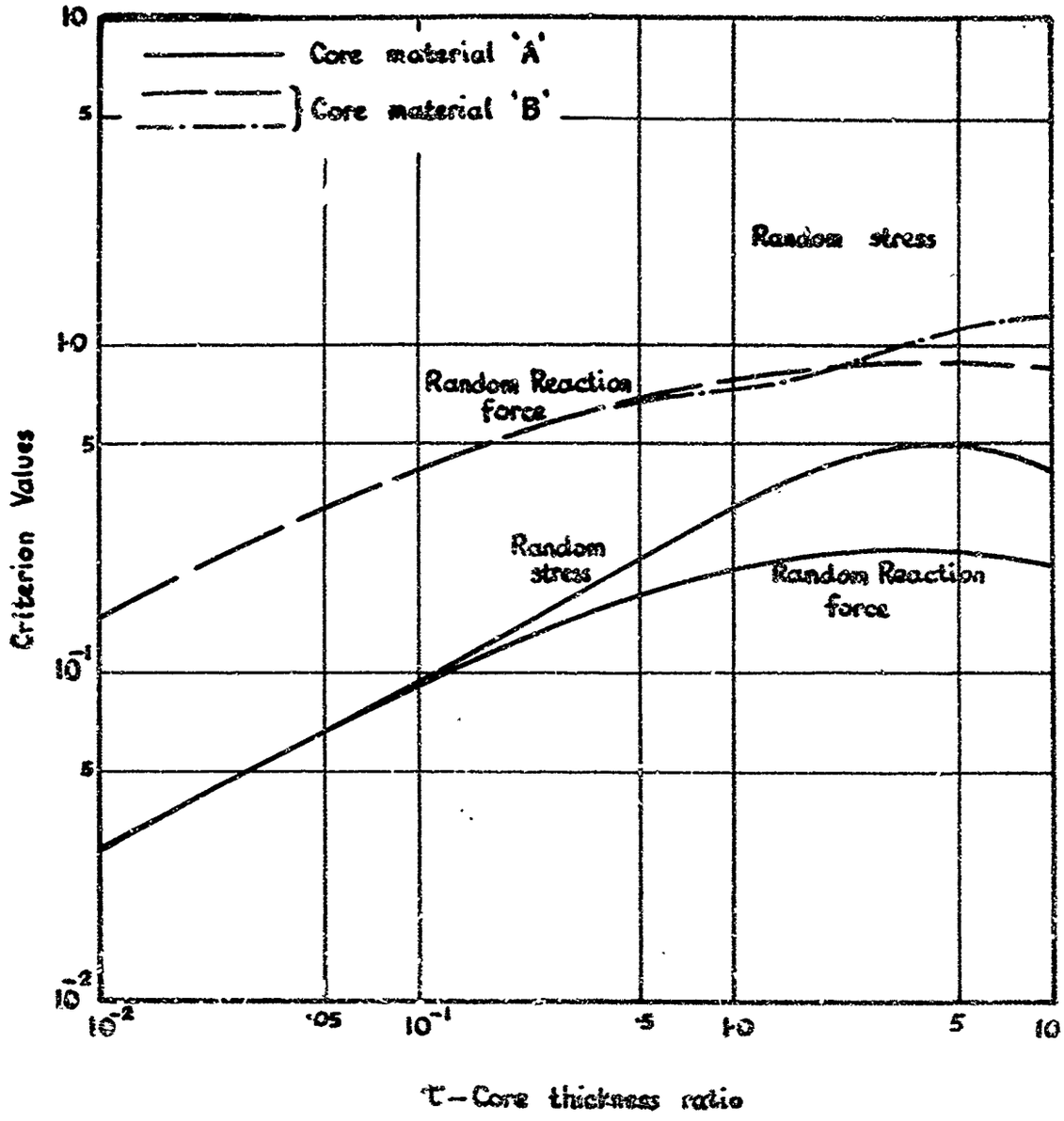

FIG. 37 THE RANDOM STRESS AND RANDOM REACTION FORCE CRITERIA FOR A 6in SQUARE SANDWICH PLATE WITH DIFFERENT CORE MATERIALS

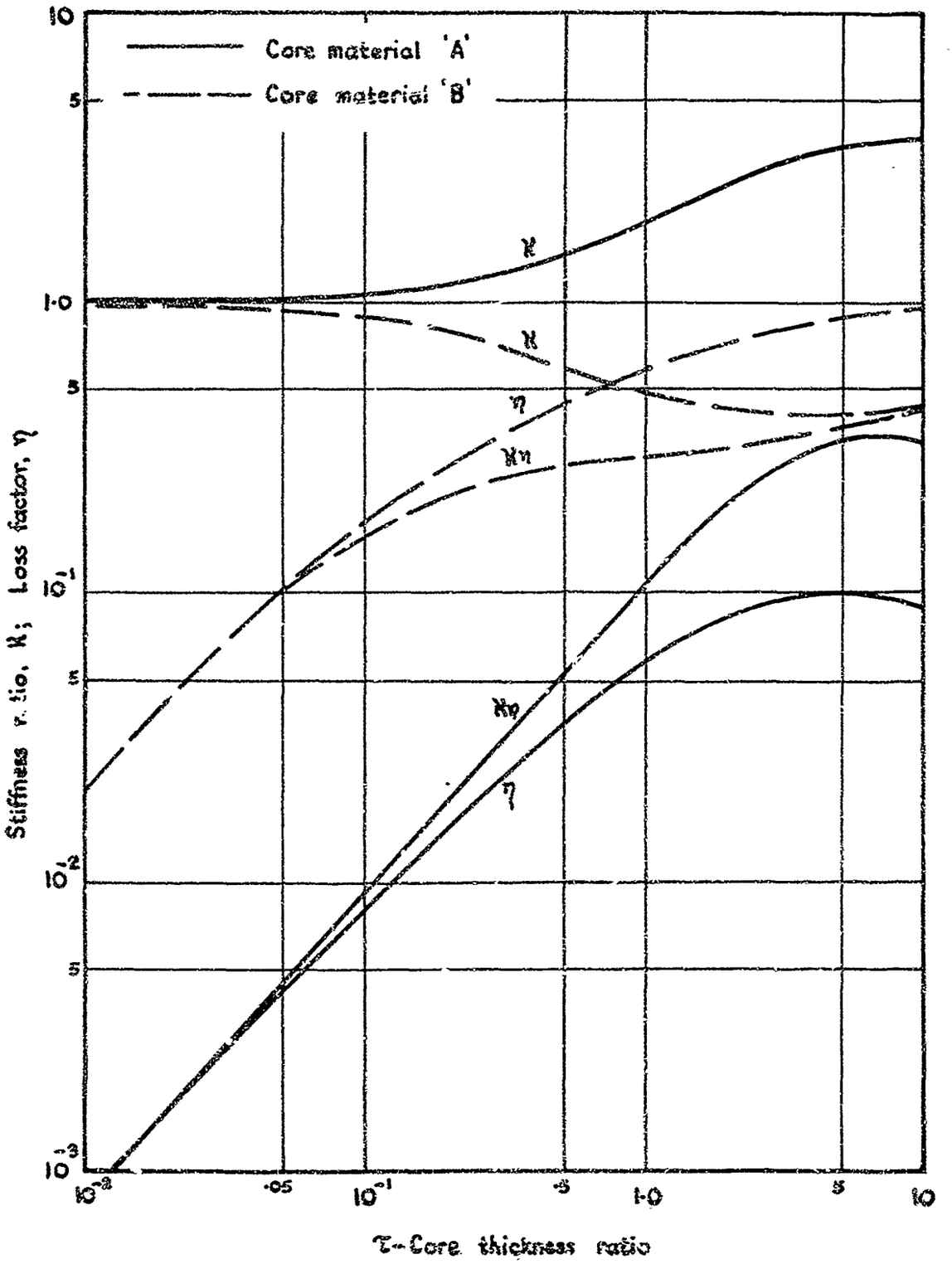

FIG. 38 THE STIFFNESS RATIO, K, LOSS FACTOR, η, AND Kη FOR A 6in. SQUARE SANDWICH PLATE WITH DIFFERENT CORE MATERIALS

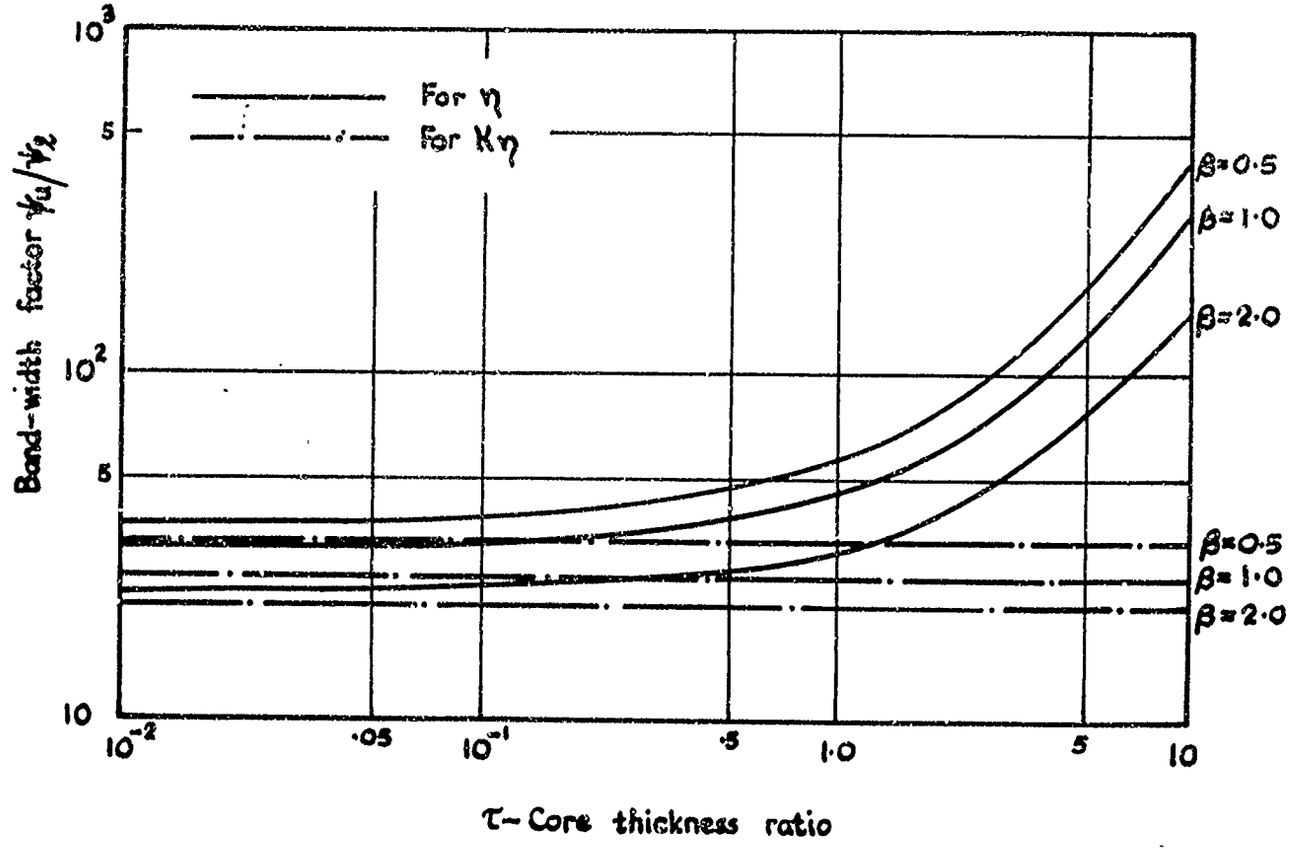

FIG. 39 THE BAND-WIDTH FACTOR, ψ_1/ψ_2, FOR η & $K\eta$

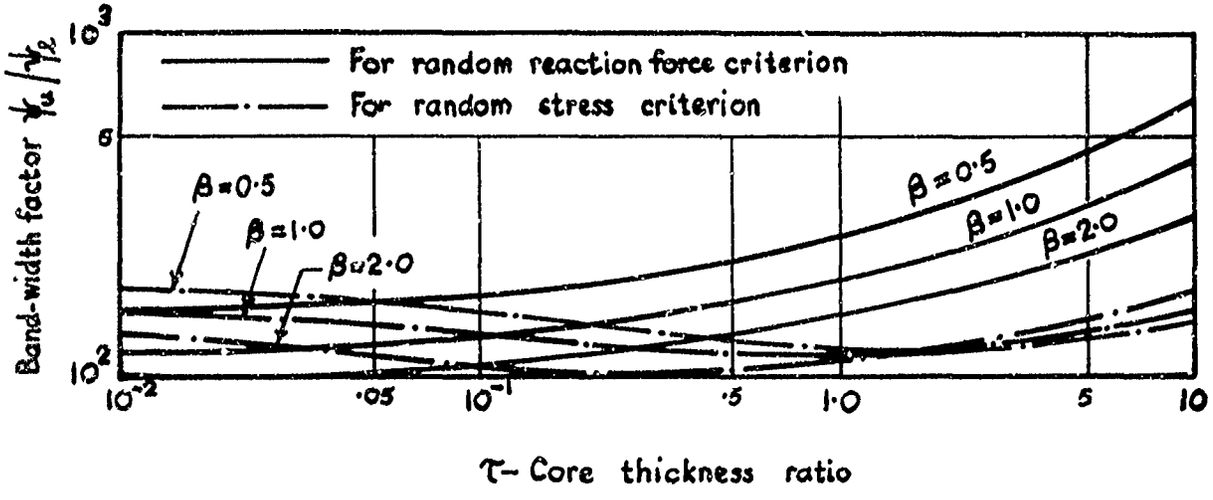

FIG.40 THE BAND-WIDTH FACTOR ψ_u/ψ_l FOR THE RANDOM REACTION FORCE AND RANDOM SURFACE STRESS CRITERIA

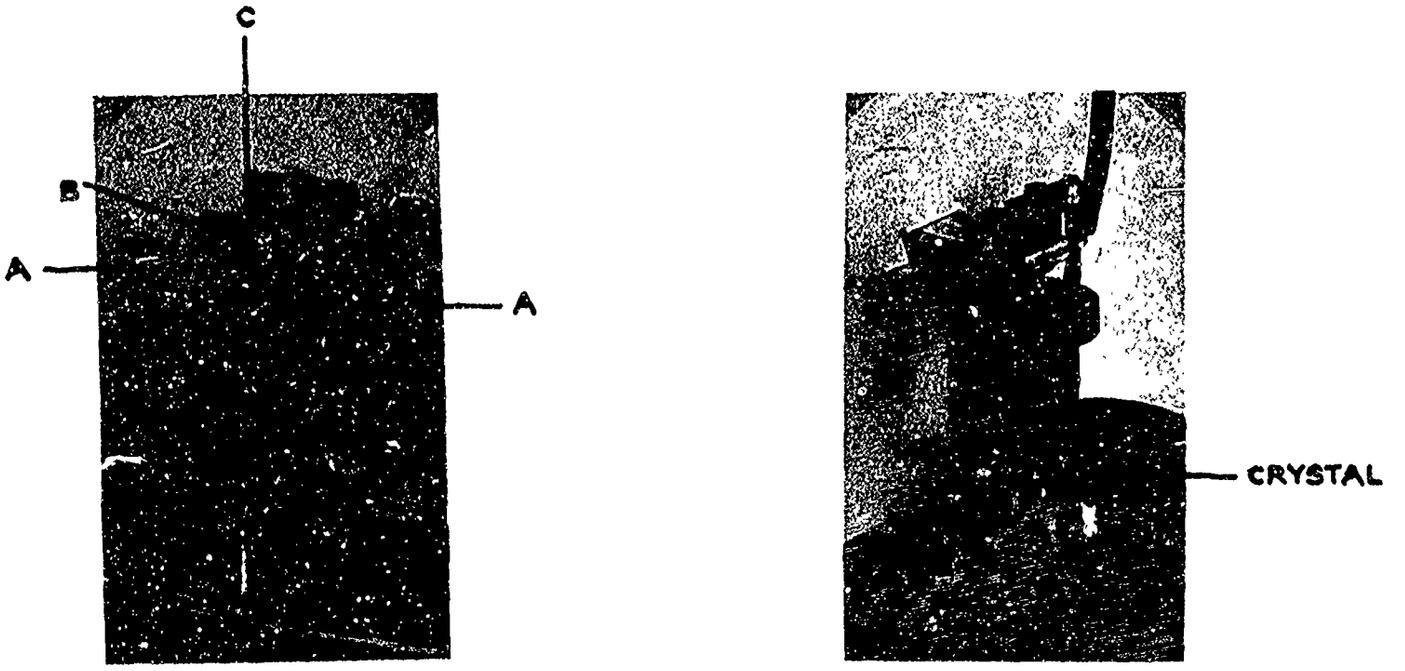

FIG.41 THE SUPPORTS OF THE SANDWICH SPECIMENS

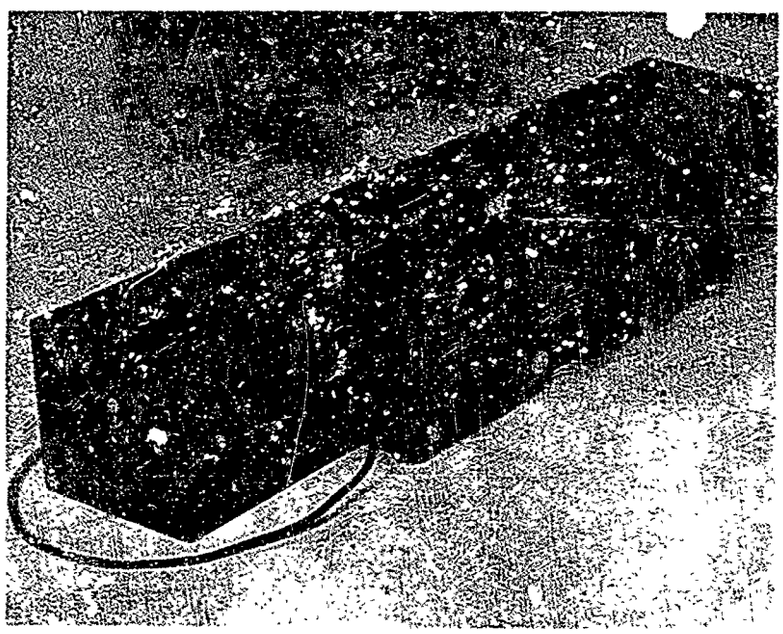

FIG. 42 THE SANDWICH SPECIMEN TEST RIG

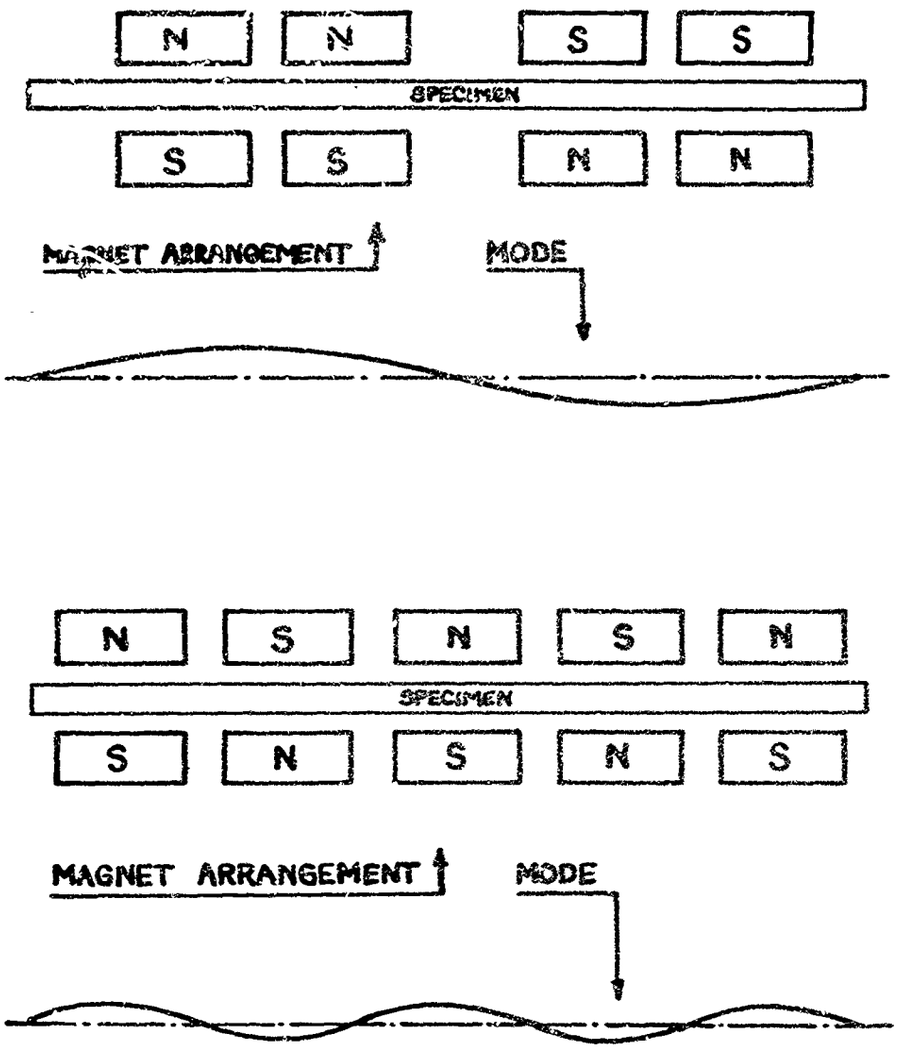

FIG. 43 MAGNET ARRANGEMENTS TO EXCITE GIVEN MODES

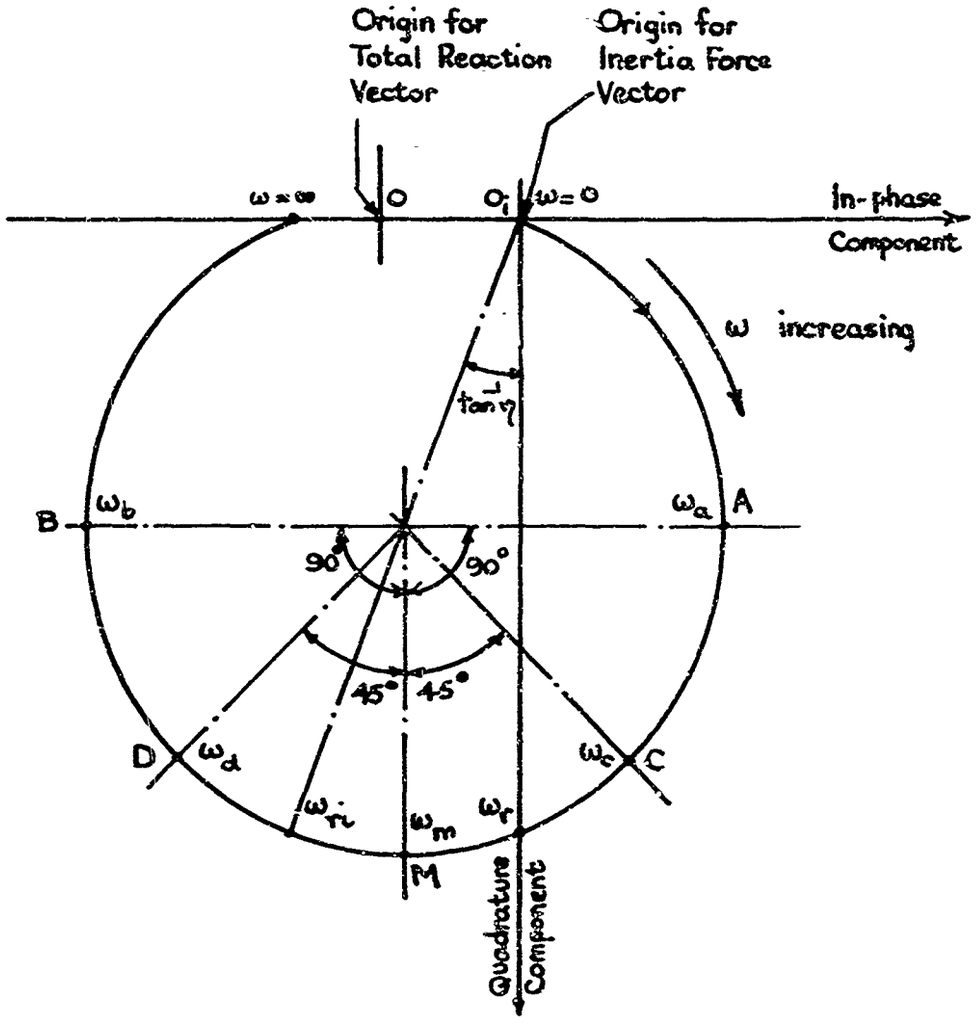

FIG. 44 VECTOR RESPONSE DIAGRAM OF INERTIA FORCE CORRESPONDING TO ONE MODE

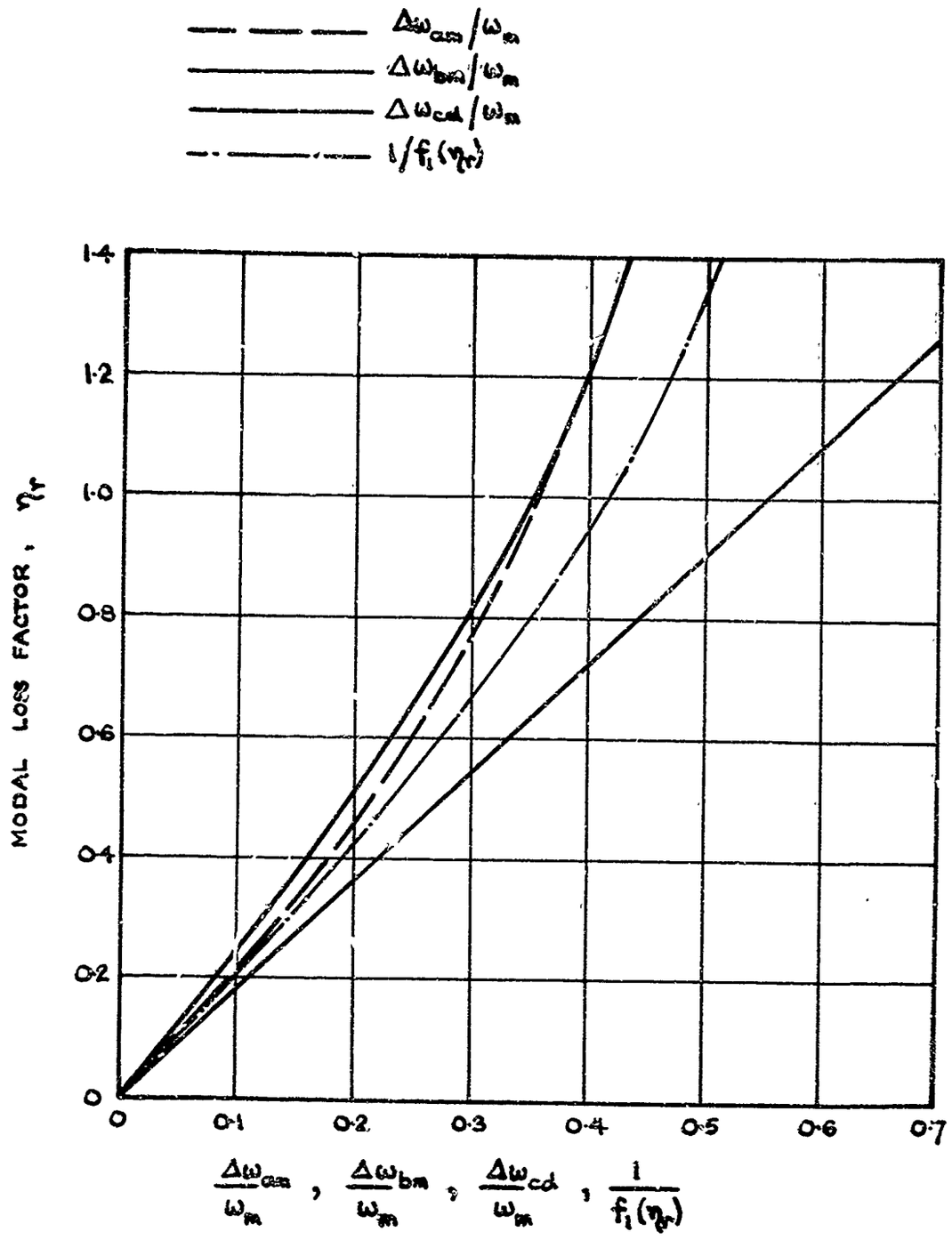

FIG.45 CURVES USED FOR DEDUCING MODAL LOSS FACTORS

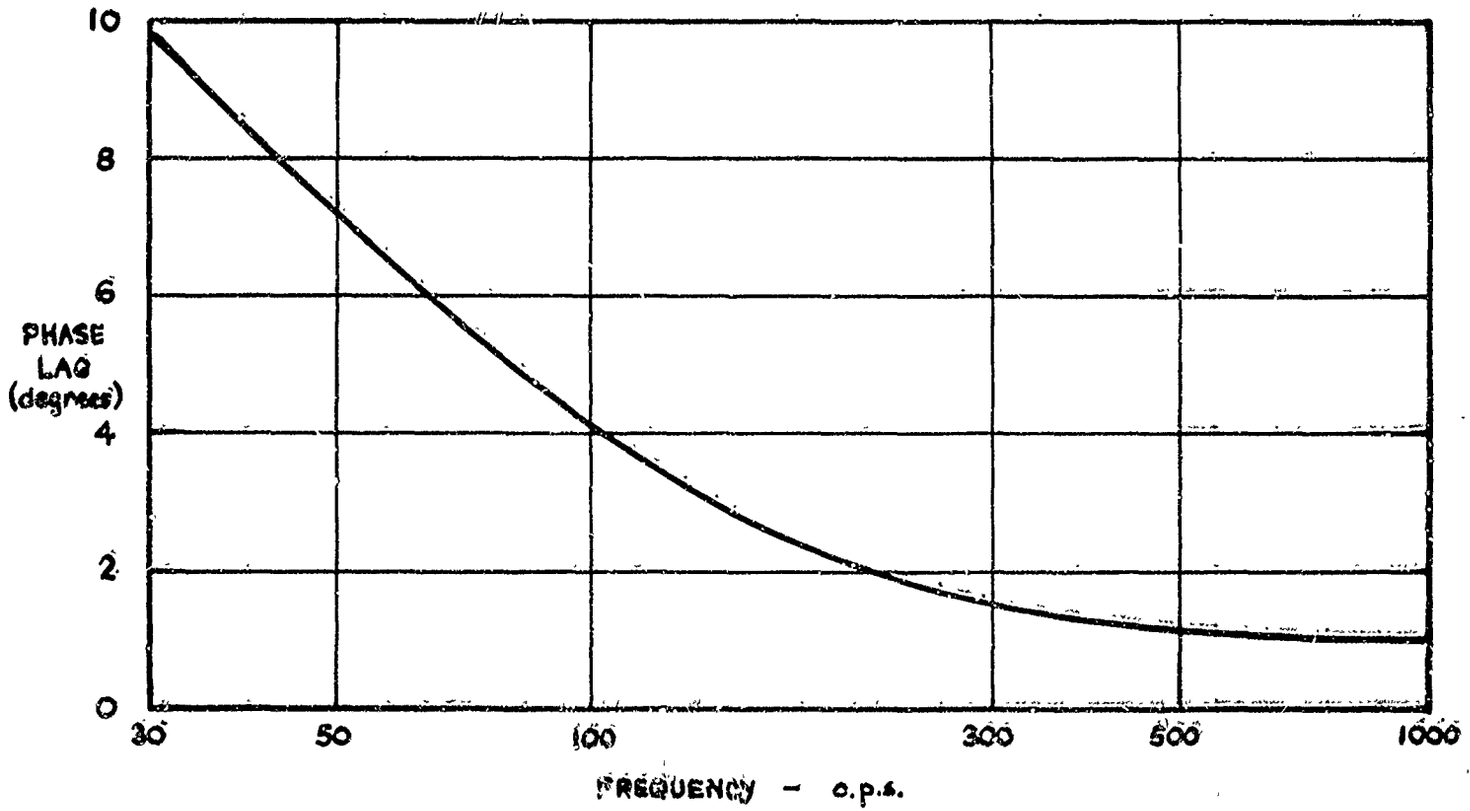

FIG.46 PHASE LAG OF REACTION TRANSDUCER OUTPUT BEHIND APPLIED FORCE

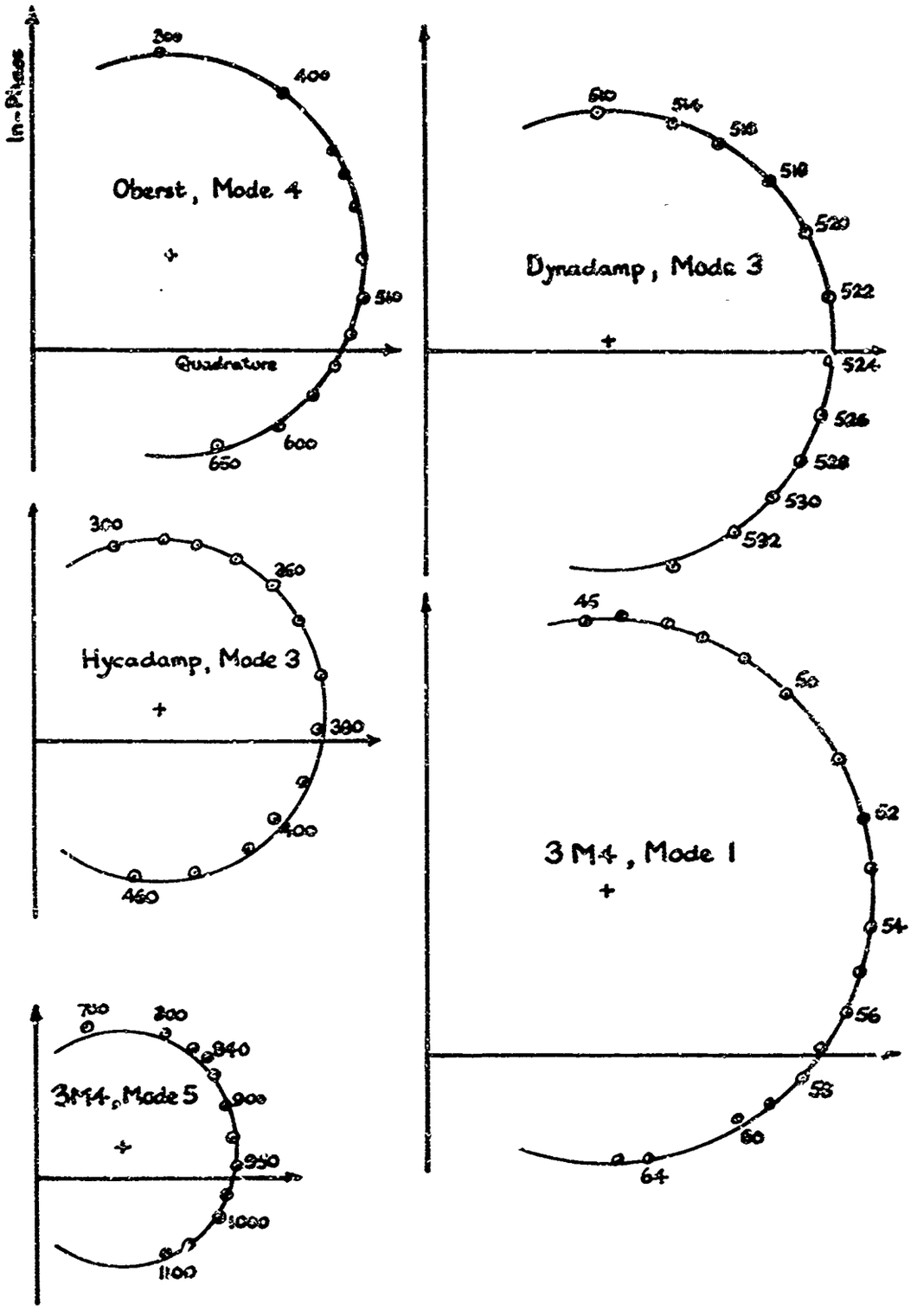

FIG. 47 SOME MEASURED VECTOR RESPONSE DIAGRAMS

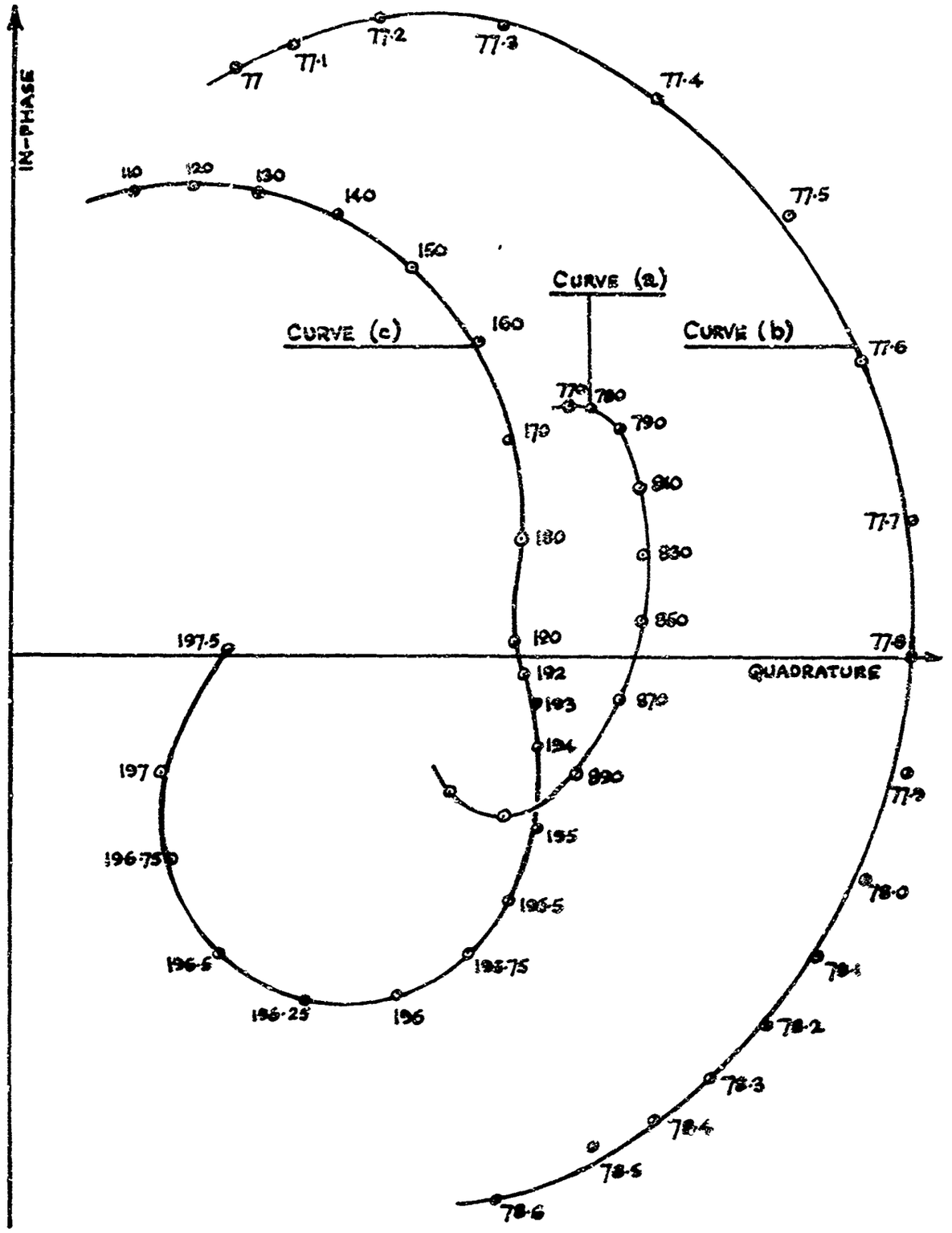

FIG. 48 SOME MEASURED VECTOR RESPONSE DIAGRAMS (CONT.)

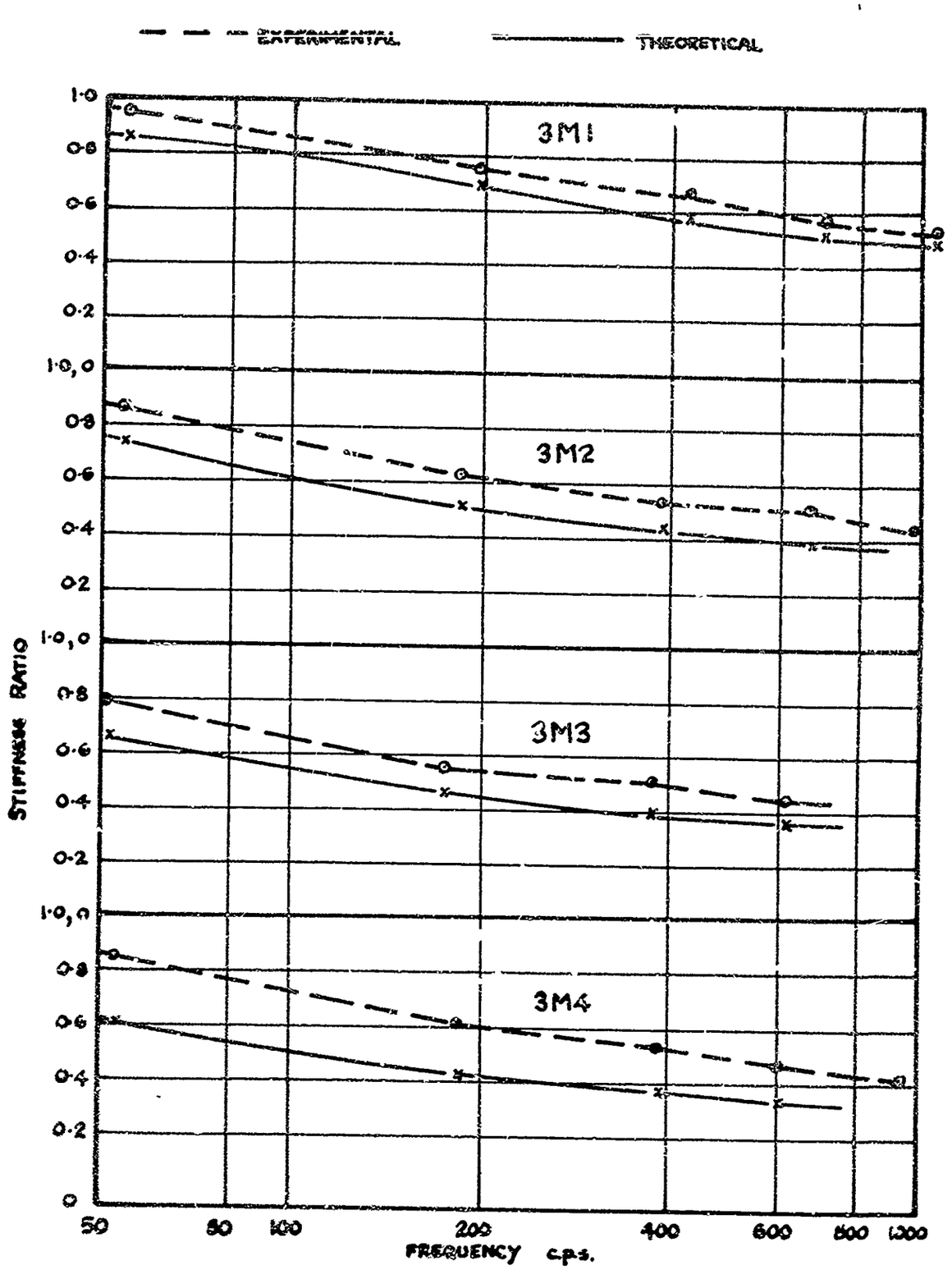

FIG. 49 EXPERIMENTAL AND THEORETICAL VALUES OF THE STIFFNESS RATIOS OF THE 3M's SPECIMENS

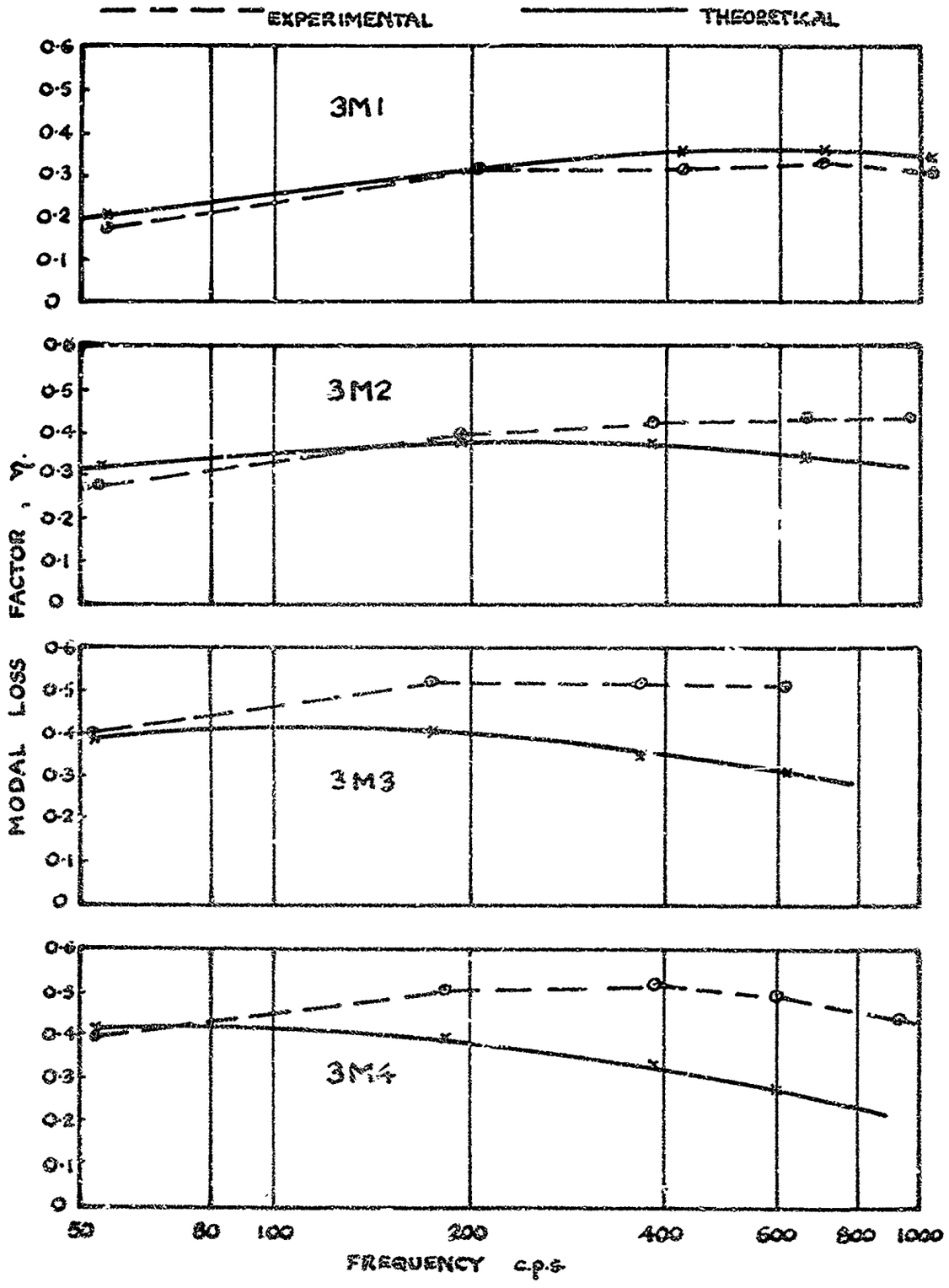

FIG. 50 EXPERIMENTAL AND THEORETICAL VALUES OF THE LOSS FACTORS OF THE 3M's SPECIMENS

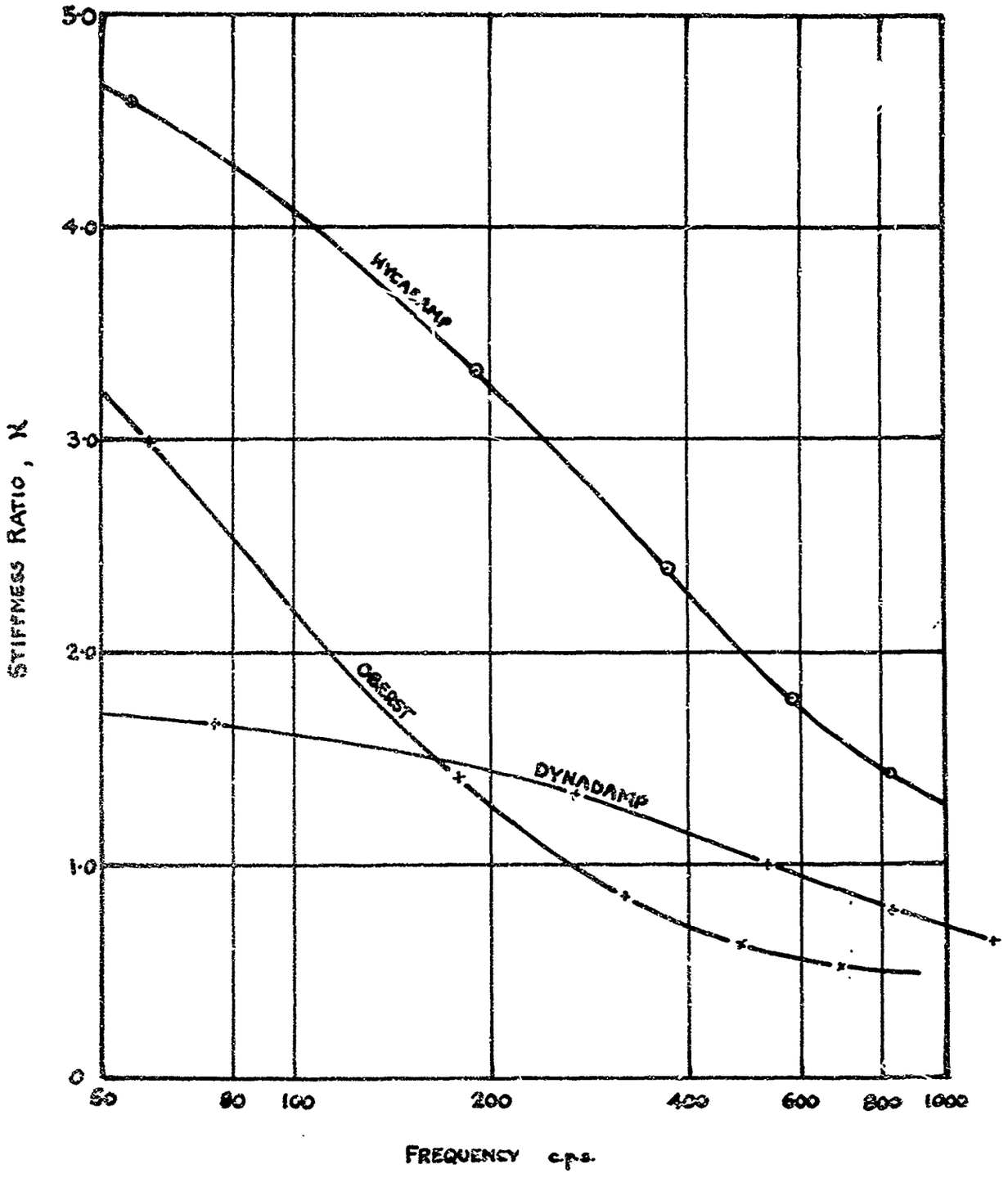

FIG. 51 MEASURED STIFFNESS RATIOS OF THE COMMERCIAL SPECIMENS

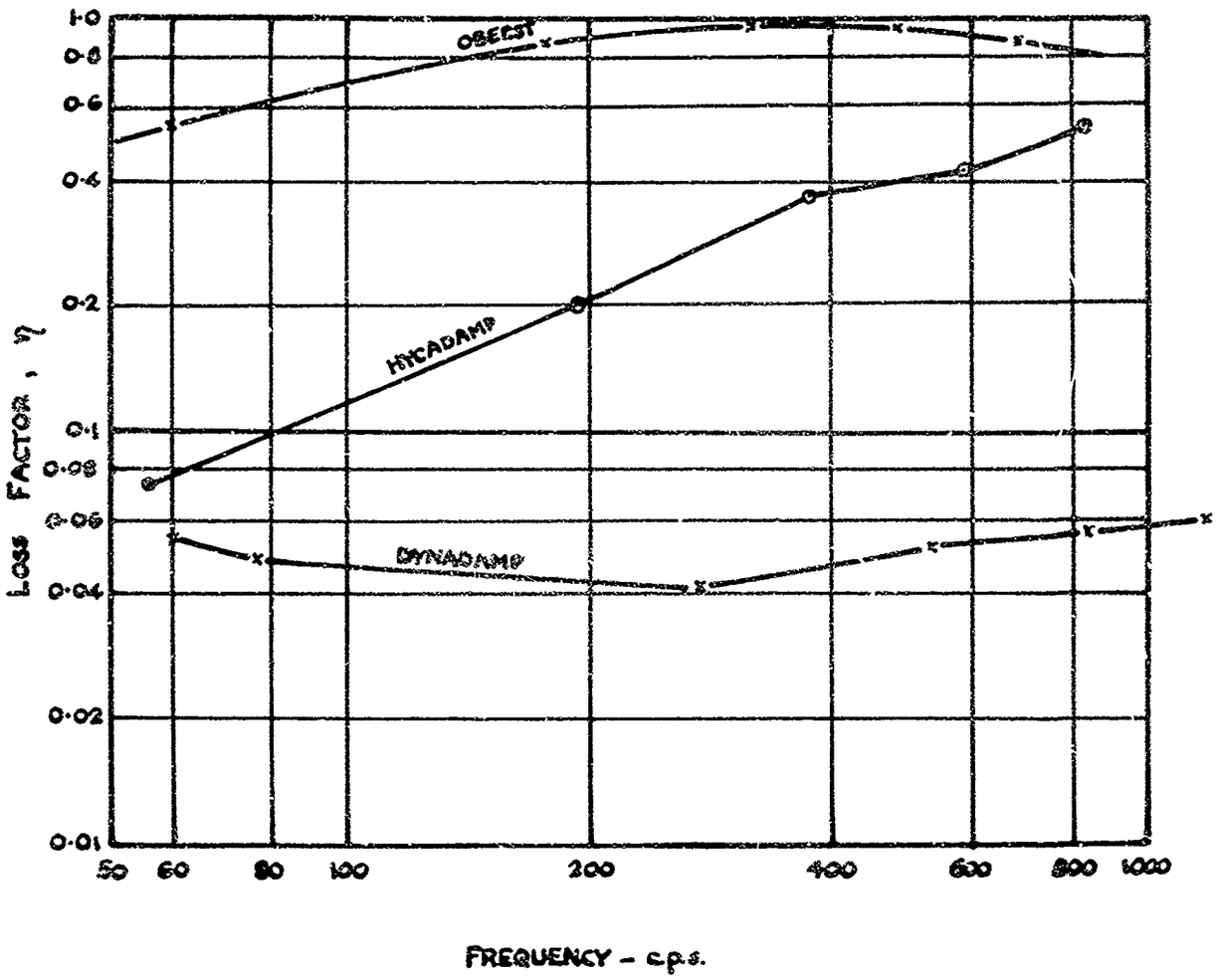

FIG. 52 LOSS FACTORS OF COMMERCIAL SPECIMENS

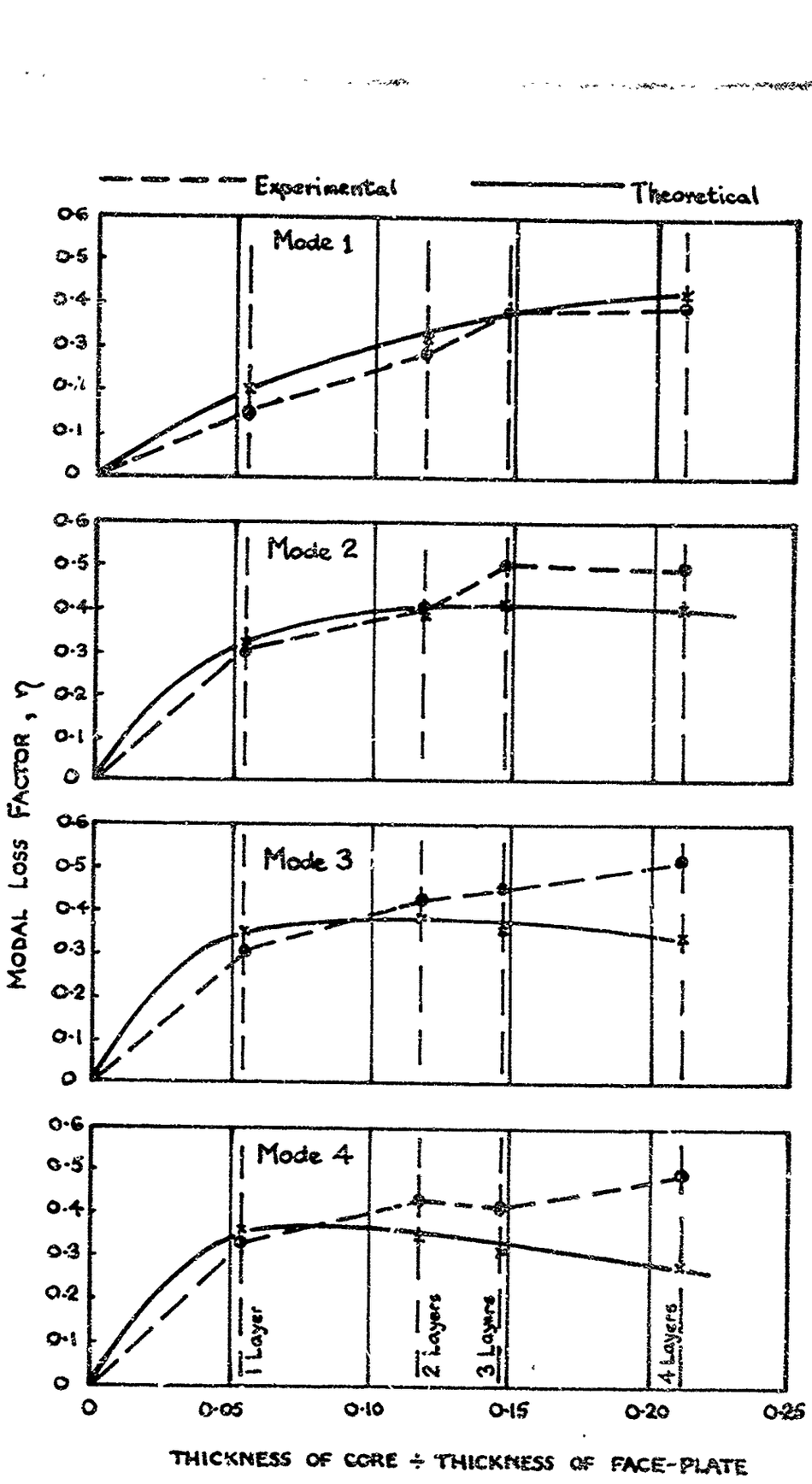

FIG.53 MODAL LOSS FACTORS OF 3M's SPECIMENS PLOTTED AGAINST CORE THICKNESS

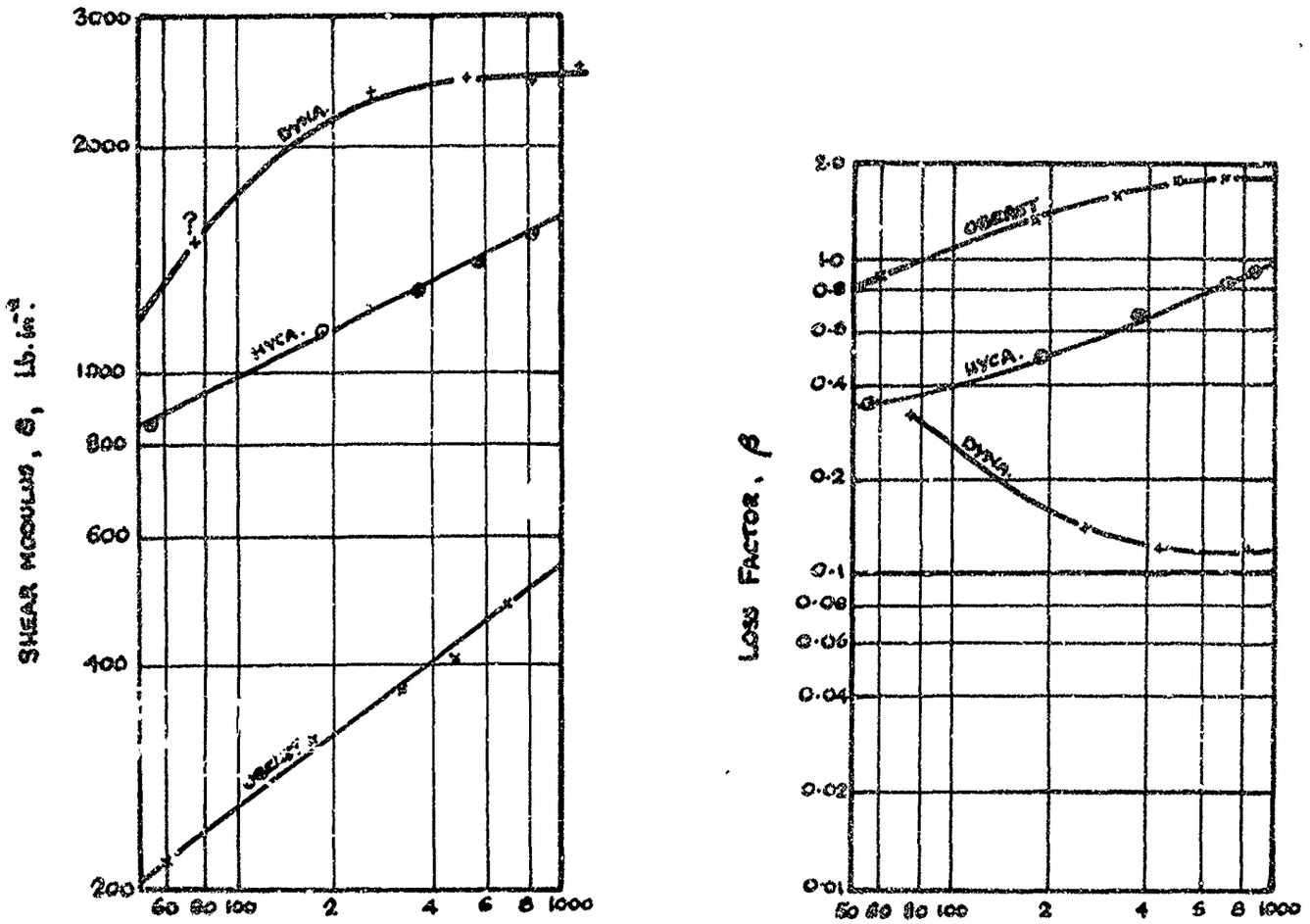

FIG. 54 THE SHEAR MODULUS, G, AND THE LOSS FACTOR, β, OF THE MATERIALS IN THE COMMERCIAL SPECIMENS

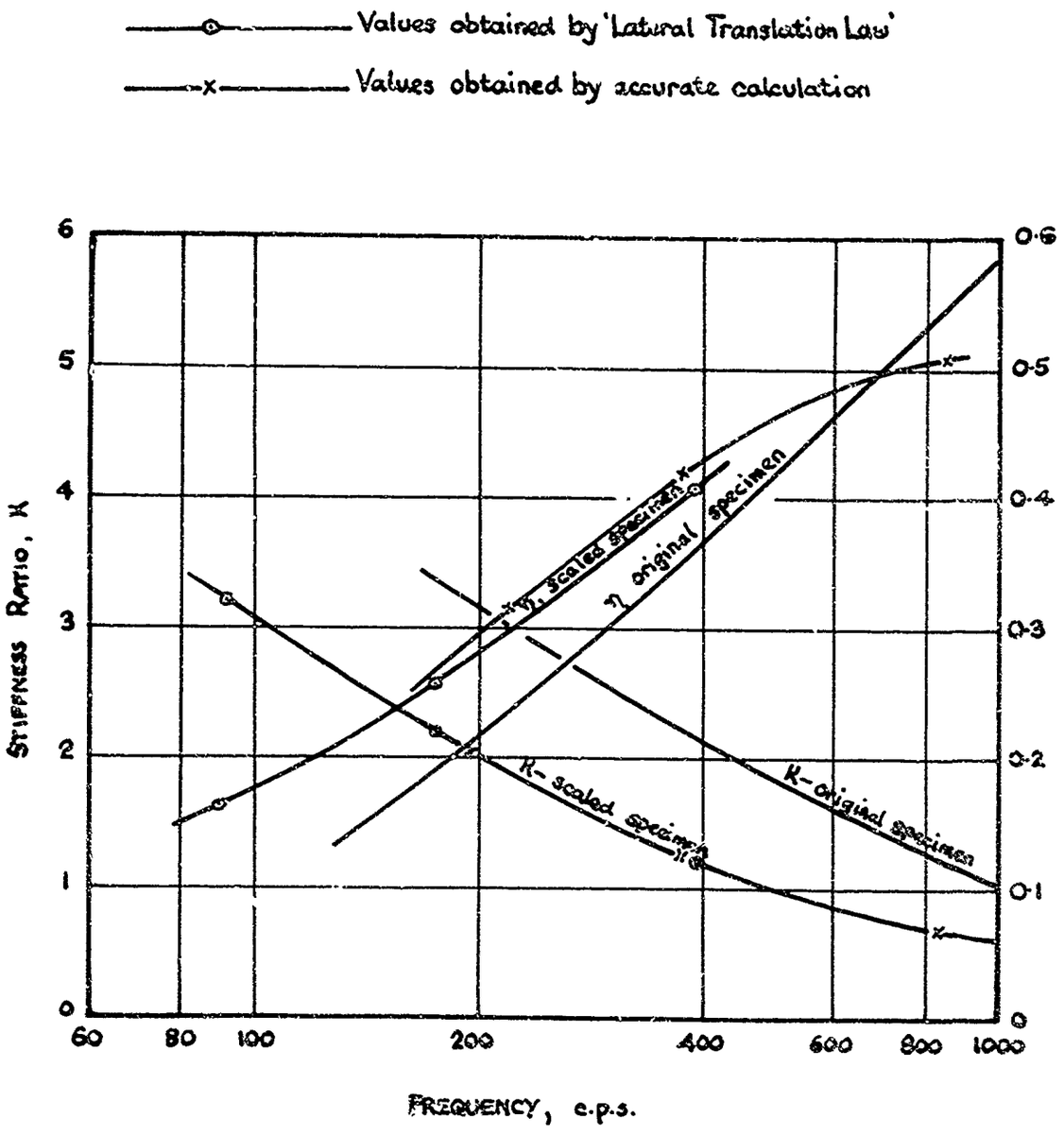

FIG. 55 THE STIFFNESS RATIOS AND LOSS FACTORS OF THE ORIGINAL AND 'SCALED-UP' HYCADAMP SPECIMENS

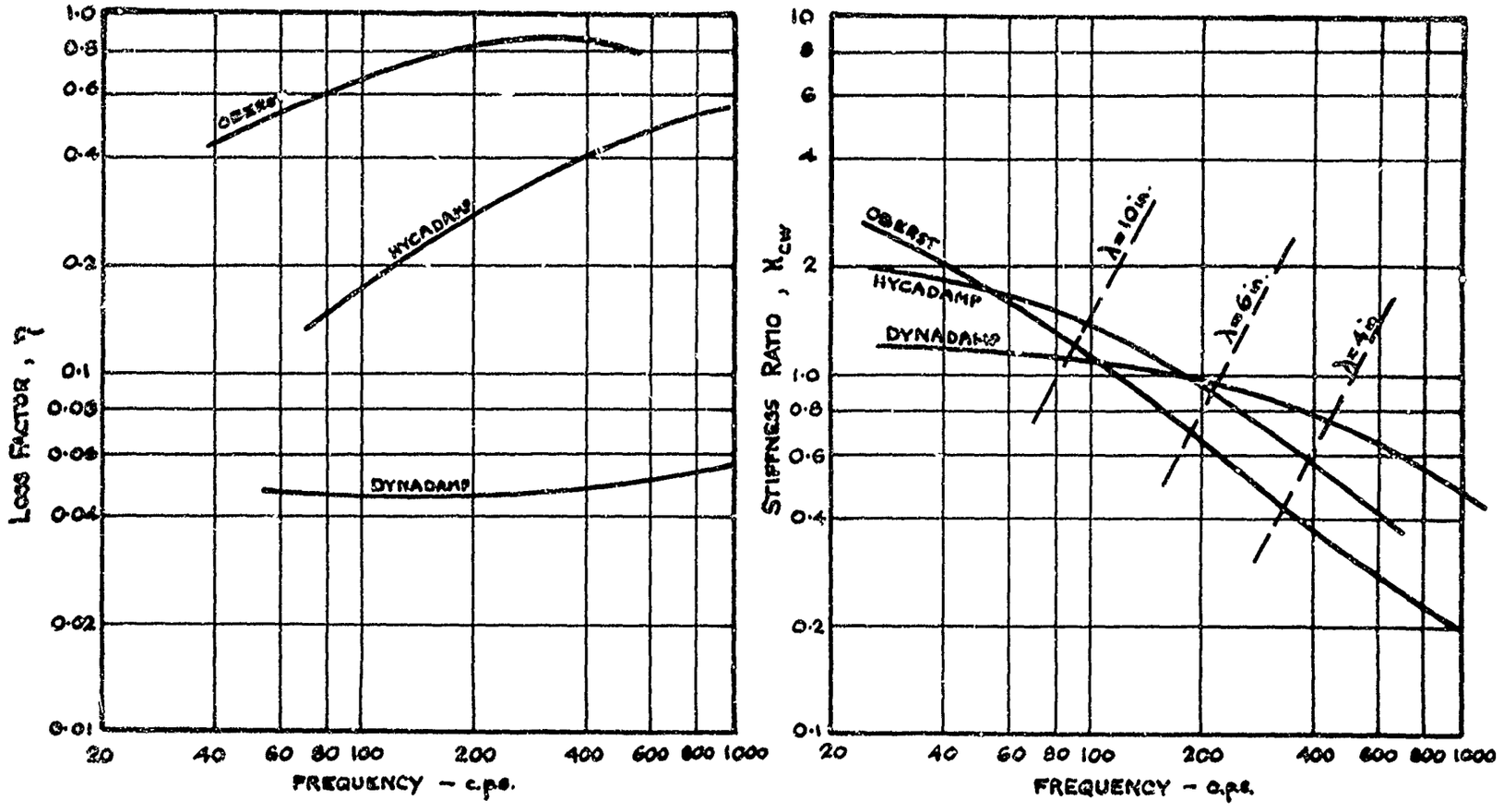

FIG. 56 THE STIFFNESS RATIOS AND LOSS FACTORS FOR THE 'SCALED' COMMERCIAL SPECIMENS

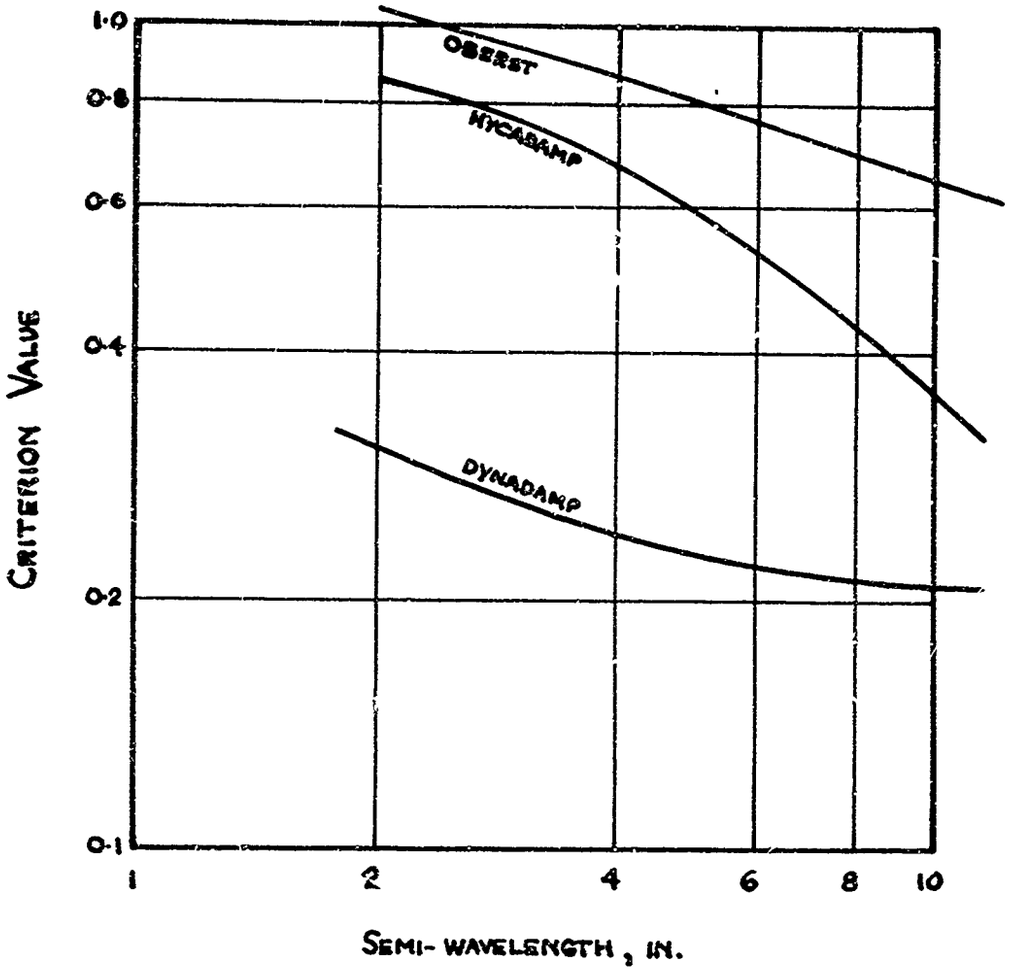

FIG. 57 THE REACTION FORCE CRITERION FOR THE SCALED COMMERCIAL SPECIMENS PLOTTED vs. MODAL WAVELENGTH

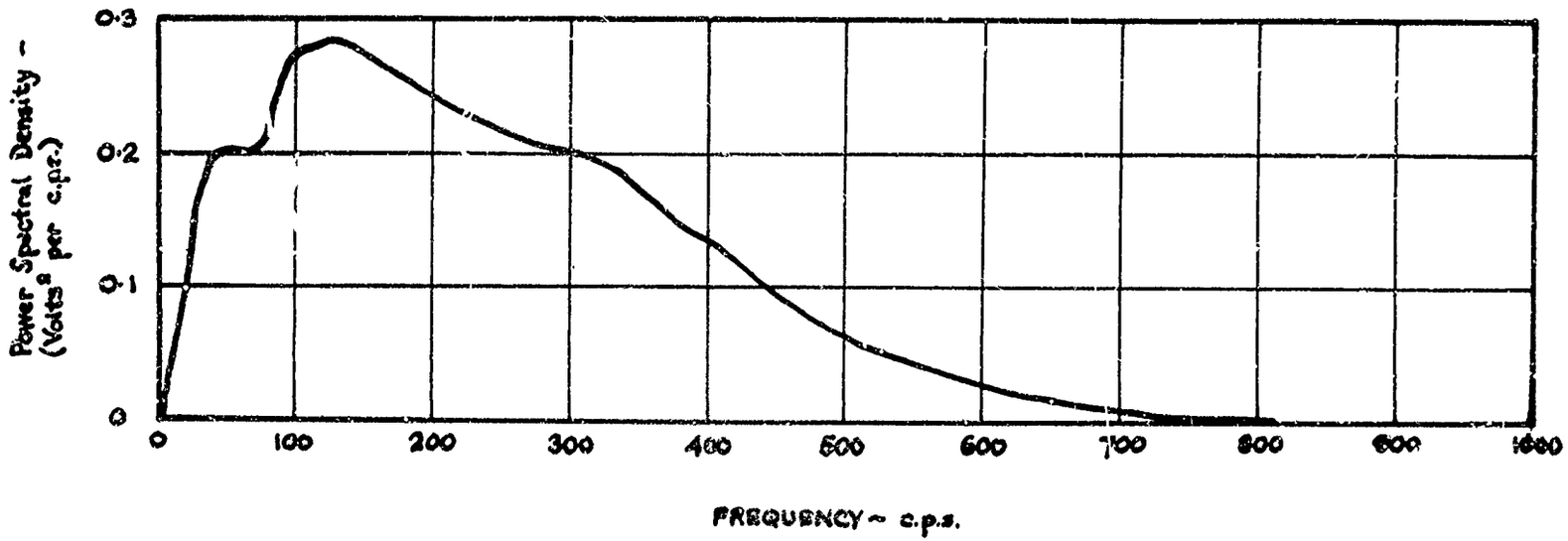

FIG. 38 MEASURED FREQUENCY SPECTRUM OF VOLTAGE ASSOCIATED WITH EXCITING CURRENT

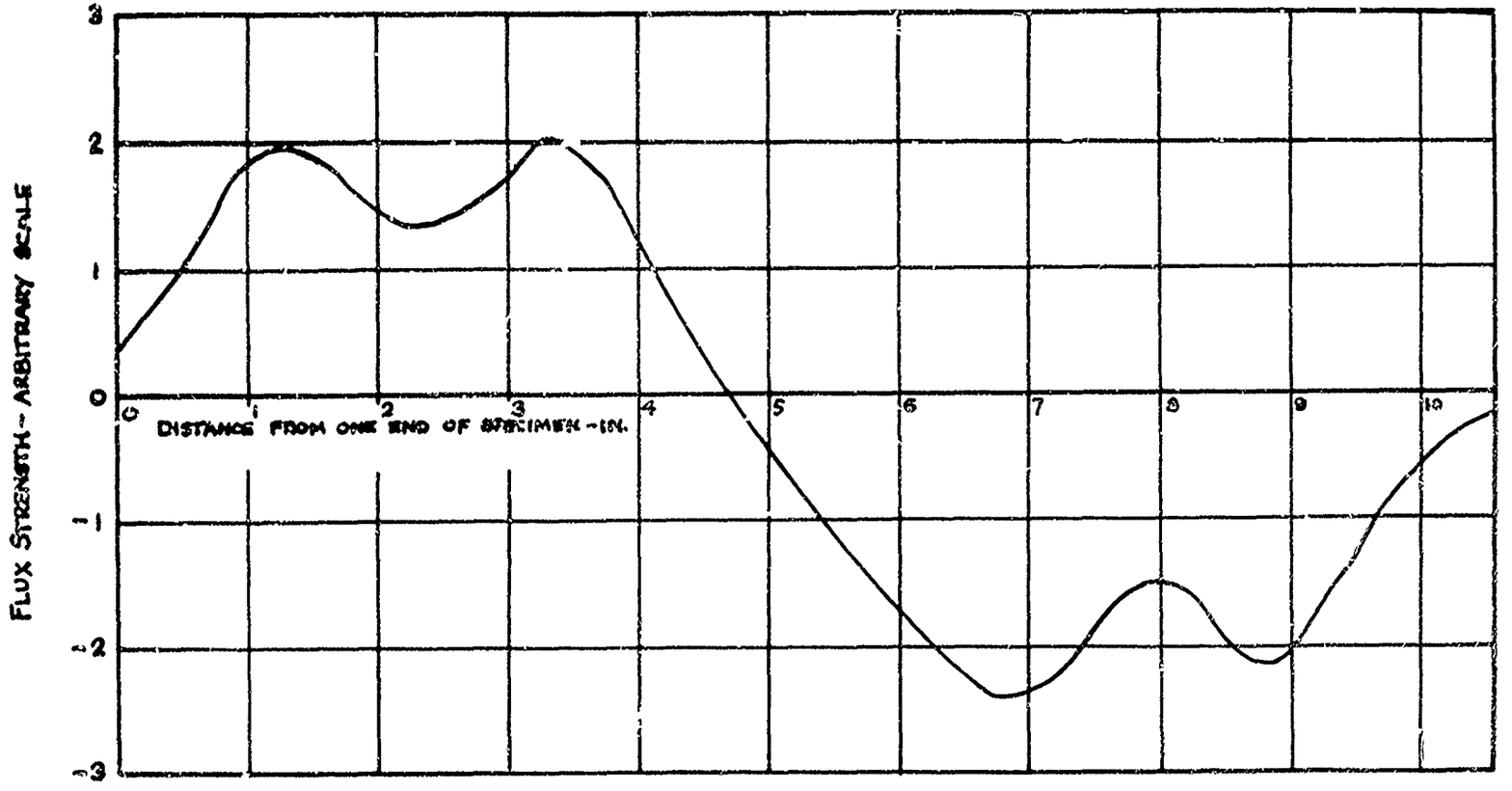

FIG. 59 FLUX DISTRIBUTION (∝ LOADING DISTRIBUTION) ALONG THE SPECIMEN

Security Classification

DOCUMENT CONTROL DATA - R&D

(Security classification of title, body of abstract and indexing annotation must be entered when the overall report is classified)

1. ORIGINATING ACTIVITY (Corporate author)
University of Southampton
Southampton, England

2a. REPORT SECURITY CLASSIFICATION
UNCLASSIFIED

2b GROUP

3. REPORT TITLE
THE EFFECT OF CERTAIN DAMPING TREATMENTS ON THE RESPONSE OF IDEALIZED AEROPLANE STRUCTURES EXCITED BY NOISE

4. DESCRIPTIVE NOTES (Type of report and inclusive dates)
Final Report - January 1963 to January 1964

5. AUTHOR(S) (Last name, first name, initial)
Mead, D. J.

6. REPORT DATE	7a. TOTAL NO. OF PAGES	7b. NO. OF REFS
August 1965	183	32

8a. CONTRACT OR GRANT NO. AF 61(052)-627	9a. ORIGINATOR'S REPORT NUMBER(S)
b. PROJECT NO. 7351	AFML-TR-65-284
c. TASK NO. 735106	9b. OTHER REPORT NO(S) (Any other numbers that may be assigned this report)
d.	

10. AVAILABILITY/LIMITATION NOTICES Qualified users may obtain copies of this report from the Defense Documentation Center (DDC), Alexandria, Va. The distribution of this report is limited because it contains technology identifiable with items on the Mutuall Defense Assistance Control List excluded from export under U.S. Export Control Act of 1949, as implemented by AFR 400-10.

11. SUPPLEMENTARY NOTES

12. SPONSORING MILITARY ACTIVITY
Metals and Ceramics Division (MAMD)
Air Force Materials Laboratory
Wright-Patterson AFB, Ohio 45433

13. ABSTRACT

This report relates to the vibration of aeroplane structures excited by jet-noise or other random pressures. A review is made of those aspects of vibration and transmitted noise which may be alleviated by increasing the structural damping. The damping of conventional untreated structures is then considered, measured values of the damping of model and full-scale structures being discussed in the light of previous studies (by the author) of acoustic and rivet damping.

The common practice of judging a damping treatment by the loss factor increment it produces is then shown to be inadequate for contemporary treatments and thin-plate structures. Alternative "criteria" are therefore derived which describe more adequately the effectiveness of the treatment in attenuating certain random and harmonic vibration phenomena. These have been used to compare two commercial unconstrained treatments and to estimate the reduction of random stresses in an aeroplane structure when the treatments are added.

The response of a two-dimensional flat sandwich plate with a damped core has next been analysed. The dependence of the modal loss factor, stiffness and criteria values on the wavelength and core properties has been studied. Optimum core thicknesses and core properties have been found

(CONTINUED)

DD FORM 1 JAN 64 1473

Security Classification

Security Classification

14. KEY WORDS	LINK A		LINK B		LINK C	
	ROLE	WT	ROLE	WT	ROLE	WT

INSTRUCTIONS

1. ORIGINATING ACTIVITY: Enter the name and address of the contractor, subcontractor, grantee, Department of Defense activity or other organization *(corporate author)* issuing the report.

2a. REPORT SECURITY CLASSIFICATION: Enter the overall security classification of the report. Indicate whether "Restricted Data" is included. Marking is to be in accordance with appropriate security regulations.

2b. GROUP: Automatic downgrading is specified in DoD Directive 5200.10 and Armed Forces Industrial Manual. Enter the group number. Also, when applicable, show that optional markings have been used for Group 3 and Group 4 as authorized.

3. REPORT TITLE: Enter the complete report title in all capital letters. Titles in all cases should be unclassified. If a meaningful title cannot be selected without classification, show title classification in all capitals in parenthesis immediately following the title.

4. DESCRIPTIVE NOTES: If appropriate, enter the type of report, e.g., interim, progress, summary, annual, or final. Give the inclusive dates when a specific reporting period is covered.

5. AUTHOR(S): Enter the name(s) of author(s) as shown on or in the report. Enter last name, first name, middle initial. If military, show rank and branch of service. The name of the principal author is an absolute minimum requirement.

6. REPORT DATE: Enter the date of the report as day, month, year, or month, year. If more than one date appears on the report, use date of publication.

7a. TOTAL NUMBER OF PAGES: The total page count should follow normal pagination procedures, i.e., enter the number of pages containing information.

7b. NUMBER OF REFERENCES: Enter the total number of references cited in the report.

8a. CONTRACT OR GRANT NUMBER: If appropriate, enter the applicable number of the contract or grant under which the report was written.

8b, 8c, & 8d. PROJECT NUMBER: Enter the appropriate military department identification, such as project number, subproject number, system numbers, task number, etc.

9a. ORIGINATOR'S REPORT NUMBER(S): Enter the official report number by which the document will be identified and controlled by the originating activity. This number must be unique to this report.

9b. OTHER REPORT NUMBER(S): If the report has been assigned any other report numbers *(either by the originator or by the sponsor)*, also enter this number(s).

10. AVAILABILITY/LIMITATION NOTICES: Enter any limitations on further dissemination of the report, other than those imposed by security classification, using standard statements such as:

(1) "Qualified requesters may obtain copies of this report from DDC."

(2) "Foreign announcement and dissemination of this report by DDC is not authorized."

(3) "U. S. Government agencies may obtain copies of this report directly from DDC. Other qualified DDC users shall request through

_____."

(4) "U. S. military agencies may obtain copies of this report directly from DDC. Other qualified users shall request through

_____."

(5) "All distribution of this report is controlled. Qualified DDC users shall request through

_____."

If the report has been furnished to the Office of Technical Services, Department of Commerce, for sale to the public, indicate this fact and enter the price, if known.

11. SUPPLEMENTARY NOTES: Use for additional explanatory notes.

12. SPONSORING MILITARY ACTIVITY: Enter the name of the departmental project office or laboratory sponsoring *(paying for)* the research and development. Include address.

13. ABSTRACT: Enter an abstract giving a brief and factual summary of the document indicative of the report, even though it may also appear elsewhere in the body of the technical report. If additional space is required, a continuation sheet shall be attached.

It is highly desirable that the abstract of classified reports be unclassified. Each paragraph of the abstract shall end with an indication of the military security classification of the information in the paragraph, represented as *(TS)*, *(S)*, *(C)*, or *(U)*.

There is no limitation on the length of the abstract. However, the suggested length is from 150 to 225 words.

14. KEY WORDS: Key words are technically meaningful terms or short phrases that characterize a report and may be used as index entries for cataloging the report. Key words must be selected so that no security classification is required. Identifiers, such as equipment model designation, trade name, military project code name, geographic location, may be used as key words but will be followed by an indication of technical context. The assignment of links, rules, and weights is optional.

Security Classification

DD FORM 1473 (Continued)

which minimise the response. Random stresses in a structure with thick-cored sandwich plating have been estimated to be not less than 10% of those in a solid-plate structure of equal weight.

Harmonic experiments on small sandwich specimens have confirmed the theory for the loss factor and stiffness. The special apparatus and techniques of measurement developed for the experiment have been used to assess three commercial sandwich specimens.

A new approach has been initiated to estimate the random response of a very heavily damped system. Its validity has been confirmed for simple random excitation conditions by experiments on the sandwich specimens.